# Contents

# Preface

The topics covered in this book represent a review of modern approaches and practical methods for analysing various problems related to reservoir engineering.

This textbook, part I **Fundamentals** and part II **Reservoir Parameter Estimation Methods**, constitutes the main content of the book. The subjects presented, are based on the course of lectures in *Reservoir Engineering 1* held by the authors at the Rogaland University Centre in the period from 1989 to 1995. Part III **Fluid Flow in Porous Media** and part IV **Enhanced Oil Recovery** are a collection of subjects extending the fundamental knowledge into areas of more advanced theoretical description. The last part V **Projects Exercises** presents quite a few exercises of the type students are asked to solve at their examination test.

The book contains a short introduction to important definitions for oil and gas reservoirs (Chapter 1). The two main parts of the book is related to petro-physics (Chapter 2 to 10), and related to two important methods in Reservoir Engineering, namely Material Balance (Chapter 11) and Well Testing (Chapter 12, 13 and 14). Modelling of fluid flow in porous media is presented through different examples using various mathematical techniques (Chapter 15 to 20). Classification and description of several methods used in enhanced oil recovery are associated with examples for oil and gas fields in the North Sea (Chapter 21 to 27)

The Preface contains a list of some of the most commonly used parameters and systems of units used in petroleum engineering.

In **Chapter 1** some basic definitions of gas and oil reserves are given and the methods of their evaluation.

**Chapter 2** is a brief introduction to the basics of petroleum geology, with some illustrative examples relevant to the Norwegian Continental Shelf. This chapter contains some basic concepts and definitions related to the origin, habitat and trapping of petroleum

In **Chapter 3** some basic concepts and definitions used in Reservoir Engineering are presented. Some laboratory techniques are explained and examples of equipment are shown. A short description of reservoir pressure distribution is also presented.

**Chapter 4** introduces porosity and some examples of experimental techniques used to estimate porosity. Some examples describing the method of error propagation are also given.

Permeability is introduced in **Chapter 5**. A short deduction of Darcy's law is given and some examples of its use is described. Measurements of gas permeability is exemplified and together with laminar and turbulent gas flow, some additional factors affecting permeability are discussed.

In **Chapter 6**, viscosity is introduced and some basic equations, describing laminar fluid flow are derived. Examples of different viscosity measuring techniques are discusses and some flow characteristics are mentioned.

Wettability and capillary pressure are discussed in **Chapter 7**. In this chapter we introduce the term surface energy to replace interfacial tension and an important relation between surface energies are derived. Examples of the effect of capillary forces are given and different experimental techniques are discussed.

Relative permeability is introduced briefly in **Chapter 8**. There has been no attempt made, to give a broad and consistent description of relative permeability in this book. The chapter is meant as an introduction to basic concepts of relative permeability and possibly an inspiration for further reading.

In **Chapter 9**, some basic aspects of compressibility related to reservoir rock and fluids are introduced. Examples are related to the behaviour of porous reservoir rocks and core samples under laboratory conditions.

**Chapter 10** lists some basic definitions and properties related to reservoir fluids. Volume-factors and other important relations are explained and examples of their use are given.

The Material Balance Equation is deduced in **Chapter 11**. The equation is applied in several examples, describing different types of reservoirs, such as gas-reservoir and oil- reservoirs with and without a gas cap.

Well test analysis is introduced in **Chapter 12**. A somewhat simplified derivation of the pressure solution for three important production periods are presented, i.e., the wellbore storage period, the semi-logaritmic period and the semi-steady state period. Dimension-less parameters are used and the set of pressure solutions are presented.

**Chapter 13** introduces some basic methods of well testing, like drawdown test, build-up test and combinations of the two, are presented. Examples of two "classical" well test analysis is also included.

Modern well test analysis, like transient testing techniques, is presented in **Chapter 14**. Use of type curves and matching techniques are shortly presented.

Part III **Fluid Flow in Porous Media** gives an introduction to mathematical modelling of oil displacement by water-flooding. This part presents a broad classification of models describing fluid flow in porous media. Basic principles behind equations of Buckley- Leverett theory and their application are presented, as well as various analytical solution techniques. Some few exercises are included at the end of this part.

**Enhanced Oil Recovery** is presented in part IV. A basic mathematical description of EOR methods are given and various methods are classified. Examples of polymer flooding is presented as well as EOR related to surfactants and different solvents. Various techniques using WAG, foams and Microbial methods are also briefly described.

Most chapters in part I and II contain several exercises, illustrating the concepts and methods presented, while all exercises in part III and IV are added at the end.

This book does not contain complicated mathematical equations or calculus. The mathematical prerequisite required are minimal, though necessary. The student should know the elements of matrix and linear algebra, probability theory and statistics, and also be acquainted with single and partial-differential equations and methods of their solution. In part III and IV, however some slightly more advanced mathematical formalism is used.

A reference list is given at the end of the book. The book does not cover all the relevant literature, nor is the reference list intended to be a complete bibliography. Only some necessary references and key publications are included in the reference list.

J.-R. Ursin & A. B. Zolotukhin
Stavanger, 1997

## Units and conversion factors

The basic knowledge of units and conversion factors is absolutely necessary in reservoir engineering, although the choice of industrial units depend on company, country or simply tradition. Since the choice of units has been largely a question of preference, the knowledge of conversion factors is practical necessary.

English and American units are most commonly used in the petroleum industry, but there is a tendency to turn to SI-units or practical SI-units, especially in the practice of the Norwegian and the other European oil companies.

In this book we will use both SI-units and industrial units in explaining the theory as well as in examples and in exercises. Since both set of units are widely used in the oil industry, it is important to be confident with both systems, -simply due to practical reasons.

A selection of some of the most frequently used parameters are listed in the table below. The *Metric unit* is seen as a practical SI-unit, often used in displaying data or calculations.

$$\textbf{Metric unit = Conversion factor} \times \textbf{Industry unit,}$$

i.e. metric unit is found by multiplying a given industry unit by an appropriate conversion factor.

| Parameter (SI unit) | Industry unit | Conversion factor | Metric unit |
|---|---|---|---|
| Area, $m^2$ | sq mile | 2.589988 | $km^2$ |
| | acre | 4046.856 | $m^2$ |
| | sq ft | 0.09290304 | $m^2$ |
| | sq in. | 6.4516 | $cm^2$ |
| Compressibility, $Pa^{-1}$ | $psi^{-1}$ | 0.1450377 | $kPa^{-1}$ |
| Density, $kg/m^3$ | $g/cm^3$ | 1000.0 | $kg/m^3$ |
| | $lbm/ft^3$ | 16.01846 | $kg/m^3$ |
| | $^o$API | 141.5/(131.5 + $^o$API) | $(\gamma_{sg})^*$ |
| Flow rate, $m^3/s$ | bbl/d | 0.1589873 | $m^3/d$ |
| | $ft^3/d$ | 0.02831685 | $m^3/d$ |
| Force, N | lbf | 4.448222 | N |
| | pdl | 138.2550 | mN |
| | dyne | 0.01 | mN |
| Length, m | mile | 1.609344 | km |
| | ft | 30.48 | cm |
| | in. | 2.54 | cm |
| Pressure, Pa | atm | 101.325 | kPa |
| | bar | 100.0 | kPa |
| | $lbf/in.^2$ (psi) | 6.894757 | kPa |
| | mm Hg ($0^oC$) | 1.333224 | kPa |
| | $dyne/cm^2$ | 0.1 | Pa |
| Mass, kg | ton | 1000 | kg |
| | lbm | 0.4535924 | kg |
| Temperature, K | $^o$C | + 273.15 | K |
| | $^o$F | ($^o$F-32)/1.8 | $^o$C |
| | R | 5/9 | K |
| Surface tension, N/m | dyne/cm | 1.0 | mN/m |
| Viscosity, Pa·s | cp (poise) | 0.001 | Pa·s |
| Volume, $m^3$ | acre-ft | 1233.489 | $m^3$ |
| | cu ft | 0.02831685 | $m^3$ |
| | bbl | 0.1589873 | $m^3$ |
| | U.S. gal | 3.785412 | $dm^3$ |
| | liter | 1.0 | $dm^3$ |

* Spesific gravity of oil.

# Chapter 1

# Oil and Gas Resources and Reserves

## 1.1 Terminology and Definitions

In the period from 1936 to 1964, the American Petroleum Institute (API) set some guiding standards for the definition of *proved reserves*. They were presented in a joint publication of API and the American Gas Association (AGA), "Proved reserves of crude oil, natural gas liquids and natural gas", in 1946. In 1964, the Society of Petroleum Engineers (SPE) recommended reserve definitions following the revised API definitions. In 1979, the U.S. Security and Exchange Commission (SEC) issued a newer set of definitions, whereby also the SPE definitions were updated in 1981. In 1983, the World Petroleum Congress issued a set of petroleum reserve definitions, which included categories ranging from *proved* to *speculative* reserves [2].

Fig. 1.1 shows a conceptual scheme of the oil and gas resources and reserves, where the following definitions are used [2]:

> **Reserves** are estimated volumes of crude oil, condensate, natural gas, natural gas liquids, and associated substances anticipated to be commercially recoverable from known accumulations from a given date forward, under existing economic conditions, by established operating practices, and under current government regulations. Reserve estimates are based on geologic and/or engineering data available at the time of estimate.

The relative degree of an estimated uncertainty is reflected by the categorisation of reserves as either "proved" or "unproved"

> **Proved Reserves** can be estimated with reasonable certainty to be recoverable under current economic conditions. Current economic conditions include prices and costs prevailing at the time of the estimate.
>
> Reserves are considered proved is commercial producibility of the reservoir is supported by actual engineering tests.
>
> **Unproved Reserves** are based on geological and/or engineering data similar to those used in the estimates of proved reserves, but when technical, contractual, economic or regulatory uncertainties preclude such reserves being classified as proved. They may be estimated assuming future economic conditions different from those prevailing at the time of the estimate.

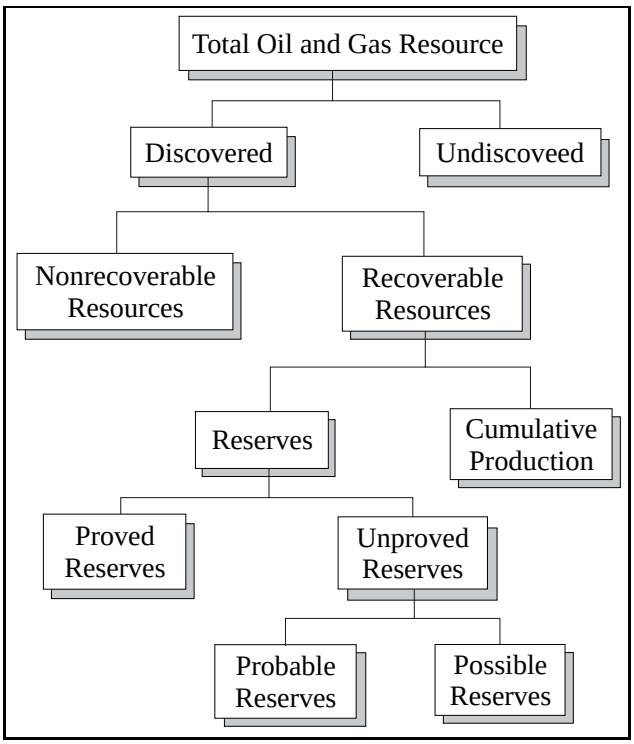


Figure 1.1: Conceptual scheme for oil and gas resources and reserves.

Unproved reserves may further be classified*probable* and *possible*, see Fig. 1.1.

**Probable Reserves** are less certain than proved reserves and can be estimated with a degree of certainty sufficient to indicate they are more likely to be recovered than not.

**Possible Reserves** are less certain than proved reserves and can be estimated with a low degree of certainty, insufficient to indicate whether they are more likely to be recovered than not.

The estimation of reserves will depend upon the actual mode of petroleum recovery, which may involve either a natural-drive mechanism improved by water or gas injection, or some special technique of enhanced oil recovery (EOR).

In general, "possible" reserves may include:

- Reserves suggested by structural and/or stratigraphic extrapolation beyond areas classified as probable, based on geological and/or geophysical interpretation.
- Reserves in rock formations that appear to be hydrocarbon-bearing based on logs or cores, but may not be productive at a commercial level.
- Incremental reserves based on infill drilling are subject to technical uncertainty.

- Reserves attributable to an improved or enhanced recovery method when a pilot project is planned (but not in operation) and the rock, fluid and reservoir characteristics are such that a reasonable doubt exists whether the estimated reserves will be commercial.
- Reserves in a rock formation that has proved to be productive in other areas of the field, but appears to be separated from those areas by faults and the geological interpretation, indicates a relatively low structurally position.

## 1.2 Methods for Resources/Reserve Estimation

### 1.2.1 Analogy-Based Approach

Another producing reservoir with comparable characteristics can be used as a possible analogue for the reservoir under consideration, either by a direct well-to-well comparison or on a unit-recovery basis. This can be done by determining an average oil or gas recovery per well in the analogue reservoir (e.g., 100,000 bbl/well) and applying a similar or adjusted recovery factor to the wells in the reservoir considered. The unit-recovery approach refers to a recovery calculated in barrels per acre-foot or Mcf per acre-foot.

In an analogue approach, one has to consider similarities of well spacing, reservoir rock lithofacies, rock and fluid properties, reservoir depth, pressure, temperature, pay thickness and drive mechanism. All possible differences between the analogue reservoir and the reservoir in question need to be considered to make a realistic adjustment of the recovery estimates.

The use of an analogue may be the only method available to estimate the reserves in a situation where there are no solid data on well performance or reservoir characteristics. However, an analogue-based approach is also the least accurate and little reliable method of petroleum reserve estimation, simply because perfect analogues can seldom be found.

### 1.2.2 Volumetric Estimates

The methods of reserve estimation based on reservoir data are volumetric and can be divided into *deterministic* and *probabilistic* (stocastic) estimates. The main difficulty in a volumetric estimate of resources/reserves is in the transfer of data obtained at a small scale (core analysis, lithofacies data, well logs, etc.) into a much larger scale ( i.e. data "upscaling" for interwell space).

#### Deterministic Methods

The principle of a deterministic approach to resources/reserve estimates is to "upscale" the information derived from the wells and supported by seismic survey, into the interwell space by using an *interpolation technique*.

The main parameters used for a volumetric estimate in this approach are:

- The reservoir "gross" isopach map, which means the bulk thickness of the reservoir rocks (formation).
- The reservoir "net" isopach map, which means the cumulative thickness of the permeable rock units only. The Net-to-Gross ratio (N/G) is an important parameter indicating the productive portion of the reservoir.

- The reservoir rock porosity (as a volume-based weighed average):

$$\overline{\phi} = \frac{\sum_i \phi_i A_i h_i}{\sum_i A_i h_i},$$

  where $\phi$ is the local porosity, $A_i$ is a subarea and $h_i$ is a subthickness (of permeable rock).

- The permeability and net-thickness product ($kh_N$) is important for the estimation of well production capacity:

$$\overline{(kh_N)} = h_N \frac{\sum_i k_i h_i}{\sum_i h_i} = \frac{N}{G} \sum_i k_i h_i,$$

  where $k_i$ is the local permeability (other symbols as above).

- Volume-based average saturation of water, gas and oil. For example water saturation:

$$\overline{S_w} = \frac{\sum_i S_{wi} \phi_i A_i h_i}{\sum_i \phi_i A_i h_i}.$$

Plotting these parameters as contoured maps (isopachs, isoporosity, isopermeability, etc.) provides the crucial information on their variation and distribution in the reservoir and makes it possible to evaluate the reservoir pore volume and its fractions saturated with oil and gas (hydrocarbon volume). The numerical value of hydrocarbon resources/reserve estimate their represents an outcome of "integrated" map analysis.

### Stochastic Methods

An alternative approach is a probabilistic estimation of resources/reserves, which takes more account of the estimate uncertainty. Stochastic reservoir description is usually based on the procedure of random-number generator. This numerical technique assumes that the main reservoir properties (porosity, permeability, N/G, ect.) all have random, possibly normal, frequency distributions, with the range of values included by core and well-log data. The maximum and minimum values are specified for each of the reservoir parameters and the random number generator then "drowns data", so to speak, and then simulates their actual density distribution in the whole reservoir.

In practice, it is necessary to repeat the stochastic simulation for different "seeds" (initial boundary values) in order to asses and quantify the actual variation of a given parameter. Each numerical realisation bears an uncertainty for the reservoir characterisation, where the probabilistic rather than deterministic, is an estimate of resources/reserves. Different realisations lead to different volumetric estimates, with different probabilities attached. The cumulative frequency distributions of these estimates, that is used to asses their likelihood will be a very unclear formulation. See Fig. 1.2.

In common usage [8] we have:

- An estimate with 90 % or higher probability is the level regarded as a *proven* value.
- An estimate with 50 % or higher probability is the level regarded as a *proven + probable* value.

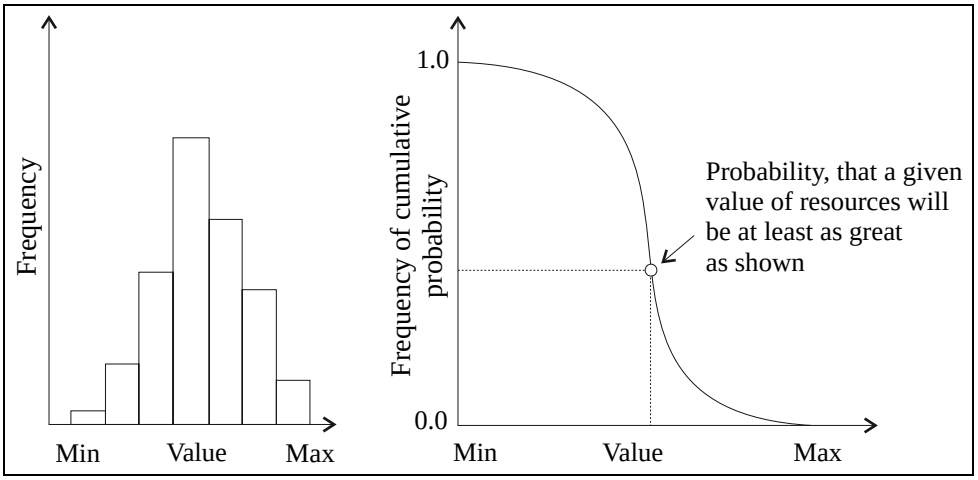


Figure 1.2: Example of stochastic volumetric estimate based on a series of random-number simulations.

– An estimate with 10 % or higher probability is the level regarded as a *proven +probable + possible* value.

As more information on the reservoir becomes available, the cumulative frequency graph may change its shape and the uncertainty of our resource/reserve estimates may decrease, see Fig. 1.3.

More generally, the problem of certainty can be considered in terms of "fuzzy" [61], probabilistic and deterministic estimates based on the data available at a particular time, as seen in Fig. 1.4. A comparison of these estimates may be more revealing that each of them is in isolation.

At the very early stages of field appraisal, the data are usually too limited for using statistical analysis and, hence, a *fuzzy* estimate of the resources/reserves may be best or only option [22, 28, 56]. The lack or scarsity of data in such cases is compensated by a subjective assessment of the reservoir characteristics (i.e. the shape of the distribution and the maximum and minimum values of a given reservoir parameter), Based on the knowledge from other reservoirs or simply a theoretical guess. A rectangular distribution means no preference and a triangular distribution means that strong preference distributions are used.

When more data have been collected and statistical analysis becomes possible, a *probabilistic* estimate can be made. The range in the possible values of the reservoir parameters would then be narrower, compared to a fuzzy assessment. When the data available are abadundant, a *deterministic* estimate can be made based on a well- specified value of a particular parameter for a particular part (zone, subunit or layer) of the reservoir.

### 1.2.3 Performance Analysis

The methods of performance analysis presently used include:

- Analysis based on Material Balance Equation (MBE) [33, 34].
- Reservoir Simulation Models (RSM) [10, 45].

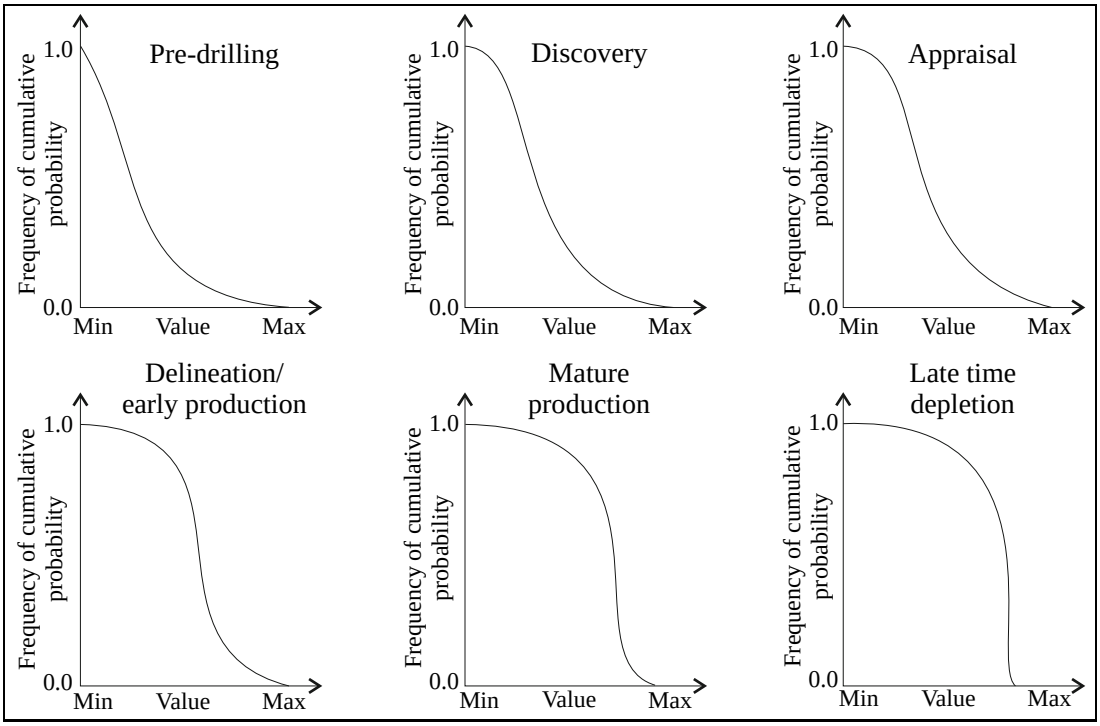


Figure 1.3: Changes in the uncertainty resources estimate with increasing data acquisition (after Archer and Wall, 1992).

- Decline Curve Analysis (DCA) [53].

The aim of all of these methods is to obtain the best reservoir performance prediction on the basis of available data.

The MBE method is based on the data obtained from previous reservoir performance and PVT analysis, but involves some assumptions for the reservoir driving mechanism in order to minimise the range of possible predictions from the dataset. The method is thus adjusted differently to reservoirs containing oil, gas or oil with a gas cap (primary or secondary).

The RSM method involves a numerical simulation technique, with the matching of the production and the reservoir's previous performance (history). The discrepancy between the simulation results (*prediction*) and the available data is minimised by adjusting the reservoir parameters and taking into account the most likely reservoir drive mechanism (*history match*).

The DCA method is to predict future performance of the reservoir by matching the observed trend of the production decline with one or several standard mathematical methods of the production *rate-time* (hyperbolic, harmonic, exponential, ect.). If successful, such a performance analysis allows to estimate both the reserves and the future performance of the reservoir. The following "decline curves" from production wells are commonly used in the DCA:

– Production rate vs. time.

– Production rate vs. cumulative oil production.

– Water cut vs. cumulative oil production.

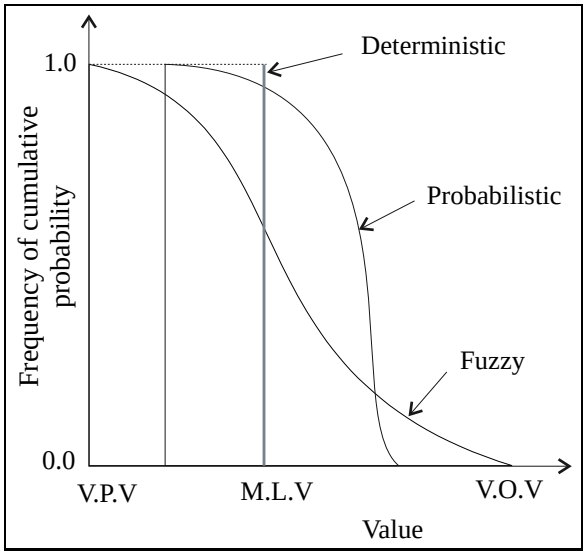


Figure 1.4: The concept of uncertainty in resources/reserves estimation illustrated by fuzzy, probabilistic and deterministic approach (data set).

– Gas-oil ratio vs. cumulative production.

– Percentage oil production vs. cumulative oil production.

– The $(\overline{p}/z)$ ratio vs. cumulative gas production.

Some of these decline curves are shown in Fig. 1.5.

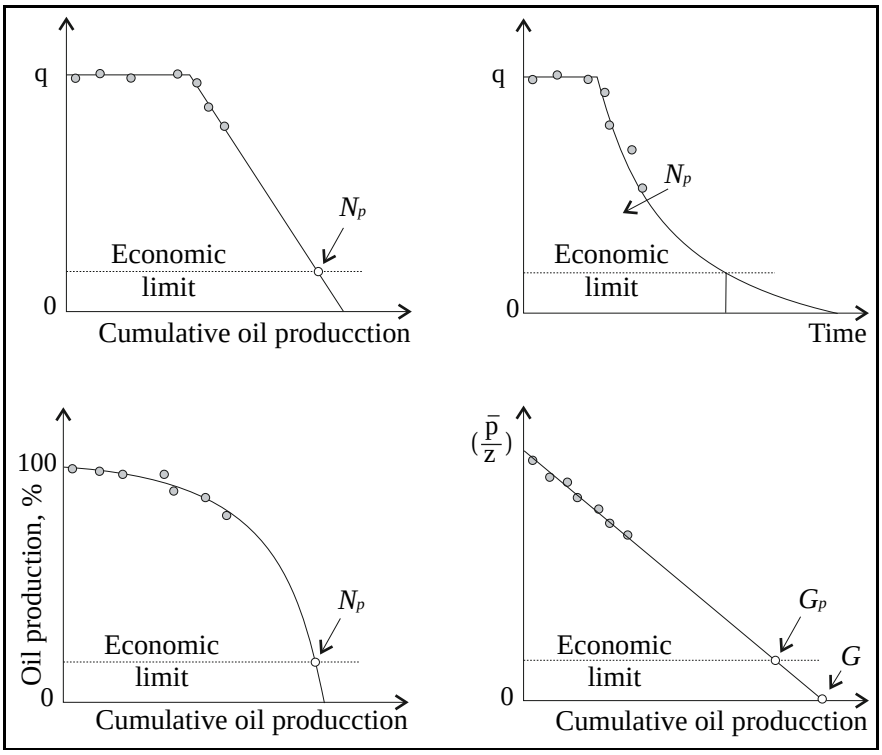


Figure 1.5: Different ways of data representation for a decline curve analysis.

# Part I

# Fundamentals

# Chapter 2

# Basic Concepts of Petroleum Geology

## 2.1 Introduction

Reservoir Engineering is a part of Petroleum Science that provides the technical basis for the recovery of petroleum fluids from subsurface sedimentary-rock reservoirs.

The Fig. 2.1 below indicates the place and role of Reservoir Engineering in the broad field of Petroleum Science.

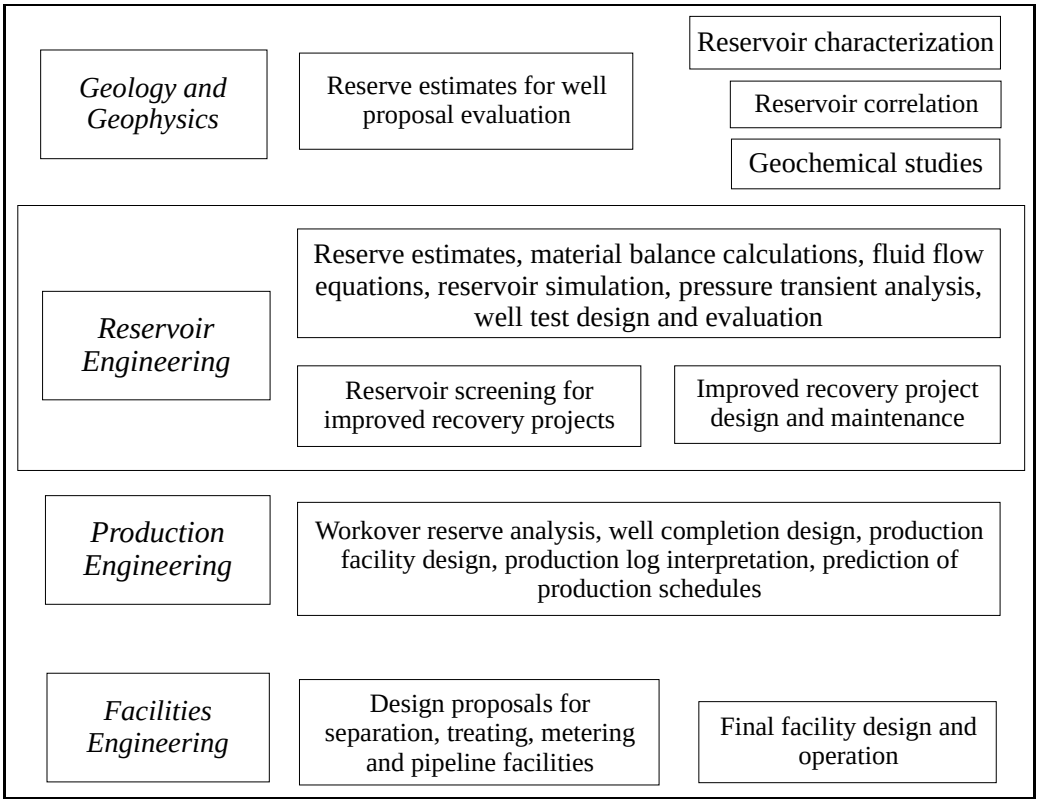


Figure 2.1: Reservoir engineering and petroleum science.

This chapter pertains to the basic concepts of Petroleum Geology and covers the following

main topics:

- The source rock of hydrocarbons.
- The generation, maturation, migration and accumulation of hydrocarbons.

## 2.2 The Basic Concepts

Petroleum is a mineral substance composed of hydrocarbons and produced from the natural accumulations of organic matter of a faunal and/or floral provenance. Petroleum is a gaseous, liquid or semisolid substance, present in the pore space of porous rocks, referred to as reservoir rocks, which are mainly of *sedimentary origin*.

### 2.2.1 Clastic Sedimentary Rocks

Sedimentary rocks results from the deposition of sedimentary particles, known as clastic material or *detritus* (from the Latin "worn down"), consisting of mineral grains and rock fragments. Sedimentary particles are derived from weathered and fragmented older rocks, igneous, metamorphic or sedimentary, usually with some chemical changes. Sediment comprising loose mineral detritus or debris is referred to as *clastic sediment* (from the Greek word "klastos", meaning broken). Some clastic sediments consist of the accumulations of skeletal parts or shells of dead organisms, commonly fragmented, and are referred to as bioclastic rocks (see next section). The particles of clastic sediment may range widely in size, and the predominant grain-size fraction is the primary basis for classifying clastic sediments and clastic sedimentary rocks. As shown in Table 2.1 clastic sediments can be divided into 4 main classes: gravel, sand, silt, and clay [49], where mud is a mixture of clay and silt, possibly including also some very fine sand. The narrower the grain-size range of a given sediment, the better its "sorting". Both the grain size and sorting have direct implications for the sediment permeability to fluids.

Table 2.1: Definition of grain-size and the terminology for sediments and sedimentary rocks.

| **Sediment grain-size fraction** | **Grain-size limits in mm** | **Unconsolidated sediment** | **Consolidated rock** |
|---|---|---|---|
| Boulder | More than 256 | Boulder gravel | Boulder conglomerate * |
| Cobble | 64 to 256 | Cobble gravel | Cobble conglomerate * |
| Pebble | 4 to 64 | Pebble gravel | Pebble conglomerate * |
| Granule | 2 to 4 | Granule grawel | Granule coglomerate * |
| Sand | 1/16 to 2 | Sand | Sandstone |
| Silt | 1/256 to 1/16 | Silt | Siltstone |
| Clay | Less than 1/256 | Clay | Claystone (clayshale, if fissile) |
| Clay & slit mixture | | Mud | Mudstone (mudshale, if fissile) |

* The term "gravelstone" is preferred by some authors on semantic basis [51].

### 2.2.2 Nonclastic Sedimentary Rocks

#### Chemical Deposits

Some sedimentary rocks contain little or no clastic particles. Such a sediment, formed by the precipitation of minerals from solution in water, is a *chemical sediment*. It forms by means of either biochemical or purely chemical (inorganic) reactions [51]. The primary porosity of such rocks is practically zero, and their possible porosity is totally dependent on the development of secondary porosity, chiefly in the form of microfractures.

#### Biogenic Deposits

Sedimentary rocks commonly contain *fossils*, the remains of plants and animals that died and were buried and preserved in the sediment as it accumulated. A sediment composed mainly or entirely of fossil remains is called a *biogenic sediment*. If the fossil debris has not been homogenised by chemical processes, the deposit can be regarded as a bioclastic sediment [51].

Main nonclastic rocks are: limestone, dolomite, salt, gypsum, chert, and coal. Chalk is a special type of biogenic limestone, composed of the sheletal parts of pleagic coccolithophorid algea, called coccoliths. The main types of sedimentary rocks and their chemical compositions are shown in list below, containing main sedimentary rock types and their chemical composition of categories [37].

**Sandstone** a siliciclastic rock formed of sand, commonly quartzose or arhosic, cemented with silica, calcium carbonate, iron oxide or clay.

Chemical composition: $SiO_2$. Density: $\sim 2.65\ g/cm^3$.

**Shale** a fissile rock, commonly with a laminated structure, formed by consolidation of clay or mud ( mainly siliciclastic)

**Argillite** (mud rock) – any compact sedimentary rock composed mainly of siliciclastic mud.

Chemical composition: $SiO_2$ .

**Dolomite** a carbonate rock, consisting largely of the mineral dolomite (*calcium magnesium carbonate*)

Chemical composition: $CaMg(CO_3)_2$. Density: $\sim 2.87\ g/cm^3$.

**Limestone** a carbonate rock consisting wholly or mainly of the mineral calcite.

Chemical composition: $CaCO_3$. Density: $\sim 2.71\ g/cm^3$.

**Calcarenite** a sandstone composed of carbonate grains, typically a clastic variety of limestone.

Chemical composition: $CaCO_3$. Density: $\sim 2.70\ g/cm^3$.

**Marl** a friable rock consisting of calcium carbonate and siliciclastic mud/clay.

Chemical composition: $SiO_2 + CaCO_3$. Density: $\sim 2.68\ g/cm^3$.

**Salt** (rock salt) – a chemical rock composed of the mineral *halite*.

Chemical composition: $NaCl$.

**Gypsum** a chemical, evaporitic rock composed of the mineral *gypsum*

Chemical composition: $CaSO_4\,2H_2O$.

**Anhydrite** a chemical, evaporitic rock composed of the mineral *anhydrite*.

Chemical composition: $CaSO_4$.

Some of the typical reservoir rocks are shown in Fig. 2.2

## 2.3 The Origin and Habitat of Petroleum

### 2.3.1 Source Rock and Generation of Petroleum

Local large concentrations of organic matter in sedimentary rocks, in the form of coal, oil or natural gas are called the *fossil fuels*.

A rock rich in primary organic matter is called a *source rock,* because it is capable of releasing large amounts of hydrocarbons in natural burial conditions. Usually this is a *shale* or *mudrock* which itself is a very common rock type, consisting about 80% of the world's sedimentary rock volume. Organic carbon-rich shale and mudrock are characteristically black or dark greyish in colour, which indicates a non-oxidised primary organic matter.

Many hypotheses concerning the origin of petroleum have been advanced over the last years. Currently, the most favoured one is that oil and gas are formed from marine phytoplankton (microscopic floating plants) and to a lesser degree from algae and foraminifera [51]. In the ocean, phytoplankton and bacteria are the principal of organic matter buried in sediment. Most of organic matter is trapped in clay mud that is slowly converted into shale under burial. During this conversion, the organic compounds are transformed (mainly by the geothermal heat) into *petroleum*, defined as gaseous, liquid or semisolid natural substances that consist mainly of *hydrocarbons*.

In terrestrial sedimentary basins, it is plants such as trees, bushes, and grasses that contribute to most of the buried organic matter in mud rocks and shales. These large plants are rich in *resins, waxes*, and *lignins*, which tend to remain solid and form coal, rather than petroleum.

Many organic carbon-rich marine and lake shales never reach the burial temperature level at which the original organic molecules are converted into hydrocarbons forming oil and natural gas. Instead, the alteration process is limited to certain wax-like substances with large molecules. This material, which remains solid, is called *kerogen*, and is the organic substance of so-called *oil shales*. Kerogen can be converted into oil and gas by further burial by mining the shale and subjecting it to heat it in a retort.

Petroleum is generated when the kerogen is subjected to a sufficient high temperature in the process of the sediment burial. The alteration of kerogen to petroleum is similar to other thermal-cracking reactions, which usually require temperatures greater than $60^oC$. At lower temperatures, during the early diagenesis, a natural biogenic methane called *marsh gas,* is generated through the action of microorganisms that live near the ground surface.

A temperature range between about $60^oC$ and $175^oC$ is most favourable for the generation of hydrocarbons, and is commonly called the *oil window*. See Fig 2.3.

At temperatures much above $175^oC$, the generation of liquid petroleum ceases and the formation of gas becomes dominant. When the formation rock temperature exceeds $225^oC$, most of the kerogen will have lost its petroleum-generating capacity [49],as illustrated by Fig. 2.3 .

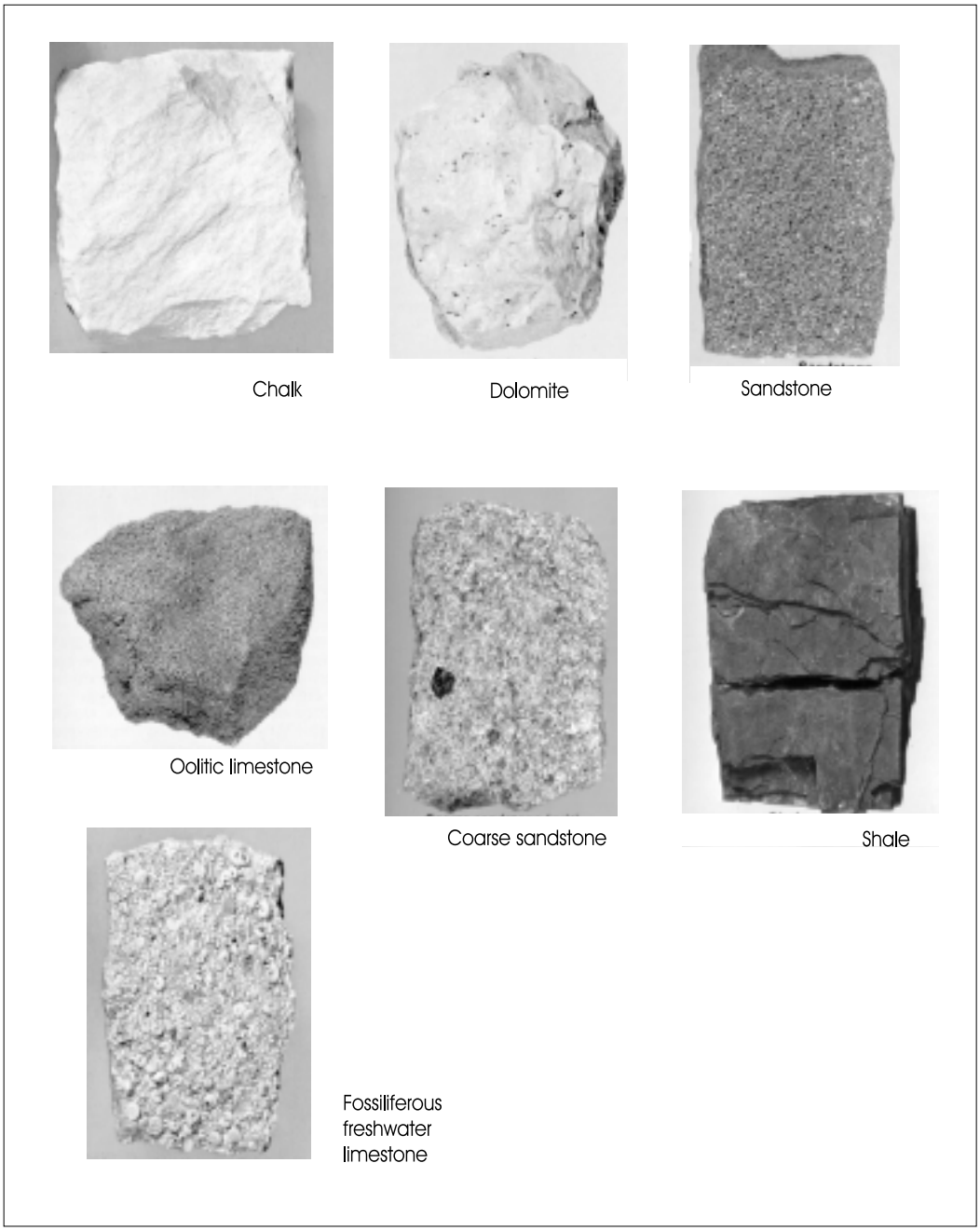


Figure 2.2: Typical reservoir rocks.

The long and complex chain of chemical reactions involved in the conversion of raw organic matter into crude petroleum is called *maturation*. Additional chemical changes may occur in the oil and gas even after these have been generated or accumulated. This explains, for example, why the petroleum taken from different oil fields has different properties, despite a common source rock. Likewise, primary differences in the source composition may be reflected in the chemistry of the petroleum.

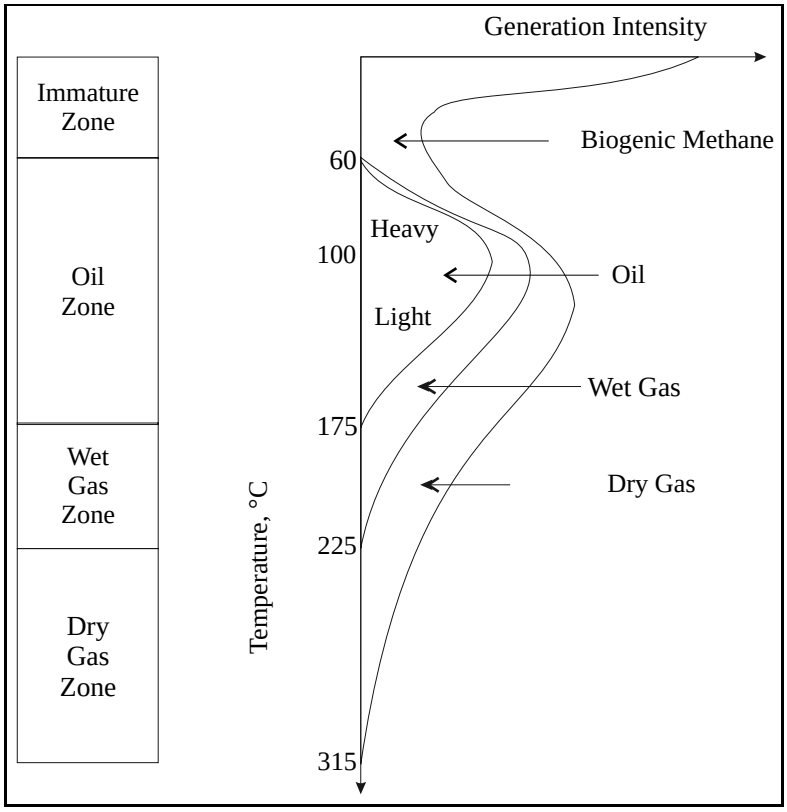


Figure 2.3: Generation of petroleum vs. burial temperature.

Two types of evidence support the hypothesis that petroleum is a product of the decomposition of natural organic matter [51],

- oil has the optical properties of hydrocarbons that are known only to derive from organic matter and
- oil contains nitrogen and certain other compounds that are known to originate from living organic matter only.

Oil source rocks are chiefly marine shales and mudrocks. Sampling of mud on the continental shelves and along the bases of continental slopes has shown that the shallowly buried mud contains up to 8% organic matter. Similar or even higher total organic-carbon (TOC) content characterizes many ancient marine shales. Geologists conclude therefore that oil is originated primarily from the organic matter deposited in marine sediments.

The fact is that most of the world's largest hydrocarbon fields are found in marine sedimentary rock successions representing ancient continental shelves. However, some lake sediments may be just as oil-prone as marine source rocks. Many oil fields in various parts of the world are in ancient lacustrine deposits (formed at the bottom or along the shore of lakes, as geological strata). Fig. 2.4 shows the distribution of the world's sedimentary basin and petroleum accumulations (from [51]).

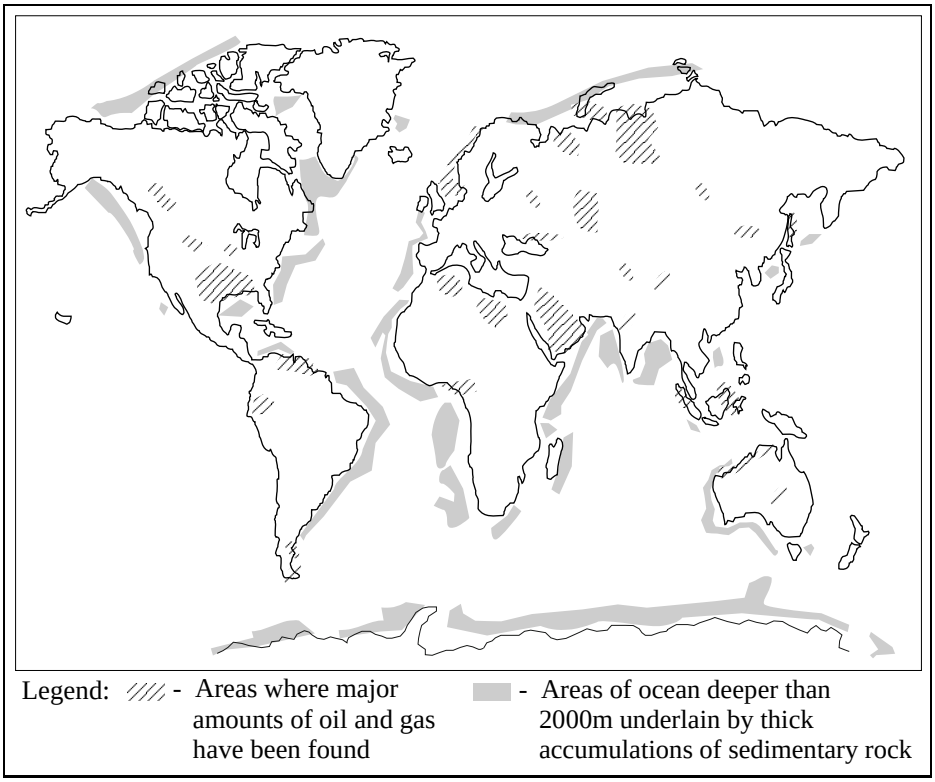


Figure 2.4: World's main sedimentary basins and petroleum accumulations.

### 2.3.2 Petroleum Migration and Accumulation

The accumulation of petroleum occur in only those areas, where geological conditions have provided the unique combination of both hydrocarbon prone source rocks and hydrocarbon traps.

Hydrocarbons are less dense than water. Once released from the source rock, they thus tend to migrate upwards in the direction of the minimum pressure, until they either escape at the ground surface, or an impervious barrier, called a *trap*.

In a trap, the oil and gas accumulate by displacing pore water from the porous rock. The top may be imperfectly sealed, which means that gas and possibly also some oil may "leak" to yet higher lying traps or up to the ground surface. The part of the trap that contains hydrocarbons is called a *petroleum reservoir*.

Water generally underlines the hydrocarbons in a trap. The water bearing part of the trap is called an *aquifer*, and is hydrolically connected with the reservoir. This means that any pressure change in the aquifer will also affect the reservoir, and the depletion of the reservoir will make the aquifer expand into this space.

Both oil and gas are generated together, in varying proportions, from a source rock which results in a primary gas cap above the oil in the reservoir. Likewise, a secondary gas cap may develop when the reservoir pressure has decreased and the lightest hydrocarbon begin to bubble out from the oil. Some "leaky" or limited-capacity traps may segregate oil and gas that have been generated together, such that these accumulate in separate reservoirs.

In summary, several factors are required for the formation of a petroleum reservoir [49]:

1. There must be a *source rock*, preferably rich in primary organic matter (carbon- rich marine or lacustrine shale). This source rock must be deeply buried to reach efficient temperatures to cause the organic matter to mature and turn into petroleum.

2. There has to be a *migration* pathway that enables the shale-released petroleum to migrate in a preferential direction.

3. There must be a *reservoir rock* that is sufficiently porous and permeable to accumulate the petroleum in large quantities.

4. There must be a *trap* that is sealed sufficiently to withhold the petroleum. Otherwise, the majority of petroleum will bypass the porous rock and be dispersed or escape to the ground surface.

5. An impermeable *seal* or caprock, is critical in preventing the petroleum from leaking out from the reservoir or escaping to the surface.

If any of these key factors is missing or inadequate, a petroleum reservoir field cannot be formed. A large isolated reservoir or group of closely adjacent reservoirs is referred to as an *oil field*.

### 2.3.3 Classification of Petroleum Reservoir-Forming Traps

In this section, a general classification of petroleum reservoir-forming traps is discussed (after [1]). In broad terms, one may distinguish between *structual* traps (related to tectonic structures) and *sratigraphic* traps (related to the sealing effect of unconformities and rock-type, or lithofacies, changes).

#### Domes and Anticlines

Domes and anticlines are structures formed by the tectonic uplift and/or folding of sedimentary rocks. When viewed from above, a dome is circular in shape as in Fig. 2.5, whereas an anticline is an elongate fold as in Fig. 2.6.

#### Salt Domes

This type of geological structure is caused by the upward intrusion of a diapiric body of salt, volcanic rock, or serpentine. In pushing up or piercing through the overlaying sedimentary rocks, the diapir may cause the formation of numerous traps on its flanks, in which petroleum may accumulate, as seen in Fig. 2.7. Some salt domes may be highly elongated, rather than cylindrical, and are called *salt walls* (e.g. southern North Sea region). Salt itself is a perfect sealing rock.

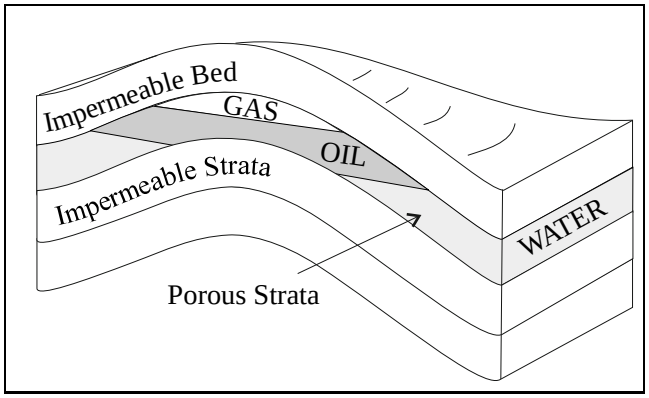


Figure 2.5: Oil and gas accumulation in a dome structure.

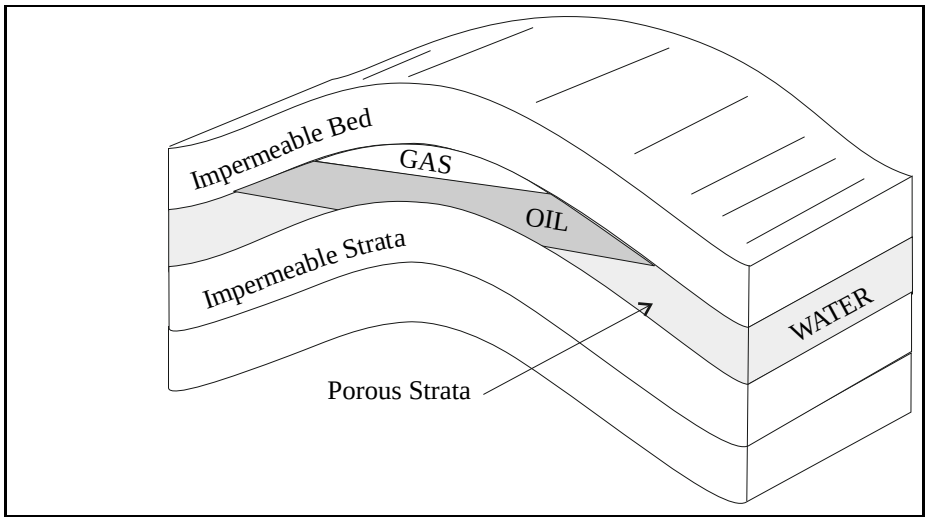


Figure 2.6: Oil and gas accumulation in an anticline structure.

**Fault Structures**

Many petroleum traps are related to faults, which commonly displace permeable rocks against the impervious one. The fault plane, where lined with a shear-produced *gouge* or heavily cemented by the percolating groundwater fragments of rock, acts on impermeable barrier that further increases the trapping effect on the migration of oil and gas. See Fig. 2.8.

**Structures Unconformity**

This type of structure is a sealing unconformity, with the permeable rocks tilted, erosionally truncated and covered by younger impermeable deposits. A reservoir may be formed where the petroleum is trapped in the updip part of the bluntly truncated and sealed, porous rock unit, as seen in Fig. 2.9.

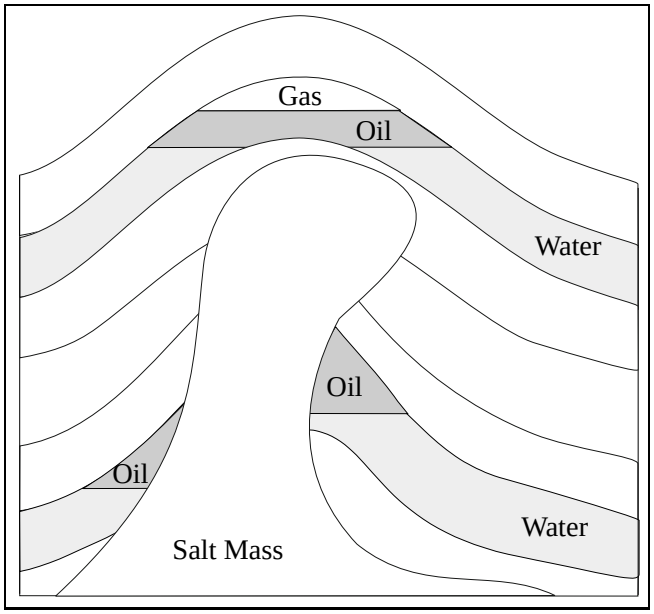


Figure 2.7: Hydrocarbon accumulation associated with a salt dome.

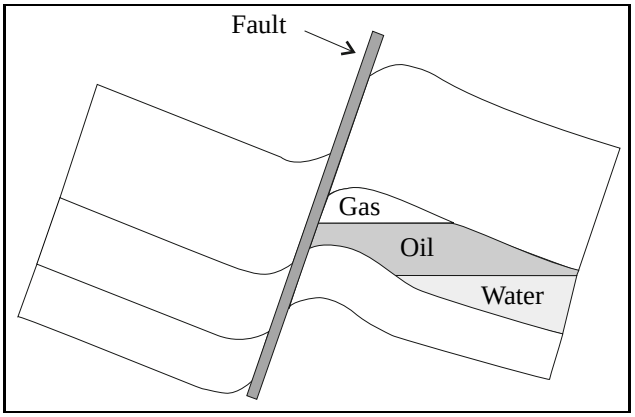


Figure 2.8: Hydrocarbon accumulation related to a fault.

### Lenticular Traps

Oil and gas may accumulate in traps formed by the bodies of porous lithofacies (rock types) embedded in impermeable lithofacies, or by the pinch-outs of porous lithofacies within impermeable ones, as seen in Fig. 2.10.

Examples of such lenticular traps include: fluvial sandstone bodies embedded in floodbasin mudrocks, deltaic or mouth-bar sandstone wedges pinching out within offshore mudrocks, and turbiditic sandstone lobes embedded in deep marine mudrocks. Similar traps occur in various limestones, where their porous lithofacies (e.g. oolithic limestone or other calcarenites) are embedded in impermeable massive lithofacies; or where porous bioclastic reefal limestones pinch out in marls or in mudrocks.

The approximate percentages of the world's petroleum reservoirs associated with those

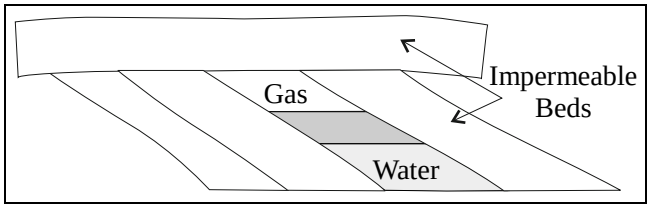


Figure 2.9: Oil and gas trapped below an unconformity.

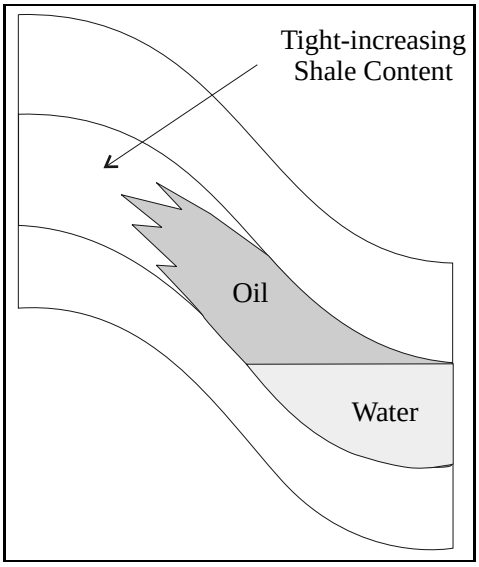


Figure 2.10: Petroleum trap formed by lithofacies change (Sandstone pinch-out).

major trap types are given in Fig. 2.11.

On of the present-day Earth's surface, over half of the continental areas and adjacent marine shelves have sediment covers either absent or too thin to make prospects for petroleum accumulation. Even in an area where the buried organic matter can mature, not all of it results in petroleum accumulations. The following statistical data may serve as a fairly realistic illustration [49]:

- Only 1% by vol. of a source rock is organic matter,
- < 30% by vol. of organic matter matured to petroleum,
- > 70% by vol. of organic matter remains as residue and
- 99% by vol. of petroleum is dispersed or lost at the ground surface in the process of migration, and only 1% by vol. is trapped.

These data lead to the following estimate: only 0.003 vol.% of the world's source rocks actually turn into petroleum that can be trapped and thus generate our petroleum resources.

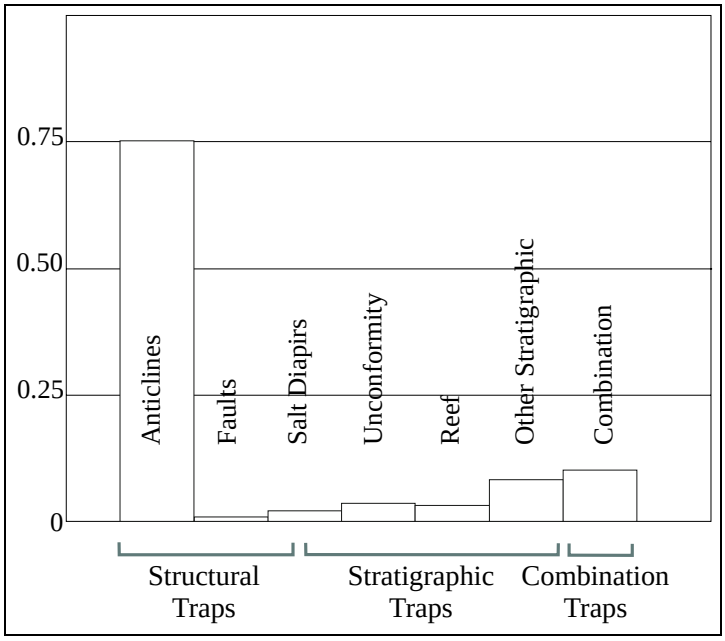


Figure 2.11: Percentages of world's petroleum accumulations associated with the major traps types.

## 2.4 Types of Hydrocarbon Traps on the Norwegian Continental Shelf

Structural traps, particularly fault and dome structures, are the most common type of trap in the Norwegian Continental Shelf [4]. Stratigraphic traps are far less common for this region, although there are several reservoirs associated with unconformities or porous lithofacies pinchouts (e.g. fluvial sandstone in the Snorre filed and turbiditic sandstone in the Frigg and Balder fields).

Table 2.2 summarises the regional information about some of the hydrocarbon fields belonging to the most common types of traps in the Norwegian continental shelf [4].

Table 2.2: Types of petroleum trap in the main fields of the Norwegian Continental Shelf [4].

| **Field** | **Type of Trap** | **Reservoir Rock** | **Rock Age** |
|---|---|---|---|
| AGAT | Stratigraphic | Sandstone | Cretaceous |
| BALDER | Stratigraphic | Sandstone | Tertiary |
| DRAUGEN | Stratigraphic | Sandstone | Jurassic |
| EKOFISK | Dome | Chalk | Cretaceous |
| ELDFISK | Dome | Chalk | Cretaceous |
| EMBLA | Structural | Sandstone | Carboniferous |
| FRIGG | Stratigraphic | Sandstone | Tertiary |
| GULLFAKS | Structural | Sandstone | Jurassic |
| HEIDRUN | Structural | Sandstone | Jurassic |
| MIDGARD | Structural | Sandstone | Jurassic |
| OSEBERG | Structural | Sandstone | Jurassic |
| SNORRE | Structural | Sandstone | Jurassic |
| SNİHVIT | Structural | Sandstone | Jurassic |
| STATFJORD | Structural | Sandstone | Jurassic |
| TROLL | Structural | Sandstone | Jurassic |
| VALHALL | Dome | Chalk | Cretaceous |

# Chapter 3

# Basic Concepts and Definitions in Reservoir Engineering

## 3.1 Continuum Mechanics

The present understanding of the subsurface processes relevant to reservoir engineering is based on the physical concepts of *continuum mechanics* [12]. According to these concepts, a porous rock formation saturated with fluids forms a continuum, which means that all the components involved (rock, water, oil and/or gas) are present in every element, or volumetric part, of the reservoir space, even if the elementary volume considered is very small and approaches zero. This conceptual approach allows us to develop a useful theory for the flow of liquid and gas through a porous medium, called the *filtration theory*. All of the most important numerical simulation programs (ECLIPSE, MORE, FRANLAB, FRAGOR, UTCHEM, etc.) are based on this theory.

The flow of fluids that occurs in the partial volume of a porous rock, even if very small, can only be described qualitatively, because of the great complexity of the phenomenon. However there are some regularities in the behaviour of the "rock-fluids" systems that can be described by continuum mechanics. For the purpose of the filtration theory, the laws of continuum mechanics are considered to be effective only if the elementary volume is sufficiently large to render the number of pores and rock grains very large or "innumerable". This condition makes the average parameters of the porous medium sufficiently representative for a description of the fluid flow processes occurring in the rock. If the elementary volumes are too small and comparable to the rock's pore or grain size, the filtration theory cannot be successfully applied. The need for this concept assumption can be explained as follows. Let us consider the flow of liquids and gas in a natural reservoir, with the scale of the flow phenomenon varying from very small to large, as seen in Fig. 3.1. In Fig. 3.1, many physical phenomena (capillary effects, fluid adhesion effects associated, etc.) occur at a scale comparable to the rock's grain size or the dimension of a fractured rock's fragment ($10^{-4} - 10^{0}$ m).

At a large scale, with the elementary volumes considered on the order of $10^{2} - 10^{4}\,m$, the effect of the micro-scale phenomena "average" and can more readily be parameterizied. Likewise, the concepts of continuum mechanics can be applied if the reservoir heterogeneity is considered at a macro-scale level (lithofaces variation, bedding, ect.), whereas all micro-heterogeneities on a scale comparable to the grain size are being considered as constants in

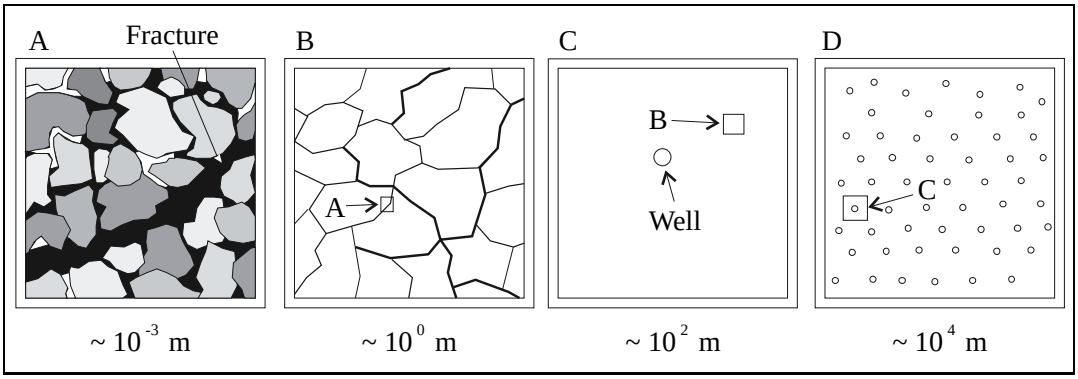


Figure 3.1: Structure of a fractured-rock reservoir at different scales of observation.

the equations of flow (parametrized connate-water saturation, residual-oil saturation, etc.) or described by some empirical relationships (functions). The fundamental definitions in the filtration theory include the distribution between *porosity* (i.e. the rock's fluid storage capacity) and *permeability* (i.e. the rock's fluid flow capacity), as well as the consideration of *fluid saturation* (i.e. the pore volume percent occupied by water, oil and gas, respectively).

## 3.2 Porosity

The porosity constitute the part of the total porous rock volume which is not occupied by rock grains or fine mud rock, acting as cement between grain particles. Absolute and effective porosity are distinguished by their access capabilities to reservoir fluids. Absolute porosity is defined as the ratio of the total void volume $V_{p_a}$, whether the voids are interconnected or not, to the bulk volume $V_b$ of a rock sample,

$$\phi_a \stackrel{\text{def}}{=} \frac{V_{p_a}}{V_b}. \tag{3.1}$$

Effective porosity implies the ratio of the total volume of interconnected voids $V_p$ to the bulk volume of rock,

$$\phi \stackrel{\text{def}}{=} \frac{V_p}{V_b}. \tag{3.2}$$

Effective porosity depends on several factors like rock type, heterogeneity of grain sizes and their packing, cementation, weathering, leaching, type of clay, its content and hydration, etc. It should be noted that porosity is a *static* parameter, unlike permeability which makes sense only if liquid or gas is *moving* in porous medium.

## 3.3 Saturation

Let us consider a representative elementary volume of the reservoir, with the pores filled with oil, gas and water. In volumetric terms, this can be written as follows:

$$V_p = V_o + V_g + V_w, \tag{3.3}$$

which leads to the definition of saturation, $S$, as a fraction of the pore volume occupied by a particular fluid:

$$S_i \stackrel{\text{def}}{=} \frac{V_i}{V_p}, \quad i = 1, ..., n$$

where $n$ denotes the total number of fluid phases present in the porous medium.

Consequently,

$$\sum_{i=1}^{n} S_i = 1.$$

If two fluids coexist (say, oil and water), they are distributed unevenly in the pore space due to the *wettability preferences*. See Fig. 3.2. Simply, the adhesive forces of one fluid against the pore walls (rock-grain surface) are always stronger than those of the other fluid. In the vast majority of petroleum reservoirs, both siliclastic and carbonate, the pore water is the wetting phase and oil is a non-wetting phase.

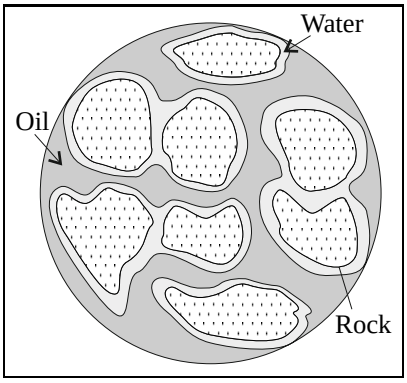


Figure 3.2: Distribution of water and oil phases in a water-wet porous medium.

Importantly, the fluid saturation ($S_o$, $S_g$ and $S_w$) in a reservoir varies in space, most notably from the water-oil contact to the reservoir top (see figures in previous chapter), and also in time during the production. In short, different parts of the reservoir may have quite different fluid saturations, and also the saturation in any elementary volume of the reservoir changes progressively during the production.

### 3.3.1 Residual Saturation

Not all the oil can be removed from the reservoir during production. Depending on the production method, or the actual "drive mechanism" of the petroleum displacement, the oil- recovery factor may be as low as 5-10% and is rarely higher than 70%. Part of the oil will remain as residue, this is called the *residual oil*. One has to distinguish between the residual oil and possibly gas saturation reached in a reservoir after the production stage, and the residual saturation

of fluid phases in a reservoir-rock sample after a well *coring* operation. A fresh, "peel-sealed" core sample is taken to the laboratory, where the reservoir saturation and the oil-recovery factor are estimated. The laboratory process is illustrated in Fig. 3.3, where water is displacing the initial oil in the core sample.

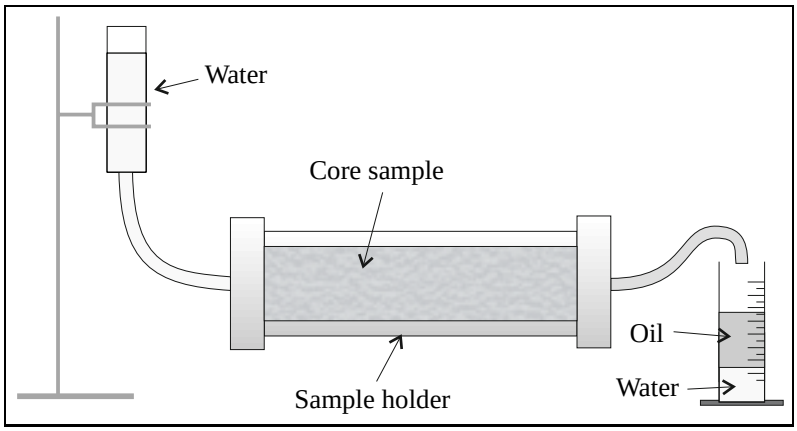


Figure 3.3: Evaluation of residual oil saturation $S_{or}$ by a laboratory displacement from a core sample.

If the pore volume $V_p$ of the core sample in known, then

$$S_{or} = \frac{V_{oi} - V_o}{V_p}, \tag{3.4}$$

where $V_{oi}$ is the initial volume of trapped oil in the core sample, and $V_o$ is the displaced or produced oil.

### 3.3.2 Laboratory Determination of Residual Oil and Water Saturation

The cores recovered from wells contain residual fluids (depleted due to the drilling-fluid invasion, the changes in pressure and temperature, etc.) that are assumed to reflect:

- The fluid saturation at the reservoir conditions.
- The possible alterations due to the drilling-fluid invasion into the core.
- The efficiency of possible oil displacement from the reservoir rock represented by the core.

The modern techniques of core-samples collection prevent dramatic alterations of the rock fluid characteristics, (foam-based drilling fluid, rubber sleeves containing the core samples and maintaining their reservoir pressure, deep freezing of retrieved cores, etc.)

Two laboratory techniques are commonly used for determining the residual oil and water saturation,

- a high temperature retort distillation method and
- the Dean-Stark method.

### The Retort Distillation Method

The core sample is weighed and its bulk volume measured or calculated. The sample is then placed in a cylindrical metal holder with a screw cup at the top and a hollow stem projecting from the bottom. The top is sealed and the sample holder is placed in a retort oven. A thermostat controller raises the temperature of the core to a selected level, at which point the water within the core is vaporised and recovered. The temperature is then increased to $\sim 650^{o}$C ($1200^{o}$F) to vaporise and then distil oil from the sample. The vaporised fluids are first collected in the sample holder and then released vertically downwards through the hollow stem (*down-draft retort*). They are subsequently condensed and measured in a calibrated receiving tube. See Fig. 3.4.

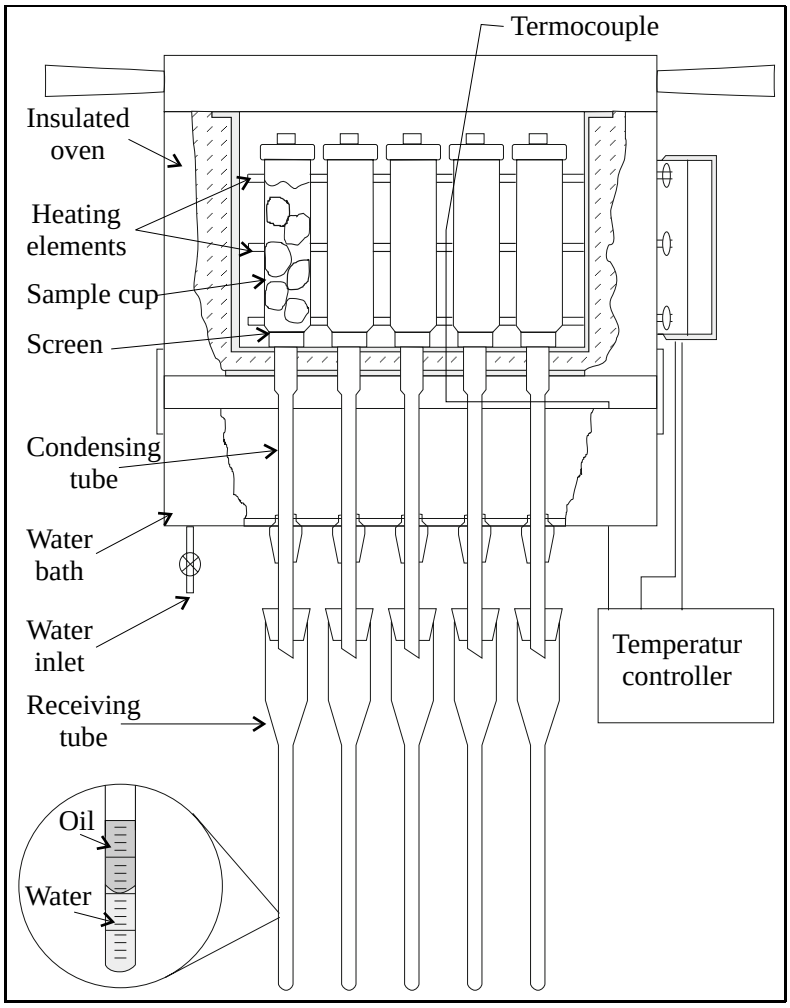


Figure 3.4: The high temperature retort distillation method.

**N.B.!** *Samples are usually destroyed in this test due to the high temperature and for this reason small-diameter samples or "plugs" (small cores from the well core), are normally used.*

The calculation of the oil and water saturation is straightforward. The following parameter values are derived from the laboratory test:

- $V_b, \rho_r$ – the sample bulk volume and rock density, determined prior to the experiment.
- $V_o; V_w$ – the recovered oil and water volumes, registered during the test..
- $V_p$ – the pore volume, which is calculated.

The water and residual oil saturation are calculated as follows:

$$S_w = \frac{V_w}{V_p}, \quad \text{and } S_o = \frac{V_o}{V_p}, \tag{3.5}$$

where the saturation are fractional parts of the pore volume. Frequently, saturation are also given in %.

**The Dean-Stark Apparatus for Measuring Initial Fluids**

When the core to be analysed is weighed, the measurement includes the weight of rock grains, and the pore fluid. The sample is then placed in the tare apparatus (to be sure that no sand grains are lost from the core sample during its analysis, which might otherwise lead to an erroneously high oil saturation!) and this unit is suspended above a flask containing a solvent, such as toluene, as shown in Fig. 3.5.

There are several requirements for choosing a proper solvent,

- it must have a boiling temperature higher than that of water,
- it must be immiscible with water and
- it must also be lighter than water.

*Toluene* satisfies all of those requirements.

When heat is applied to the solvent, it vaporises. The hot solvent vapour rises, surrounds the sample and moves up to the condensing tube, where it is cooled and condensed. The condensate collects into the calibrated tube until the fluid there reaches the spill point, where upon the solvent condensate drips back onto the sample containing the reservoir fluids. The solvent mixes with the oil in the sample and both are returned to the solvent flask below. See Fig. 3.5. The process continues until the sample's temperature has risen above the boiling point of water. At that point, the water vaporises, rises in the condensing tube, condenses therein and falls back into the calibrated tube. Because it is heavier than the solvent, it collects at the bottom of the tube, where its volume can be directly measured. When successive readings indicate no additional water recovery, the water volume is recorded for further calculations. After all the oil and water have been recovered from the sample, it is dried and weighed again. The difference between the original and final weights equals to the weight of the oil and water originally present in the sample. Because the water collected in the calibrated tube is distilled, with a density of 1.0 $g/cm^3$ and a known volume, the weight of oil in the sample can be calculated. This information is subsequently combined with the estimated porosity of the clean, dry sample, the volumes of the oil and water can be converted into percent pore-space fraction (saturation).

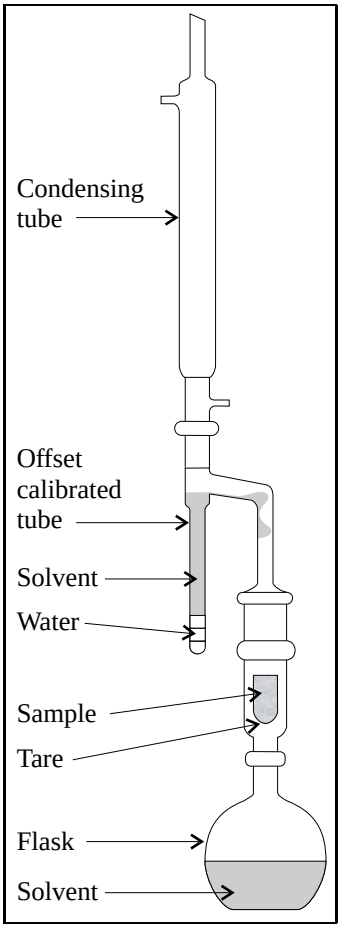


Figure 3.5: The Dean-Stark apparatus.

**N.B.** *The samples in the process are not destroyed and can be further used in other measurements, i.e., pore volume pycnometry or perhaps capillary measurements, ect..*

The calculation of the oil and water saturation is straightforward. The following parameters are derived from the laboratory test:

- $W_i$ – the initial weight of the core sample, determined prior to the tests.
- $W_d$ – the weight of the dry, clean core sample, determined directly after the tests.
- $\phi$, $V_b$ – the rock's porosity and the core sample's bulk volume, determined after the tests.
- $V_w$ – the reservoir volume of water, registered during the test.
- $V_o$ – the recovered volume of oil, which is calculated.

Water and oil (residual) saturation is calculated according to Eqs. (3.5), where both the retort distillation method and the Dean-Stark method are capable of yielding fluid saturation values within $\pm 5\%$ of the true values.

## 3.4 Reservoir Pressure and Distribution of Fluid Phases.

The migration and accumulation of petroleum in a reservoir leads to the replacement of the original pore water by gas and oil , even though the rock pores remain "water-wet" (i.e, their walls are covered with a thin film of water). The density difference makes the gas accumulate at the top of the reservoir, and the oil directly below. Water underlies the petroleum, as an aquifer, but is continuously distributed throughout the reservoir as the wetting fluid. See Fig. 3.6.

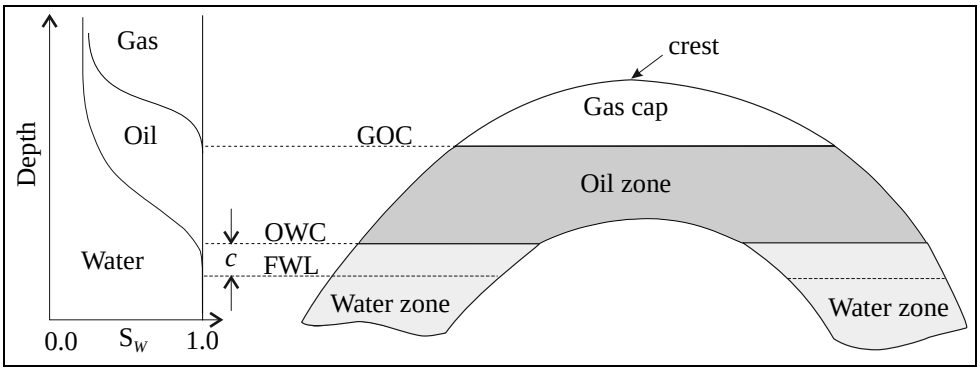


Figure 3.6: The distribution of fluid phases in a reservoir.($S_w$ is the water saturation.)

The following fluid interfaces in the reservoir are important:

- The Gas-Oil Contact (GOC) – a surface separating the gas cap from the underlying oil zone (also referred to as the oil "leg" or oil "column"). Below the GOC, gas can be present only as a dissolved phase in oil.
- The Oil-Water Contact (OWC) – a surface separating the oil zone from the underlying water zone. Below the OWC, oil is generally absent.
- The Free-Water Level (FWL) – an imaginary surface at which the pressure in the oil zone equals to that in the water zone, i.e. $p_o = p_w$. In other words, FWL is the oil-water contact in the absence of the capillary forces associated with a porous medium, i.e. in a well.

However, the term "oil-water contact" does not have a single, unique meaning in reservoir engineering considerations. The continuos distribution of water saturation in the reservoir zone (see $S_w$ in Fig. 3.6) affects strongly the relative mobility of the oil phase, which in turn makes it necessary to distinguish the following saturation interfaces:

- The Free-Oil Level (FOL) – the level above which the oil saturation is sufficiently high to allow full oil mobility (100% oil productivity) and the water saturation is low enough to make water immobile. In most reservoirs, this is the level where $S_o$ exceeds ca. 70%, which means $S_w < 30\%$.
- The Economic OWC – the level above which enough oil will be mobile, rendering the whole overlying part of the reservoir economical viable. In most reservoirs, this is the

level where $S_o$ exceeds ca. 50%, although the actual threshold value may vary, depending upon reservoir conditions.

- The Productive OWC – The level above which oil become mobility. This may mean $S_w$ as high as 80-85% and $S_o$ of merely 15-20%.

- The Edge-Water Level – which is the OWC as defined earlier (level of $S_w$ = 100%), located below the productive oil-water contact. In strict terms, this is not always the "100% water level", as our common terminology refers to it, because the oil saturation may still be in the order of some percent. This is the base of the reservoir, or the oil- column level below which the capillary forces render oil completely arrested, or "imbibed", by the rock pores (such that only thermal distribution can possibly remove the oil from the "dead-end" pores). Therefore, some engineers prefer to refer to this surface as the capillary oil displacement level or threshold pressure level.

Needless to add, the distribution of these surfaces is of crucial importance when it comes to physical (fluid dynamics) and economical (oil recovery) considerations. The interfaces are usually determined on the basis of analysis and well (drill-stem) tests. The FWL would then appear to be the only rock-independent OWC, representing the absolute base of the oil column, as shown in Fig. 3.6.

The total pressure at any reservoir depth, due to the weight of the overlying fluid saturated rock column, is called the *overburden pressure*, $p_{ov}$.

The total pressure at any depth is the sum of the overlaying fluid-column pressure ($p_f$) and the overlaying grain- or matrix-column pressure ($p_m$), as sketched in Fig. 3.7, and thus,

$$p_{ov} = p_f + p_m.$$

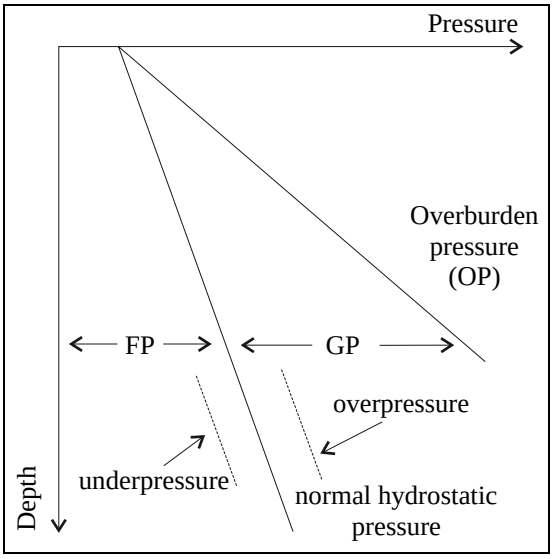


Figure 3.7: Overburden pressure as the combined grain- and fluid column pressure.

Because the overburden pressure $p_{ov}$ is constant at any particular depth $D$, then the differential overburden pressure is zero, i.e. [21]:

$$dp_f = -dp_m.$$

This means that any reduction of the fluid pressure, as it occurs during production, will lead to a corresponding increase in the grain pressure. Rock compressibility is therefore an important parameter to be considered when petroleum (preferably oil) production is estimated.

## 3.5 Pressure Distribution in Reservoirs

The hydrostatic water pressure at any depth $D$, can be calculated as follows:

$$p_w(D) = \int_{D_0}^{D} (\frac{dp}{dz})_w dz + p_w(D_0), \tag{3.6}$$

where $(dp/dz)_w$ denotes the pressure gradient of the water phase at depth $z$, and $D_0$ is an arbitrary depth with a known pressure (for instance, the pressure at the sea bottom or the pressure at the sea surface). The hydrostatic pressure is therefore identical to the water pressure, at any reservoir depth, as long as there is a continous phase contact in the water, all the way up to the sea surface.

If the hydrostatic pressure gradient considered to be constant we can write,

$$p_w(D) = (\frac{dp}{dD})_w (D - D_0) + p_w(D_0), \tag{3.7}$$

and if $D_0$ is taken at the sea level, the equation becomes,

$$\begin{aligned} p_w(D) &= (\frac{dp}{dD})_w D + 14.7 \text{ (in psia), or} \\ p_w(D) &= (\frac{dp}{dD})_w D + 1.0 \text{ (in bar)} \end{aligned} \tag{3.8}$$

Typical "normal" pressure gradients for the water, oil and gas phases are:

$$\begin{array}{lcll} (dp/dD)_w & = & 0.45 \text{ psi/ft} & = & 10.2\text{kPa/m}, \\ (dp/dD)_o & = & 0.35 \text{ psi/ft} & = & 7.9 \text{ kPa/m}, \\ (dp/dD)_g & = & 0.08 \text{ psi/ft} & = & 1.8 \text{ kPa/m} \end{array}$$

Abnormally high or low reservoir pressure can appear when the reservoir is "sealed" off from the surrounding aquifer, as a result of geological processes. The reservoir pressure can then be corrected, relative the hydrostatic pressure, by using a constant ($C$) in the above pressure equations. The constant $C$ accounts for the fact that the reservoir pressure is not in hydrostatic equilibrium, where the pressure in the reservoir is somewhat higher or lower than otherwise expected.

The water pressure for a general reservoir is then as follows,

$$p_w(D) = (\frac{dp}{dD})_w D + 14.7 + C, \text{ (in psia,)} \tag{3.9}$$

where $C$ is positive when over-pressure is observed and negative for a under-pressured reservoir.

In order to evaluate the pressure distribution in a reservoir, let us consider the reservoir which cross-section, as shown in Fig. 3.8 (see also [21]).

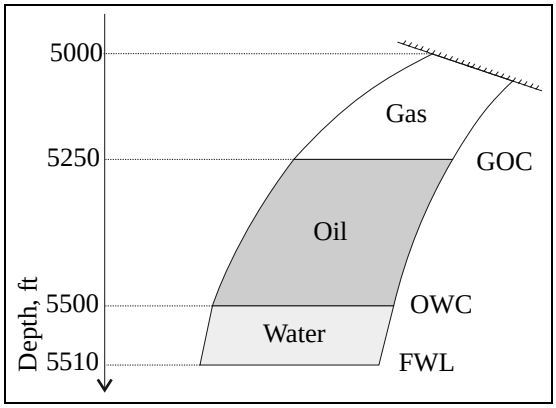


Figure 3.8: Cross-section of a reservoir.

Assuming normal pressure condition, we can evaluate the fluid-phase pressures at the different reservoir "key" levels.

- Water phase:

$$\begin{aligned}(p_w)_{FWL} &= 0.45 \cdot 5510 + 14.7 = 2494.2 \text{ psia} \\ (p_w)_{OWC} &= 0.45 \cdot 5500 + 14.7 = 2489.7 \text{ psia} \\ (p_w)_{GOC} &= 0.45 \cdot 5250 + 14.7 = 2377.2 \text{ psia} \\ (p_w)_{top} &= 0.45 \cdot 5000 + 14.7 = 2264.7 \text{psia}\end{aligned}$$

- Oil phase:

$$\begin{aligned}(p_o)_{FWL} &= = 0.35 \cdot 5510 + C_o = 2494.2 \text{psia} \\ \text{which gives: } C_o &= 565.7 \text{psia} \\ (p_o)_{OWC} &= 0.35 \cdot 5500 + 565.7 = 2490.7 \text{psia} \\ (p_o)_{GOC} &= 0.35 \cdot 5250 + 565.7 = 2403.2 \text{psia} \\ (p_o)_{top} &= 0.35 \cdot 5000 + 565.7 = 2315.7 \text{psia}\end{aligned}$$

- Gas phase:

$$\begin{aligned}(p_g)_{GOC} &= 0.08 \cdot 5250 + C_g = 2403.2 \text{psia} \\ \text{which gives: } C_g &= 1983.2 \text{psia} \\ (p_g)_{top} &= 0.08 \cdot 5000 + 1983.2 = 2383.2 \text{ psia}\end{aligned}$$

The different phase pressures (water, oil and gas) are derived from a common reference which normally is the FWL pressure, $(p_w)_{FWL}$. At this level there is no pressure difference

between water and oil and the two pressures are identical, i.e., $(p_w)_{FWL} = (p_o)_{FWL}$. Ideally there is no oil present in the zone between the FWL and the OWC, since the oil pressure is too low to allow the oil phase to enter the pore space (the largest pore throats). Accordingly, the OWC becomes the level in the reservoir where the water saturation becomes less than one and consequently the water saturation is ideally considered to be 100% in this zone.

Similar to the FWL, the definition of the GOC, is the level in the reservoir where the pressures in the oil and gas phases are identical. Often this pressure is referred to as the *reservoir pressure*.

Different phase pressures are observed at the same elevation in the reservoir, as seen in Fig 3.9. The pressure difference between two coexisting phases is called *capillary* pressure and denoted $(P_c)_{ij}$, where the subscripts $i$ and $j$ refer to oil-water, gas-oil or gas-water.

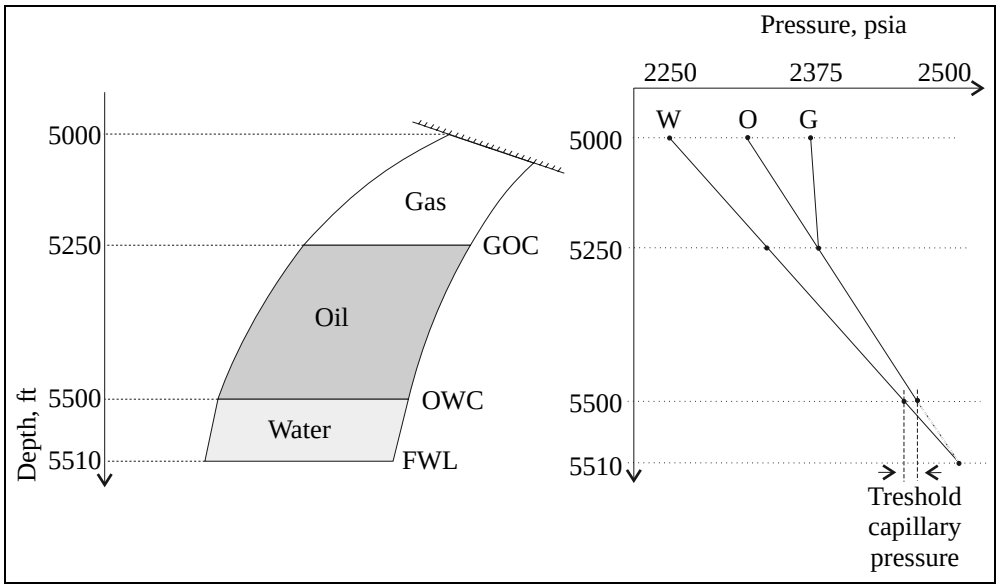


Figure 3.9: Pressure distribution in a reservoir (hypothetical example).

The capillary pressure at the top of the reservoir, shown in Figs. 3.8 and 3.9, can be evaluated as follows,

$$(P_c)_{ow}^{top} = (p_o)_{top} - (p_w)_{topt} = 2315.7 - 2264.7 = 51.0 \text{ psi(a)} = 3.5 \text{ bar}$$
$$(P_c)_{go}^{top} = (p_g)_{top} - (p_o)_{top} = 2383.2 - 2315.7 = 67.5 \text{ psi(a)} = 4.6 \text{ bar}$$
$$(P_c)_{gw}^{top} = (p_g)_{top} - (p_w)_{top} = 2383.2 - 2264.7 = 118.5 \text{ psi(a)} = 8.1 \text{ bar}$$

The capillary calculations and the Fig. 3.9, show that the phase pressures are different at the same elevation in the reservoir, and that the capillary pressure is additive, i.e. [7]:

$$(P_c)_{gw} = (P_c)_{ow} + (P_c)_{go}, \tag{3.10}$$

At static (initial reservoir) conditions, the distribution of phases within a reservoir is governed by counteracting gravity and capillary forces. While gravity forces tend to separate

reservoir fluids accordingly to their densities, the capillary forces, acting within and between immiscible fluids and their confining solid substance, resist separation. The balance of these two forces result in an equilibrium distribution of phases within the reservoir prior to its development, as shown in Fig. 3.6

**Example: Water pressure in a vertical cylindrical tube**

The water pressure at a depth $D$ is found using Eq. 3.6, where $p_w(D_0)$ is the atmospheric pressure, $p_{atm.}$.

The water pressure at any depth is,

$$p = \frac{F}{A} \qquad \Rightarrow \qquad dp = d\left(\frac{F}{A}\right),$$

where $F/A$ is force due to water weight per cross-section area. We may therefore write the pressure change as,

$$dp = d\left(\frac{mg}{A}\right) = d\left(\frac{\rho_w g V_w}{A}\right) = d\left(\frac{\rho_w g A D}{A}\right) = \rho_w g\, dD$$

In the equation above, $\rho_w$ is the water density, $g$ is the gravitational constant and $D$ is the water depth.

Substituting the last results into Eq.3.6 we obtain the following general formula for water pressure at depth $D$,

$$p_w(D) = \int_0^D \rho_w g\, dD + p_{atm.}$$

**NB!** The pressure variation in a reservoir is determined by the fluid densities alone (when the gravitational coefficient is considered constant).

## 3.6 Exercises

1. Determine the porosity and lithology of a core sample, given the following data:

   Weight of dried core sample: 259.2 $g$
   Weight of 100% water-saturated core sample: 297 $g$
   (the density of water is 1.0 $g/cm^3$)
   Weight of core sample in water: 161.4 $g$

   Define the terms *absolute* and *effective* porosity and decide which term to use when characterising the core sample.

2. A laboratory cylindrical cup contains 500 $cm^3$ water and weighs 800 $g$. Carbonate sand (limestone, $CaCO_3$) is poured into the cup until the level of sand and water coincide. Calculate the bulk volume and porosity of this saturated porous medium knowing that the total weight of cup and its content (water and limestone) is 2734 $g$. How do you define the porosity ?

3. A glass cylinder has been filled with dolomite grains up to the 2500 $cm^3$ mark. The mass of dolomite is 4714 $g$. Calculate and characterise the sand's porosity.

4. Estimate numerically the change in carbonate-rock porosity caused by a complete dolomitization of calcite, accounting to the chemical reaction,

   $$2CaCO_3 + Mg^{2+} = CaMg(CO_3)_2 + Ca^{2+},$$

   will yield a carbonate rock's porosity of 13% .

5. Calculate the porosity of a sandstone core sample given the data from core analysis:

   Bulk volume of dried sample: 8.1 $cm^3$,
   Weight of dried sample: 17.3 $g$,
   Sand grain density: 2.67 $g/cm^3$.

6. Calculate the density of formation water when the pressure gradient is measured, $dp/dz$ = 10.2 $kPa/m$.

7. A reservoir water pressure of 213 *bar* is measured at a sub-sea depth of 2000 $m$. Evaluate the pressure situation in the reservoir and determind whether there is an over- /underburden pressure, when the water pressure gradient is 10.2 $kPa/m$.

8. Formation water salinity will influence hydrostatic pressure estimation. Given that uncertainty in salinity may lead to an uncertainty in water density of $\Delta\rho$ = 1.11 - 1.31 $g/cm^3$, determine the pressure change inside a reservoir where the depth from the *top* down to the FWL is 150 $m$.

(answ. 1. 28%, effective, 2.65 $g/cm^3$, sandstone, 2. 41%, absolute, 3. 34%, absolute, 4. 4%, 6. 20%, 7. 1.4 $g/cm^3$, 8. 8.1 bar, 9. 3 bar)

# Chapter 4

# Porosity

## 4.1 General Aspects

According to the definition, already presented, the porosity is the fluid-storage capacity of a porous medium, which means the part of the rock's total volume that is not occupied by solid particles. It should also be noted that porosity is a *static* parameter, defined *locally* as an average over the representative elementary volume of porous rock media considered.

Genetically, the following types of porosity can be distinguished :

- Intergranular porosity.
- Fracture porosity.
- Micro-porosity.
- Vugular porosity.
- Intragranular porosity.

Rock media having both fracture and intergranular pores are called double-porous or fracture-porous media.

From the point of view of pores susceptibility to mechanical changes one should distinguish between *consolidated* and *unconsolidated* porous media. A consolidated medium means a rock whose grains have been sufficiently compacted and are held together by cementing material. An important characteristic of consolidated porous media is the ability to restore elastically, to a great extent, to their shape (volume) after the removal of the overburden pressure.

Porosity is a statistical property dependent on the rock volume taken into consideration. If the volume selected is too small, the calculated porosity can deviate greatly from the "true" statistical average value [35]. Only a volume selected large enough (a representative volume) will result in a representative and correct statistical average (see Fig. 4.1).

## 4.2 Models of Porous Media

The geometric character of rock's permeable pore space is in reality quite complicated, and may vary greatly from one rock type to another. In practice, it is impossible to counter the

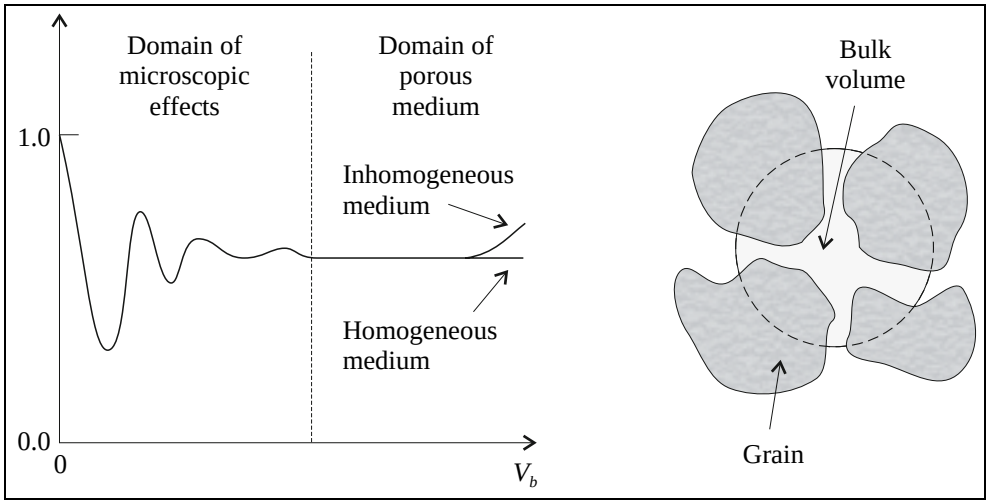


Figure 4.1: Definition of a representative elementary volume for porosity measurements [35].

pore-system geometry in a detailed and faithful way. Therefore, several idealised models have been developed to approximate porous rock media and their varied characteristics.

### 4.2.1 Idealised Porous Medium Represented by Parallel Cylindrical Pores

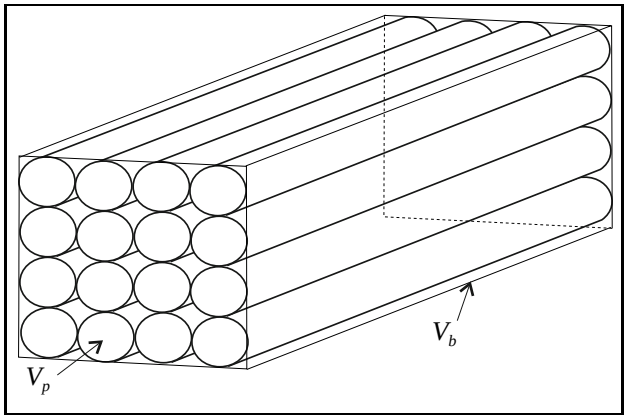


Figure 4.2: Idealised porous medium represented by a system of parallel cylindrical pores (pipes).

Estimation of porosity accounting to this model, see Fig. 4.2, is as follows:

$$\phi = \frac{V_p}{V_b} = \frac{\pi r^2 \cdot n \cdot m}{2rn \cdot 2rm} = \frac{\pi}{4} = 0.785, \text{ or } 78.5\%,$$

where $r$ is the pipe radius and $m \cdot n$ is the number of cylinders contained in the bulk volume.

It is rather obvious that rocks do not have pores like this and that this model gives a unrealistically high porosity value. This model may though, be used in some situations where fluid flow under simplified conditions is modelled.

### 4.2.2 Idealised Porous Medium Represented by Regular Cubic-Packed Spheres

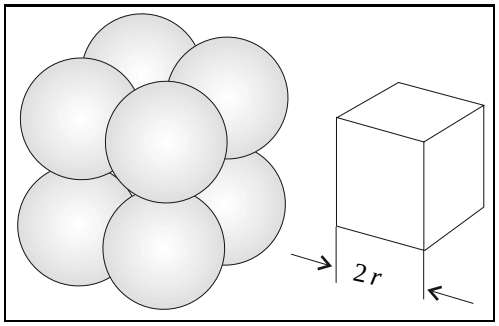


Figure 4.3: Idealised porous medium represented by a regular system of cubic-packed spheres.

The estimation of porosity according to this model, see Fig. 4.3, is as follows:

$$V_b = (2r)^3 \text{ and } V_m = \frac{1}{8}(\frac{4}{3}\pi r^3)\cdot 8 = \frac{4}{3}\pi r^3,$$

and

$$\phi = \frac{V_b - V_m}{V_b} = \frac{8r^3 - \frac{4}{3}\pi r^3}{8r^3} = 1 - \frac{\pi}{6} = 0.476 \text{ or } 47.6\%$$

where $V_m$ is the "matrix" volume or the volume of bulk space occupied by the rock.

### 4.2.3 Idealised Porous Medium Represented by Regular Orthorhombic-Packed spheres

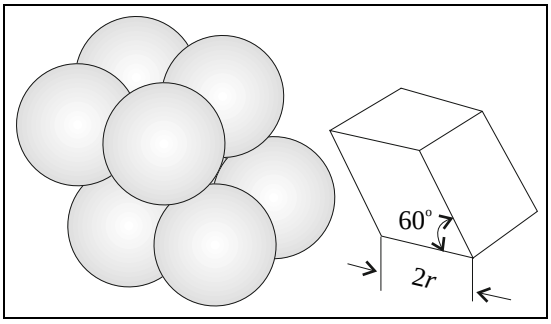


Figure 4.4: Idealised porous medium represented by a regular system of orthorhombic-packed spheres.

The estimation of porosity according to this model, see Fig. 4.4, is as follows:

$$V_b = 2r\cdot 2r\cdot h = 4r^2\cdot 2r\sin(60^o) = 4\sqrt{3}r^3 \text{ and } V_m = \frac{4}{3}\pi r^3,$$

where $h$ is the height of the orthorhombic-packed spheres. The matrix volume is unchanged and thus,

$$\phi = 1 - \frac{V_m}{V_b} = 1 - \frac{4\pi r^3}{12\sqrt{3}r^3} = 1 - \frac{\pi}{3\sqrt{3}} = 0.395 \text{ or } 39.5\%$$

### 4.2.4 Idealised Porous Medium Represented by Regular Rhombohedral-Packed spheres

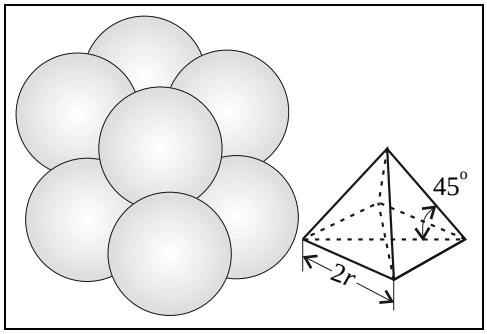


Figure 4.5: Idealised porous medium represented by regular system of rhombohedral-packed spheres.

The estimation of porosity according to this model, see Fig. 4.5 and it follows from Fig. 4.5 that,

$$h = \sqrt{4r^2 - 2r^2} = \sqrt{2}r,$$

where $h$ is the height in the tetrahedron and

$$V_b = 2r \cdot 2r \cdot \sqrt{2}r = 4\sqrt{2}r^3 \text{ and } V_m = \frac{4}{3}\pi r^3,$$

which gives

$$\phi = 1 - \frac{4\pi r^3}{12\sqrt{2}r^3} = 1 - \frac{\pi}{3\sqrt{2}} = 1 - 0.74 = 0.26 \text{ or } 26.0\%$$

### 4.2.5 Idealised Porous Medium Represented by Irregular-Packed Spheres with Different Radii

Real reservoir rock exhibits a complex structure and a substantial variation in grain sizes and their packing, which results in variation of porosity and other important reservoir properties, often associated with the hetrogeniety of porous medium.

Fig. 4.6 shows an example of an idealised porous medium represented by four populations of spheres (I - IV) sorted by different radii and the histogram showing the hypothetical grain -size distribution.

By drawing a graph with radii of the spheres plotted on the horizontal axis and heights equal to the corresponding frequencies of their appearance plotted on the vertical axis, one can obtain a histogram of distribution of particles (spheres) in sizes.

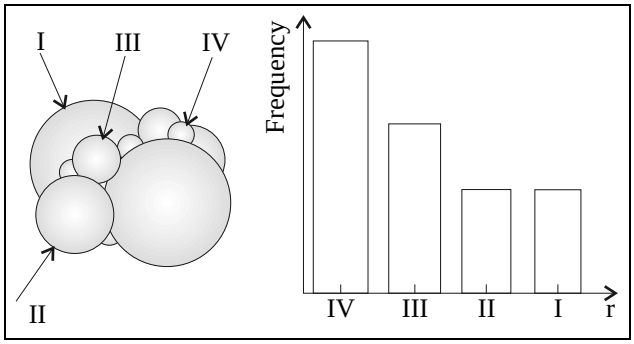


Figure 4.6: Idealised porous medium represented by an irregular system of spheres with different radii.

The different models, described above, may serve as a "mental image" or idealised concretization of a rather complex porous structure of porous rocks. The advantage of idealised models, in general and in particular in the case of porous media, is the opportunity they offer for simple quantification and representation of characteristic parameters. Since rock porosity has so many representations, it is important to maintain a representative image, though idealized, of the rock porosity, for further analysis and improved undersanding.

**Example: Porous medium of irregular system of spheres**

A porous medium is blended with three types of sediment fractions: fine pebble gravel with porosity ($\phi_{pebble} = 0.30$), sand ($\phi_{sand} = 0.38$) and fine sand ($\phi_{f.sand} = 0.33$).

The three sediments are mixed in such proportions that the sand fills the pore volume of the fine pebbles and that the fine sand fills the pore volume of the sand.

The volume of fine pebble gravel is equal to the bulk volume, i.e., $V_b = V_{pebble}$. Since the sand fills the pore volume of the pebble and the fine sand the pore volume of the sand, the following table is listed:

| | |
|---|---|
| Volume of sand: | $V_{sand} = \phi_{pebble} V_{pebble}.$ |
| Volume of fine sand: | $V_{f.sand} = \phi_{sand} V_{sand}.$ |
| Pore volume of fine sand: | $V_p = \phi_{f.sand} V_{f.sand}.$ |

The total porosity is then defined,

$$\begin{aligned} \phi = \frac{V_p}{V_b} &= \frac{\phi_{f.sand}\phi_{sand}\phi_{pebble}V_{pebble}}{V_{pebble}}, \\ &= 0.3 \cdot 0.38 \cdot 0.33 = 0.037. \end{aligned}$$

The porosity of the porous medium is $\sim 4\%$.

## 4.3 Porosity Distribution

The multiple sampling of porosity measurements for reservoir rocks at different depths and in different wells gives a data set that can then be plotted as a histogram, to reveal the porosity's frequency distribution. See Fig. 4.7. The distribution may appear to be unimodal (left) or polymodal (right). Such histograms may be constructed separately for the individual zones, or units, distinguished within the reservoir, and thus give a good basis for statistical estimates (mean porosity values, standard deviations, etc.).

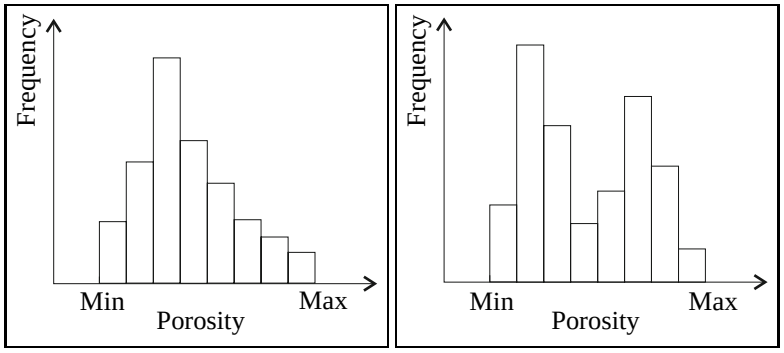


Figure 4.7: Unimodal and polymodal porosity distributions.

Numerical simulation of fluid flow in porous media, related to laboratory tests on core samples as well as full field production estimation, require a realistic picture of the rock porosity and its variation throughout the reservoir. This picture is not easily obtainable since porosity is measured locally (in the well) and porosity extrapolations introduce large uncertainty in the estimated average values.

The grouping of porosity data according to the reservoir zones, depth profile or graphical co-ordination, may reveal spatial trends in the porosity variation , see Fig. 4.8. The recognition of such trends is very important for the development of a bulk picture of the reservoir as a porous medium and representation of the reservoir porosity in mathematical simulation models (reservoir characterisation, lateral correlation, numerical modelling, etc.)

Mechanical diagenesis (compaction) and chemical diagenesis (cementation) have a profound effect on a sedimentary rock's porosity. This burial effect is illustrated by the two typical examples of sand and clay deposits in Fig. 4.9.

## 4.4 Measurement of Porosity

### 4.4.1 Full-Diameter Core Analysis

A full-diameter core analysis is used to measure the porosity of rocks that are distinctly heterogeneous, such as some carbonates, and fissured, vugular rocks, for which a standard core-plug analyse is unsuitable. The same core-plug is a non-representative elementary volume for this type of rock. The porosity measurement in such rocks requires samples that are as large as can be obtained (portions of full-diameter drilling cores). In heterogeneous rocks, the local porosity may be highly variable, as it may include micro-porosity, intergranular porosity, vugues,

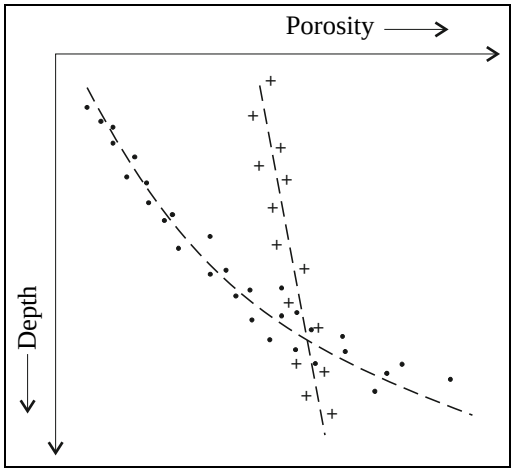


Figure 4.8: Examples of trends of porosity distribution in the depth profiles of two reservoir sandstone.

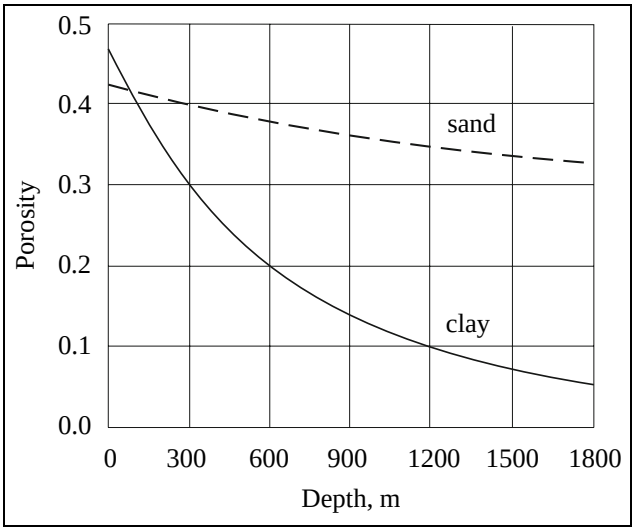


Figure 4.9: Sediment compaction burial and porosity change.

fractures, or various combinations of these. A full-diameter core sample usually has a diameter of 5 inches (12.5 cm) and the length of 10 inches (25 cm).

The full-diameter core technique does not differentiate between the actual types of porosity involved, but yields a singe porosity value that represents their effective combination. Several laboratory techniques used for porosity measurements, and the procedure is generally similar for full-diameter cores and core "plugs".

### 4.4.2 Grain-Volume Measurements Based on Boyle's Law

This gas transfer technique involves the injection and decompression of gas into the pores of a fluid-free (vacuum), dry core sample, see Fig. 4.10. Either the pore volume or the grain volume can be determined, depending upon the instrumentation and procedures used.

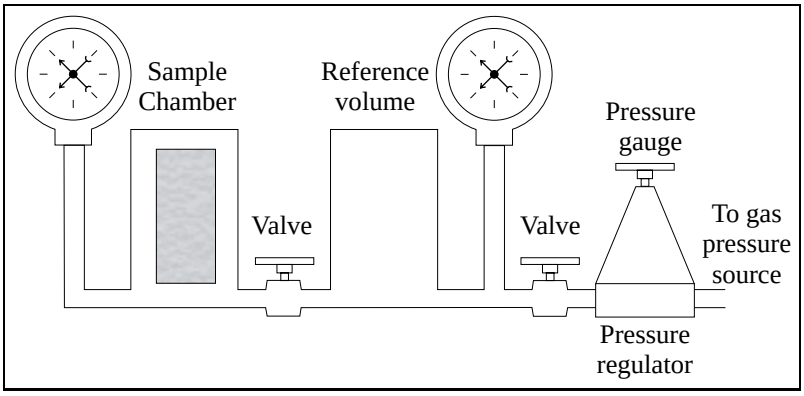


Figure 4.10: Porosity measurements based on the Boyle's law.

To perform the laboratory measurement, Helium gas is often used due to its following properties,

- the very small size of helium molecules makes the gas rapidly penetrate small pores,
- helium is an inert gas that and will not be absorbed on the rock surfaces and thus yield erroneous results.

Other gases, such as $N_2$ and $CO_2$, might be good alternatives to Helium. The advantage of $CO_2$ is it's hydrophilic ability, which increase the effect of dehydrating the core sample. $N_2$ is also used, simply due to its availability.

**The Calculation of the Grain Volume**

Using the ideal gas law,

$$pV = nRT$$

where the temperature, $T$= const, one obtains $p_1V_1 = p_2V_2$, and in the case of vacuum inside the sample chamber (Fig. 4.10,

$$p_1V_{ref} = p_2(V_{ref} + V_s - V_g),$$

where $V_{ref}$, $V_s$ and $V_g$ are the reference volume, the volume of the sample chamber and the grain volume, respectively. See Fig. 4.10.

Assuming adiabatic conditions, one obtains,

$$V_g = \frac{p_2V_{ref} + p_2V_s - p_1V_{ref}}{p_2}, \tag{4.1}$$

where $p_1$ denotes initial pressure in the reference cell, and $p_2$ the final pressure in the system. Successive measurements will increase the accuracy, due to effects of dehydration of the porous core sample.

### 4.4.3 Bulk-Volume Measurements

This technique utilizes the Archimedes' principle of mass displacement:

1. The core sample is first saturated with a wetting fluid and then weighed.
2. The the sample is then submerged in the same fluid and its submerged weight is measured.

The bulk volume is the difference between the two weights divided by the density of the fluid.

Fluids that are normally used are,

- water which can easily be evaporated afterwards,
- mercury which normally not enters the pore space in a core sample due to its non-wetting capability and its large interfacial energy against air.

The laboratory measurements, using this technique, are very accurate, where uncertainties in the order of $\pm$ 0.2%, is normally obtained.

**Example: Uncertainty analysis in measuring the bulk volume using Archimedes' principle.**

The bulk volume of a porous core sample can be measured in two steps, first by weighing the sample in a cup of water; $m_1$ (assuming 100% water saturation) and then weighing the sample in air as it is removed from the cup; $m_2$.

The bulk volume is then written,

$$V_b = \frac{m_2 - m_1}{\rho_w}.$$

Differentiating the equation above gives us,

$$dV_b = \frac{\partial V_b}{\partial m_2} dm_2 + \frac{\partial V_b}{\partial m_1} dm_1 + \frac{\partial V_b}{\partial \rho_w} d\rho_w,$$

$$dV_b = \frac{m_2 - m_1}{\rho_w} \left[ \frac{dm_2}{m_2 - m_1} - \frac{dm_1}{m_2 - m_1} - \frac{d\rho_w}{\rho_w} \right].$$

If the density measurement as well as the two mass-measurements above, is considered to be independent measurements, the relative uncertainty in the bulk volume is written,

$$\left( \frac{\Delta V_b}{V_b} \right)^2 = 2 \left( \frac{\Delta m}{(m_2 - m_1)} \right)^2 + \left( \frac{\Delta \rho_w}{\rho_w} \right)^2,$$

where the uncertainty introduced in the process of weighing the two masses is considered to be identical, i.e., $\Delta m = \Delta m_1 = \Delta m_2$.

The uncertainty equation above may also be written,

$$\left(\frac{\Delta V_b}{V_b}\right)^2 = 2\left(\frac{\Delta m}{\rho_w V_b}\right)^2 + \left(\frac{\Delta \rho_w}{\rho_w}\right)^2.$$

If the relative uncertainty in determined the water density is estimated to 0.1% and the weighing accuracy is equal to 0.1 $g$, we find a relative uncertainty in the bulk volume of approximately 0.5%. The bulk volume of the core sample is approximately 30 $cm^3$ and water density is assumed equal to 1 $g/cm^3$.

(Note that the uncertainty related to the assumption of 100% water saturation prior to the first mass measurement, in some experimental tests could be larger than the effective uncertainty related to the measuring technique.)

### 4.4.4 Pore-Volume Measurement

Pore volume measurements can be done by using the Boyle's law, where the sample is placed in a rubber sleeve holder that has no voids space around the periphery of the core and on the ends. Such a holder is called the Hassler holder, or a hydrostatic load cell, see Fig. 4.11.

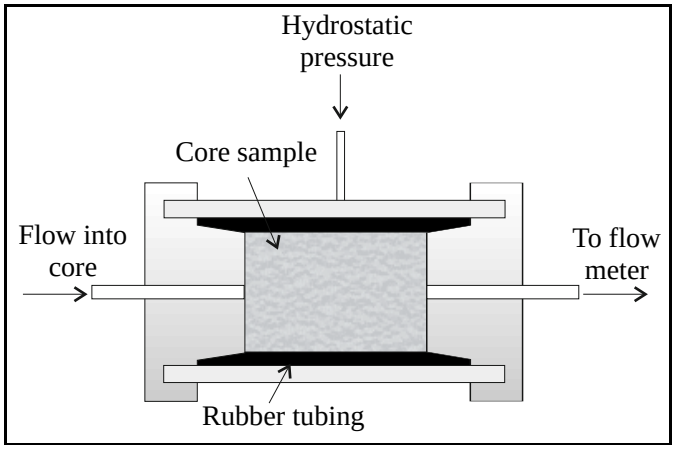


Figure 4.11: Hydrostatic load cell (Hassler holder) used for a direct measurement of pore volume.

Helium or one of its substitutes is injected into the core plug through the end stem. The calculation of the pore volume $V_p$ is as follows:

$$p_0 V_p + p_1 V_{ref} = nRT \quad (4.2)$$

$$p_2(V_p + V_{ref}) = nRT \quad (4.3)$$

and

$$V_p = \frac{(p_1 - p_2)}{(p_2 - p_0)} V_{ref} \text{ where } (p_1 > p_2 > p_0)$$

It is important to notice that the Hassler core holder has to be coupled to a volume of known reference $V_{ref}$, as seen in Fig. 4.10, when the pore volume $V_p$, is measured.

### 4.4.5 Fluid-Summation Method

This technique is to measure the volume of gas, oil and water present in the pore space of a fresh or preserved (peel-sealed) core of known bulk volume. If the core has been exposed to the open air for some time, some of the oil and water can evaporate and the saturation will be measured inaccurately.

The volumes of the extracted oil, gas and water are added to obtain the pore volume and hence the core porosity.

The core sample is divided into two parts. One part (ca. 100 g) is crushed and placed in a fluid-extraction retort (see figure in previous chapter), where the metal-holder unit has a cap to prevent the evaporation of gases at the top.

The vaporised water and oil originally contained in the pores, move down and are subsequently condensed and collected in a calibrated glassware, where their volumes are measured.

The second part of the rock sample (ca. 30 g) with a roughly cylindrical shape, is weighed and then placed in a pump chamber filled with mercury (a pycnometer) in which its bulk volume is determined, measuring the volume of the displaced mercury. Then the pressure of the mercury, $p_{Hg}$, is raised to 70 bar (1000 psi). At this pressure, the mercury enters the sample and compresses the gas, filling the pore space originally occupied with the gas. With an appropriate calculation, the volume of the mercury "imbibed" in the rock gives the gas volume $V_g$.

The bulk volume and weight of the fresh sample allow the computation of the effective bulk density of the rock. This in turn is used to convert the weight of the first part of the sample, which was 100 g (to be retorted), into an equivalent bulk volume.

The oil, water and gas volumes are each calculated as fractions of the bulk volume of the rock sample and the three values are added to yield the porosity value .

The laboratory procedure provides the following information:

- First subsample gives the rock's weight $W_{s1}$ and the volumes of oil $V_{o1}$ and water $V_{w1}$ are recorded.
- Second subsample gives the volume of gas $V_{g2}$ and the rock's bulk volume $V_{b2}$.

From the second subsample, the fraction of the bulk volume occupied by gas (i.e., the fraction of the gas-bulk volume) can be calculated,

$$f_g = \frac{V_{g_2}}{V_{b_2}} = \phi S_g$$

where the subscript 2 is omitted for $f_g$, $S_g$, and $\phi$, because these values are representative for both parts of the sample.

Denoting the apparent bulk density of the fluid-saturated rock sample as $\rho_{app}$, we can write,

$$W_{s_1} = V_{b_1} \cdot \rho_{app} \text{ and } W_{s_2} = V_{b_2} \cdot \rho_{app} \quad \rightarrow V_{b_1} = V_{b_2} \frac{W_{s_1}}{W_{s_2}}$$

The formation oil- and water-volume factor are calculated as follow,

$$f_o = \frac{V_{o_1}}{V_{b_1}} = \phi S_o,$$

$$f_w = \frac{V_{w_1}}{V_{b_1}} = \phi S_w,$$

and the sum of the fluid-volume factor then gives the porosity value:

$$f_o + f_w + f_g = \phi(S_o + S_w + S_g) = \phi$$

**Example: Use of pycnometer in matrix volume calculation.**

The pycnometer is a lab-tool occasionally used for measuring bulk- and pore volumes of core samples. A pycnometer is in principle a contained volume, a cell, where a defined amount of mercury can be injected or withdrawn. The sketch below illustrates the working principle of the pycnometer.

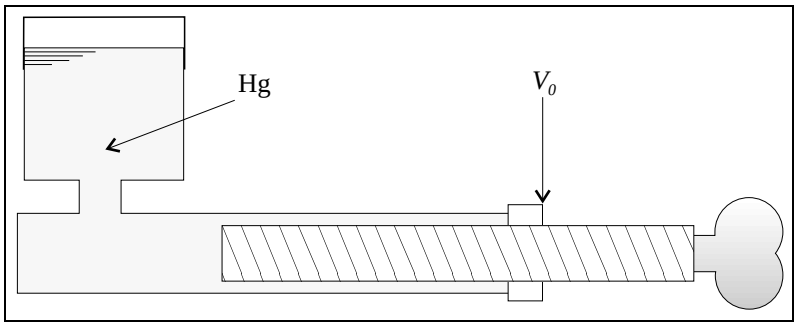


Figure 4.12: Sketch of the pycnometer.

In order to define the matrix volume, $V_m$ of a core sample, the following measuring steps are carried out:

1. The pycnometer cell is fully saturated with mercury.
2. The pycnometer piston is withdrawn and a gas (air) volume of $V_0$ is measured.
3. The core sample is placed in the cell, and the cell volume is sealed. The equilibrium condition inside the cell is written; $p_0(V_0 - V_m)$, where $p_0$ is the atmospheric pressure and $V_m$ is the matrix of the sample (the rock's grain volume).
4. Mercury is injected into the cell and a new gas volume, $V_1$ and gas pressure, $p_1$ is measured. NB: The mercury does not enter the pore system of the core sample, due to its high interfacial tension. (Mercury, as laboratory fluid, has become less popular due to its toxic characteristics and is quite often replaced by other fluids.)
5. New equilibrium is reached and we write; $p_1(V_1 - V_m)$.

Finally, the matrix volume is found as follows:

$$V_m = \frac{p_1 V_1 - p_0 V_0}{p_1 - p_0}.$$

_____ . _____

## 4.5 Uncertainty in Porosity Estimation

Experimental data is always contaminated with measuring uncertainty. For characteristic parameter estimation, like determination of the porosity, we will expect the uncertainty in the measured parameters to introduce an error in the estimate of the porosity found.

Porosity will normally be a function of $V_p$, $V_m$ and/or $V_b$. Since the three parameters are dependent, i.e.

$$V_b = V_p + V_m, \tag{4.4}$$

only two of them should appear in the uncertainty analysis.

If we define porosity as,

$$\phi = \frac{V_p}{V_b},$$

we may differentiate the equation and we obtain,

$$\frac{d\phi}{\phi} = \frac{dV_p}{V_p} - \frac{dV_b}{V_b}.$$

The pore- and bulk volumes are independent measurements, i.e., the results $V_p$ and $V_b$ are independent parameters and so are their uncertainties, $\Delta V_p$ and $\Delta V_m$.

The relative error or uncertainty in the porosity is then given by

$$\frac{\Delta\phi}{\phi} = \sqrt{\left(\frac{\Delta V_p}{V_p}\right)^2 + \left(\frac{\Delta V_b}{V_b}\right)^2}. \tag{4.5}$$

In laboratory experiments we wish to reduce uncertainties to a minimum. Eq. (4.5) tells us that it is not sufficient to reduce the uncertainty in only one of the measured parameters, leaving the other unchanged, since the total relative uncertainty is mainly influenced by the largest relative uncertainty.

**Example: Error propagation**

From laboratory measurements one has estimated the relative uncertainty related to the pore volume to be, $\triangle V_p/V_p$ = 5.0% and the relative uncertainty related to the matrix is, $\triangle V_m/V_m$ = 7%.

The porosity is defined,

$$\phi = \frac{V_p}{V_b} = \frac{V_p}{V_p + V_m}.$$

We could start to differentiate the porosity with respect to $V_p$ and $V_m$, given the equation above, but instead we intend to differentiate Eq. (4.4) and then substitute the results into Eq. (4.5).

Differentiation of Eq. (4.4) gives,

$$\left(\frac{\triangle V_b}{V_b}\right)^2 = \left(\frac{\triangle V_p}{V_p + V_m}\right)^2 + \left(\frac{\triangle V_m}{V_p + V_m}\right)^2,$$

and substitution in Eq. (4.5) gives,

$$\frac{\triangle\phi}{\phi} = \sqrt{\left(\frac{\triangle V_p}{V_p}\right)^2 + \left(\frac{\triangle V_p}{V_p+V_m}\right)^2 + \left(\frac{\triangle V_m}{V_p+V_m}\right)^2},$$

or written differently,

$$\frac{\triangle\phi}{\phi} = \sqrt{\left((1+\phi^2)\frac{\triangle V_p}{V_p}\right)^2 + \left((1-\phi)^2\frac{\triangle V_m}{V_m}\right)^2}.$$

If the porosity is, $\phi$ = 0.2 (or 20%), then the relative uncertainty in the porosity is $\sim$ 7.57% and the porosity with uncertainty is written,

$$\phi \pm \triangle\phi = (20 \pm 1.5)\%.$$

Note that if the equation $\phi = V_p/(V_p+V_m)$ is differentiated directly, the result would be slightly different because the differentiation was used only once, compared to the process above where a two step differentiation is performed. Every extra operation in the error propagation increases the final uncertainty.

## 4.6 Porosity Estimation from Well Logs

Porosity of reservoir rock can be estimated not only by using methods, as has been described above, but also from geophysical well logs, often called wireline logs. This method of porosity evaluation is not very accurate, but has the advantage of providing continous porosity data. Once these logs are obtained and converted into a porosity log, they can be calibrated using core-sample porisity data and serve as additional reliable source of porosity distribution evaluation.

Porosity can be estimated from:

- Formation resistivity factor (F).
- Microresistivity log (from which F can be derived).
- Neutron - gamma log.
- Density (gamma - gamma) log.
- Acoustic (sonic) log.

The *Formation resistivity factor* is defined as the ratio of the resistivity of the porous sample saturated with an ionic solution $R_o$ of the bulk resistivity of the same solution $R_w$, i.e. [23]

$$F = \frac{R_o}{R_w}. \tag{4.6}$$

The Formation resistivity factor measures the influence of pore structure on the resistance of the core sample. There are several relationships which can be used for the porosity evaluation using F-values [23],

- $F = \phi^{-m}$, where $m$ is the cementation constant (Archie, 1942).
- $F = (3 - \phi)/2\phi$ (Maxwell, 1881).
- $F = X/\phi$, where $X$ is the electric tortuosity of the sample (Wyllie, 1957).

For more information regarding porosity evaluation using geophysical well logs, see reference [7, 23, 37].

## 4.7 Exercises

1. Calculate the bulk volume of a preserved (paraffin-coated) core sample immersed in water, given the following data:

   weight of dry sample in air: 20 g,
   weight of dry sample coated with paraffin: 20.9 g (density of paraffin is : 0.9 g/cc),
   weight of coated sample immersed in water: 10 g (density of water is: 1g/cc)

   Determine the rock's porosity, assuming a sand-grain density of 2.67 g/cc.

2. Calculate the bulk volume of a dry core sample immersed in mercury pycnometer, given the following data:

   weight of dry sample in air: 20 g,
   weight of mercury-filled pycnometer at $20\,^oC$: 350 g,
   weight of mercury-filled pycnometer with the sample at $20\,^o$C; 235.9 g.
   density of mercury: 13.546 g/cc.

3. Determine the sandstone's grain density and porosity, given the following data:

   weight of crushed dry sample in air: 16 g,
   weight of crushed sample plus absorbed water: 16.1 g,
   weight of water-filled pycnometer: 65 g,
   weight of water-filled pycnometer with the sample: 75 g.

4. Determine the sandstone's grain volume and porosity using Boyl's law, given the following data:

   volume of chamber containing the core sample: 15 cc,
   volume of chamber containing air: 7 cc,
   bulk volume of core sample: 10 cc

5. Calculate the effective porosity of a sandstone sample using the following data:

   weight of dry sample in air: 20 g,
   weight of saturated sample in air: 22.5 g,
   density of water is : 1.0 g/cc),
   weight of saturated sample in water: 12.6 g.

6. A core sample is saturated with an oil ($\rho_o = 35^oAPI$), gas and water. The initial weight of the sample is 224.14 g. After the gas is displaced by water ($\rho_w = 1 g/cm^3$), the weight is increased to 225.90 g. The sample is the placed in a *Soxhlet* distillation apparatus, and 4.4 $cm^3$ water is extracted. After drying the core sample, the weight is now 209.75 g. The sample bulk volume, 95 $cm^3$ is measured in a mercury pycnometer.

   Find the porosity, water saturation, oil saturation, gas saturation and lithology of the core sample. (Notice that the oil density is $\rho[g/cm^3] = 141.4/(131.5 + \rho[^oAPI])$, when the water density at that particular temperature and pressure is 1 $g/cm^3$)

7. Another core sample is brought to the laboratory for compositional analysis, where 80 g of the sample is placed in a mercury pycnometer and the volume of gas found is 0.53 $cm^3$. A piece of the same sample, weighing 120 g is placed in a retorte, where the water and oil volume is measured to 2.8 $cm^3$ and 4.4 $m^3$, respectively. A third piece of the

sample, weighing 90 g is placed in a pycnometer and the bulk volume is measured to be 37.4 $cm^3$. Assume oil and water densities as in the exercise above and find the same characteristic parameters.

8. Calculate the porosity of the sample described below:

   mass of dry sample: 104.2 $g$,
   mass of water saturated sample: 120.2 $g$,
   density of water 1.001 $g/cm^3$,
   mas of saturated sample immersed in water: 64.7 $g$.

   Is this effective porosity or the total porosity of the sample? What is the most probable lithology of the matrix material? Explain .

9. A core, 2.54 $cm$ long and 2.54 $cm$ in diameter has a porosity of 22%. It is saturated with oil and water, where the oil content is 1.5 $cm^3$.

   a) What is the pore volume of the core?
   b) What are the oil and water saturations of the core?

10. If a formation is 2.5 $m$ thick, what is the volume of oil-in-place (in $m^3$ and in $bbl$) of a 40.47 hectare large area, if the core described in the excercise above is representative of the reservoir?

**Answer to questions:**

1. 24.3%, 2. 9.95 $cm^3$, 3. 2.67 $g/cm^3$, 1.6%, 4. 20%, 5. 25%, 6. 19%, 14.5%, 75.8%, 9.6%, 2.73 $g/cm^3$, 7. 16%, 35.1%, 55.1%,10%, 2.69 $g/cm^3$, 8. 29%, 2.64 $g/cm^3$, 9. 2.831 $cm^3$, 53%, 47%, 10. 738235.6 $bbl$

# Chapter 5

# Permeability

## 5.1 Introduction

Permeability in a reservoir rock is associated with it's capacity to transport fluids through a system of interconnected pores, i.e. communication of interstices. In general terms, the permeability is a *tensor*, since the resistance towards fluid flow will vary, depending on the flow direction. In practical terms, however, permeability is often considered to be a *scalar*, even though this is only correct for isotropic porous media.

If there were no interconnected pores, the rock would be impermeable, i.e., it is natural to assume that there exists certain correlations between permeability and effective porosity. All factors affecting porosity will affect permeability and since rock permeability is difficult to measure in the reservoir, porosity correlated permeabilities are often used in extrapolating reservoir permeability between wells.

*Absolute* permeability could be determined in the laboratory by using inert gas (nitrogen is frequently used) that fills the porous rock sample completely and limits the possibility of chemical interaction with the rock material to a minimum. Since the gas molecules will penetrate even the smallest pore-throats, all pore channels are included in the averaging process when permeability is measured.

When several phases or mixtures of fluids are passing through a rock locally and simultaneously, each fluid phase will counteract the free flow of the other phase's and a reduced phase permeability (relative to absolute) is measured, i.e. *effective* permeability.

## 5.2 Darcy's Law

The first important experiments of fluid flow through porous media, were reported by Dupuit in 1854, using water-filters. His results showed that the pressure drop across the filter is proportional to the water filtration velocity. In 1856 Henry Darcy proved that flow of water through sand filters, obeys the following relationship:

$$q = K \cdot A \frac{h}{\Delta l}, \tag{5.1}$$

where $h$ is a difference in manometer levels, i.e. hydrostatic height difference,
$A$ is cross-sectional area of the filter,
$\Delta l$ is thickness of the filter in the flow direction and
$K$ is a proportionality coefficient.

In Darcy's experimental results, as in Eq. (5.1), viscosity $\mu$, was not included because only water filters were investigated and hence, the effects of fluid density and viscosity had no real experimental significance.

Experiments repeated after Darcy, have proved that if the manometric level, $h$, is kept constant, the same flow rate (or flow velocity) is measured, irrespective of the orientation of the sand filter (see Fig. 5.1).

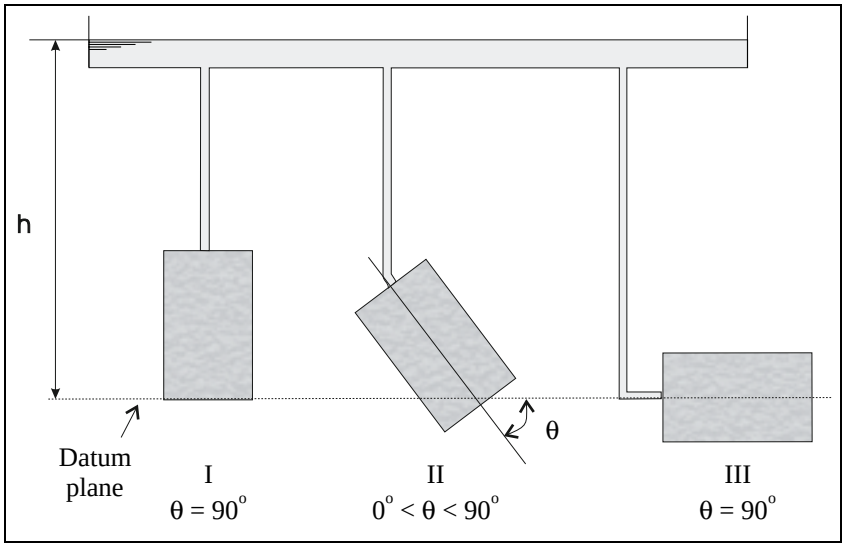


Figure 5.1: Orientation of the sand filter with respect to the direction of gravitation.

The pressure difference across the sand filter in Fig. 5.1, for the 3 cases are given,

$$\begin{aligned} \text{I}: &\quad \Delta p_I = \rho g(h - \Delta l), \\ \text{II}: &\quad \Delta p_{II} = \rho g(h - \Delta l \cdot \sin\theta), \\ \text{III}: &\quad \Delta p_{III} = \rho g h, \end{aligned}$$

where $\Delta l$ is the thickness or length of the sand filter in the flow direction.

Since the water velocity is proportional to the manometric level (observation made by Darcy), the flow velocity is proportional to,

$$v \propto (\Delta p + \rho g \Delta z),$$

where $\Delta z$ is the elevation in the gravitational field. ($\Delta z$ accounts for the inclined flow direction relative to horizontal flow.)

If the sand filter is made longer, a reduced flow velocity is expected and similarly if the water is replaced by a fluid of higher viscosity, a reduced flow velocity is expected.

$$v \propto \frac{1}{\mu}\frac{\Delta p + \rho g \Delta z}{\Delta l}.$$

The proportionality, above, can be replaced by equality, by introducing a proportionality coefficient $k$,

$$v = \frac{k}{\mu}\frac{\Delta p + \rho g \Delta z}{\Delta l}, \tag{5.2}$$

where $k$ is the permeability.

The pressure at any point along the flow path is related to a reference height or datum plane $z_0$, where $\Delta z = z - z_0$ and e.g. $z_0 = 0$ at a level where the reference pressure is 1 atm. A pressure difference $\Delta(p+\rho gz) = (p+\rho gz)_2 - (p+\rho gz)_1$ will create a fluid flow between the two points, unless the pressure $p$ is equal to the static pressure $-\rho gh$. In these cases no flow is expected and static equilibrium is established, as observed in any reservoir where the fluid pressure increases with depth.

Fluid flow in a porous rock is therefore given by the pressure *potential* difference $\Delta(p+\rho gz)$, i.e. the sum of pressure difference and elevation in the gravity field. In a historical context, the pressure potential has been associated with the energy potential (energy pr. mass) and the following definition has been used,

$$\Phi \stackrel{\text{def}}{=} \frac{p}{\rho} + gz.$$

Substituting the pressure potential difference $\Delta\Phi$ in Eq. (5.2), one can rewrite the equality equation based on Darcy's deduction,

$$q = A\frac{k}{\mu}\rho\frac{\Delta\Phi}{\Delta l}$$

where $k$ is the permeability of the porous medium (filter, core sample/plug, etc.), $\mu$ is the viscosity of the fluid and $l$ is the length of the porous medium in the direction of flow and $\Phi$ is the pressure potential. The flow rate $q = dV/dt$, is volume pr. time.

The Darcy's law in differential form is,

$$q = A\frac{k}{\mu}\rho\frac{d\Phi}{dl} = \lim_{\Delta l \to 0}\left(A\frac{k}{\mu}\rho\frac{\Delta\Phi}{\Delta l}\right). \tag{5.3}$$

For linear and horizontal flow (parallel to the x-axis) of incompressible fluid, the elevation is constant, i.e. $dz/dx = 0$, and Dracy's law is written,

$$q = -A\frac{k}{\mu}\frac{dp}{dx}, \tag{5.4}$$

where the minus sign "-", in front of the pressure gradient term, compensates for a negative pressure gradient in the direction of flow (since fluids move from high to low potential). Velocity and flow rate are pr. definition positive parameters (see the example below).

At this point it is important to notice that the permeability, $k$, is introduced in Eqs. (5.4) and (5.3), as a *proportionality constant* and not as a physical parameter. The permeability does pr. definition, not carry any characteristic information about the porous medium. When

permeability is related to the transport capability of the porous medium, as often is the case in practical situations, the fact that this information about the porous medium is missing in Eq. (5.4), is often overlooked. The proportionality constant $k$, called permeability, describes not only the porous medium transport capability, as such, but represents all information about the porous medium etc., which is otherwise not described by any of the other parameters in Eq. (5.4).

**Example: Linear horizontal core flow**

The minus sign "-" in the horizontal flow equation Eq. 5.4 is justified by considering linear core flow.

Let's assume a constant liquid flow rate $q$, through a core sample, as shown in Fig. 5.2. The pressures $p_1$, $p_2$ and the positions $x_1$, $x_2$ are labelled according to standard numbering and orientation.

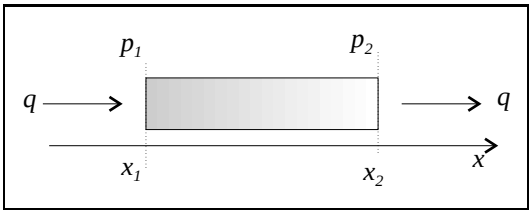


Figure 5.2: Horizontal flow in a core sample.

Assuming a homogeneous porous medium and integration from position 1 to 2, the pressure term is written as follows,

$$\frac{dp}{dx} = \frac{p_2 - p_1}{x_2 - x_1} = -\frac{p_1 - p_2}{x_2 - x_1},$$

where $p_1 > p_2$ in positive flow direction. Since $x_2$ obviously is larger than $x_1$, the value of $dp/dx$ is pr. definition negative, i.e. the minus sign "-" is needed to balance the equation.

———— · ————

The fluid velocity related to the cross-section area $A$ is called the *superficial* (i.e. filtration) or *bulk* velocity, and the linear flow velocity is written,

$$u = \frac{q}{A} = -\frac{k}{\mu}\frac{dp}{dx}. \tag{5.5}$$

The real velocity of fluid flow in the pores is called the *interstitial* (true) velocity, $v_{pore}$ and is necessarily higher than the bulk velocity, since the flow cross-section area is, on average, $\phi$ times smaller than the bulk cross-section $A$. The directions of pore flow are inclined relative to the general flow direction and a characteristic inclination angle $\alpha$ is assigned to describe this effect. This effect will increase the pore velocity even more, as illustrated in Fig. 5.3. If, in addition, the porous medium contains a residual saturation of a non-flowing phase, e.g. a connate water saturation $S_{wc}$, the pore flow velocity is affected through the reduction of the

flow cross-section area. The sum of these effects will cause the pore flow velocity to become considerably higher than the bulk velocity,

$$v_{pore} = \frac{q}{A}\frac{1}{\phi}\frac{1}{1-S_{wc}}\frac{1}{cos^2\alpha}. \tag{5.6}$$

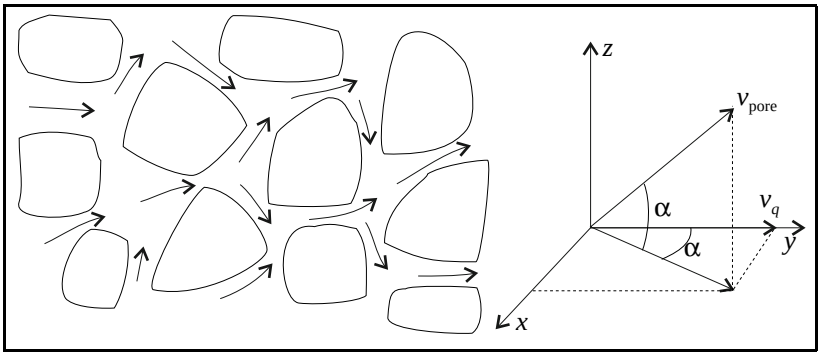


Figure 5.3: Pore flow velocity in a porous medium.

Experimental tests from different porous rocks have shown that an average inclination angle, $\overline{\alpha} \simeq 36^o$ and that this angle may vary between $12^o$ to $45^o$. If a typical porosity of 25% and a connate water saturation of 10% are assumed, then the pore velocity will be about 7 times higher than the bulk velocity.

**Example: Linear inclined core flow**

When the direction of flow is inclined, with an angle $\theta$ to the horizontal flow direction, the gravitational force has to be considered, since the fluids are moving up or down in the gravitational field.

In order to keep a constant flow rate $q$, through a porous medium of length $\Delta l$, a pressure difference $\Delta p$ is applied. See Fig. 5.4.

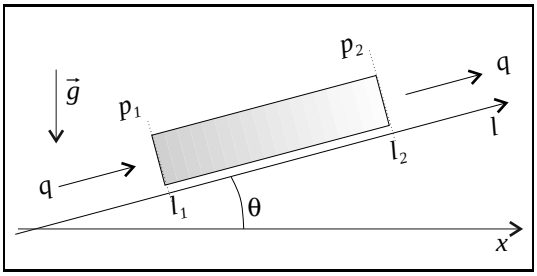


Figure 5.4: Core flow at a dip angle $\theta$ to the horizontal axis

Flow at an angle to the horizontal direction is described by Eq. (5.3), where the minus sign is describing linear flow,

$$q = -A\frac{k}{\mu}\frac{d(p+\rho gz)}{dl}.$$

$z$ is the elevation in the gravitational field and from Fig.5.4 it's evident that $z = l\sin\theta$, where $l$ is the direction of flow. The flow equation becomes,

$$q = -A\frac{k}{\mu}\frac{dp}{dl} - A\frac{k}{\mu}\rho g\sin\theta.$$

Integration from position 1 to 2, gives

$$\left(q + A\frac{k}{\mu}\rho g\sin\theta\right)\Delta l = A\frac{k}{\mu}\Delta p.$$

The pressure difference is given,

$$\Delta p = \frac{\mu\Delta l}{Ak}q + \rho g\Delta l\sin\theta,$$

where horizontal linear flow is $\Delta p_{\theta=0} = q(\mu\Delta l)/(Ak)$.

In order to maintain a constant flow rate through the core sample, the pressure difference needs to be adjusted relative to the inclination angle (dip angle). In a up-dip situation, as in Fig. 5.4, the pressure difference has to be larger relative to the horizontal case, since the fluid is pushed upwards in the gravitational fields, i.e.,

$$\begin{aligned} 0 \le \theta < 90^o \quad &\Rightarrow \quad \Delta p \ge \Delta p_0 \\ -90^o < \theta < 0 \quad &\Rightarrow \quad \Delta p < \Delta p_0 \end{aligned}$$

## 5.3 Conditions for Liquid Permeability Measurements.

Permeability in core samples is measured in the laboratory using Darcy's law for horizontal flow, Eq. (5.4). In these tests, some important conditions have to be satisfied before permeability could be estimated from the measured data. These conditions are the following:

- Horizontal flow.
- Incompressible fluid.
- 100% fluid saturation in the porous medium.
- Stationary flow current, i.e. constant cross-section in flow direction.
- Laminar flow current (satisfied in most liquid flow cases).
- No chemical exchange or - reactions between fluid and porous medium.

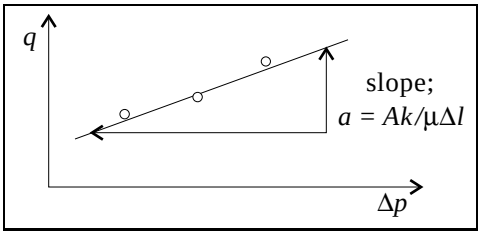


Figure 5.5: Experimental determination of liquid permeability.

Having satisfied all the above conditions, permeability is found by integrating the linear flow equation where the permeability is experimentally determined using the formula,

$$q = \frac{Ak}{\mu \Delta l} \Delta p, \tag{5.7}$$

where the flow rate $q$ and the pressure difference $\Delta p$ are the measured data. Permeability is found by plotting the measured data as shown in Fig. 5.5.

The linear best fit through all experimental data-points will give a slope, from which the permeability can be calculated using Eq. (5.7) [54].

The importance of linear representation of the measured data is the advantage of visual inspection, which may reveal non-linear effects in the data, e.g. at high or low flow rates, or uncertainty in laboratory measurements, e.g. large spread in data around the linear fit.

## 5.4 Units of Permeability

Dimensional analysis applied to the Darcy's law, shows that permeability has the dimension of surface area, $L^2$. It is not convenient to measure permeability of porous media in $cm^2$ or in $m^2$. By convention the unit for the permeability is called the *Darcy*. The following definition of the Darcy has been accepted:

> The permeability is 1 Darcy if a fluid with viscosity of 1 $cp$ is flowing at a rate of 1 $cm^3/s$ through a porous medium with a cross-section of 1 $cm^2$, creating a pressure difference of 1 $atm/cm$.

Applying *Darcy-units* to Eq. (5.4), we get the following equality:

$$1\frac{\mathrm{cm}^3}{\mathrm{s}} = -1\mathrm{cm}^2 \frac{1\mathrm{D}}{1\mathrm{cp}} \left( -\frac{1\mathrm{atm}}{1\mathrm{cm}} \right),$$

where the Darcy-units are preferably used in connection with laboratory tests.

There are two systems of units which are widely used in petroleum field engineering;

- Field units.
- SI units (international system of units).

The value 1 Darcy is defined in SI-units by substitution:

$$\begin{aligned} q &= 10^{-6}\,\frac{\mathrm{m}^3}{\mathrm{s}}, \\ \mu &= 1\,cp = 10^{-3}\,\frac{\mathrm{kg}}{\mathrm{m\ s}}, \\ \frac{dp}{dl} &= 1\,\frac{\mathrm{atm}}{\mathrm{cm}} = 1.01\cdot 10^5\,\frac{\mathrm{Pa}}{\mathrm{cm}} = 1.01\cdot 10^7\,\frac{\mathrm{kg}}{\mathrm{m}^2\ \mathrm{s}^2} \text{ and} \\ A &= 10^{-4}\,\mathrm{m}^2 \\ k &= \frac{q\mu}{A\cdot dp/dl} = 0.987\cdot 10^{-12}\ \mathrm{m}^2 = 0.987\mu\mathrm{m}^2. \end{aligned}$$

Here: $\mu\mathrm{m}^2 = (\mu\mathrm{m})^2$.

It follows from these evaluations that,

$$1\ \mathrm{D} = 0.987\ \mu\mathrm{m}^2.$$

Instead of the unit 1 Darcy, the 1/1000 fraction is used, which then is called millidarcy (mD).

It is important to remember that permeability is a tensor, which means that permeability might have different values in different directions. Vertical permeability (i.e. normal to the bedding of formations) is usually much lower in comparison than the horizontal permeability (measured along the bedding of formations). In its turn, the horizontal permeability can be different in different directions. These permeability features should be taken into account while measuring permeability.

**Example: Core sample liquid permeability.**

A cylindrical core sample is properly cleaned and all remains of hydrocarbons are removed from the pore space. The core is saturated with water and then flushed horizontally. The core length is 15 *cm*, it's diameter is 5 *cm* and the water viscosity is 1.0 *cp*.

The permeability might be determined by plotting the data in a "rate/pressure" diagram, as shown in Fig. 5.5, or more directly, by calculating the permeability value for each data-pair, using the formula,

$$k = \frac{\mu\Delta l}{A}\frac{q}{\Delta p},$$

where $A = \pi(d/2)^2$ and $d$ is the core sample diameter.

The pressure drop $\Delta p$, is measured for three different flow-rates and permeability is calculated using the above formula,

| $q_w\ [cm^3/s]$ | 1.0 | 3.0 | 10.0 |
|---|---|---|---|
| $\Delta p$ [atm] | 7.2 | 24.5 | 76.0 |
| $k\ [D]$ | 0.106 | 0.093 | 0.101 |

The average or representative permeability is $\overline{k}$ = 0.1 *D* or 100 *mD*.

Laboratory measurements, always contain uncertainty related to the technology used to obtain the lab-data. This uncertainty could be examined by plotting the data-pairs in an appropriate way, e.g. as shown in Fig. 5.5. The advantage of data-plotting, compared to straight forward calculations, as in this example, is the opportunity to verify that the data used in the averaging process are "good" or representative .

## 5.5 Gas Permeability Measurements

Due to certain interactions between the liquids and the porous rock, absolute permeability is routinely measured in the laboratory by flowing gas (usually inert gas) through the core sample.

Because gas is a highly compressible substance, i.e. the gas rate is pressure dependent, the Darcy's law may not be utilised directly. Considering mass flow of gas $q\rho$, one can write,

$$q\rho = -A\frac{k\rho}{\mu}\frac{dp}{dx},$$

where $\rho$ is the density of the gas at certain pressure.

It follows from the perfect gas law ($pV = nRT$) that,

$$\rho(p) = \frac{\rho(p_0)}{p_0}p, \text{ or simply } \rho = \frac{\rho_0}{p_0}p,$$

which when substituted into the previous equation equation yields,

$$q\rho = -A\frac{k\rho_0 p}{\mu p_0}\frac{dp}{dx}. \tag{5.8}$$

Here the subscript "0" refers to a certain pressure value, for instance, the pressure at normal or standard conditions.

Taking into account the invariant quantity,

$$q\rho = q_0\rho_0,$$

one finally obtains,

$$q_0 = -A\frac{kp}{\mu p_0}\frac{dp}{dx}, \tag{5.9}$$

or integrated from $p_1$ to $p_2$,

$$q_0 = A\frac{k}{2\mu p_0}\frac{p_1^2 - p_2^2}{\Delta l}. \tag{5.10}$$

Another useful form in which Eq. (5.10) can be written is,

$$q_0 = A\frac{k}{\mu}\frac{\overline{p}}{p_o}\frac{\Delta p}{\Delta l}, \tag{5.11}$$

where $\overline{p} = (p_1 + p_2)/2$ is a mean (average) pressure in the core during the measurements.

Combining the invariant mass flow; $q\rho = \overline{q\rho}$ and the results generated from the perfect gas law; $\rho\overline{p} = \overline{\rho}p$ with Eq. (5.11), one obtains,

$$\overline{q} = -A\frac{k}{\mu}\frac{\Delta p}{\Delta l}, \tag{5.12}$$

where $\overline{q}$ is the mean or average flow rate. Eq. (5.12) has exactly the same form as Darcy's law for horizontal liquid flow, except for the fact that the flow rate is the mean flow rate. In a homogeneous porous rock, the mean flow rate is equal to the gas rate at the centre of the core sample.

The Hassler core holder is commonly used for permeability measurements. It provides measurements of permeability in both vertical and horizontal directions.

For permeability measurements in the vertical direction gas is injected through the core plug in the axial direction (see Fig. 5.6, left). The core plug is placed in an impermeable rubber sleeve protecting the gas flow at the outer-face of the core plug.

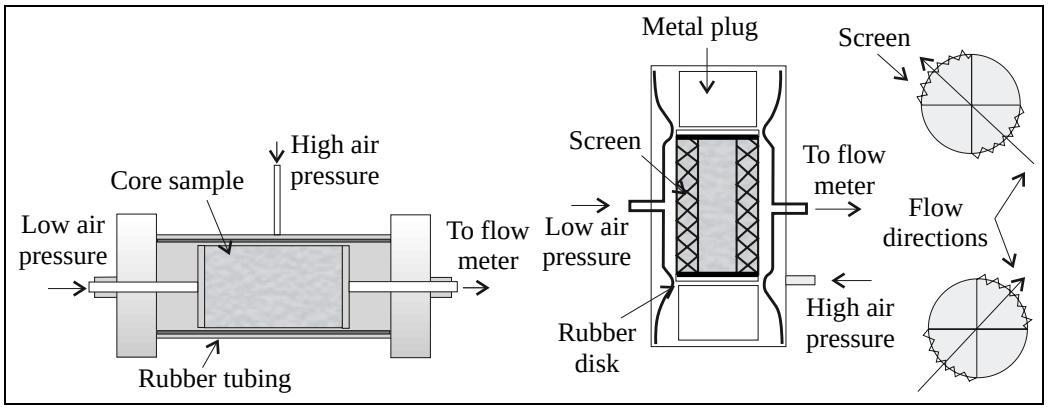


Figure 5.6: Full diameter vertical and horizontal permeability measurement apparatus (from IHRDC, 1991).

Horizontal permeability measurements require a sealing of the top surfaces of the core with non-permeable rubber disks (see Fig. 5.6, right). The area of cylindrical surface at the inflow and outflow openings is covered with a screen and the sample is then placed into the core holder. Under high air pressure the rubber tubing is collapsed around the core. Low pressure air is introduced into the center of the holder and passes through the rubber boot and intersects with the screen, and then flows vertically through the screen. The air then flows through the full diameter sample along its full height and emerges on the opposite side, where the screen again allows free flow of the air to exit. The screen are selected to cover designated outer segments of the full diameter sample. In most cases the circumference of the core is divided into four equal quadrants. In this test the flow length is actually a function of the core diameter, and the cross-sectional area of flow is a function of the length and diameter of the core sample.

It is common to furnish two horizontal permeability measurements on all full diameter samples. The second measurement is made at the right angles to the first.

**Example: Core sample gas permeability.**

A gas permeability test has been carried out on a core sample, 1 *in* in diameter and length. The core has been cleaned and dried and mounted in a Hassler core holder, of the type seen in Fig. 5.6.

The gas is injected and the pressure, $p_1$ measured, at one end of the core sample, while the gas rate, $q_2$ is measured at the other end, at atmospheric pressure, i.e., $p_2 = 1atm.$

The gas permeability could be estimated using Eq. (5.10), written as follows,

$$q_2 = A\frac{k}{2\mu p_2}\frac{p_1^2 - p_2^2}{\Delta l}.$$

Given the pressure $p_1$ and the gas rate $q_2$, the mean pressure in the core sample, $\overline{p}$ and the pressure drop across the core, $\Delta p$, are calculated from the equation above. The gas permeability $k$ is found as a function of the mean core pressure.

The following data is given:

| $p_1$ $[mmHg]$ | $q_2$ $[cm^3/min]$ | $\overline{p}$ $[atm.]$ | $\Delta p$ $[atm.]$ | $k$ $[mD]$ |
|---|---|---|---|---|
| 861 | 6.4 | 1.066 | 0.133 | 6.8 |
| 1276 | 35.6 | 1.33 | 0.667 | 6.3 |
| 2280 | 132.8 | 2.00 | 2.00 | 5.0 |

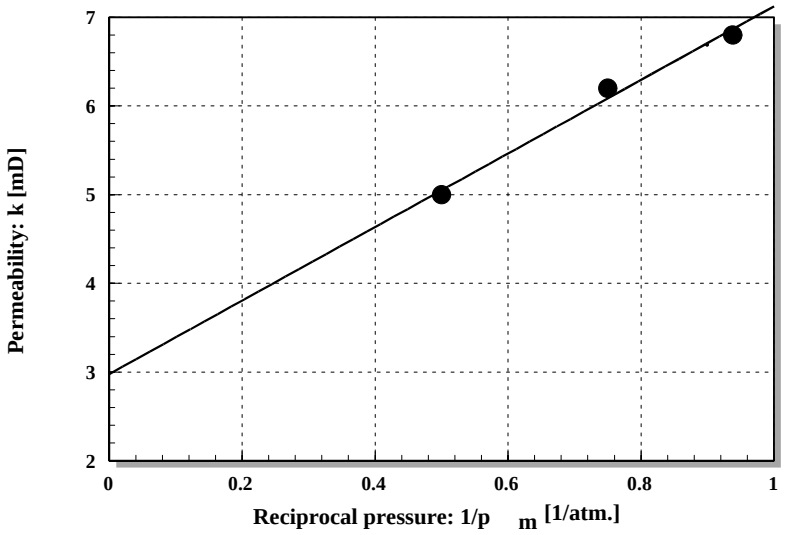


Figure 5.7: Gas permeability plotted as the reciprocal of mean pressure.

Note that the gas permeability is pressure dependent. As the mean pressure in the core sample increases it is expected that the gas permeability will approach the absolute (liquid) permeability, since at such high pressure the gas itself, will start to behave as a liquid.(This asymptotic limit is not reached unless the pressure, e.g. in air, is more than 1000 *bar*.)

The absolute gas permeability of the core sample is therefore found as the asymptotic value of permeability, when $\overline{p} \to \infty$ or more conveniently, when $1/\overline{p} \to 0$, as seen in Fig.5.7. The data, taken from the table is plotted and the absolute permeability is found $k_{liquid} = 3.0\,mD$.

———— · ————

### 5.5.1 Turbulent Gas Flow in a Core Sample

When gas permeability in core samples are measured, turbulent flow may be experienced in parts of the pore system, preferably in the larger pores and pore channels.

In order to adjust for the occurance of turbulence, the horizontal flow equation can be expanded by adding a term particularly describing the turbulent flow situation. For this purpose the Fanning Eq. (5.13), is used describing turbulent flow in a circular tube [7],

$$v^2 = \frac{R}{\rho F}\frac{\Delta p}{\Delta x}, \tag{5.13}$$

where $R$ is the tube radius, $\rho$ is the gas density and $F$ is the Fanning friction factor characterising the tube (i.e. roughness, wetting, etc.).

According to the Fanning equation one may assume that pressure drop across a pore channel is proportional to the square of the average gas velocity in the pore.

The horizontal flow equation, including a turbulent term can be written as,

$$\frac{\Delta p}{\Delta x} = \frac{\mu}{k}\overline{v} + \beta\overline{v}^2,$$

where $\overline{v}$ is the average or mean flow velocity and $\beta$ is the turbulent constant .

Considering the average gas flow velocity, $\overline{v} = \overline{q}/A$ and rearranging the above equation somewhat, one gets,

$$\frac{\Delta p}{\Delta x}\frac{A}{\mu}\frac{1}{\overline{q}} = \frac{1}{k} + \frac{\beta}{A\mu}\overline{q}.$$

In an experimental situation one normally do not know the average core rate $\overline{q}$. Instead the gas rate is measured at the exhaust end, $q_0$. Recall from above the relation,

$$\overline{q} = \frac{p_0}{\overline{p}}q_0.$$

Substituting for average gas rate in the horizontal flow equation one gets an equation particularly adapted for experimental application,

$$\frac{A}{\Delta x \mu p_0}\frac{\Delta p\overline{p}}{q_0} = \frac{1}{k} + \frac{\beta p_0}{A\mu}\frac{q_0}{\overline{p}}. \tag{5.14}$$

Eq. (5.14) is a linear equation where $1/k$ is the constant term.

In order to use Eq. (5.14), special care has to be taken to *how* data is plotted. Since $\overline{p} = (p_1 + p_2)/2$ and $\Delta p = (p_1 - p_2)$, are both functions of $p_1$, one of them has to be kept fixed when producing linear plots.

Assuming there are three sets of data; set a, b and c. For each set there are three measurements; 1, 2 and 3, all together nine measurements.

| | | |
|---|---|---|
| $\overline{p}_a$ | $\Delta p_{a,1}$ | $q_{0,a,1}$ |
| $\overline{p}_a$ | $\Delta p_{a,2}$ | $q_{0,a,2}$ |
| $\overline{p}_a$ | $\Delta p_{a,3}$ | $q_{0,a,3}$ |
| $\overline{p}_b$ | $\Delta p_{b,1}$ | $q_{0,b,1}$ |
| $\overline{p}_b$ | $\Delta p_{b,2}$ | $q_{0,b,2}$ |
| $\overline{p}_b$ | $\Delta p_{b,3}$ | $q_{0,b,3}$ |
| $\overline{p}_c$ | $\Delta p_{c,1}$ | $q_{0,c,1}$ |
| $\overline{p}_c$ | $\Delta p_{c,2}$ | $q_{0,c,2}$ |
| $\overline{p}_c$ | $\Delta p_{c,3}$ | $q_{0,c,3}$ |

For each data set; a, b and c, a straight line is plotted through the measured data points and the constant $1/k$ is evaluated, as shown in the Fig. 5.8.

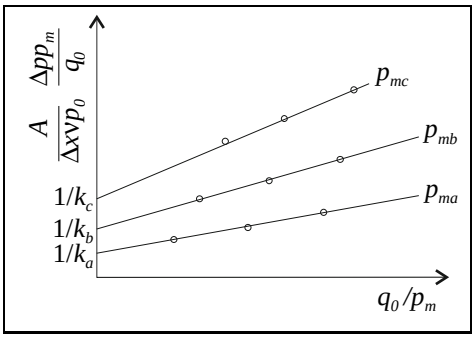


Figure 5.8: Plotting linear data where the average pressure $\overline{p} = p_m$ is kept constant.

The three permeability values found form Fig. 5.8; $k_a$, $k_b$ and $k_c$ are now plotted, in accordance with the linear Eq. (5.14), as shown in the Fig. 5.9.

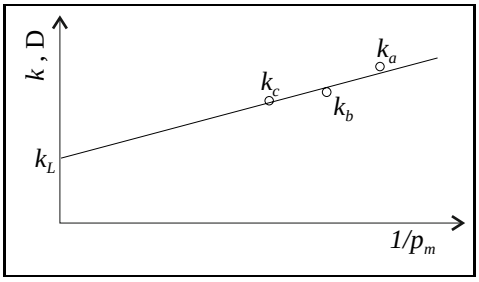


Figure 5.9: Absolute permeability as function of inverse average pressure, $\overline{p} = p_m$

When turbulence is considered, gas permeability is found using a step like plotting process, where data having the same average core pressure are plotted together in the first step. Secondly, permeabilities are plotted as functions of the inverse average pressure, from where the absolute (liquid) permeability is found.

## 5.6 Factors Affecting Permeability Values

General considerations show that permeability is a characteristic parameter describing flow behaviour in porous media. Since the permeability is introduced as a proportional coefficient in Darcy's law, it is evident that other characteristics than the porous medium have important influence on the numeric value of the permeability. In the case of overburden pressure, experiments have shown that the permeability is even more dependent on the overburden pressure than the porosity.

Permeability measurements are also (sometimes strongly) affected by the fluid, e.g. used in laboratory tests, due to some interaction between the fluid and the porous medium. To avoid this effect, gases (helium, nitrogen, carbon-dioxide and air) are often used for permeability measurements. The use of gases introduce other problems, such as turbulent flow behaviour, increased uncertainty in gas rate measurements and at low pressure, the *Klinkenberg effect*.

It follows from Eq. (5.11), that the rock permeability to gas is not the same as for liquids, since gas permeability is pressure dependent, i.e. $k = k(\overline{p})$,

$$k = \frac{q_o \mu}{A} \frac{p_o}{\overline{p}} \frac{\Delta l}{\Delta p}, \tag{5.15}$$

where the latter statement means that different average core pressures $\overline{p}$, provide different values of the rock permeability to gas.

These facts should be considered when permeability from laboratory measurements is related to reservoir permeability.

### 5.6.1 The Klinkenberg Effect

It has been observed that at low average pressures, measurements of gas permeability give erroneously high results, as compared to the non-reactive liquid permeability measurements (absolute permeability). This effect is known as the *gas slippage effect* or as the *Klinkenberg effect*, investigated by Klinkenberg in 1941. Klinkenberg found that the gas permeability of a core sample varied with both the type of gas used in the measurements and the average pressure $\overline{p}$, in the core.

One of the conditions for the validity of Darcy's law, as presented in Eqs. (5.7) or (5.11), is the requirement of laminar flow, i.e. that the fluid behaves "classically" with respect to intermolecular interactions in the gas. At low gas pressure, in combination with small (diameter) pore channels, this condition is broken.

At low $\overline{p}$, gas molecules are often so far apart, that they slip through the pore channels almost without interactions (no friction loss) and hence, yield a increased flow velocity or flow rate. At higher pressures, the gas molecules are closer together and interact more strongly as molecules in a liquid. Compared to laminar flow, at a constant pressure difference, the Klinkenberg dominated flow will yield a higher gas rate than laminar flow,

$$q_{Klinkenberg} > q_{laminar}.$$

Experiments show that when gas permeability is plotted versus the reciprocal average pressure $\overline{p}$, a straight line can be fitted through the data points. Extrapolation of this line to infinite mean pressure, i.e. when $1/\overline{p} \to 0$, gives the absolute (liquid) permeability. The permeability

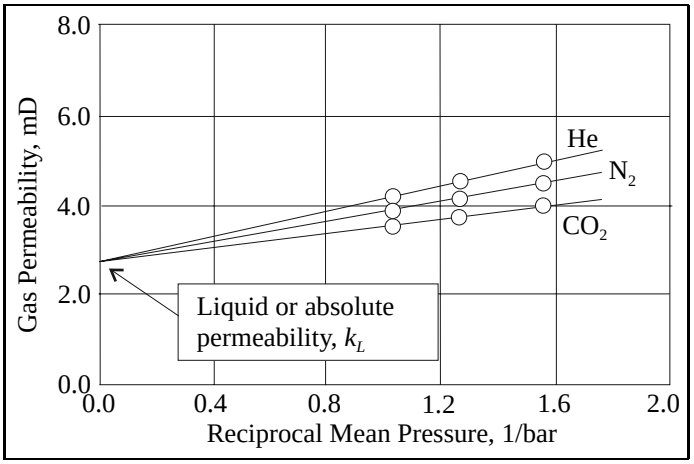


Figure 5.10: Klinkenberg permeability determination.

value at $1/\overline{p} \to 0$ is comparable to the permeability obtained if the core were saturated with a non-reactive liquid (see Fig. 5.10.

In early core analysis the Klinkenberg permeability was estimated by using a steady-state technique for permeability measurements, at different mean pressures $\overline{p}$, or by using the following correlation's;

$$k_m = k_L \left(1 + \frac{b}{\overline{p}}\right), \tag{5.16}$$

where $k_m$ and $k_L$ are the measured- and the absolute (liquid) permeability, respectively. The parameter $b$ depends on the type of gas used and reflects, to some extent, properties of the rock (Fig. 5.10).

Corrections to measured gas permeability due to the Klinkenberg effect are normally moderate to small corrections, as seen for the table below.

| Non-corrected permeability, [mD] | Klinkenberg corrected permeability, [mD] |
|---|---|
| 1.0 | 0.7 |
| 10.0 | 7.8 |
| 100.0 | 88.0 |
| 1000.0 | 950.0 |

In most laboratory measurements of gas permeability, it is safe to neglect the Klinkenberg effect if the gas pressure is higher than 10 bar. In reservoirs, the pressure will be much higher and consequently the significance of the Klinkenberg effect of no importance.

**Example: Onset of the Klinkenberg effect**

The onset of the Klinkenberg effect is considered in a system comprised of a bundle of identical capillary tubes. For such a system, using Poiseuille's law for tube flow, it is shown that the permeability can be written,

$$k = \frac{\pi}{4}\frac{r^2}{8}, \tag{5.17}$$

where $r$ is the individual tube radius.

Irrespective of the fact that a bundle of cylindrical tubes is far from being a realistic model of a porous medium, one can estimate the permeability at which the Klinkenberg effect starts to become a significant effect.

As an example helium gas might be chosen in the flow experiment. Helium has a *mean free path*, $\lambda_{He} = 0.18 \cdot 10^{-6} m$ at atmospheric pressure and temperature of $20^o$C [59]. At higher pressures, lower *mean free paths* are observed, i.e. $\lambda < \lambda_{He}$.

Since the Klinkenberg effect is said to become important when the *mean free path* of the gas and the size (diameter) of the pore channels are comparable, there is a maximum permeability limit, below which the Klinkenberg effect becomes active.

Substituting the helium *mean free path* for the diameter of the tube radius in Eq. (5.17); $r = \lambda_{He}/2$, it follows,

$$k_{He} = \frac{\pi}{4}\frac{(\lambda_{He}/2)^2}{8}, \tag{5.18}$$

Using helium gas, the Klinkenberg effect would be active at standard conditions in a "porous" medium, as above, for permeabilities less than $k_{He}$ = 0.8 mD. In an experiment where $N_2$ or $CO_2$ is used, the expected *mean free paths* are shorter and consequently the permeability limits are lower than in the $He$ case.

For many gases, the mean free paths of their molecules at standard conditions (room temperature and atmospheric pressure) are in the range: 0.01 to 0.1 $\mu$m, whereas the mean free paths of $CO_2$ and $N_2$ are respectively 0.04 $\mu$m and 0.06 $\mu$m.

## 5.7 Exercises

1. Prove that the numeric constant for converting $dyn/cm^2$ to atm, is equal to $1.0133 \times 10^6$,.

2. Darcy's law is given,

$$q = A\frac{k}{\mu}\frac{\Delta p}{\Delta L},$$

where; k:[Darcy], $\mu$:[cp], A:[$cm^2$], q:[$cm^3/s$], L:[cm] and p:[atm].

Convert this equation to "Oil Field Units" where; k:[mD], $\mu$;[cp], A:[$ft^2$], q:[bbl/d], L:[ft] and p:[psi].

3. The cylindrical pore model consists of cylindrical tubes stacked on top of each other. Assuming a tube radius equal to $r$ and that the fluid flow velocity through the tubes, is given by Poiseuilles equation,

$$v = \frac{r^2}{8\mu}\frac{\Delta p}{\Delta l}.$$

   a) Calculate the porosity of the cylindrical pore model $\phi$,

   b) Show that the permeability is written as $k = \phi r^2/8$.

   c) Consider the average permeability of a serial coupling of two tubes with tube radius $R$ and $r$, where $R \gg r$. Find an expression for the average permeability and evaluate the consequences of relative increase/decrease in the pore radius, as shown in the figure below.

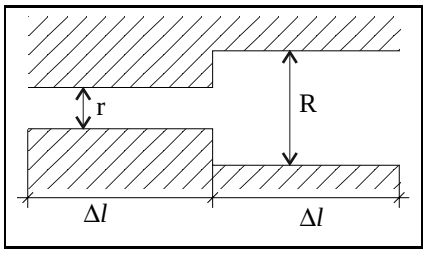


4. A reservoir has cylindrical geometry where the following parameters are defined;

| | |
|---|---|
| $p_e$ [atm] | Pressure at the outer boundary |
| $p_w$ [atm] | Pressure in the well |
| $r_w$ [cm] | Well radius |
| $r_e$ [cm] | Radius at the outer boundary |
| $h$ [cm] | Reservoir height |

Use Darcy's law to derive a general equation for a cylindrical reservoir in the cases of horizontal flow, when we have,

   a) incompressible fluid and

   b) ideal gas.

5. Use the laws of Darcy and Poiseuilles to estimate the lowest measurable permeability of a sandstone core sample, without detecting the Klinkenberg effect. The measurements are done under laboratory conditions, using $N_2$.

6. Calculate the air permeability, in two ways, for a cylindrical core sample where the following data is given. Verify that the two approaches used above give the same answer. (Use the equation for gas rate at the effluent end $q_b$ and the equation for the average gas rate $\overline{q}$.)

| | | | |
|---|---|---|---|
| Length | 3.0 in, | $p_1$ | 55 psig, |
| Diameter | 1.5 in, | $p_2$ | 20 psig, |
| $q_b$ | 75 $cm^3/s$, | Atm. pressure | 13 psia, |
| $p_b$ | 14.65 psia, | $\mu$ | 0.0185 cP. |

   $q_b$ and $p_b$ is the flow rate and back pressure, respectively.
   (NB: $p_{psia} = p_{psig} + p_{atm.pressure}$)

7. An oil well is producing from a cylindrical reservoir with a drainage area of 20 acres. Calculate the well pressure, given the following data:

| | | | | | |
|---|---|---|---|---|---|
| $r_w$ | = | 6 in, | $\mu$ | = | 5 cP, |
| k | = | 75 mD, | h | = | 10 ft, |
| $p_e$ | = | 5000 psia, | q | = | 175 BOPD, |

   BOPD is short for "Barrel of Oil Produced per Day".
   Calculate the pressure in the reservoir at a distance 5 ft from the well. What is the pressure drop from the well to this position, in percentage of the total pressure difference in the reservoir?

8. Show that the average permeability $\overline{k}$ for $n$ horizontal layers, stacked on top of each other (in parallel), is given by the formula [8] (see Figure below),

$$\overline{k} = \frac{\sum_{j=1}^{n} k_j h_j}{\sum_{j=1}^{n} h_j},$$

   where $k_j$ and $h_j$ are the permeability and thickness of the layers.

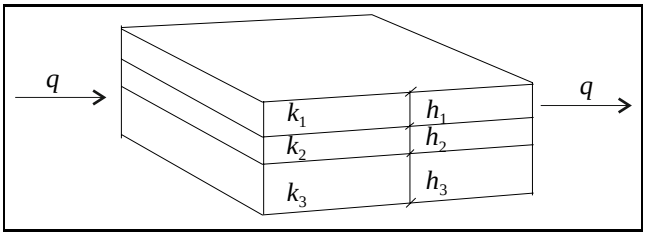


9. Linear flow in horizontal layers.

   Calculate the total flow rate in $ft^3/d$ at the pressure $p_b$ for gas flow through parallel layers, where the following data is given:

| | | | | | |
|---|---|---|---|---|---|
| width | 200 ft, | length | 400 ft, | $p_{atm.}$ | 15.0 psia, |
| $h_1$ | 2 ft, | $k_1$ | 200 mD, | $p_{in}$ | 500 psig, |
| $h_2$ | 6 ft, | $k_2$ | 150 mD, | $p_{out}$ | 400 psig, |
| $h_3$ | 4 ft, | $k_3$ | 400 mD, | $p_b$ | 14.65 psia. |

Gas viscosity $\mu_g = 0.0185\,cp$. (Notice: $p_{psia} = p_{psig} + p_{atm.}$)

10. Show that the average permeability of rectangular porous media coupled in series is given by the formula [8] (see Figure below),

$$\bar{k} = \frac{\sum_{j=1}^{n} L_j}{\sum_{j=1}^{n} L_j / k_j},$$

where $L_j$ is the length of the media in the direction of flow.

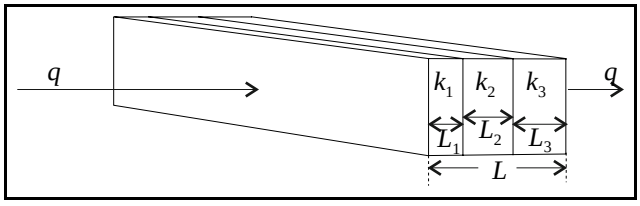


11. Linear and horizontal flow through linear beds in series.

Calculate the total oil rate $bbl/d$ through all media, when the following data is given:

| | | | | | |
|---|---|---|---|---|---|
| width | 100 ft, | height | 50 ft, | $\mu_o$ | 10 cP, |
| $L_1$ | 100 ft, | $k_1$ | 100 mD, | $p_{in}$ | 100 psig, |
| $L_2$ | 200 ft, | $k_2$ | 50 mD, | $p_{out}$ | 50 psig, |
| $L_3$ | 200 ft, | $k_3$ | 200 mD, | $p_{atm.}$ | 15.0 psia, |

12. Show that the average permeability for $n$ radial layers in a cylindrical reservoir is given by the formula [8] (see Figure below),

$$\bar{k} = \frac{\ln(r_e/r_w)}{\sum_{j=1}^{n} ln(r_j/r_{j-1})/k_j},$$

where $r_e$ and $r_w$ is the radius to the outer boundary of the reservoir and the well radius, respectively. $k_j$ is permeability to the layer with outer radius $r_j$.

Are the formulas above valid both for gas- and liquid flow?

13. Radial and horizontal flow through cylindrical layers.

An oil well has a intermediate zone with reduced reservoir permeability $k_1$. Calculate the pressure at the outer boundary $p_e$ when the oil rate is 100 $bbl/d$ and the following data is given:

| | | | | | |
|---|---|---|---|---|---|
| $r_w$ | 6 in, | $k_1$ | 50 mD, | $p_w$ | 2000 psia, |
| $r_1$ | 10 ft, | $k_2$ | 200 mD, | $\mu_o$ | 5 cp, |
| $k_3$ | 330 ft, | | | h | 20 ft. |

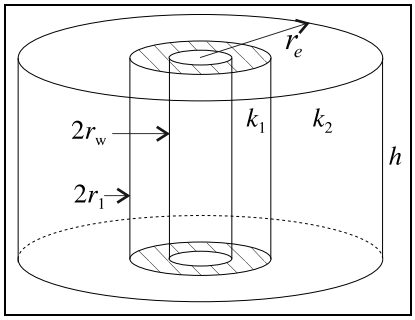


What is the pressure at outside the damaged zone ($r_1$) ?

14. Absolute permeability of a core sample is being measured by water flooding. The core sample is mounted in a transparent cylindrical tube, as shown in the figure below, and the air-water surface is monitored as function of time.

    The tube is placed in a vertical position and the water is assumed to flow through the whole core sample, evenly distributed over the surface.

    Calculate the absolute permeability of the sample when the air–water surface uses 400 seconds to move 18 cm.

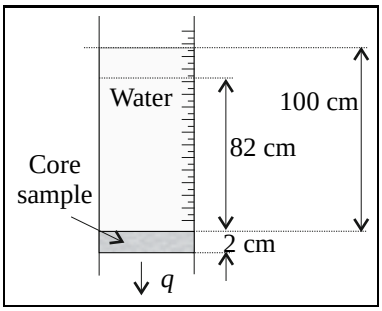


Additional data;

| | |
|---|---|
| Density of water | $1\ g/cm^3$ |
| Water viscosity | 1 cp |
| Gravitational constant | $980\ cm/s^2$ |
| Thickness of core sample | 2 cm |

**Answers to questions:**

3. $\pi/4$, 5. 0.1 *mD*, 6. 0.1 *D*, 7. 262 atm, 288 atm,
9. $1.57 \cdot 10^6\ ft^3/d$, 11. 4710 $bbl/d$, 13. 2272 *psi*, 14. 1 *D*.

# Chapter 6

# Viscosity

## 6.1 Ideal Fluids

The frictional forces in fluid flow result from the *cohesion* and *momentum interchange* between molecules in the fluid. Viscosity of a fluid is a measure of its resistance to shear or angular deformation [47].

The main characteristic of an ideal fluid is the absence of tangential stresses (*shear stresses*), which means that all the stresses are symmetrical.

## 6.2 Viscous Fluids

### 6.2.1 Horizontal Flow of Viscous Fluid

A commonly used type of the rheology law, is the equation of rheology of viscous fluid otherwise called *Newton's equation of viscosity*. It states that there is a straight proportionality between the tangential (shear) component $\tau$ (friction component) of a stress tensor and the flow derivative of the shear rate, i.e.,

$$\tau = \mu \frac{dv_x}{dy}, \tag{6.1}$$

where $\tau$ is a shear stress, $\mu$ is the fluid viscosity, $v_x$ is the fluid flow velocity in $x$-direction (direction of flow) and $y$ is the direction normal to flow, subjected to exchange of stresses.

The shear stress $\tau$, is also considered as the momentum transfer between fluid layers pr. time pr. area, i.e. a sort of momentum density, where the shear stress $\tau$ and $dv/dy$ have the following dimensions:

$$\tau = \left[\frac{\mathrm{N}}{\mathrm{m}^2}\right], \quad \frac{dv}{dy} = \left[\frac{\mathrm{m}}{\mathrm{s}\cdot\mathrm{m}}\right] = \left[\frac{1}{\mathrm{s}}\right],$$

where the viscosity $\mu$ dimension is defined,

$$\mu = \frac{\tau}{dv/dy} = \left[\frac{\mathrm{N}\cdot\mathrm{s}}{\mathrm{m}^2}\right].$$

By definition we say,

$$1\ \text{Pa}\cdot\text{s} = 1\frac{\text{N}\cdot\text{s}}{\text{m}^2} = 10\ \text{p (Poise)}\ = 10^3\text{cp}\ .$$

Conventionally viscosity is measured in centipoise (cp), expressed by means of the units above:

$$1cp = 1mPa\cdot s.$$

Typical values of the oil, water and air viscosity at atmospheric pressure, are given in Table 6.1 [48].

Table 6.1: **Typical Values of Viscosity of Some Fluids**

| Temperature $C^0$ | Viscosity Castor Oil, Poise [p] | Viscosity Water, Centipoise [cp] | Viscosity Air, Micropoise [$\mu$p] |
|---|---|---|---|
| 0 | 53.00 | 1.792 | 171 |
| 20 | 9.86 | 1.005 | 181 |
| 40 | 2.31 | 0.656 | 190 |
| 60 | 0.80 | 0.469 | 200 |
| 80 | 0.30 | 0.357 | 209 |
| 100 | 0.17 | 0.284 | 218 |

**Example: Water viscosity at reservoir conditions.**

Water viscosity is primarily a function of temperature, though salinity has also a slight influence on $\mu_w$. Pure water viscosity is listed in the Table 6.1, but due to correction for salinity and reservoir temperature, the normal range of viscosity at reservoir conditions is from 0.2 to 1.0 $cp$.

The following correlation for estimation of the water viscosity at reservoir temperature can be used [57],

$$\mu_w = 4.33 - 0.07T + 4.73\cdot 10^{-4}T^2 - 1.415\cdot 10^{-6}T^3 + 1.56\cdot 10^{-9}T^4,$$

where $\mu_w$ is measured in $cp$ and temperature in Fahrenheit ($^oF$).

At a reservoir temperature of 110 $^oC$ (230 $^oF$), the water viscosity will be,

$$\begin{aligned}\mu_w &= (4.33 - 0.07\cdot 230 + 4.73\cdot 10^{-4}\cdot 230^2 - 1.415\cdot 10^{-6}\cdot 230^3 \\ &\quad +1.56\cdot 10^{-9}\cdot 230^4)cp \\ &= 0.40cp.\end{aligned}$$

(Note that at temperatures above 100 $^oC$ water at reservoir conditions will still be in a liquid phase since the reservoir pressures is quite high as compared to surface conditions.)

### 6.2.2 Continuity Equation for Viscous Flow

When a liquid is flowing in an open channel, as shown in Fig. 6.1, collisions between individual liquid molecules is an ongoing and continuous process. Momentum is transferred between the different molecules in such a way, as to collectively co-ordinate the behaviour of all molecules. As a result of these molecular interactions the liquid flow might be characterised as *a convective movement*.

Liquid flow, i.e. a river silently flowing down stream over a flat bottom is considered, as sketched in Fig. 6.1. Since the bottom surface is not moving, all molecules adjacent to the bottom, will experience retardation when colliding with this surface. The collective flow velocity close to the bottom will therefore be approximately zero. (Due to thermal energy, molecules will have thermal velocity different from zero). For those molecules belonging to the layers above the bottom layer, flow velocity will increase with elevation.

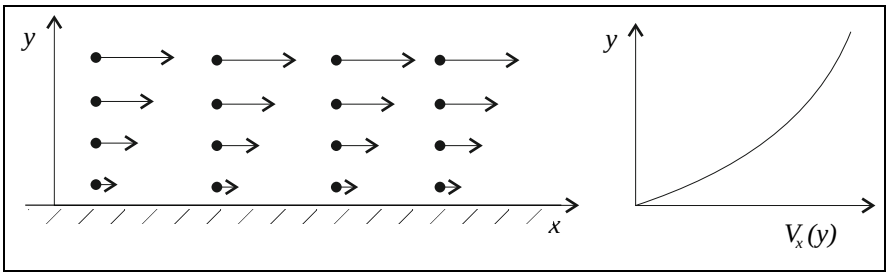


Figure 6.1: Cross-section view of fluid flow in an open channel.

In an attempt to quantify the somewhat idealised picture of fluid flow, as shown in Fig. 6.1, it is quite fruitful to consider the quantity of *transferred momentum pr. time pr. area*; $j_p$, as the source of change in velocity between adjacent layers. The parameter $j_p$ is often characterised as the *momentum intensity* or as the *shear stress*, $\tau$ and it's units is written: $N/m^2$.

In analogy with Fick's law for molecular diffusion and Fourier's law for thermal conductivity, the momentum transfer between two adjacent molecular layers is defined, to be proportional to the change in fluid flow velocity pr. distance between the two layers; $d\ v_x/d\ y$. By introducing a proportionality constant $\mu$, the identity Eq. (6.2) is written,

$$j_p = \mu \frac{\partial\ v_x}{\partial\ y}. \tag{6.2}$$

Viscosity is here defined as a proportionality constant, similar to what was done in the case of defining absolute permeability. The liquid viscosity $\mu$, is considered to be a characteristic constant, given by Eq. (6.2). This constant carries information about the liquid, and is conditionally dependent on the proportionality in Eq. (6.2).

In accordance with classical tradition, the momentum transfer between liquid layers is considered as being confined in a box with cross-section, $S$. Fig. 6.2 shows the box where the momentum flux is perpendicular to the liquid flow direction.

The change of momentum intensity inside the box in Fig. 6.2 is defined by the difference of momentum intensity through the surfaces $S$ and $S'$, where the box width $dy$ is small,

$$j_p S - j_p' S' = (j_p - j_p')S = \frac{\partial\, j_p}{\partial y} S dy,$$

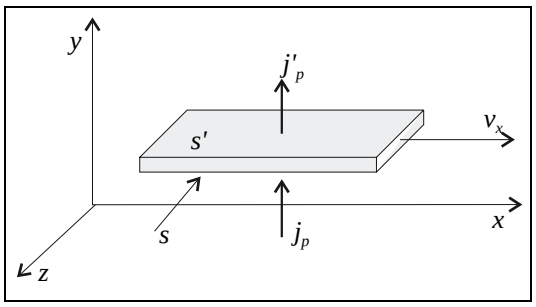


Figure 6.2: Momentum transfer between layers $S$ and $S'$ in Newtonian viscous flow.

where $dy$ is the width of the box and $S = S'$ is the cross-section.

The momentum density inside the box is defined by $P_\rho$. The change of momentum pr. time inside the box is then given as,

$$\frac{\partial P_\rho}{\partial t} S dy.$$

Combining the two expressions above, one gets,

$$\frac{\partial P_\rho}{\partial t} = \frac{\partial j_p}{\partial y}. \tag{6.3}$$

In Eq. (6.3), the $\partial P_\rho / \partial t$ is considered as the sum of all forces acting on the box. In addition to viscous forces, as considered in Eq. (6.3), a general external forces is added, e.g. gravitation is always is active.

Let $f$ symbolise a force of more general origin, and the continuity equation is written,

$$\frac{\partial P_\rho}{\partial t} = \frac{\partial j_p}{\partial y} + f. \tag{6.4}$$

Substituting the momentum intensity given in Eq. (6.2) and using the definition of momentum density as, $P_\rho = \rho v_x$, where $\rho$ is the liquid density, the general continuity equation is given,

$$\frac{\partial v_x}{\partial t} = \frac{\mu}{\rho} \frac{\partial^2 v_x}{\partial y^2} + \frac{f}{\rho}. \tag{6.5}$$

**Example: Falling sphere viscosity measurement.**

A metal sphere falling in a viscous fluid reaches a "terminal" (constant) velocity $v_s$, at which the viscous retarding force plus the buoyancy force equals the weight of the sphere, as seen in Fig. 6.3.

The force $F_s$, acting on a sphere of radius $r$, moving with a thermal speed $v_s$ through a fluid with viscosity $\mu$ is given by *Stoke's law*,

$$F_s = 6\pi\mu r v_s.$$

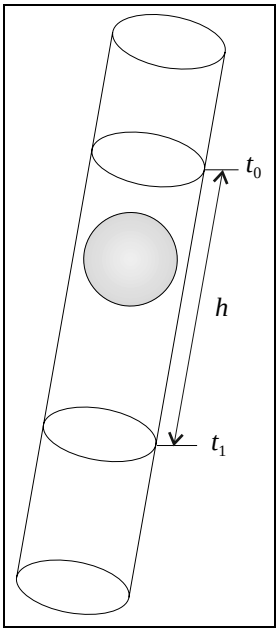


Figure 6.3: Falling sphere viscosity measurement.

If $\rho_s$ is the density of the metal sphere and $\rho_f$ is the density of the fluid, the weight of the sphere will balance the viscous force plus the buoyancy force at the terminal sphere velocity when the sum of forces acting on the sphere is zero. This gives,

$$\frac{4}{3}\pi r^3 g\rho_s = 6\pi\mu r v_s + \frac{4}{3}\pi r^3 g\rho_f,$$

where $g$ is the constant of gravitation.

Viscosity can be estimated by measuring the falling speed of a metal sphere in e.g. a cylindrical tube,

$$\mu = \frac{2}{9}r^2 g(\rho_s - \rho_f)\frac{1}{v_s},$$

or alternatively, by measuring the time $\Delta t$, it takes for the metal sphere to fall (at constant speed) a distance $h$ in the fluid ($v_s = h/\Delta t$),

$$\mu = C(\rho_s - \rho_f)\Delta t,$$

where the $C$ is a characteristic constant, determined through calibration with a fluid of known viscosity.

In a Hoeppler viscometer, different types of spheres (density and radius) can be used and the accuracy in the viscosity estimate is normally better than 1%.

### 6.2.3 Viscous Flow in a Cylindrical Tube

Looking at viscous flow in a cylindrical tube, the same technique as previously used, in the open channel case is applied. The only difference being the geometry of the problem. Viscous flow in a tube is characterised by a radial decreasing flow velocity, due to the boundary effect of the tube wall.

In the process of developing the continuity equation for this example, a thin layer, $dr$ of liquid is considered at a radius $r$, as shown in Fig. 6.4.

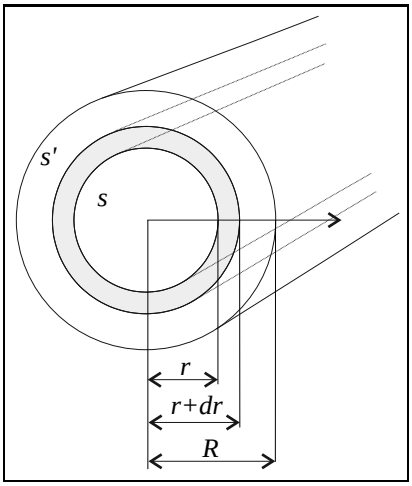


Figure 6.4: Cross-section of viscous flow through a cylindrical tube.

The momentum flux through the cylindrical volume, of length $\Delta l$, is written on differential form,

$$j_p S - j_p' S' = j_p 2\pi r \Delta l - j_p' 2\pi (r+dr)\Delta l = -\left(\frac{\partial j_p}{\partial r} + \frac{j_p'}{r}\right) 2\pi r dr \Delta l.$$

In this example, the flux area $S$ is varying and $S \neq S'$.

Defining the change in the momentum density inside the cylindrical volume; $2\pi r dr \Delta l$, as

$$\frac{\partial P}{\partial t} 2\pi r dr \Delta l,$$

the general equation for laminar flow in a tube is written,

$$\frac{\partial P}{\partial t} = -\left[\frac{\partial j_p}{\partial r} + \frac{j_p}{r}\right] + f. \tag{6.6}$$

In Eq. (6.6), the momentum intensity $j_p$ is substituted as defined in Eq. (6.2) and the Eq. (6.2) is redefined in accordance to the geometric conditions in our example,

$$j_p = -\mu \frac{\partial v_x}{\partial r}, \tag{6.7}$$

where the minus sign "-" is introduced because the flow velocity, $v_x$ is decreasing when the radius, $r$ is increasing.

Using this new definition, Eq. (6.7), the continuity equation for viscous flow in a cylindrical tube is written,

$$\frac{\partial v}{\partial t} = \frac{\mu}{\rho}\left(\frac{\partial^2 v}{\partial r^2} + \frac{1}{r}\frac{\partial v}{\partial r}\right) + \frac{f}{\rho}. \tag{6.8}$$

Solution of Eq. (6.8) under stationary conditions is a straight-forward calculation. At a constant pressure drop $\Delta p$ along the tube, no velocity variation is observed, i.e. $\partial v/\partial t = 0$. The somewhat simplified Eq. (6.8) is written,

$$\begin{aligned} \frac{\partial^2 v}{\partial r^2} + \frac{1}{r}\frac{\partial v}{\partial r} + \frac{f}{\mu} &= 0 \\ \Longrightarrow \qquad \frac{\partial}{\partial r}\left(r\frac{\partial v}{\partial r}\right) &= -r\frac{f}{\mu}. \end{aligned} \tag{6.9}$$

The general solution of Eq. (6.9) is found by integrating twice, resulting in,

$$v = -\frac{1}{4}\frac{f}{\mu}r^2 + C_1 \ln r + C_2 \tag{6.10}$$

The general constants in Eq. (6.10) are found by considering the boundary conditions, particular for this example, where the flow is directed along the x-axis:

1. Since the maximum flow velocity, $v_x(r=0)$ in the centre of the tube is obviously less than infinity ($\infty$); $C_1 = 0$.

2. Since the flow velocity is zero along the tube wall;
   $v_x(r=R) = 0$ and $C_2 = 1/4(f/\mu)R^2$.

The particular solution of Eq. (6.9) for viscous flow in a tube with a radius of R is then given as,

$$v = \frac{1}{4}\left(R^2 - r^2\right)\frac{f}{\mu} \tag{6.11}$$

If the outer force, driving the liquid through the tube is the pressure drop $\Delta p$ along a tube length $\Delta l$, i.e. $f = \Delta p/\Delta l$, the following equation can be written,

$$v = \frac{1}{4\mu}\left(R^2 - r^2\right)\frac{\Delta p}{\Delta l}. \tag{6.12}$$

Eq. (6.12) gives the velocity profile in the tube and defines the laminar viscous flow pattern. The flow, as shown in Fig. 6.5, is characterised by a parabola shaped velocity distribution where the maximum flow is reached in the tube centre.

The basic consideration behind these derivations is related to Eq. (6.2) and (6.7) where it is assumed a linear relation between momentum transfer and the flow velocity of adjacent layers. This type of flow is called laminar flow and is the kind of flow pattern one gets for Newtonian fluids at "normal" flow velocities.

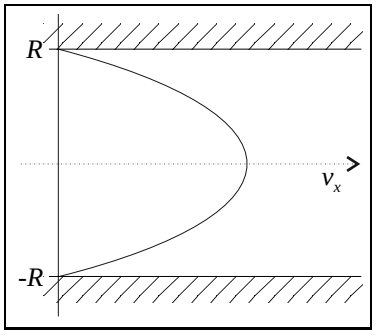


Figure 6.5: Velocity profile in cylindrical tube flow.

### 6.2.4 Viscous Flow Through a Porous Medium Made Up of a Bundle of Identical Ttubes

It follows from the results obtained above that the incremental flow rate through a fraction of the total cross-section of a capillary tube can be expressed as,

$$dq(r) = v(r) \cdot 2\pi r \cdot dr = \frac{2\pi r}{4\mu}\left(R^2 - r^2\right)\frac{\Delta p}{\Delta l}dr.$$

The total flow rate can be found by integration as shown in Fig 6.4,

$$q = \int_0^R \frac{dq}{dr}dr = \frac{\pi\Delta p}{2\mu\Delta l}\int_0^R (R^2 - r^2)dr = \frac{\pi R^4}{8\mu}\frac{\Delta p}{\Delta l}$$

For the sake of convenience we may present the last equation in the following form,

$$q = A\frac{R^2}{8\mu}\frac{\Delta p}{\Delta l}, \tag{6.13}$$

which is known as the *Poiseuille's equation*, where $A$ is the cross-section of the capillary tube.

Considering a porous medium as a bundle of identical capillary tubes, the total flow $q_p$ through the medium is defined,

$$q_p = \sum_i q_i = \sum_i A_i\frac{R_i^2}{8\mu}\frac{\Delta p}{\Delta l} = A\frac{k}{\mu}\frac{\Delta p}{\Delta l}, \tag{6.14}$$

where $A_i = \pi R_i^2$ is the capillary tube cross-section and $A$ is the cross-section of the porous medium.

From Eq. (6.14), the permeability of the medium where $n \times m$ capillary tubes are packed together is found,

$$k = \frac{\pi}{32}R^2 = \phi\frac{R^2}{8},$$

where the porosity of a bundle of capillary tubes is given by; $\phi = \pi/4$.

**Example: Capillary tube viscosity measurements.**

The fluid viscosity may also be estimated by measuring the volume of fluid flowing through a capillary tube pr. time, as shown in Fig. 6.6. Rewriting Eq. (6.13), an expression for the dynamic fluid viscosity is written,

$$\mu = \frac{\pi R^4}{8}\frac{\Delta p}{\Delta L}\frac{\Delta t}{\Delta V}.$$

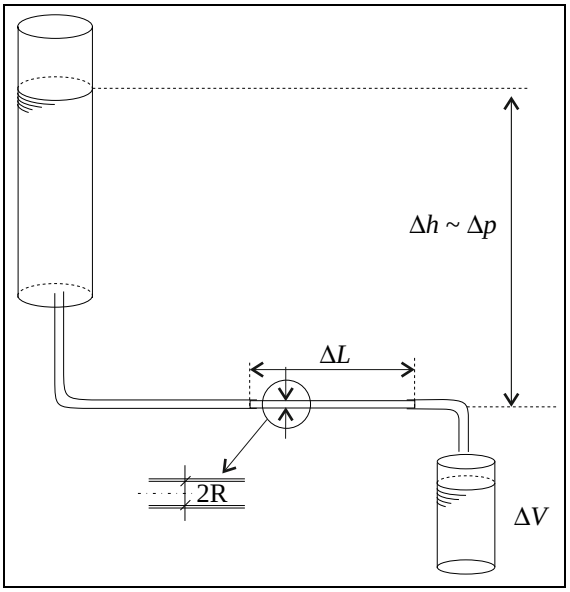


Figure 6.6: Capillary tube viscosity measurement.

For horizontal flow through a capillary tube of length $\Delta L$ and radius $R$, the time $\Delta t$ it takes to fill a certain volume $\Delta V$ is measured. The flow pressure $\Delta p$, is fixed during the process, e.g. by maintaining a constant fluid level at a certain elevation above the capillary tube.

The accuracy in these measurements is strongly related to the fabrication accuracy of the capillary tubes, as can be seen from the formula above. If the relative uncertainty is considered,

$$\frac{\Delta\mu}{\mu} = 4\frac{\Delta R}{R},$$

which means that if the relative accuracy in the tube-radius is $\pm$ 2–3%, then the relative accuracy in the viscosity is about $\pm$10%, i.e. a small variation in capillary tube fabrication induces large uncertainty in the viscosity measurements.

———— · ————

**Example: Rotating cylinder viscosity measurement.**

As yet an other example of the same ideas, the motion of a fluid between two coaxial cylinders is considered. Due to the elastic forces in the fluid, a viscous

shear will exist in the fluid at a certain radius distance between the two cylinders if one cylinder is rotating with an angular velocity and the other is kept constant, as seen in Fig. 6.7.

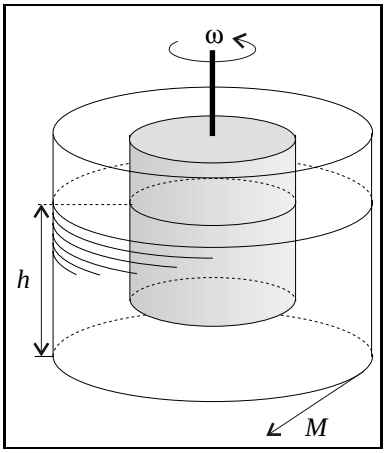


Figure 6.7: Rotating cylinder viscosity measurement.

If the inner cylinder, with a radius $r_{inner}$, is rotating with a constant angular velocity $\omega$ and the outer cylinder, with a radius $r_{outer}$, is held stationary by a spring balance which measures the torque (angular momentum) $M$ on it, the fluid viscosity is measured by the torque acting across the cylindrical surface.

Derivation of the formula for the torque is done in agreement with what is shown above,

$$M = 4\pi h\mu\omega\left(\frac{1}{r_{inner}^2} - \frac{1}{r_{outer}^2}\right)^{-1},$$

where $h$ is the fluid height level on the two cylinders.

For a certain viscometer, the viscosity as function of angular momentum and angular velocity is estimated,

$$\mu = C\frac{M}{\omega},$$

where $C$ is the characteristic constant for the viscometer.

———— · ————

## 6.3 Some Fluid Flow Characteristics

For laminar flow in a cylindrical tube we have derived *Poiseuille's equation,*

$$v = \frac{q}{A} = \frac{R^2}{8\mu}\frac{\Delta p}{\Delta l}. \tag{6.15}$$

For turbulent flow in a tube, an empirical law, called *Fanning's equation,* has been found ,

$$v^2 = \frac{R}{\rho F}\frac{\Delta p}{\Delta l},$$

where $F$ is the Fanning friction factor. This factor is dependent of the tube surface roughness, but also on the *flow regime* established in the tube.

The flow regime is again strongly correlated to the *Reynolds number*, which characterises the fluid flow in the tube. The Reynolds number, *Re* is defined as a dimensionless number balancing the turbulent and the viscous (laminar) flow, i.e. $(\Delta p/\Delta l)_T/(\Delta p/\Delta l)_L$,

$$Re = \frac{2Rv\rho}{\mu}. \tag{6.16}$$

In Eq. (6.16), $2R$ is the spatial dimension where the flow occur, i.e. the diameter of a capillary tube or the width of an open channel. $v$ and $\rho$ are respectively, the average flow velocity and density and $\mu$ is the fluid viscosity.

From experimental studies an upper limit for laminar flow has been defined at a Reynolds number; $Re = 2000$. Above this number, turbulent flow will dominate. (This limit is not absolute and may therefore change somewhat depending on the experimental conditions.)

In the case of porous flow, the velocity $v$ in Eq. (6.16) should be the pore flow velocity, where $v_{pore} = q/(\phi A(1-S_{or}))$ and $R$ is the pore radius.

The Reynolds number for flow in a porous medium is written,

$$Re = \frac{2v_B\rho}{\phi\mu(1-S_{or})},$$

where $v_B = q/A$ is the bulk velocity.

Typical parameters for laboratory liquid flow experiments are as follows,

| | | |
|---|---|---|
| $R$ | pore dimension | $10\ \mu\ m = 10\cdot 10^{-6}\ m$, |
| $v_B$ | bulk velocity | $1\ cm/s = 0.01\ m/s$, |
| $\rho$ | fluid density | $1.0\ g/cm^3 = 1000\ kg/m^3$, |
| $\phi$ | porosity | 0.25, |
| $\mu$ | viscosity | $1\ cP = 1\cdot 10^{-3}\ kg/m\cdot s$, |
| $S_{or}$ | residual oil saturation | 10%= 0.1 . |

Using the tabulated numbers above, we find a Reynolds number $Re \approx 1$, for laboratory core flow, which is far below the limit of turbulent flow.

In the case of reservoir flow, the "normal" reservoir flow velocity is approximately 1 foot/day or 3.5 $\mu m/s$, which indicates that turbulent liquid flow under reservoir conditions is not very likely to occur.

For a gas, turbulent flow may occur if the potentials are steep enough. If the formula for Reynolds number and Poiseuille's law Eq. (6.15) is compared,

$$Re = \frac{2Rk\Delta p}{\Delta l}\frac{\rho}{\mu^2},$$

where the only fluid dependent parameters are the density and the viscosity.

Comparing the Reynolds number for typical values of gas and oil gives,

$$\frac{Re_{gas}}{Re_{oil}} = \frac{(\rho/\mu^2)_{gas}}{(\rho/\mu^2)_{oil}} = \frac{0.2g/cm^3/(0.02cP)^2}{0.8g/cm^3/(2.0cP)^2} \approx 2500,$$

which demonstrates the possibilities for turbulence when gas is flowing in a porous medium (preferably near the well).

## 6.4 Dependency of Viscosity on Temperature

It is a well known fact that viscosity of liquids and gases depends on temperature. Viscosity of liquids decreases with respect to temperature while viscosity of gases increases.

The dependency of viscosity of gases on temperature can be expressed by the Satterland's equation,

$$\mu = K\frac{T^{3/2}}{T+C}, \tag{6.17}$$

where $K$ and $C$ are constants depending on the type of gas.

Another commonly used equation can be written as,

$$\mu = \mu_0(\frac{T}{T_0})^n, \tag{6.18}$$

where $n$ depends on the type of gas ($1 < n < 0.75$).

Liquids often show an exponential type of relationship between their viscosity and temperature, see Fig. 6.8 and Table 6.1.

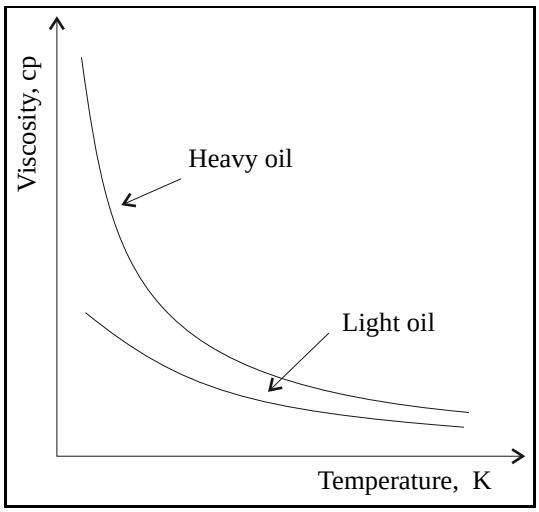


Figure 6.8: Relationship between viscosity of fluids and temperature.

## 6.5 Non-Newtonian Fluids

### 6.5.1 Viscous-Plastic Fluids

Rheology of viscous-plastic fluids was investigated by Bingham (1916) and Shvedov (1889) . The main feature of such fluids is that of elasticity in addition to viscosity. Rheology equation describing this distinguished characteristic can be presented in the following way:

$$\tau = \tau_0 + \mu' \frac{dv}{dy}, \text{ when } \tau > \tau_0. \tag{6.19}$$

Here $\tau_0$ is the breaking shear stress, $\mu'$ is the so-called structural viscosity. When $\tau < \tau_0$ , there is no fluid flow, i.e. the medium behaves as a solid body.

Some oils, drilling mud, and cement slurries represent viscous-plastic fluids.

### 6.5.2 Pseudo-Plastic Fluids

Some fluids do not have breaking shear stress but rather, their apparent viscosity depends on a shear rate:

$$\tau = k(\frac{dv}{dy})^n, n < 1$$

which means that their apparent viscosity

$$\mu = \frac{\tau}{dv/dy} = k(\frac{dv}{dy})^{n-1} \tag{6.20}$$

decreases when $dv/dy$ grows.

## 6.6 Exercises

1. Water at $20^oC$ is flowing through a pipe of radius 20 cm. If the fluid velocity in the centre of the pipe is 3 mm/s, what is the fluid velocity;

   a) 10 cm form the centre of the pipe (ie. halfway between the centre and the walls) ?

   b) at the walls of the pipe?

2. A viscous liquid flows through a tube with laminar flow. Prove that the volume rate of flow is the same as if the velocity were uniform at all points of a cross section and equal to half the velocity at the center of the tube.

3. Water at $20^oC$ is flowing in a horizontal pipe that is 15 m long. A pump maintains a gauge pressure at 800 Pa at a large tank at one end of the pipe. The other end of the pipe is open to air.

   a) The diameter of the pipe is 8 cm, what is the expected volumetric flow rate?

   b) What gauge pressure must the pump provide to achieve the same flow rate for a pipe with a diameter like 4 cm?

   c) For the pipe in part a), what does the volume flow rate become if the water is at a temperature of 60 $^oC$?

4. A copper sphere of mass 0.20 g is observed to fall with a terminal velocity of 0.08 m/s in an unknown liquid. If the density of copper is 8900 kg/m$^3$ and that of the liquid is 2800 kg/m$^3$, what is the viscosity of the liquid? Apply Stokes law.

5. Find the formula that describes the velocity distribution in the open flow case, $v_x(y)$. Assume maximum flow velocity, $v_m$ at maximum liquid (water) level, $y_m$.

6. Establish a correlation between the Reynolds number, *Re* and the Fannings factor, $F$. Use the two equations for laminar and turbulent flow.

**Answers to questions:**

1. a) $v = 2.25m/s$, b) $v = 0$, 3. a) $q = 53.6l/s$, b) $\Delta p = 12800Pa$, c) $q = 116.5l/s$,
4. $\mu = 509cp$,

# Chapter 7

# Wettability and Capillary Pressure

## 7.1 Introduction

The exploitation of hydrocarbons is a complex process of controlling interactions in systems involving crude oil, water, gas and rock formations. In such complicated systems, it is important to recognise the effect of the surface properties of oil/rock, water/rock and, in combination, the interface oil/water. A central property, when giving an overall picture of the interfacial conditions, is the *surface* or *interfacial tension* (or more correctly the surface or interfacial *energy*). This property is very sensitive to chemical changes at the interface.

In this chapter, the interaction between wettability and surface tension is revealed. Due to the great significance of the surface/interfacial tension, several experimental methods have been developed in order to measure this physical property. Some of the most commonly used techniques are reviewed.

## 7.2 Surface and Interfacial Tension

An interface is known as the boundary region between two adjacent bulk phases. The equilibrium bulk phases can be:

- Liquid-vapor (LV).
- Liquid-liquid (LL).
- Liquid-solid (LS).
- Solid-vapor (SV).

(Gases are basically miscible and thus, no interfacial tension is observed between gases.)

Any surface that is in the state of lateral tension, leads to the concept of *surface tension*. For curved interfaces, the definition is similar but slightly more complex. The surface tension, denoted by $\sigma$, can be related to the work or energy required to establish the surface area.

If two fluids, say water and oil is forming an interface, as seen in Fig. 7.1, the molecules attached to the oil-water interface do necessarily have less kinetic energy than the bulk molecules, on average. The molecules on or close to the interface may not move with the same degree of freedom and speed, due to the constraint put on them by the interface. Since the total energy of

the molecules is mainly a function of temperature, the potential energy of molecules attached to the interface is greater than the potential energy of the bulk molecules.

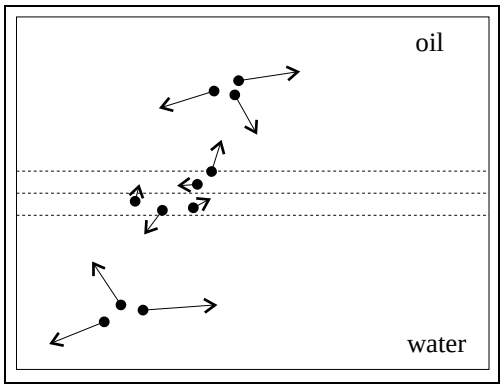


Figure 7.1: Molecular motion in bulk and close to the oil-water interface.

Generally speaking, a molecule at a surface is in a state of higher potential energy than a bulk molecule, due to anisotropy and intermolecular interactions. This means that energy is required to move a molecule from the interior to the surface of a phase, i.e., to increase the surface area of the system. Since a proportionality exist between surface area and potential energy of the system of molecules and since equilibrium is reached at minimum potential energy (actually minimum Gibbs energy), the surface area of a system is always minimised.

Keeping the temperature, pressure and amount of material in the system constant, the following expression for surface tension may be written,

$$\sigma = \left(\frac{\partial G}{\partial A}\right)_{T,p,n_i}. \tag{7.1}$$

Here $G$ is the Gibbs free energy and $A$ is the surface area. The unit of surface tension is therefore, the unit of energy pr. area, i.e., $J/m^2$ or more commonly $N/m$. Note, that what is called surface or interface *tension* is in fact surface or interface *energy* and quite often it is more advantageous to use the energy perspective than it is to deal with tension and forces.

The surface tension between a pure liquid and its vapour phase is usually in the range of 10 to 80 m$N/m$. The stronger the intermolecular attractions in the liquid, the greater is the work needed to bring bulk molecules to the surface, i.e., the larger is the interfacial tension $\sigma$. In Table 7.1 some typical values for surface - and interfacial tensions are listed.

## 7.3 Rock Wettability

Laboratory experiments have proved that rock wettability affects oil displacement. The term *wettability* can be defined as "the tendency of one fluid to spread or to adhere to a solid surface in the presence of other immiscible fluids" [29].

The evaluation of reservoir wettability can be made through measurements of interfacial tensions, i.e., tensions acting at the fluid-fluid and rock-fluid interfaces, and the *contact angle*. Note that wettability itself is a microscopic characteristic, that has to be measured by using micro-scale laboratory investigation techniques.

Table 7.1: Surface tension, $\sigma_{LV}$ and interfacial tension to water, $\sigma_{LW}$ for some liquids at temperature, T = 293$^o$K. Note: Surface tension $\sigma_{LV}$, is here defined as the interfacial tension between a liquid and its vapor.

| Liquid | $\sigma_{LV}$ (m$N/m$) | $\sigma_{LW}$ (m$N/m$) |
|---|---|---|
| Water | 72.8 | – |
| n-octane | 21.7 | 51.7 |
| n-dodecane | 25.4 | 52.9 |
| n-hexadecane | 27.5 | 53.8 |
| dichoromethane | 28.9 | 27.7 |
| benzene | 28.9 | 35.0 |
| mercury | 476.0 | 375.0 |

The angle $\theta$ is influenced by the tendency of one of the fluids, i.e. water, of the immiscible pair, to spread on the pore wall surface in preference to the other (oil). The qualitative recognition of preferred spread is called a wettability preference, and the fluid which spreads more is said to be the wetting phase fluid. Contact angles are measured, by convention, through the fluid whose wettability is studied or through the fluid which is wetting the solid surface. A table of typical fluid pairs of interest in reservoir engineering is shown in the Table 7.2, together with contact angles and interfacial tensions [8].

Table 7.2: Fluid pair wettability under reservoir and laboratory conditions.

| **System** | | **Conditions** | | |
|---|---|---|---|---|
| Wetting phase | Non-wetting phase | T = temperature P = pressure | $\theta$ | $\sigma$ (dynes/cm) |
| Brine | Oil | Reservoir, T, P | 30 | 30 |
| Brine | Oil | Laboratory, T, P | 30 | 48 |
| Brine | Gas | Laboratory, T, P | 0 | 72 |
| Brine | Gas | Reservoir, T, P | 0 | (50) |
| Oil | Gas | Reservoir, T, P | 0 | 4 |
| Gas | Mercury | Laboratory, T, P | 140 | 480 |

The degree of wettability exhibited, depends both on the chemical compositions of the fluid pair, particularly the asphaltine content of the oil, and on the nature of the pore wall. Pure quartz sandstone or calcite surfaces are likely to be wetted preferentially by water. The presence of certain authigenic clays, particularly chamosite, may promote oil wet character.

The differences in contact angle somehow indicate different wettability preferences which

can be illustrated by the following rule of thumb presented in Table 7.3 and in Fig. 7.2 [19].

Table 7.3: Wettability preference expressed by contact angle.

| Contact angle values | Wettability preference |
|---|---|
| 0 – 30 | Strongly water wet |
| 30 – 90 | Preferentially water wet |
| 90 | Neutral wettability |
| 90 – 150 | Preferentially oil wet |
| 150 – 180 | Strongly oil wet |

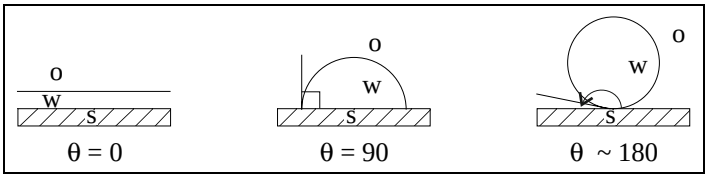


Figure 7.2: Example of wetting preference.

## 7.4 Contact Angle and Interfacial Tension

With two immisible fluids (oil and water) present in the reservoir, there are three interfacial tension parameters to be assessed; $\sigma_{os}$, $\sigma_{ws}$ and $\sigma_{wo}$. The three interfacial tension are not independent parameters, and in order to reveal the relationship between them a "gedanken" experiment is carried out on a droplet of water, surrounded by oil, placed in a contact with a water-wet reservoir rock, as seen in Fig. 7.3.

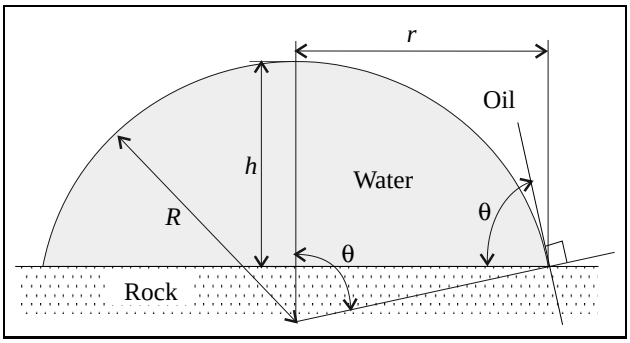


Figure 7.3: Geometry of the water droplet in oil, placed in a contact with a water-wet reservoir rock.

The following definitions will be used:

- surface tension between the oil and solid; $\sigma_{os}$,

- surface tension between the water and solid; $\sigma_{ws}$,
- interfacial tension between the oil and water phases; $\sigma_{ow}$,
- contact angle at the oil-water-solid interface measured through the water; $\theta$,
- surface area of the water droplet; $A_d$,
- area of the reservoir rock occupied by the water droplet; $A_s$.

The water droplet is assumed to be in equilibrium with the surrounding medium. A small deformation of the surface area, will deform the droplet slightly and force the droplet to expand on the solid surface. The deformation is described by the equilibrium equation, expressing the change in energy due to the change in area.

$$\sigma_{ws} dA_s + (-\sigma_{os} dA_s) + \sigma_{ow} dA_d = 0 \tag{7.2}$$

Elaborating on Eq. (7.2), the following relationships are valid (see also Fig. 7.3),

$$\begin{array}{lll} A_s = \pi r^2 & \Rightarrow & dA_s = 2\pi r dr \\ A_w = \pi(r^2 + h^2) & \Rightarrow & dA_w = 2\pi(r dr + h dh) \\ V_w = \frac{\pi h}{6}(3r^2 + h^2) & & \end{array}$$

Incompressible liquids give,

$$dV_w = \frac{\partial V_w}{\partial r} dr + \frac{\partial V_w}{\partial h} dh = 0,$$

which leads to

$$dh = -\frac{2rh}{h^2 + r^2} dr.$$

Using these results, Eq. (7.2) is rewritten,

$$\sigma_{ws} - \sigma_{os} + \sigma_{ow} \left(1 - \frac{2h^2}{h^2 + r^2}\right) = 0, \tag{7.3}$$

and taking into account that (see Fig. 7.3),

$$\begin{array}{l} R\sin\theta = r \\ R\cos\theta = R - h \end{array}$$

and

$$(1 - \frac{2h^2}{h^2 + r^2}) = \cos\theta,$$

a final result is obtained,

$$\sigma_{os} - \sigma_{ws} = \sigma_{ow} \cos\theta, \tag{7.4}$$

which is known as the Young-Dupre equation [15].

## 7.5 Capillary Pressure

Capillary pressure may be defined as the pressure difference across a curved interface between two immiscible fluids. By convention, the $P_c$ term is positive for unconfined immiscible fluid pairs, where $P_c$ is defined as the pressure difference between the non- wetting and the wetting phase.

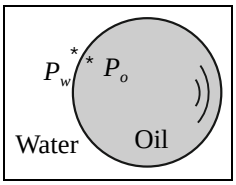


Figure 7.4: Pressure difference across a curved (spherical) interface.

Using an example with an oil drop floating in water where the density of oil and water are assumed similar, as seen in Fig. 7.4, the capillary pressure is written,

$$P_c = p_o - p_w.$$

If the droplet is small, one may assume the interfacial tension to be far more important than the gravitational force acting on the droplet and thus, since the surface area is minimised, the droplet takes the form of a perfect sphere. A small perturbation, i.e. a small reduction of the sphere volume, is described by an equation taking into account the energy change due to the volume and the surface change. The equilibrium condition is ecpressed as the change in potential and surface energy,

$$p_w dV + \sigma_{ow} dA = p_o dV.$$

Substituting definition of the capillary pressure $p_c$, in the latter equation, one we successively obtain,

$$P_c = \sigma_{ow}\frac{dA}{dV} = \sigma_{ow}\frac{dA}{dr}\left(\frac{dV}{dr}\right)^{-1} = \sigma_{ow}\frac{8\pi r}{4\pi r^2} = \sigma_{ow}\frac{2}{r}.$$

Capillary pressure can be of significant magnitude, since this is the energy needed to form a droplet that can pass through a porous channel . Taking typical values of a pore radius and an interfacial tension of oil and water, the capillary pressure can be obtained by the following evaluation:

$$r \sim 1\mu m \text{ and } \sigma_{ow} = 0.025\frac{N}{m} \Rightarrow P_c \simeq \cdot 10^4 \frac{N}{m^2} = 0.5\, bar$$

### 7.5.1 Capillary Pressure Across Curved Surfaces

For two immiscible liquids as part of a real physical system, a spherical interface is an odd observation. Normally, a curved surface is characterised by two radii of curvature; $R_1$ and $R_2$, as seen in Fig 7.5.

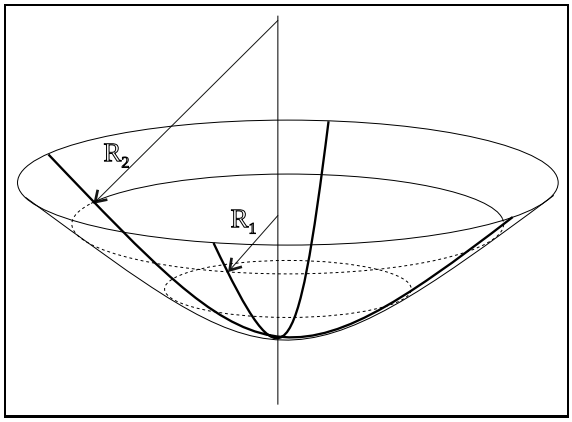


Figure 7.5: Curved surface and radii of curvature.

With a pressure difference across the interface in the two phases, the interface will show a net curvature with the larger pressure on the concave side. The relationship between the pressure difference $\Delta p = P_c$ and the curvature is given by Laplace equation,

$$P_c = \sigma \left( \frac{1}{R_1} + \frac{1}{R_2} \right), \tag{7.5}$$

where $R_1$ and $R_2$ are the principal radii of curvature and $\sigma$ is the interfacial tension. For a spherical droplet $R_1 = R_2 = r$ and $\Delta p = 2\sigma/r$. Across a planar interface/surface $R_1 = R_2 = \infty$ and $\Delta p = 0$.

**Example: Surface tension and surface energy**

The process of displacing water through a porous medium is comparable to the formation of droplets of sizes equal to the capillary pore throats.

What is then the energy needed to transform 1 $cm^3$ of pure water to droplets with an average radius of 1 $\mu m$, when the surface tension of water to vapor is 0.073 m$N/m$?

The energy in question, is the energy needed to increase the initial water surface $A$, of the initial volume $V$ to $N$ number of droplets with area, $A_d$ and volume ,$V_d$.

The area increase is,

$$\Delta A = N \cdot A_d - A = \frac{V}{V_d} A_d - A = \frac{3}{r} V - A,$$

where the droplet area and volume are respectively; $4\pi r^2$ and $(4/3)\pi r^3$.

Since the increased area $\Delta A$ is directly proportional to the increase in potential energy $\Delta E_p$, which can be expressed by Eq. (7.1),

$$\Delta E_p = \sigma_{air,w} \Delta A = \sigma_{air,w} \left( \frac{3}{r} V - A \right).$$

If the initial water area is considered to be small (or negligible) to the area of the droplets, a potential energy equal to about 0.22 $J$ is found.

### 7.5.2 Interfacial Tension

Assuming pairs of immicsible unconfined fluids the following phenomena, as illustrated in Fig. 7.6 can be observed, depending on the sign of interfacial tension:

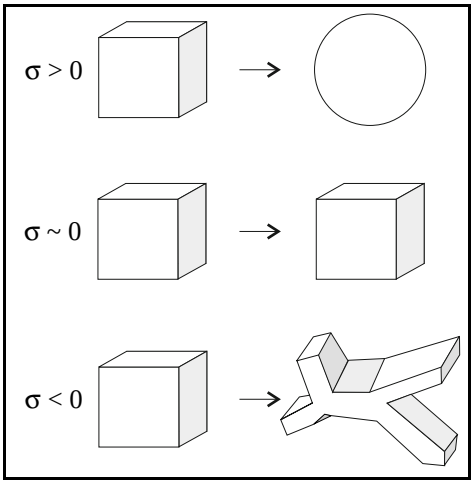


Figure 7.6: Formation of interface as function of the sign of the interfacial tension in pairs of immicsible unconfined fluids.

- When the surface tension is positive, $\sigma > 0$, confined molecules, have a preference for keeping their own company. The surface against the second type of molecules is minimised and in the case of small droplets, spherical interfaces are formed.

- In the cases when $\sigma \approx 0$, liquids are classified as "truely" miscible. In these cases no preference with respect to mixing of the two fluids is observed. (However, diffusion will lead to mixing of the two fluids.)

- When the surface tension is negative, $\sigma < 0$, molecules of one type will prefer (have affinity for) the company of the second type of molecules. We may observe a chemical reaction where the final state is stable in time. An example of such a process is the hydrophilic ability of pure ethanol to mix with air more or less instantaneously.

### 7.5.3 Capillary Pressure in a Cylindrical Tube

When a non-wetting fluid is displacing a wetting fluid, as is the case when oil is displacing water in a water-wet porous rock, a curved interface is formed in the capillary tube. To reveal the relation between the capillary pressure, the interfacial tension and the radius in a cylindrical tube, two immiscible fluids (oil + water) are confined in a cylindrical capillary of radius $r_c$, as shown in Fig. 7.7.

Using the Eq. (7.5) for the pressure difference between the two sides of the interface,

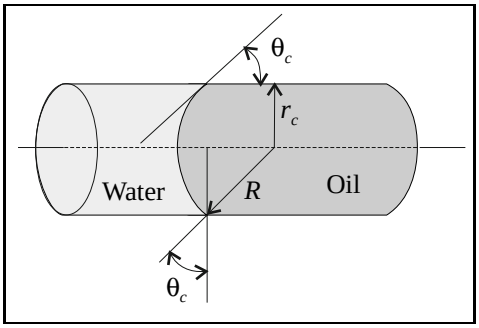


Figure 7.7: Idealised model of a pore channel filled with two immiscible fluids forming a curved interface between them.

$$p_o - p_w = \sigma_{ow}\left(\frac{1}{R_1}+\frac{1}{R_2}\right),$$

where $R_1$ and $R_2$ are main radii of the curvature, expressing the radius of the interfacial surface $R$ by means of the contact angle $\theta_c$ and the capillary radius $r_c$ in the cylindrical tube. When $R_1 = R_2 = R$ and

$$R = \frac{r_c}{\cos\theta_c},$$

the capillary pressure is written,

$$P_c = p_o - p_w = \sigma_{ow}\left(\frac{1}{R_1}+\frac{1}{R_2}\right) = \frac{2\sigma_{ow}\cdot\cos\theta_c}{r_c}, \tag{7.6}$$

where Eq. (7.6) is the capillary pressure in a cylindrical tube of radius $r$.

**Example: Oil - water displacement in a capillary tube**

Displacement processes in porous media are very often a competition between viscous- and capillary forces. In this example, the process by which oil displaces water in a cylindrical tube is considered in analogy with the production of oil from a water-wet reservoir where oil is forced through capillary pores which initially contained water.

Consider a dynamical situation, as sketch in Fig. 7.8 where the oil front has reached a position $x$ in to the cylinder (pore). The pressure drop along the cylindrical tube is partly the viscous pressure drop $\Delta p_o + \Delta p_w$, in the oil- and water zone and partly the capillary pressure drop, $P_c$ across the oil-water interface:

$$\begin{aligned}\Delta p_V &= \Delta p_o + \Delta p_w = \frac{q}{Ak}\left[\mu_o x + \mu_w (L-x)\right],\\ P_c &= \frac{2\sigma_{ow}\cos\theta}{r}.\end{aligned}$$

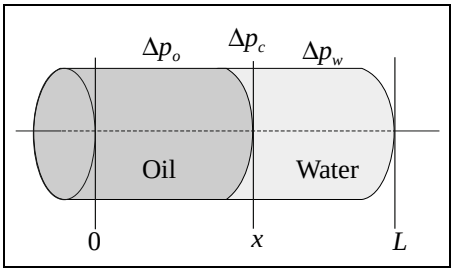


Figure 7.8: Cross-section view of a cylindrical "pore channel".

The flow rate is $q = Av$, where $A$ and $v$ is respectively the cross-section area and the pore velocity. The permeability of the tube is known as, $k = r^2/8$, and $r$ is the tube radius.

The strength between the two forces is considered by simply comparing their pressure drops,

$$\frac{\Delta p_V}{P_c} = 4\left[\frac{v\mu_o}{\sigma_{ow}\cos\theta}\frac{x}{r} + \frac{v\mu_w}{\sigma_{ow}\cos\theta}\frac{L-x}{r}\right].$$

In the equation above, the relation $v\mu/(\sigma\cdot\cos\theta)$ is the only term containing dynamical parameters. In analogy with the definition of Reynolds number, a dimension-less number could be defined,

$$N_c = \frac{v\mu}{\sigma\cos\theta}.$$

The *Capillary number* $N_c$, describes the competition between the viscous- and the capillary force.

In a situation where the two forces are assumed to be equally important, i.e. $\Delta p_v/P_c \sim 1$, a set of "typical values" could be chosen and the average pore velocity is found,

$$\left.\begin{array}{l}\Delta p_V/P_c = 1\\ \theta = 60^o\\ L/r = 5\\ \mu_o \approx \mu_w = 1\,\mathrm{m}Pa\cdot s\\ \sigma_{ow} = 50\,\mathrm{m}N/m\end{array}\right\} \quad v_{pore} \approx 1.3\,m/s.$$

Reservoir flow is commonly considered to be of the order of 1 foot pr. day, which is equal to 3.5 $\mu m/s$. From this comparison , it is obvious (even when the appropriate bulk velocity $u = v_{pore}/(\phi(1-S_r)\cos^2\alpha)$ is taken into account) that under reservoir flow conditions, capillary forces are totally predominant and that viscous forces play a minor role when microscopic flow pattern is considered. This means that the capillary forces alone decide which pore channels are going to be swept and which are not, in the reservoir.

The Capillary number for reservoir flow becomes $N_c = 1.5\cdot 10^{-5}$ (using the numbers above), while the Capillary number at the "breaking point" when the viscous force becomes equally important to the capillary force is $8\cdot 10^{-3}$.

The capillary number for field water-floods ranges from $10^{-6}$ to $10^{-4}$. Laboratory studies have shown that the value of the Capillary number is directly related to the ultimate recovery of oil, where an increase in the Capillary number implies an increase in the oil recovery. The Capillary number is generally varied by increasing the flow rate (pore velocity) and/or lowering the interfacial tension.

## 7.6 Capillary Pressure and Fluid Saturation

Results from drainage and imbibiation laboratory experiments have shown that the capillary pressure $P_c = p_o - p_w$ is dependent on the following parameters (see Fig. 7.9):

- surface tensions; $\sigma_{os}$, $\sigma_{ws}$ and $\sigma_{ow}$,
- contact angle measured through the water phase; $\theta_c$,
- rock porosity; $\phi$,
- rock permeability; $k$,
- fluid saturations; $S_w$ and $S_w$

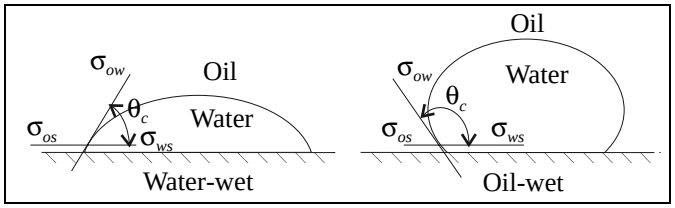


Figure 7.9: Wettability of oil-water-solid system.

The task is to define (if possible) a correlation between capillary pressure $P_c$ and the parameters, mentioned above, being responsible for the numeric variation of the capillary pressure in the experiments.

Relying upon the data obtained, the following dependency can be expressed,

$$P_c = f(\phi,\ k,\ \sigma_{os},\ \sigma_{ws},\ \sigma_{ow},\ \theta_c,\ S_o,\ S_w) \tag{7.7}$$

Since some of the parameters are dependent on others,

$$\begin{aligned} S_o &= 1 - S_w, \\ \sigma_{os} - \sigma_{ws} &= \sigma_{ow} \cdot \cos\theta_c, \end{aligned}$$

the list of independent parameters is shortened and Eq. (7.7) is written;

$$P_c = f(\phi,\ k,\ \sigma_{ow} \cdot \cos\theta_c,\ S_w) \tag{7.8}$$

A dimensional analysis of Eq. (7.8) can be carried out using the following notation for dimensions,

$$\text{M – mass,} \quad \text{L – length,} \quad \text{and T – time,}$$

which gives the following dimensions for all the parameters in Eq. (7.8):

$$\begin{array}{lll} [P_c] = M \cdot L^{-1} \cdot T^{-2}, & [k] = L^2, & [\sigma_{ow} \cdot \cos\theta_c] = M \cdot T^{-2}, \\ [\phi] = 1, & [S_w] = 1 & \end{array} \tag{7.9}$$

Comparing all the parameters of the right-hand side of Eq. (7.8), it appears that both dimension parameters $k$ and $\sigma_{ow}$ have independent dimensions. This means that dimension of the capillary pressure can be defined through dimensions of those parameters, i.e.,

$$[P_c] = [k]^{\alpha} \cdot [\sigma_{ow} \cdot \cos\theta_c]^{\beta}.$$

Using notation (7.9), the last relation is written in the form,

$$M \cdot L^{-1} \cdot T^{-2} = L^{2\alpha} \cdot M^{\beta} \cdot T^{-2\beta},$$

which is followed by,

$$\begin{array}{rrcrcl} M: & 1 & = & \beta, & & \\ L: & -1 & = & 2\alpha, & \Rightarrow & \alpha = -1/2 \text{ and } \beta = 1. \\ T: & -2 & = & -2\beta, & & \end{array}$$

Thus, a dimension-less parameter $F$ can be composed,

$$F = \frac{P_c}{\sigma_{ow} \cdot \cos\theta_c} \cdot \sqrt{k},$$

and by making use of this result, Eq. (7.8) can be rewritten in dimension-less form,

$$F = F(\phi,\, S_w),$$

or using the initial notation,

$$P_c = \frac{\sigma_{ow} \cdot \cos\theta_c}{\sqrt{k}} \cdot F(\phi,\, S_w).$$

It can be shown that parameters $\phi$ and $S_w$ and their functions, can only appear in correlations where they form a product,

$$P_c = \frac{\sigma_{ow} \cdot \cos\theta_c}{\sqrt{k}} \cdot F_1(\phi) \cdot F_2(S_w) \tag{7.10}$$

Thus by using the dimension analysis (the $\pi$-theorem) [11], the number of independent variable parameters is reduced and an almost exact form of the correlation between the capillary pressure $P_c$, fluids and rock parameters is obtained.

The following correlation is widely used for reservoir simulation tasks [13, 15],

$$P_c = \frac{\sigma_{ow} \cdot \cos\theta_c}{\sqrt{(k/\phi)}} \cdot J(S_w), \tag{7.11}$$

where $J(S_w)$ is known as the $J$-function (after Leverett).

## 7.7 Pore Size Distribution

It is obvious that the capillary pressure is strongly affected by the distribution of pore channel sizes, represented by the $1/r$ relationship. The capillary pressure does also represent the response of interfacial tensions and rock wettability. Generally, is the capillary pressure characteristic of the reservoir heterogeneity.

To reveal the relation between the capillary pressure and the microscopic heterogeneity of the reservoir, the following example is considered: An idealised model of the porous medium consisting of cylindrical capillaries with different radii $r_i$, where all pore channels have the same type of wettability and, as a consequence, a fixed contact angle $\theta$. It is also assumed, that a certain invariant distribution-function $\chi(r)$ defines a fraction of pore channels with capillary radii belonging to the interval $(r, r+dr)$ as,

$$\chi(r) = \frac{n(r, r+dr)}{N},$$

where N is the total number of pore channels.

Let $V_i$ be the pore volume of a single capillary with radius $r_i$ and $V$ be the total pore volume of the porous medium considered, i.e.,

$$V = \sum_{i=1}^{N} V_i.$$

Now let us consider a process of imbibition for a strongly water-wet rock initially saturated with oil, as shown in Fig. 7.10.

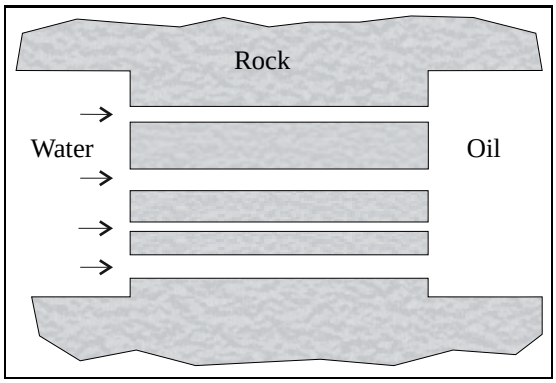


Figure 7.10: Illustration of imbibition process in an idealised model of porous medium.

Assume that at the starting point, the pressure in the oil phase $p_o$, is high enough to protect the water invading the pore channels. Then gradually decreasing the outlet pressure (pressure in the oil phase), the water will invade the pores. It is quite obvious that the water enters only those capillary channels with capillary pressure $P_c$, exceeding the difference between the outlet and inlet pressure $\Delta p_o(t)$. Hence, at a certain time only those channels will be filled with water, which satisfy the condition,

$$P_c \geq \Delta p_o(t),$$

or, substituting Eq. (7.6) into the last inequality,

$$r_c \leq \frac{2\sigma_{ow}\cos\theta_c}{\Delta p_o(t)}.$$

Then the volume of water which has invaded the porous medium can be defined as,

$$V_c = N\int_0^{r_c} \chi(r)\pi r^2 l dr,$$

where $l$ is the length of a single pore channel.

Defining the total pore volume as,

$$V = N\int_0^{\infty} \chi(r)\pi r^2 l dr,$$

the relations between the water saturation $S_w$, and the capillary pressure $P_c$, is

$$\begin{aligned} S_w &= \frac{V_c}{V} = \frac{\int_0^{r_c}\chi(r)r^2dr}{\int_0^{\infty}\chi(r)r^2dr}, \text{ and} \\ P_c &= \frac{2\sigma_{ow}\cdot\cos\theta_c}{r_c}, \end{aligned} \tag{7.12}$$

which explicitly indicates that microscopic reservoir heterogeneity strongly affects the capillary pressure.

Since the pore size distribution varies between the different layers in a reservoir, it is expected that the capillary pressure curve shape will also vary from layer to layer. This phenomenon is frequently observed in laboratory tests, by using a mercury injection technique, on core samples taken from different elevations in the same well.

**Example: Pore size distribution and capillary pressure curve**

In this example, it will be shown how data from a mercury drainage experiment could be used to produce a capillary pressure curve and how these data could be used further, to define the pore size distribution for the core sample tested.

First, the core sample is properly cleaned, dried and placed in vacuum for some time, before it is sealed in a mercury pycnometer. A series of $N+1$, representative pressure measurements $p_i$, is recorded inside the pycnometer and the injection volume $V_i$ is read as the pore sample is invaded by more and more mercury. The experimental data is as follows:

| $p_{Hg}$ | $p_0$ | $p_1$ | $p_2$ | $p_3$ | $\cdots$ | $p_N$ |
|---|---|---|---|---|---|---|
| $V_{Hg}$ | $V_0$ | $V_1$ | $V_2$ | $V_3$ | $\cdots$ | $V_N$ |

The capillary pressure $P_c$, is here the pressure difference between the mercury pressure $p_{Hg}$, and the gas pressure in the core sample $p_g$,

$$P_c = p_{Hg} - p_g = \frac{2\sigma\cos\theta}{r}.$$

The gas is the wetting phase since mercury definitely does not wet any core sample. The wetting saturation is therefore written,

$$S_g = 1 - S_{Hg} = \frac{V_N - V_i}{V_N - V_0}.$$

Based on the data in the table above, the following parameters are calculated,

| $S_g$ | 1 | $S_1$ | $S_2$ | $S_3$ | $\cdots$ | 0 |
|---|---|---|---|---|---|---|
| $r$ | $r_0$ | $r_1$ | $r_2$ | $r_3$ | $\cdots$ | $r_N$ |
| $P_c$ | $P_{c,0}$ | $P_{c,1}$ | $P_{c,2}$ | $P_{c,3}$ | $\cdots$ | $P_{c,N}$ |

The pore size distribution $D(r)$ is representing the relative increase in pore volume as function of the pore throat radius,

$$D(r) \stackrel{def}{=} -\frac{1}{\Delta V}\frac{dV}{dr},$$

where $\Delta V = V_N - V_0$ and $dV = V_i - V_{i-1}$, taken from the above tabulated data. The minus sign "-" is added due to convenience.

The pore size distribution is then rewritten,

$$D(r) = -\frac{1}{\Delta V}\frac{1}{dr}\frac{\partial V}{\partial S}\frac{\partial S}{\partial P_c}dP_c.$$

Remembering the definition of the wetting phase saturation $S_g = (V_N - V)/(V_N - V_0)$, one may write,

$$\frac{\partial S}{\partial V} = -\frac{1}{\Delta V} \qquad \Rightarrow \qquad \frac{\partial V}{\partial S} = -\Delta V,$$

and by substituting in the pore size distribution equation, one gets,

$$D(r) = \frac{1}{dr}\frac{dP_c}{(\partial P_c/\partial S)}.$$

Using the definition of the capillary pressure $P_c = 2\sigma\cos\theta/r$, gives

$$dP_c = \frac{\partial P_c}{\partial r}dr = -\frac{P_c}{r}dr.$$

Substituting this last expression into the pore size distribution, one gets,

$$D(r) = -\frac{P_c}{r}\frac{1}{(\partial P_c/\partial S)}.$$

Fig. 7.11 shows the two curves for the capillary pressure and the pore size distribution, respectively. When $P_c(S_g)$ is known, then $D(r)$ can be calculated, using the following steps.

1. For a certain gas saturation $S_g$, the corresponding capillary pressure $P_c(S_g)$ is calculated.

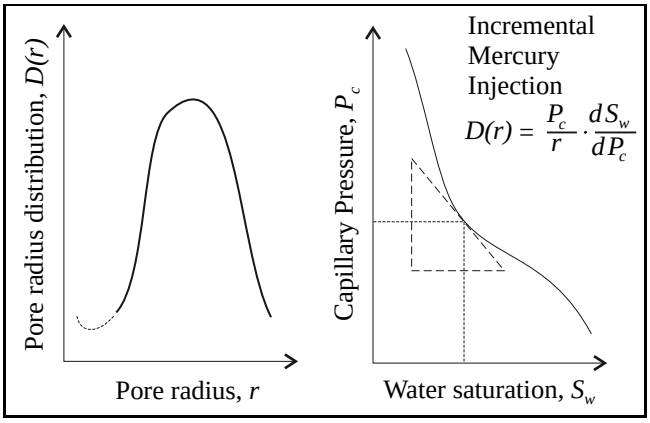


Figure 7.11: Capillary pressure curve and corresponding pore size distribution [8].

2. The pore radius related to this pressure is $r = 2\sigma\cos\theta/P_c$.
3. The tangent to the curve $P_c(S_g)$ through the co-ordinate $(S_g, P_c(S_g))$ gives the slope defined by $\partial P_c/\partial S$.

In Fig. 7.11 the pore size distribution is drawn in accordance with the enumerated list.

## 7.8 Saturation Distribution in Reservoirs

The equilibrium fluid saturation distribution in a petroleum reservoir, prior to production is governed by the pore space characteristics. This is as a result of the non-wetting phase, normally hydrocarbons, entering pore space initially occupied by the wetting fluid, normally water, during migration of hydrocarbons from a source rock region into a reservoir trap. A pressure differential is required for the non-wetting phase to displace wetting phase and this is equivalent to a minimum threshold capillary pressure and is dependent on pore size.

The physical significance of threshold pressure in an oil reservoir may be appreciated by the analogy with a capillary rise of water in different vertical glass tubes suspended in an open tray of water, as seen in Fig. 7.12. Since $P_c \propto 1/r$ it is observed that entry of the non-wetting phase should be most difficult in the smallest tube (highest threshold pressure). For a water-air system, the following relation exist,

$$P_c = g\rho_w h, \Rightarrow P_{c(3)} > P_{c(2)} > P_{c(1)} \text{ where } r_3 < r_2 < r_1.$$

The threshold capillary pressure, found in reservoir is proportional to the height above the free water level (FWL), where a 100% water saturation is found.

The FWL is a property of the reservoir system, while an oil-water contact observed in a particular well will depend on the threshold pressure of the rock type present in the vicinity of the well.

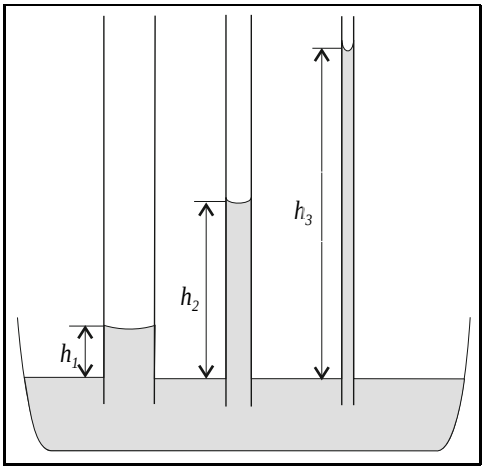


Figure 7.12: Capillary water elevation in cylindrical tubes as function of tube radii.

The relation between height above the free water level and the capillary pressure is derived from consideration of the gravity-capillary pressure force equilibrium. Using a free water level as the datum plane and defining its position in the reservoir as the place where the oil phase pressure $p_o$ equals the water phase pressure $p_w$, one obtains,

$$P_{c(FWL)} = p_o - p_w = 0.$$

At some height $h$, above FWL, the pressures are,

$$p_o = p_{FWL} - \rho_o g h$$
$$p_w = p_{FWL} - \rho_w g h$$

Therefore, the capillary pressure at a depth equivalent to $h$ above the FWL is,

$$P_c = p_o - p_w = (p_{FWL} - \rho_o g h) - (p_{FWL} - \rho_w g h) = gh(\rho_w - \rho_o)$$

Since $P_c = P_c(S_w,\ r)$ there exist a dependence,

$$h = h(S_w,\ r),$$

which indicated that saturation at height $h$, will depend on both the water saturation and the pore radius (see example: "Equilibrium in a capillary channel"),

$$h_{S_w} = \frac{2\sigma_{ow}\cos\theta_c}{rg(\rho_w - \rho_o)}.$$

Similarly, the threshold height $h_t$ is equivalent to the height of an observed water-oil contact above FWL. In a particular rock type, this height is given,

$$h_t = \frac{P_{ct}}{g(\rho_w - \rho_o)}.$$

In real reservoir systems it is expected that a number of rock type units or layers will be encountered. Each unit can have its own capillary pressure characteristic and the static saturation distribution in the reservoir will be a superposition of all units, as seen in Fig. 7.13.

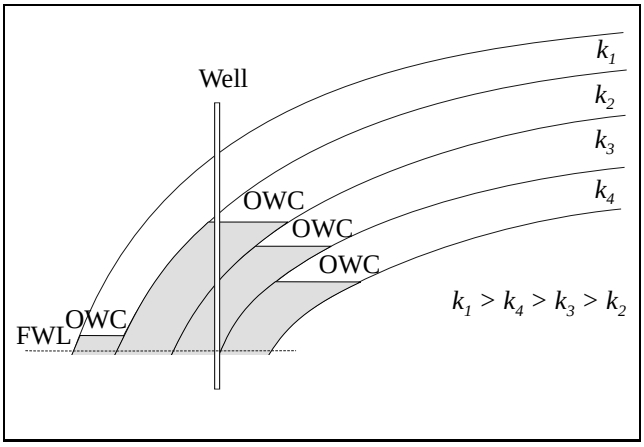


Figure 7.13: Observed water-oil contacts and their relationship with free water level (FWL) in a layered reservoir with a common aquifer [8].

**Example: Equilibrium in a capillary tube**

In this example, the relation between elevation of water above FWL in reservoirs is coupled to the pore dimension (pore radius).

Equilibrium in a vertical water wet capillary tube, as shown in Fig. 7.14, is related to the saturation of water in a reservoir, where oil is the non-wetting fluid.

For a small perturbation $\Delta h$, a small part of the tube surface will experience a change in fluid coverage, when oil is replacing water as being the contact fluid. The change in surface energy, caused by oil displacing water in a small fraction of the capillary tube (see close up in Fig. 7.14), is given by the difference in surface tension (or surface energy),

$$\Delta E_s = 2\pi r(\sigma_{os} - \sigma_{ws})\Delta h.$$

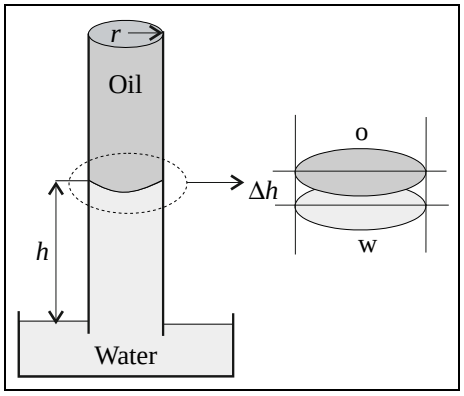


Figure 7.14: Perturbation around equilibrium in a water-wet capillary tube.

The corresponding potential energy change, due to change in elevation is written,

$$\Delta E_p = \pi r^2 \Delta h(\rho_w - \rho_o)gh.$$

If small perturbations close to equilibrium are considered, the surface- and the potential energy changes is expected to be equal, i.e. $\Delta E_s = \Delta E_p$. Using the Young- Dupre equation, the following relation is given,

$$\sigma_{ow}\cos\theta = \frac{g}{2}(\rho_w - \rho_o)rh.$$

In a oil reservoir where the fluids are well defined , i.e. where the densities and the oil- water interfacial tension are known parameters, the pore radius $r$ and the height above FWL $h$ are reciprocal variables. This means that the saturation of initial water present in the reservoir above a certain height $h$ is localised in those pores having a radii less than $r$.

From the above consideration, the capillary pressure has a "dual" characteristic,

$$P_c = g(\rho_w - \rho_o)h = \frac{2\sigma_{ow}\cos\theta}{r},$$

where the capillary pressure is the pressure difference between oil- and water phase at a certain elevation $h$ in the reservoir, and at the same time, the pressure difference across a curved surface in inside a pore channel of radius $r$. This dual characteristic of the capillary pressure gives the condition for the coexistence of oil and water in porous rock.

## 7.9 Laboratory Measurements of Capillary Pressure

Laboratory measurements of capillary pressure are based on the fact that $P_c \propto \sigma\cos\theta/r$, where $r$ characterizes the porous medium with respect to the pore throats and the pore size distribution . This implies that for any given porous medium and any pairs of fluids, the following relationship is valid,

$$\frac{P_{c1}}{(\sigma\cos\theta_c)_1} = \frac{P_{c2}}{(\sigma\cos\theta_c)_2}.$$

Practical use is made of this relationship in conducting laboratory tests with fluids other than reservoir condition fluids. For example, air and brine with a $(\sigma\cos\theta_c)_{lab}$ value of 72 dynes/cm may be used to measure capillary pressure for air- brine in the laboratory. The relationship for the reservoir oil-brine pair capillary pressure is obtained using the appropriate value of $(\sigma\cos\theta_c)_{res}$=26 dynes/cm, where,

$$P_{c,res} = P_{c,lab}\frac{(\sigma\cos\theta_c)_{res}}{(\sigma\cos\theta_c)_{lab}}.$$

The migration of hydrocarbons into an initially water filled reservoir rock and subsequent equilibrium vertical saturation distribution is modelled in the laboratory by a non-wetting phase displacing a wetting phase (*drainage capillary pressure test*). Air and brine are frequently used as the pseudo reservoir fluids, and the displacement is affected by increasing air pressure in a series of discrete steps in water saturated core plugs sitting on a semi-permeable porous diaphragm. As a result of an increase in pressure (equivalent to $P_c$ since $P_c = p_{air} - p_{brine}$) the water saturation decreases and its value is established by weighting the core plugs. The apparatus layout is shown in Fig. 7.15.

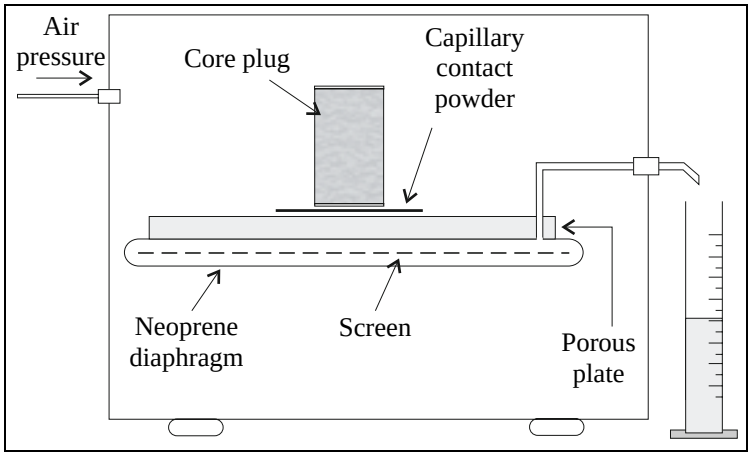


Figure 7.15: Gas-liquid drainage capillary pressure measurement. Portion of liquid in saturated core is displaced at a particular pressure level by either gas or liquid. Liquid saturation measured after equilibrium saturation has been reached. Repetition for several successive pressure levels [8].

In laboratory tests the final irreducible wetting phase saturation value is often beyond the breakdown pressure of the porous plate and is sometimes obtained by centrifuge spinning at a rotational force equivalent to about 150 psi (10.34 bar), and measuring the quantity of any produced wetting phase.

The pore size distribution in a given rock type is usually determined by a mercury injection test. Although this test is destructive, in the sense that the sample cannot be used again, it has the advantage that high pressures can be attained, where mercury, the non-wetting phase with respect to air, can be forced into very small pores.

**Example: Height of water - oil transition zone.**

A laboratory air-brine capillary pressure of 1.25 bar has been measured in a reservoir core sample at residual water saturation. The air-brine interfacial tension is 0.070 $N/m$ and the brine-oil interfacial tension for the reservoir fluids is 0.022 $N/m$.

The height of the water-oil transition zone is the height from FWL and up to the point in the reservoir where connate water saturation is reached,

$$h_{res} = \frac{P_{c,res}}{g(\rho_{brine} - \rho_{oil})},$$

where $P_{c,res}$ is the capillary pressure in the reservoir at this water saturation. $\rho_{brine}$ and $\rho_{oil}$ is respectively 1074 $kg/m^3$ and 752 $kg/m^3$.

In the case of identical wetting preferences for the core sample and the reservoir, one may assume proportionality between capillary pressure and the interfacial tension in the two situations,

$$P_{c,res} = P_{c,lab}\frac{\sigma_{res}}{\sigma_{lab}}.$$

Combining these two equation, the height of the transition zone is found,

$$h_{res} = \frac{\sigma_{res}}{\sigma_{lab}}\frac{P_{c,lab}}{g(\rho_{brine} - \rho_{oil})},$$

which gives, $h_{res}$ = 12.5 $m$.

## 7.10 Drainage and Imbibition Processes.

When two or more fluids flow through a porous medium simultaneously, the phase pressures $p_i$, generally speaking, are not identical. The difference between the phase pressures of two coexisting phases is defined as the capillary pressure. The capillary pressure is inversely proportional to a generalised interfacial curvature, which is usually dominated by the smallest local curvature (radius) of the interface, as illustrated in Fig. 7.16.

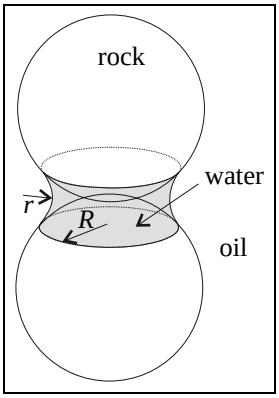


Figure 7.16: Local curvature of the interface of two coexisting liquids.

An idealised permeable medium is considered by the arrangements of decreasing pore sizes (a single pore bounded by the decreasing sizes sphere assemblage) and initially saturated with a wetting phase (w) into which a non-wetting phase (nw) is alternatively injected and then

withdrawn. The forcing of a non-wetting phase into a pore (non-wetting saturation increasing) is a *drainage* process. The reverse (wetting saturation increasing) is an *imbibition* process. We imagine the pores have an exit for the wetting fluid somewhere on the right.

Beginning at zero non-wetting saturation, injection up to the saturation shown in *condition 1* in Fig. 7.17, is first considered. At static conditions, the pressure difference between the exit and entrance of the assemblage is the capillary pressure at that saturation. When the wetting fluid is introduced into the pore from the right, the non-wetting fluid disconnects leaving a trapped or non-flowing glob in the largest pore (*condition 2*).

The capillary pressure curve from condition 1 to condition 2 is an imbibition curve that is different from the drainage curve because it terminates ($P_c = 0$) at a different saturation. At the static condition 2, the entrance - exit pressure difference is zero since both pressures are being measured in the same wetting phase.

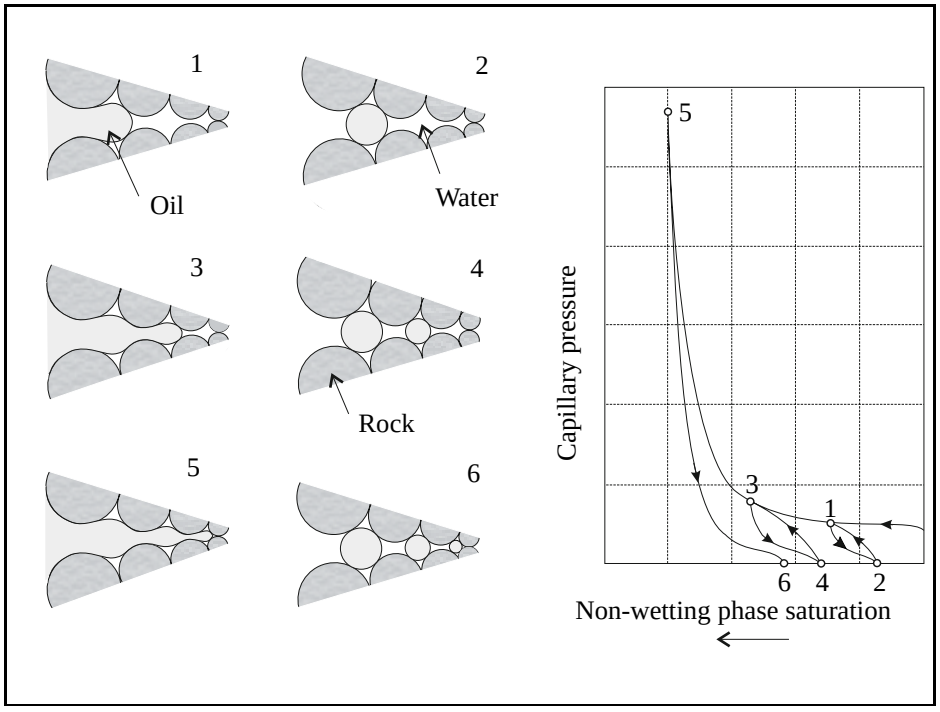


Figure 7.17: The distribution of a non-wetting phase at various saturations.

Going from *condition 2* to *condition 3* is a second drainage process, that results in even higher non-wetting saturation, a higher capillary pressure, and a higher trapped non-wetting phase saturation after imbibition (*condition*). At the highest capillary pressure (*condition 5*), all pores of the subtracted volume contain the non- wetting phase, and a post - imbibition trapped saturation is maximum. The capillary pressure curve going from the largest non-wetting phase saturation to the largest trapped non-wetting phase saturation is the imbibition curve (*condition 6*). Note, that the termination of any imbibition curve is at zero capillary pressure.

This representation, being quite simple, explains many features of actual capillary pressure curves. Imbibition curves are generally different from drainage curves, but the difference shrinks at high non-wetting phase saturations where more of the originally disconnected globs

are connected. This phenomenon is called *trapping hysteresis or drag hysteresis* and is caused by differences in advancing and receding contact angles.

### 7.10.1 Hysterisis in Contact Angle

When oil is moving to cover a rock surface which previously has been wetted by water, it has been experimental proven that the contact angle is smaller than in the case when water is replacing oil, over the same surface.

This effect is called the *hysterisis in contact angle* and has to do with the inherent memory of a physical system, which relates prehistoric events to present experience. In practical terms this means that the back and forth movement is energy dependent, typical for non-reversible systems.

The hysterisis is detected by measuring the advancing $\theta_a$, and residing $\theta_r$ contact angles of an oil drop suspended between two horizontal plates (made of polished rock material; quartz or calcite) submerged in water, as shown in Fig. 7.18. One plate is fixed and the other can move smoothly to either side. The oil drop is left to age between the plates for some time, until the two contact angles are equal. When the mobile plate is moved, the two contact angles are measured. The test is repeated after some time, when the two angles have stabilised.

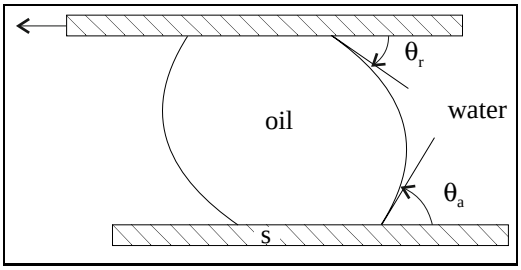


Figure 7.18: Measurement of hysterics in contact angle.

The hysterics observed, where the receding angle is smaller than the advancing angle, is an expression of the fact that energy is lost in cyclic systems. In relation to multiphase flow in porous media, the hysterics has two important effects:

- One is to stabilise the capillary surfaces (interfaces) between the fluids in the pore system, such as to preserve the fluid distribution in the reservoir, unless a finite capillary pressure difference is imposed.

- The second effect is related to the dissipation of energy towards the capillary walls, when the interface is advancing through the pore. The effect of this dissipation of energy is experienced as a resistance towards flow and is often materialised through "rip off" of small droplets, which then becomes practically immobile.

### 7.10.2 Capillary Hysterisis

It is seen that capillary pressure depends both on wetting phase saturation and the direction of its variation. A typical curve of the capillary pressure in case of two-phase flow, is shown in the Fig. 7.19.

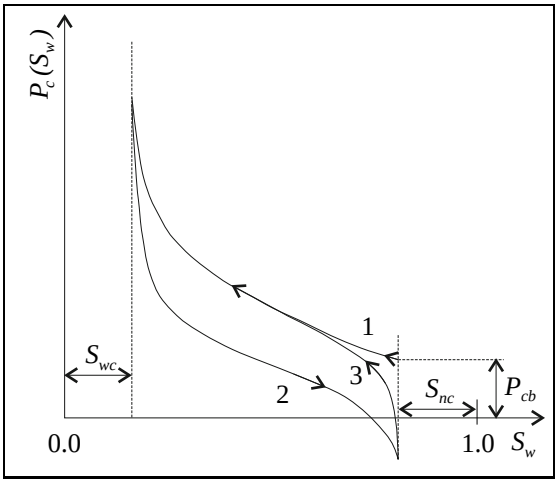


Figure 7.19: Typical type of capillary pressure curve for a two-phase flow problem: 1 drainage, 2 imbibition and 3 secondary drainage.

Two ways in which one phase can be substituted by the other in a porous medium are usually considered. The first is the process of displacement where the wetting phase is displaced by the non-wetting one, and the second is the process of imbibition, where the non-wetting phase is displaced by the wetting one. The value $P_{cb}$ is defined as threshold capillary pressure which should be exceeded to provide displacement. If displacement is preceded by imbibition the capillary pressure curve is as the curve 3 in the Fig. 7.19, which is different from the curve 1. The presence of two different curves of imbibition and displacement is called capillary hysteresis. The presence of the negative capillary pressure near the saturation point $S_w = S_{nc}$ was first discovered by Welge (1949). The hysteresis effect i demonstrated by the two curves 2 and 3 in Fig. 7.19.

## 7.11 Exercises

1. Calculate the energy needed to transform 1 $cm^3$ of water into droplets with an average radius of 1 $\mu m$. In analogy with displacement processes in porous media, assume an interfacial tension $\sigma_{o,w}$ = 0.025 $N/m$.

2. Show that the general expression for capillary pressure

$$P_c = \sigma \left( \frac{1}{R_1} + \frac{1}{R_2} \right),$$

could be written

$$P_c = \frac{2\sigma \cos\theta}{r},$$

for a cylindrical tube. Define the parameters; $r$, $R_{1,2}$, $\theta$ and $\sigma$.

3. A capillary glass-cylinder is positioned vertically in a cup of water. Calculate the height of water inside the cylinder when the inner diameter is 0.1 $cm$. The surface tension between water and air is 72 $dyn/cm$, and the water is assumed to wet the glass 100 %.

4. In order to displace water by air form a porous plate, a pressure of 25 psig is needed. Find the diameter, given in $\mu$m, of the largest pore channel disconnecting the porous plate, when the surface tension $\sigma_{air,w}$ is 72 dyn/cm.

5. A horizontal cylinder, filled with oil, is 0.1 $m$ long and has a inner diameter of 0.01 $mm$. The oil has a viscosity similar to water, 1 $mPa \cdot s$. What is the pressure drop along the cylinder, when the average flow velocity is found to be 0.01 $mm/s$ ?

   An equal amount of water and oil is pumped through the cylinder and the water and oil is assumed to move through the tube as droplets, with an average length of 0.03 $mm$ pr. droplet. The advancing contact angle is $40^o$ and the receding angle is $20^o$. Calculate the pressure drop through the tube, assuming the same flow velocity as above. The interfacial tension between water and oil is 25 m$N/m$.

6. A core sample is placed in a core holder in a centrifuge. The radial distance to the core sample is given by the two position vectors $r_1$ and $r_2$. The length of the sample is therefore; $r_2 - r_1$. At a rotation frequency $\omega$, air will displace some of the water in the sample. The radial distance $r_d$, corresponds to the threshold pressure $P_d$ at that particular rotation frequency. See the figure below.

   a) Show that the pressure difference for one phase is given by:

$$P_2 - P_1 = \frac{1}{2}\rho\omega^2(r_2^2 - r_1^2), \qquad \text{when} \qquad P_2 = P(r_2), \qquad P_1 = P(r_1)$$

   b) Show that

$$P_c(r) = \frac{1}{2}\Delta\rho\omega^2(r_2^2 - r^2)$$

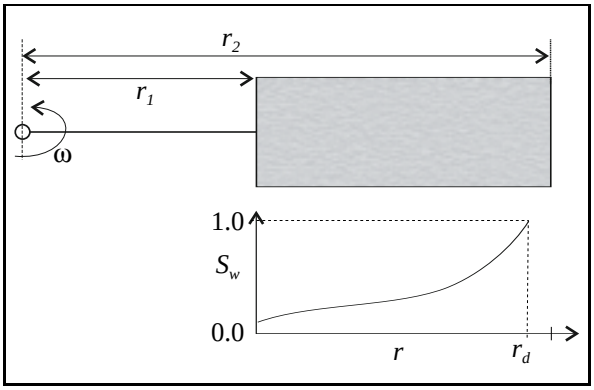


when its known that

$$P_{c1} = P_c(r_1) = \frac{1}{2}\Delta\rho\,\omega^2(r_2^2 - r_1^2)$$

and when

$$P_d = \frac{1}{2}\Delta\rho\,\omega^2(r_2^2 - r_d^2)$$

It is assumed that $P_{c2} = P_c(r_2) = 0$.

c) The water saturation can be written,

$$S_{w1} = S_w(r_1) = \frac{d(\bar{S_w}P_{c1})}{dP_{c1}}$$

when $r_1 \sim r_2$, assuming the length of core sample to be short compared to the radius of rotation. (This is an approximation, only partly true.)

Use the equations above to derive the a formula giving the capillary pressure as function of the water saturation ($P_c$–curve), when the capillary pressure is given in *kPa*.

The following data is given for a core sample, saturated with sea-water and rotated in air.

$r_1$ = 4.46 cm
$r_2$ = 9.38 cm
$\Delta\rho$ = 1.09 $g/cm^3$
$V_p$ = 8.23 $cm^3$

| RPM* | 415 | 765 | 850 | 915 | 1005 | 1110 | 1305 |
|---|---|---|---|---|---|---|---|
| $\Delta V[cm^3]$ | 0.00 | 0.00 | 0.10 | 0.15 | 0.30 | 0.50 | 1.10 |
| RPM | 1550 | 1835 | 2200 | 2655 | 3135 | 3920 | 4850 |
| $\Delta V[cm^3]$ | 2.20 | 2.90 | 3.61 | 4.21 | 4.72 | 5.24 | 5.75 |

RPM*: Rotation pr. Minute and $\Delta V$: produced volume.

7. In the laboratory, a capillary pressure difference of 5 *psi* has been measured between water and air in a core sample. Calculate the corresponding height above the OWC in the reservoir from where the core originates, when the following information is given (assume capillary pressure at the OWC to be zero).

| Laboratory | Reservoir |
|---|---|
| $\sigma = 75\,dyn/cm$ | $\sigma = 25\,dyn/cm$ |
| $\Delta\rho_{w/air} = 1.0\,g/cm^3$ | $\Delta\rho_{o/w} = 0.2\,g/cm^3$ |

8. In a laboratory experiment, capillary data from two water saturated core samples was obtained by using air as the displacing fluid.

| 1000 mD core sample | | 200 mD core sample | |
|---|---|---|---|
| $P_c[psi]$ | $S_w$ | $P_c[psi]$ | $S_w$ |
| 1.0 | 1.00 | 3.0 | 1.00 |
| 1.5 | 0.80 | 3.6 | 0.90 |
| 1.8 | 0.40 | 4.0 | 0.60 |
| 2.2 | 0.20 | 4.5 | 0.30 |
| 3.0 | 0.13 | 5.5 | 0.20 |
| 4.0 | 0.12 | 7.0 | 0.18 |
| 5.0 | 0.12 | 10.0 | 0.18 |

Calculate the distribution of vertical water saturation in the stratified reservoir given by the figure below, i.e. determine $S_w$ as function hight in the reservoir.

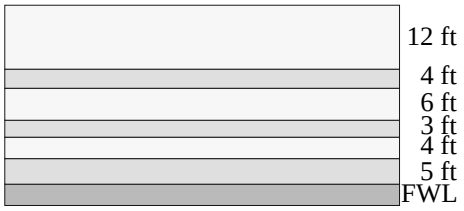


Additional data:

Laboratory: $\sigma_{w/air} = 50\,dyn/cm$
Reservoir: $\sigma_{o/w} = 23\,dyn/cm$
$\rho_o = 0.81\,g/cm^3$
$\rho_w = 1.01\,g/cm^3$

9. Use the air - water capillary pressure curve for laboratory conditions, below, to calculate the saturations; $S_o$, $S_g$ and $S_w$ at the reservoir level (hight) 120 $ft$ above the oil-water contact (assume $P_c = 0$ at this level). The distance between the contacts (OWC and GOC) is 70 $ft$.

Additional data:

Laboratory: $\sigma_{w/air} = 72\,dyn/cm$
Reservoir: $\sigma_{o/g} = 50\,dyn/cm$
$\sigma_{w/o} = 25\,dyn/cm$
$\rho_o = 53\,lb/ft^3$
$\rho_w = 68\,lb/ft^3$
$\rho_g = 7\,lb/ft^3$

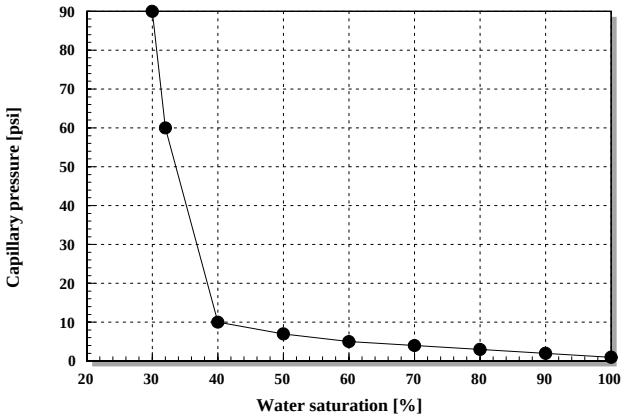


10. An oil water capillary pressure experiment on a core sample gives the following results:

| $P_{c,o/w}$ [psi] | 0 | 4.4 | 5.3 | 5.6 | 10.5 | 15.7 | 35.0 |
|---|---|---|---|---|---|---|---|
| $S_w$ [%] | 100 | 100 | 90.1 | 82.4 | 43.7 | 32.2 | 29.8 |

Given that the sample was taken from a point 100 ft above the oil-water contact, what is the expected water saturation at that elevation? If the hydrocarbon bearing thickness from the crest (top) of the structure to the oil-water contact in 175 ft, what is the average water saturation over this interval? ($\rho_w = 64\,lbs/ft^3$ and $\rho_o = 45\,lbs/ft^3$)

11. If we assume an interfacial tension; $\sigma\cos\theta = 25\ dyn/cm$ and a permeability and porosity respectively 100 *mD* and 18 %, in the exercise above, we may construct the capillary curve for a laboratory experiment using mercury as non-wetting phase. In the laboratory experiments one assume the lithology to be unchanged, but the permeability and porosity to be respectively 25 *mD* and 13 %. Find laboratory capillary curve when the interfacial tension to mercury is 370 $dyne/cm$.

**Answers to questions:**

1. $\Delta E = 0.075\,J$, 3. $h = 3\,cm$, 4. $d = 0.5\,\mu m$, 5. $\Delta p = 3.2\,mbar$, $\Delta p = 29\,bar$, 7. $h = 5.8\,m$, 9. $S_o = 0.2$, $S_g = 0.62$ , $S_w = 0.36$, 11. $\overline{S_w} = 0.41$.

# Chapter 8

# Relative Permeability

## 8.1 Definitions

Relative permeability is a concept used to relate the absolute permeability (100% saturation with a single fluid) of a porous system, to the effective permeability of a particular fluid in the system, when that fluid occupies only a fraction of the total pore volume.

When measuring a flow-rate of a fluid versus the pressure difference in a core sample, we can obtain (single phase flow),

$$q = \frac{k_e A}{\mu} \frac{\triangle p}{\triangle x},$$

and

$$k_e = \frac{q}{A} \frac{\mu \triangle x}{\triangle p}.$$

Here $k_e$ is called *effective* permeability. For 100% saturation, the effective permeability is identical to the absolute permeability; i.e. $k_e = k$.

In multiphase flow a generalisation of Darcy law has been accepted [12],

$$q_j = k_{je} \frac{A}{\mu_j} \frac{\triangle p_j}{\triangle x},$$

where $j$ denotes a fluid phase $j$, and $k_{je}$ is called the effective (phase) permeability.

According to the last equation we can obtain,

$$k_{je} = \frac{q_j}{A} \frac{\mu_j \triangle x}{\triangle p_j}.$$

In a vast number of laboratory experiments it has been observed that a sum of effective permeability's is less than the total or absolute permeability, i.e.,

$$\sum_{j=1}^{n} k_{je} < k.$$

Moreover, effective (phase) permeability was noticed to be a function of quite a number of parameters, such as: fluid saturation, rock property, absolute permeability, fluid property, and reservoir conditions (pressure, temperature),

$$k_{je} = f(k, p, T, S_1, S_2, \ldots, S_n, \ldots) \quad j \in [1, n].$$

In two phase systems the latter relationship is expressed as functions of a single (by convention, wetting) saturation.

The *effective* permeability can be decomposed into the *absolute* permeability and the *relative* permeability, as shown below,

$$k_{ej} = k_{rj} \cdot k.$$

The relative permeability is a strong function of the saturation of phase $S_j$. Being a rock-fluid property, the functionality between $k_{rj}$ and $S_j$ is also a function of rock properties (e.g. pore size distribution) and wettability. It is not, in general, a strong correlation between relative permeability and fluid properties, though when certain properties (e.g. interfacial tension) change drastically, relative permeability can be affected [40].

It is important to note that the phase permeability is a tensorial function (as the absolute permeability) and that the relative permeability is not.

Though there have been attempts to calculate relative permeability on theoretical grounds, by far the most common source of them, has been experimental measurements. This implicates that it is important to keep definitions of mobility, phase permeability and relative permeability separate and clear.

Functions $k_j(S_j)$ depend both on the structure of the porous medium and on the saturation distribution of the phases. However in mathematical modelling of two-phase and multi-phase flow it is conventional to assume that relative permeabilities are the functions of saturation only. This assumption considerably simplifies the task of laboratory experiments carried out in order to determine relative permeabilities.

In the presence of two coexisting phases, the typical curves of relative permeability are as shown in Fig. 8.1.

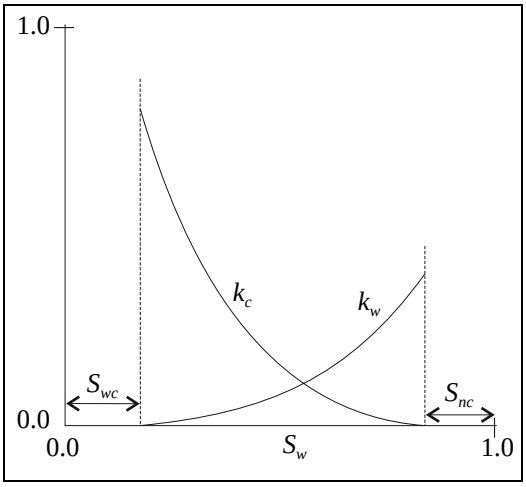


Figure 8.1: Typical type of relative permeability characteristics for a two-phase flow, where $S_w$ is the wetting phase and $S_n$ is the non-wetting phase.

One important feature in the behaviour of the rel.perm.-curves should be emphasised. If saturation of one of the phases becomes less than some definite value: $S_w < S_{wc}$ or $S_n < S_{nc}$, then the corresponding relative permeability for that phase becomes zero and the phase becomes immobile. This means that continuity of the phase is broken or disturbed and the phase

remains in a passive or loose state. The values $S_{jc}$, $j = w$, where $n$[1] are defined as residual saturation of the $i$-th phase. Let us note that those values depend on thermodynamic condition of the reservoir (reservoir pressure, temperature, number of phases, type of rock, etc.).

## 8.2 Rock Wettability and Relative Permeabilities

It should be noted that evaluations of phase- and relative permeabilities can be done through measurements of capillary pressure, which shows the evidence of strong correlation between them. Because of certain links between them, we would expect micro-heterogeneity and rock wettability to have a certain influence on relative (phase) permeability. Typical water-oil relative permeabilities are presented for strongly water-wet and oil-wet formations in Fig. 8.2 (left) and 8.2 (right), respectively.

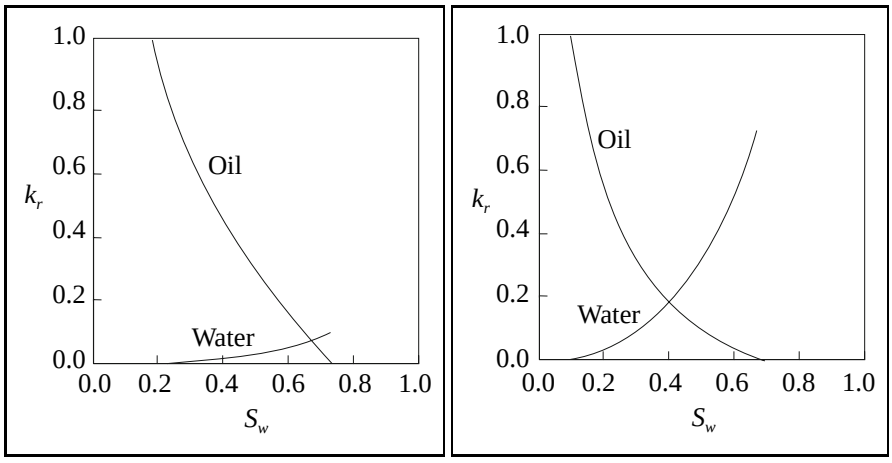


Figure 8.2: Characteristics of typical relative permeability for a two-phase flow, where $S_w$ is the wetting phase and $S_n$ is the non-wetting phase (left: a water-wet formation and right: an oil-wet formations).

The difference in the flow properties that indicates different wettability preferences can be illustrated by the following rule of thumb [29]:

[1]Here *w* and *n* denote *wetting* and *non-wetting* phase, respectively.

| | Water-wet | Oil-wet |
|---|---|---|
| Connate water saturation | Usually greater than 20 to 25 percent PV | Generally less than 15 percent PV, frequently less than 10 percent |
| Saturation at which oil and water permeabilities are equal (crossover saturation) | Greater than 50 percent water saturation | Less than 50 percent water saturation |
| Relative permeabilities to water at maximum water saturation; i.e. flood-out | Generally less than 30 percent | Greater than 50 percent and approaching 100 percent |

Let us note that the endpoint values of the relative permeabilities are usually (if not always) less than 1 and which are measures of wettability. The non-wetting phase occurs in isolated globules, several pore diameters in length, that occupy the center of the pores. Trapped wetting phase, on the other hand, occupies the cavities between rock the grains and coats the rock surfaces. Thus we would expect the trapped non-wetting phase to be a bigger obstacle to the wetting phase, then the trapped wetting phase is to the non-wetting phase. The wetting phase endpoint relative permeability will, therefore, be smaller than the non-wetting phase endpoint. The ratio of wetting to non-wetting endpoints proves to be a good qualitative measure of the wettability of the medium. For extreme cases of preferential wetting, the endpoint relative permeability to the wetting phase can be 0.05 or less. Others view the crossover saturation ($k_{r2} = k_{r1}$), of the relative permeabilities is a more appropriate indicator of wettability, perhaps because it is less sensitive to the value of the residual saturations (see the rule of thumb, above).

## 8.3 Drainage/Imbibition Relative Permeability Curves

In a gas-oil systems, the direction of displacement is particularly important, as the process can represent a drainage process, such as gas drive (gas displacing oil immiscibily) or an imbibition process, such as:

1. Movement of an oil zone into receding depleting gas cap.

2. Movement of an aquifer into receding depleting gas cap.

In gas-oil systems the third phase, water, which is always present in the reservoir, is considered to stay at irreducible saturation and play no part in the displacement processes. It is therefore argued that experiments in the laboratory can be conducted with or without irreducible water present and that effective permeabilities could be correlated to total liquid saturation ($S_L$), rather than gas saturation. The relation is based on a definition of liquid saturation,

$$S_L = S_o + S_w = 1 - S_g.$$

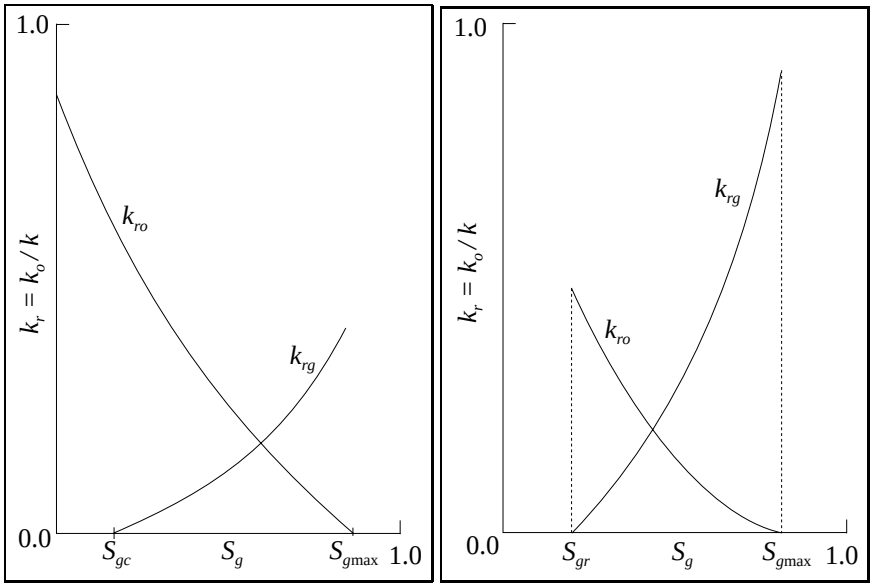


Figure 8.3: Gas-oil relative permeabilities [8].

In a system where gas saturation increases from zero, as in a liquid drainage process, it is observed that gas does not flow until some *critical* gas saturation ($S_{gc}$) has been attained. This is attributed to the physical process of the gas phase becoming continuous through the system, as a condition for gas flow. In liquid *imbibition* processes (gas saturation decreasing from a maximum initial value) the gas permeability goes to zero when the residual or trapped gas saturation ($S_{gr}$) is reached. See Fig. 8.3.

## 8.4 Residual Phase Saturations

As we know from the previous discussion, increasing pressure gradients force the non-wetting phase into the pore channels, causing the wetting phase to retreat into the concave contacts between the rock grains and other cavities in the pore body. At very high pressure differences, the wetting phase approaches mono-layer coverage and a low saturation.

The residual non-wetting phase is trapped in the large pores in globules several pore diameters in length. Repeated experimental evidence has shown that under most conditions, the $S_{nwr}$ could be as large as $S_{wr}$.

According to experimental observations there is a strict evidence of a relationship between residual non-wetting or wetting phase saturations and the so-called local capillary number. This relationship is called the capillary de-saturation curve (CDC). Typically, these curves are plots of percent residual (non-flowing) saturation for the non-wetting ($S_{nwr}$) or wetting ($S_{wr}$) phases on the *y* axis versus a capillary number on a logarithmic *x* axis. The capillary number $N_c$ is a dimension-less ratio of viscous forces to local capillary forces, and can be variously defined. One of the examples is shown below (after Dombrovsky and Brownell):

$$N_c = \frac{k \mid \nabla \vec{\Phi} \mid}{\sigma_{ow} \cdot \cos \theta_c}$$

where $\vec{\Phi}$ is the potential of flow.

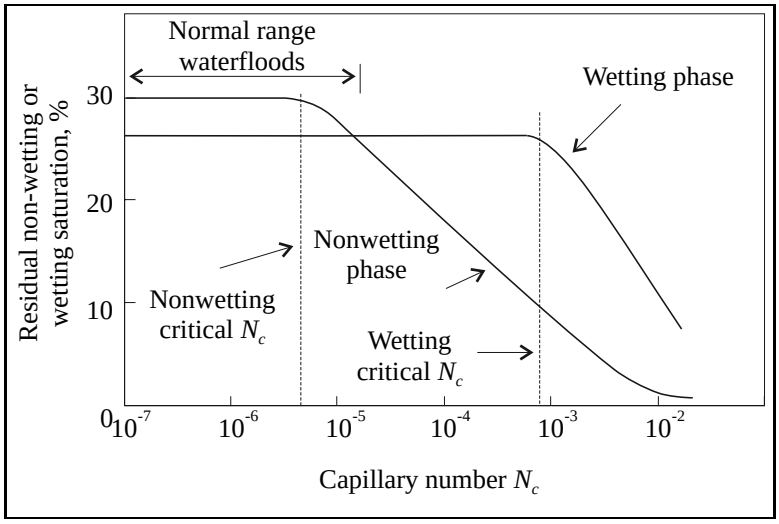


Figure 8.4: Schematic capillary de-saturation curve [40].

It is important to mention that chemical additives reduce capillary forces at the interface of the oil/water system, resulting in increased capillary number $N_c$ and reduced residual oil saturation, being either wetting or non-wetting phase. The reduction of interfacial tension at the interface allows the trapped oil to become mobile and be displaced by the water.

## 8.5 Laboratory Determination of Relative Permeability Data

Laboratory determination of effective permeability is generally conducted as a special core analysis test on representative and carefully preserved core plug samples. A reservoir condition test is conducted at reservoir pore pressure conditions and reservoir temperatures with real or simulated reservoir fluids. Such reservoir condition tests may model displacement under unsteady state, or steady state conditions. Different equipment arrangements for those test are shown in Figs. 8.5 and 8.6.

Unsteady state rel.perm. test simulate the flooding of a reservoir with an immiscible fluid (gas or water). The determination of rel. perm. is based on observation of the fractional flow of displacing phase fluid from the outlet end of the core plug and its relationship with saturation. The displacement theory of Buckley and Leverett is combined with that of Weldge in a technique described by Johnson, Bossler and Naumann [38]. The detection of the breakthrough time of the displacing phase at the outlet core face is critical in the representation of relative permeability, and severe errors can occur with heterogeneous samples. Flow rates are determined according to the method of Rappoport and Leas in order to minimize the effect of capillary pressure forces in retaining wetting phase fluid at the outlet end face discontinuity. The unsteady state or dynamic displacement test is most frequently applied in reservoir analysis of strong wetting preference, and with homogeneous samples.

For reservoirs with more core-scale heterogeneity and with mixed wettability, the steady state laboratory test is preferred. The steady state process provides simultaneous flow of displacing and displaced fluids through the core sample at a number of equilibrium ratios. At each

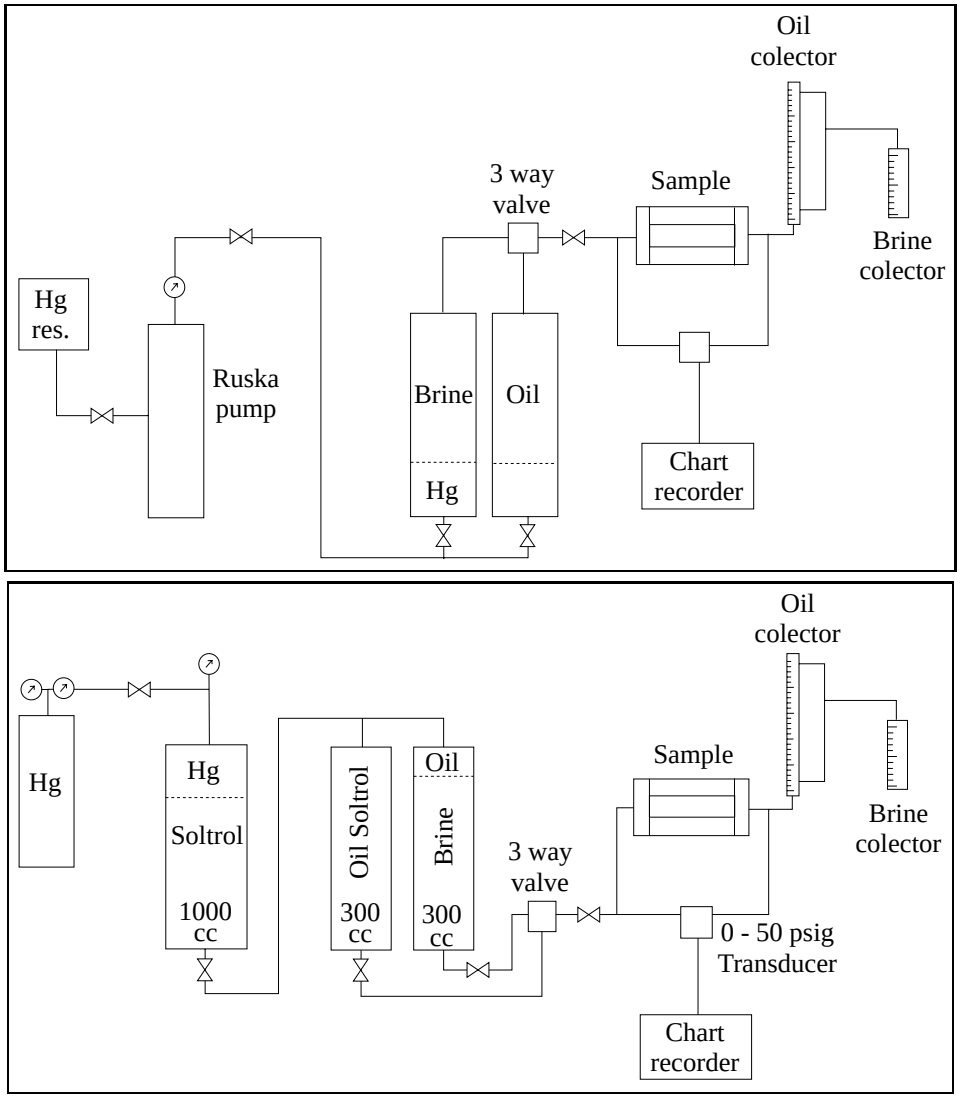


Figure 8.5: Unsteady state relative permeability measurement at constant rate (above) and at constant pressure (below).

ratio from 100% displaced phase to 100% displacing phase an equilibrium condition must be reached at which the inflow ratio of fluids equals to the outflow ratio, and at which the pressure difference between inlet and outlet is constant. At such a condition the Darcy law equation is applied to each phase to calculate effective permeability at the given steady state saturation. Capillary pressure tends to be ignored and a major difficulty is the determination of saturation at each stage. Between five and ten stages are usually needed to establish rel.perm. curves.

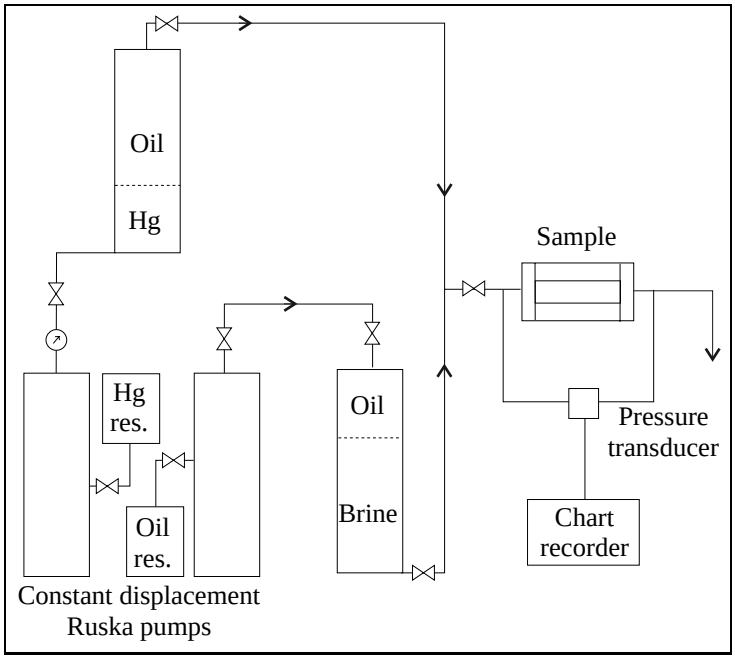


Figure 8.6: Steady state relative permeability measurement [8].

## 8.6 Exercises

1. Use Darcy's law for radial flow and show that the fractional flow for water, $f_w$, can be written:

$$f_w = \frac{q_w}{q_w + q_o} = \frac{1}{1 + k_{ro}\mu_w / k_{rw}\mu_o}$$

Assume the capillary forces to be negligible and $dP_o/dr = dP_w/dr$.

The following laboratory data is given:

| $S_w$ | $k_{ro}$ | $k_{rw}$ | $P_c^{lab}[psi]$ | |
|---|---|---|---|---|
| 1.00 | 0.00 | 1.00 | 1.0 | |
| 0.90 | 0.04 | 0.78 | 3.4 | $\rho_o = 0.85 g/cm^3$ |
| 0.80 | 0.14 | 0.58 | 3.9 | $\rho_w = 1.00 g/cm^3$ |
| 0.70 | 0.29 | 0.39 | 4.5 | $\sigma_{res.} = 22 dyn/cm$ |
| 0.60 | 0.49 | 0.23 | 5.7 | $\sigma_{lab} = 75 dyn/cm$ |
| 0.50 | 0.73 | 0.09 | 8.4 | $\mu_o = 15.0 cp$ |
| 0.40 | 1.00 | 0.00 | 18.0 | $\mu_w = 1.0 cp$ |
| 0.30 | 1.00 | 0.00 | $\infty$ | |

Use critical oil saturation, $S_{oc} = 0.05$ and the data above to construct a graph showing the water fraction as function of height above the WOC.

What is the water fraction at 15 m above the WOC ?

2. The laboratory data below is recorded at stationary conditions, measuring the relative permeability for a oil-water injection experiment.

| $q_o[cm^3/time]$ | $q_w[cm^3/time]$ | $\Delta P$ [psi] | $V_w$ [$cm^3$] |
|---|---|---|---|
| 90 | 0 | 49.25 | 2.17 |
| 75 | 5 | 91.29 | 2.87 |
| 60 | 9 | 109.52 | 3.63 |
| 45 | 20 | 123.30 | 4.65 |
| 30 | 34 | 137.05 | 5.93 |
| 15 | 85 | 164.30 | 7.95 |
| 0 | 122 | 147.00 | 9.86 |

$V_w$ is the volume of water in the core sample, determined by weighing. $q_o$ and $q_w$ is the oil- and water rate through the sample, respectively. $\Delta P$ is the pressure drop.

Additional data is given:

| | | | |
|---|---|---|---|
| Absolute permeability | 16.7 mD | length of core sample | 9 cm |
| Diameter of core sample | 3.2 cm | Oil viscosity | 2.0 cp |
| Water viscosity | 1.1 cp | Porosity | 0.20 |

1 atm. equals 14.65 psi

Draw the rel.perm. curves for $k_{ro}$ and $k_{rw}$ using the data above.

**Answers to questions:**

1. 25%

# Chapter 9

# Compressibility of Reservoir Rock and Fluids

## 9.1 Introduction

Compressibility is a universal phenomenon, of significant importance where all substances are compressible, some more compressible than others. Compressibility is therefore an important "drive mechanism" in underground petroleum production.

Oil and gas are naturally existing hydrocarbon (HC) mixtures, quite complex in chemical composition which exist at elevated temperatures and pressures in the reservoir. When produced to the surface, the temperature and pressure of the mixture are reduced, where the state of the HC mixture at the surface depends upon the composition of the HC fluid found in the reservoir. The fluid remaining in the reservoir at any stage of depletion undergoes physical changes as the pressure is reduced due to removal of quantities of oil, gas and initial water from the reservoir.

It is necessary to study the physical properties of these naturally existing HC and in particular, their variation with pressure and temperature, in order to fully understand and control the production process. This information is important in estimating the performance of the fluids in the reservoir.

Compressibility, as physical phenomenon, plays a key role in general underground petroleum production. Nearly all production of oil, gas and formation water is related to volume expansion when the reservoir pressure decreases due to removeal of reservoir fluids.

## 9.2 Compressibility of Solids, Liquids and Gases

For a mixture of HC it is quite obvious that pressure and temperature are essential parameters. The state of equilibrium is defined by these two parameters and consequently also the phase behaviour of the fluid, i.e. the fractional volume of oil and gas.

In the case of formation rock and the saturation of fluids contained therein, pore volume and fluid changes due to the pressure decline is the dominating phenomenon, responsabile for reservoir fluid production, since the reservoir temperature changes slightly or remain constant in most cases. Volumes of reservoir fluid brought to the surface will experience change in both

pressure and temperature, i.e. the final state of oil and gas is characterised by volume changes due to both drop in pressure and in temperature.

The general behaviour of materials can be described by the compressibility and expansion terms;

$$c = -\frac{1}{V}\left(\frac{\partial V}{\partial p}\right)_T, \tag{9.1}$$

$$\beta = \frac{1}{V}\left(\frac{\partial V}{\partial T}\right)_p, \tag{9.2}$$

where $c$ is the isothermal compressibility, $c \geq 0$ and $\beta$ is the isobaric thermal expansion, $\beta \geq 0$.

In practice, it is normal to use an average compressibility factor of the different HC components. In relation to reservoir production, it is common practise to distinguish between the following definitions of compressibility:

- Rock matrix compressibility; $c_r$.
- Rock bulk compressibility; $c_b$.
- Liquid compressibility (oil or initial water); $c_o$ and $c_w$.
- Gas compressibility; $c_g$.

### 9.2.1 Rock Stresses and Compressibility

When rocks are subjected to external load or force, internal stresses are developed and if the stresses are sufficiently strong, deformation such as volume and shape changes of the rock will be the result. The stresses on any plane surface through a rock sample under in situ. conditions are composed of a normal stress vector (perpendicular to the plane) and two shear stresses, parallel to the plane surface. The general stress condition may be characterised by a stress tensor, with nine components as shown in Fig. 9.1. The stress tensor is often written in matrix form;

$$\begin{pmatrix} \sigma_x & \tau_{xy} & \tau_{xz} \\ \tau_{yx} & \sigma_y & \tau_{yz} \\ \tau_{zx} & \tau_{zy} & \sigma_z \end{pmatrix}$$

Due to the general conditions of equilibrium, the stress tensor will be symmetric around the diagonal, which means that $\tau_{xy} = \tau_{yx}$ and so on. There are thus only six independent stress components in the stress tensor:

3 normal stresses: $\sigma_x$, $\sigma_y$ and $\sigma_z$ and

3 tangential (shear stresses): $\tau_{xy}$, $\tau_{yz}$, $\tau_{zx}$.

Underground gas and oil reservoirs experience stresses due to the overload of rock material and water and the lateral confinement stresses exerted on the reservoir from the surrounding rock masses, see Fig. 9.2. It is possible to show that there exist one set of ortogonal axis with

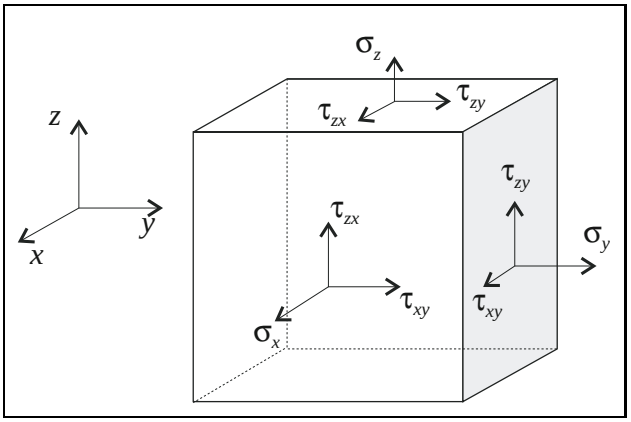


Figure 9.1: Stress conditions of formation rock media.

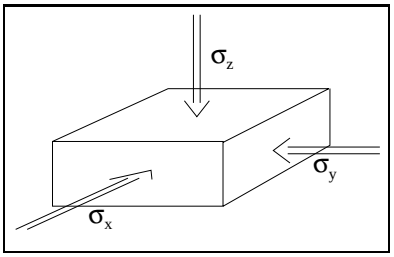


Figure 9.2: Principal stresses on reservoir rock..

respect to which all shear stresses are zero and the normal stresses have their extreme values. These stresses are called the *principal stresses*

For most reservoirs, the principal normal stresses are orientated as shown in Fig. 9.2, where the major principle stress $\sigma_z$ is acting parallel to the force of gravity, while the two lateral stresses $\sigma_x$ and $\sigma_y$ are acting in the horizontal plane, e.g. $\sigma_z > \sigma_x, \sigma_y$.

The average normal stress is generally defined by,

$$\overline{\sigma} = \frac{1}{3}(\sigma_x + \sigma_y + \sigma_z). \tag{9.3}$$

The collective action of the principal stresses will cause the rock material to deform. The relative longitudinal deformation is given by the *principal strain*,

$$\varepsilon_i = \frac{\Delta l_i}{l_i} = \frac{l_i - l_i'}{l_i}, \text{ where } i = x, y, z, \tag{9.4}$$

where $l_i$ is the initial length of the rock in the i'th direction, $l'$ is the length after deformation.

The sum of principal strains will give the relative volume change $\Delta\varepsilon = (\varepsilon_x + \varepsilon_y + \varepsilon_z)$, where $\varepsilon_V = \Delta V/V$. (In case of non-zero shear stresses, a displacement or rotation of the rock may be experienced.)

The stress - strain relationship is dependent on several parameters of which the following are the most important; the composition and lithology of the rocks, the degree of cementation of the rock material, the type of cementing material, the compressibility of the rock matrix, the porosity of the rock material and the pressure and temperature in the reservoir.

In the following, the rock will be assumed to be isotropic, which means equal properties in all directions. For simplicity, it is also assumed that the stresses are refered to the principal stress directions.

Within the elastic limit of volume deformation of any rock material, Hooke's law states that there exist a proportionality between stress, $\sigma$ and strain, $\varepsilon$, where $\sigma_1$, $\sigma_2$ and $\sigma_3$ are the principar stress directions.

$$\sigma_1 = E\varepsilon_1, \tag{9.5}$$

where $E$ is the Young's modulus of elasticity and the subscript indicate change in stress and strain in the same direction and where the stresses normal to this direction are constant.

If a cylindrical rock sample is subjected to a compressive stress, $\sigma_1$, parallel to its long axis, it will shorten, $\varepsilon_1$ and the diameter will increase. The ratio of transverse strain to the axial strain is expressed by the Poisson ratio $\nu$. If the transverse strain is defined by $\varepsilon_2$ and $\varepsilon_3$, then the transverse deformation is given,

$$\nu = \frac{\varepsilon_2}{\varepsilon_1} = \frac{\varepsilon_3}{\varepsilon_1}, \tag{9.6}$$

where $\varepsilon_1$ is the principal strain direction.

The significance of Poisson's ratio, coupling axial and transverse strain, indicates that deformation along one principal axis is caused by a combination of all three principal stresses. This observation is presented in Hooke's law in three dimensions:

$$E\varepsilon_x = \sigma_x - \nu(\sigma_y + \sigma_z), \tag{9.7}$$

$$E\varepsilon_y = \sigma_y - \nu(\sigma_x + \sigma_z), \tag{9.8}$$

$$E\varepsilon_z = \sigma_z - \nu(\sigma_x + \sigma_y). \tag{9.9}$$

In writing Hooke's law this way, the strains are reddered to the condition of zero stresses. It is often convenient to write Hooke's law in changes of stresses, $\Delta\sigma_x$ etc. In that case srain are refered to the initial conditions.

The total deformation due to all three principal stresses acting on the rock material is given by $\Delta V = (\varepsilon_x + \varepsilon_y + \varepsilon_z)V$. Using Hooke's law, Eqs. (9.7) to (9.9), the relative volume change is given,

$$\frac{\Delta V}{V} = \frac{3\overline{\sigma}(1-2\nu)}{E} \tag{9.10}$$

Relative volume deformation of the rock is also described by the compressibility Eq. (9.1) on differential from,

$$\frac{\Delta V}{V} = c_r \Delta\sigma. \tag{9.11}$$

In introducing $c_r$, one assumes that the rock is completely solid with no pores or cracks within it.

Combining equation Eq. (9.10) and Eq. (9.11) proves that the compressibility and the elasticity are "two sides of the same case",

$$c_r = \frac{3(1-2\nu)}{E}, \tag{9.12}$$

where also the elastic constants $E$ and $\nu$, refer to the solid rock material.

In Eq.(9.12) the important relation between the compressibility and the elastic properties of the rock material is established. Under the assumption that the deformation of the rock is within the range of the elasticity (see Fig. 9.3), compressibility is constant, i.e.

$$\frac{dV}{V} = -c_r d\sigma, \tag{9.13}$$

according to Eq.(9.1) the deformed volume $V$ is equal to,

$$V = V_0 e^{-c_r(\sigma-\sigma_0)} \simeq V_0[1-c_r(\sigma-\sigma_0)]. \tag{9.14}$$

The approximation is valid when $c_r\Delta\sigma$ is small, i.e. $c_r(\sigma-\sigma_0) \ll 1$.

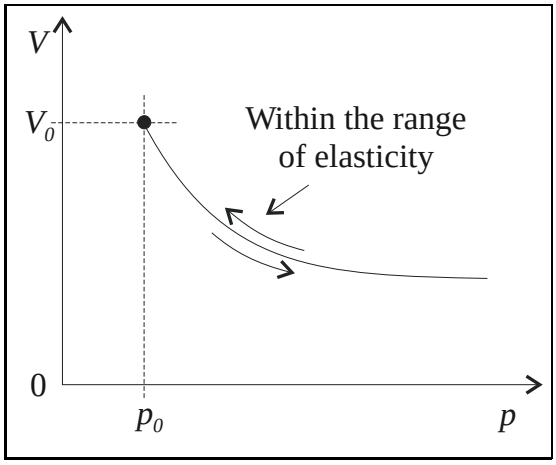


Figure 9.3: Deformation of rock bulk volume under conditions of elastic behaviour (constant compressibility factor).

The dimension of compressibility $c_r$ is reciprocal pressure, as follows from Eq.(9.1) or (9.14), i.e.

$$[c_r] = [\sigma]^{-1}$$

For normal reservoir rock like quarts, the compressibility is; $c_{quarts} \sim 2.5 \cdot 10^{-6}\ bar^{-1}$.

### 9.2.2 Compressibility of Liquids

Deformation of liquids can be explained, following the same chain of arguments as seen for solid (rock) material. Within the elastic limit of the liquid, one can expect the compressibility to be constant and in accordance to Eq.(9.1) and in analogy with Eq.(9.14),

$$V_l = V_{l_0} e^{-c_l(p-p_0)} \simeq V_{l_0}[1-c_l(p-p_0)], \tag{9.15}$$

where the last approximation is valid when $c_l(p - p_o) \ll 1$.

Various liquids may behave quite differently depending on the composition of that liquid. Water is not particularly compressible and has a compressibility factor $c_w \sim 4.6 \cdot 10^{-5}\, bar^{-1}$. Oil, on the other hand, may have a varying compressibility factor, depending on the composition of oil, i.e. the mixture of light and heavy HC and the amount of gas contained in the oil.

Black oils may have a compressibility $\sim 25 \cdot 10^{-5}\, bar^{-1}$, while light oils can have substantially higher compressibility, depending on the content of the solution gas.

### 9.2.3 Compressibility of Gases

Experience tells us that gases are very compressible. Gas compressibility can be defined equally to solids and liquids, using the definition in Eq.(9.1), in an attempt to consistently describe the nature of compressibility as a universal characteristic, also valid for gases.

In the case of a perfect gas,

$$pV = nRT, \tag{9.16}$$

where
- $p$: absolute pressure of the gas phase,
- $V$: volume which it occupies,
- $T$: absolute temperature of gas,
- $n$: number of moles of gas equal to its mass divided by its gaseous molecular weight and
- $R$: the gas constant.

Combining Eqs.(9.1) and (9.16) one obtain,

$$c_g = -\frac{1}{V}\frac{\partial V}{\partial p} = \frac{1}{p}. \tag{9.17}$$

Form this deduction it must be conclude that compressibility of gases is not constant, but varies as the reciprocal pressure (under the assumption of constant temperature).

**Example: Compressibility of real gas**

The real gas law is,

$$pV = znRT,$$

where $z$ is the deviation factor, expressing the non-ideal deviation from perfect gas behaviour.

Since compressibility describes the volume deformation, we may assume the volume to be a function of pressure, temperature and a non-ideal factor, i.e. $V = V(p,T,z)$.

Differentiation of the volum function,

$$\begin{aligned} dV &= \frac{\partial V}{\partial p}dp + \frac{\partial V}{\partial T}dT + \frac{\partial V}{\partial z}dz, \\ &= -\frac{V}{p}dp + \frac{V}{T}dT + \frac{V}{z}dz. \end{aligned}$$

At reservoir condition, $T$ is constant and consequently,

$$-\frac{1}{V}\frac{dV}{dp} = \frac{1}{p} - \frac{1}{z}\frac{dz}{dp}.$$

Compressibility for real gases in the reservoir is then given by,

$$c_g = \frac{1}{p} - \frac{1}{z}\frac{dz}{dp}.$$

The deviaton factor $z$, is a non-trivial function of pressure and temperature. The z-factor is usually expressed as a function of the so-called *pseudo reduced pressure* $p_{pr}$ and *pseudo reduced temperature* $T_{pr}$, as seen in Fig. 9.4, i.e.

$$z = z(p_{pr}, T_{pr}),$$

where pseudo reduced pressure and temperature are defined as,

$$p_{pr} = \frac{p}{p_{pc}}, \qquad T_{pr} = \frac{T}{T_{pc}},$$

where $p_{pc}$ and $T_{pc}$ are *pseudo critical pressure* and *pseudo critical temperature*, respectively.

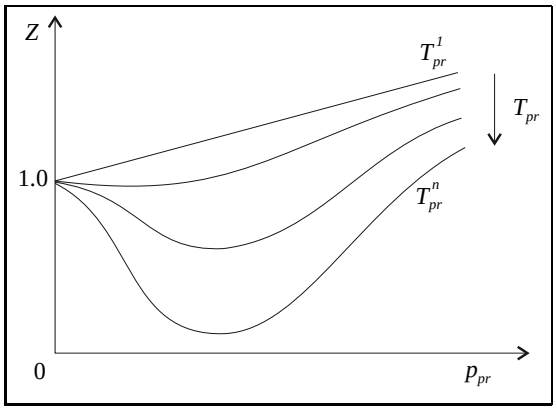


Figure 9.4: z-factor as a function of pseudo reduced pressure $p_{pr}$ and temperature $T_{pr}$.

Critical pressure and temperature for a mixture of $m$ numbers of HC components are defined,

$$p_{pc} = \sum_i^m n_i p_{ci}, \qquad T_{pc} = \sum_i^m n_i T_{ci},$$

where $p_{ci}$ and $T_{ci}$ are critical pressure and temperature of the different HC components and $n_i$ is the volume fraction or the mole fraction of each component given by Avogadro's law.

## 9.3 Deformation of Porous Rock

The elastic deformation or compressibility of porous rock is complicated by the fact that it is subjected to an external confining stress $\sigma$, and in addition to an internal pore pressure $p$, acting on the surface of the pore walls. The total external stress acting on the porous rock is partly counterbalanced by the pore presssure and the forces acting through the rock matrix. This is depicted in Fig. 9.5, where the total stress will be the pressure acting on the outer surface, while the pore pressure and the forces acting through the rock matrix are the counteracting pressures [62].

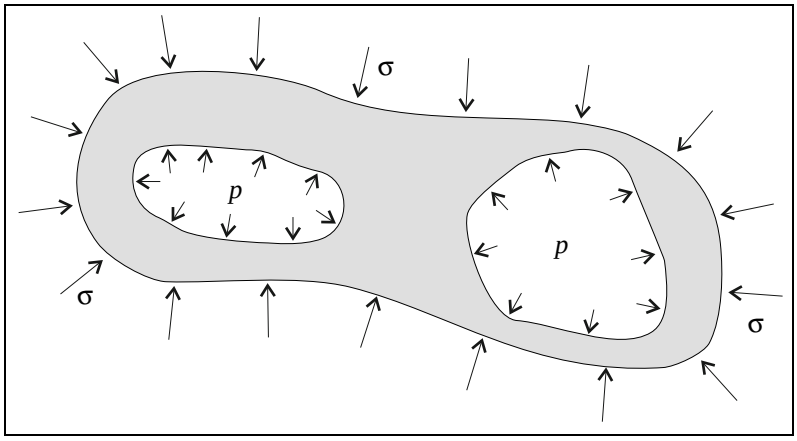


Figure 9.5: Stresses working on a porous rock.

Experience in rock and soil mechanics has shown that the deformation of porous and premeable materials depend on the effective stress which is the difference between the applied total stress and the pore pressure. Effective stress was originally introduced by Terzaghi and is defined as,

$$\sigma' = \sigma - p, \tag{9.18}$$

later the defineition of effective stress has been generalized to,

$$\sigma' = \sigma - \alpha p,$$

where the constant $\alpha$, often called the Biot constant is a number equal or less than one, $\alpha \leq 1$. For most reservoir rocks $\alpha$ will become close to one and may be neglected. It should be noted however that the consept of effective stress does not follow from strictly theoretical considerations, but must be regarded as a close approximation. For porous rocks, the stresses in Hooke's law should be replaced by effective stresses.

When a reservoir is produced the reservoir pressure will in most cases be reduced. The overburden load will however remain more or less constant and thus the vertical effective stress will increase, causing compaction of the reservoir rock. The horizontal stresses may also change with pore pressure and the development of complete stress conditions may be difficult to determine.

For reservoir engineering, it is first of all the volumetric behaviour that is important. The volumetric changes are given by the average applied stress and one will therefore for simplicity in the following assume a hydrostatic applied stress field on the porous rock.

Variation of the effective stress on the rock due to withdrawal of reservoir fluid (oil, gas or initial water) will cause deformation in the bulk volume $V_b$, as well as deformation in the pore volume $V_p$. Generally, both the external stress $\sigma$ and the pore pressure $p$ may provoke changes in the bulk or/and pore volume. The bulk and pore volume are therefore defined as function of both external stress and pore pressure, i.e.

$$\begin{aligned} V_b &= V_b(\sigma, p), \\ V_p &= V_p(\sigma, p). \end{aligned} \tag{9.19}$$

Differentiation of Eqs. (9.19) gives the relative volume change,

$$\begin{aligned} \frac{dV_b}{V_b} &= \frac{1}{V_b}\left(\frac{\partial V_b}{\partial \sigma}\right) d\sigma + \frac{1}{V_b}\left(\frac{\partial V_b}{\partial p}\right) dp, \\ \frac{dV_p}{V_p} &= \frac{1}{V_p}\left(\frac{\partial V_p}{\partial \sigma}\right) d\sigma + \frac{1}{V_p}\left(\frac{\partial V_p}{\partial p}\right) dp. \end{aligned} \tag{9.20}$$

Using Eq. (9.1) the definition of isothermal compressibility, a set of four compressibilities may be defined and Eq. (9.20) is written,

$$\begin{aligned} \frac{dV_b}{V_b} &= -c_{b\sigma} d\sigma + c_{bp} dp, \\ \frac{dV_p}{V_p} &= -c_{p\sigma} d\sigma + c_{pp} dp, \end{aligned} \tag{9.21}$$

where the "minus" sign demonstrates the fact that when $\sigma$ increases, both the bulk and pore volume will decrease, while when $p$ increases, then the bulk and pore volume will increase.

The four compressibilites defined in Eqs. (9.21) are all not independent and through elastic theory it is possible to resolve the relation between them. The purpose of this process is to express the pore compressibility as function of the compressibilities of bulk volume and rock material, $c_p = c_p(c_b, c_r)$.

### 9.3.1 Compressibility Measurements.

If a porous rock sample is brought to the laboratory and the external stress $\sigma$, on the sample is increase while the pore pressure is kept constant $dp = 0$, as seen in Fig. 9.6, left, Eqs. (9.21) gives,

$$\frac{dV_b}{V_b} = -c_{b\sigma} d\sigma, \tag{9.22}$$

Since $c_{b\sigma}$ depends on the elastic moduli of the matrix rock material and the geometry of the pore space, it must in general be considered to be an independent parameter, characterised as the bulk compressibility, i.e. $c_{b\sigma} = c_b$.

If, on the other hand, the rock sample is exposed to an external stress equal to the internal pressure, such that $d\sigma = dp$, see Fig. 9.6, right, then Eqs. (9.21) is written,

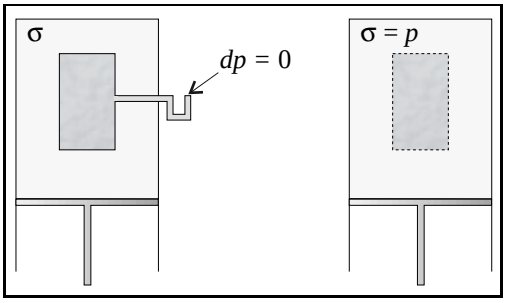


Figure 9.6: Stresses working on a porous rock.

$$\begin{aligned} \frac{dV_b}{V_b} &= (-c_b + c_{bp})d\sigma, \\ \frac{dV_p}{V_p} &= (-c_{p\sigma} + c_{pp})d\sigma, \end{aligned} \tag{9.23}$$

where $d\sigma = dp$ and where $c_{b\sigma} = c_b$.

When the pore pressure increases/decreases equally to the confining stress, then the effect of the pores with respect to the deformation of the porous rock, is only related to the rock matrix material itself. Seen from the outside the material would behave as a completly solid rock. Under these condition, the compressibility of the rock sample is equal to the compressibility of the rock material $c_r$. From Eqs. (9.23), the following relation between compressibilities are deduced;

$$\begin{aligned} -c_b + c_{bp} &= -c_r, \\ -c_{p\sigma} + c_{pp} &= -c_r, \end{aligned} \tag{9.24}$$

where the minus sign for $c_r$ reflects the fact that the rock will compress under these conditions.

### 9.3.2 Betti's Reciprocal Theorem of Elasticity.

If both the external stress and the pore pressure are changing, then the bulk and pore volume are deformed accordingly,

$$\begin{aligned} dV_b &= dV_b(\sigma) + dV_b(p), \\ dV_p &= dV_p(\sigma) + dV_p(p), \end{aligned} \tag{9.25}$$

where $dV(\sigma)$ is the volume change relative to the external stress and $dV(p)$ is the volume change relative to the pore pressure.

Betti's theorem states that the hypothetical work given by the volume expansion of the bulk volume due to the pore pressure $dV_b(p)$ times the change in the external stress $d\sigma$, is equal to the work given by the volume expansion of the pore volume due to the external stress $dV_p(\sigma)$ times the change in the pore pressure $dp$, i.e.

$$dV_b(p) \cdot d\sigma = dV_p(\sigma) \cdot dp. \tag{9.26}$$

Using Eqs. (9.21) in Eq. (9.26), one gets,

$$-V_b c_{bp} dp \cdot d\sigma = -V_p c_{p\sigma} d\sigma \cdot dp, \tag{9.27}$$

where $c_{bp} = c_b$. The minus sign for the first term reflects that the force and displacement are in opposite directions. Since porosity is defined $\phi = V_p/V_b$, the bulk compressibility is given,

$$c_{bp} = \phi c_{p\sigma} \tag{9.28}$$

Combining Eqs. (9.24 and Eq. (9.28) on gets,

$$c_p = \frac{c_b - (1+\phi)c_r}{\phi}, \tag{9.29}$$

where $c_{pp} = c_p$ is the pore volume compressibility. This formula, developed by Geertsma [31], relates the pore compressibility to the bulk and rock compressibilities which are the parameters normally measured, like in experiments sketched in Fig. 9.6.

## 9.4 Compressibility for Reservoir Rock Saturated with Fluids

Compressibility of homogenous matter like the rock material $c_r$ and the contained saturations of fluids, e.g. oil, water and/or gas, are all defined by Eq. (9.1). A discrete version of this definition, where the pressure drop $\Delta p$ is sufficiently small, gives

$$c = \frac{1}{V}\frac{\Delta V}{\Delta p} \quad \Rightarrow \quad \Delta V = cV\Delta p. \tag{9.30}$$

The compressibility of the fluids $c_f$ contained in the pore volume is defined by the compressibility of the different phases; $c_w$, $c_o$ and $c_g$. Since the pore volume is expanded by the fluid phase volumes: $V_f = V_w + V_o + V_g$, a change in the pore pressure will cause the fluid volume to change. The fluid compressibility is written,

$$\begin{aligned} \Delta V_f &= \Delta V_w + \Delta V_o + \Delta V_g, \\ c_f &= c_w \frac{V_w}{V_p} + c_o \frac{V_o}{V_p} + c_g \frac{V_g}{V_p}, \\ &= c_w S_w + c_o S_o + c_g S_g, \end{aligned} \tag{9.31}$$

where $S$ is the fluid phase saturation ($S_w + S_o + S_g = 1$).

Of interest in relation to the production of oil and gas, is the total compressibility of the rock - fluid system. This compressibility accounts for the expansion of fluid, given by the fluid compressibility $c_f$ and the reduction of the pore volume when the pore pressure is reduced, given by $c_p$ in Eq. (9.29),

$$\begin{aligned} c_t &= c_p + c_f, \\ &= \frac{c_b - (1+\phi)c_r}{\phi} + c_w S_w + c_o S_o + c_g S_g, \\ &= \frac{1}{\phi}[c_b - (1+\phi)c_r + \phi(c_w S_w + c_o S_o + c_g S_g)]. \end{aligned} \tag{9.32}$$

The effective HC compressibility is a useful term, related to the pore space occupied by the hydrocarbons,

$$c_{HC} = c_o S_o + c_g S_g.$$

An equally important term is the effective compressibility responsible for the expansion of initial water and reduction of the pore volume, when pressure is released as a result of HC production. This term, a non-HC compressibility is defined,

$$c_{non-HC} = \frac{c_b - (1+\phi)c_r + \phi c_w S_w}{\phi}.$$

**Example: Porosity variation in the reservoir**

When the reservoir pore pressure is reduced, due to oil or gas production, the equilibrium of stresses in the reservoir is changed. This change in the effective stress on the rock material will cause the porosity $\phi = V_p/V_b$ to change.

By differentiation the porosity one gets,

$$\frac{d\phi}{\phi} = \frac{dV_p}{V_p} - \frac{dV_b}{V_b}. \tag{9.33}$$

Substituting Eqs. (9.21) in Eq. (9.33) and remembering that $c_{pp}$ is the pore compressibility $c_p$ and $c_{b\sigma}$ is the bulk compressibility $c_b$,

$$\frac{d\phi}{\phi} = (c_p dp - c_{p\sigma} d\sigma) - (c_{bp} dp - c_b d\sigma). \tag{9.34}$$

Combining Eqs. (9.24) and Eq. (9.29) with Eq. (9.34) gives,

$$d\phi = -c_b(1-\phi) - c_r d(\sigma - p), \tag{9.35}$$

where the porosity change $d\phi$ is proportional to the change in the effective stress. It should be noted that in this case, the dependence on the effective stress is an exact theoretical result.

Under reservoir conditions, the confinement stress is constant, i.e. $d\sigma = 0$ and thus the change in porosity is,

$$\Delta\phi = c_r \left( \frac{c_b}{c_r}(1-\phi) - 1 \right) \Delta p, \tag{9.36}$$

where the pressure drop $\Delta p$, due to fluid production from the reservoir is small enough to keep the material within the elastic limit.

In a non-porous rock, i.e. when $\phi \to 0$, the bulk compressibility will be equal to the rock matrix compressibility, $c_b = c_r$, which then define the lower bound, where by $c_b/c_r \geq 1$. In typical sandstone porous rocks, the ratio $c_b/c_r$ is often found to be between 4 to 100. For sandstone reservoirs with a typical porosity larger than 5-10 %, the terms in the bracket in Eq. (9.36) will always be positive.

When the pore pressure is reduced, $p_1 > p_2$ (Fig. 9.7), a porosity deformation is observed, $\phi_1 > \phi_2$, i.e. the porosity is reduced in the reservoir when the pressure is reduced, which is an important drive mechanism for undersaturated oil reservoirs.

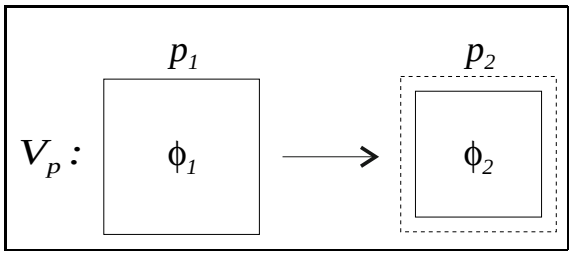


Figure 9.7: Constant confinement pressure and reduced pore pressure leads to a reduction in the pore volume.

**Example: Porosity variation in formation core samples**

Reservoir porosity is seen to decrease with the pore pressure, under the assumption of constant confinement stress. What about the porosity change in rock samples which are brought to the surface for further experimental investigations? This question is quite important since laboratory measurements on core material from wells, is one of the very few direct sources of information available regarding reservoir characteristics.

Eq. (9.35) gives the porosity change relative to the change in the pressure difference $(\sigma - p)$. At initial conditions in the reservoir, the pressure difference is normally such that the confinement pressure is larger than the pore pressure, i.e. $(\sigma - p)_R > 0$. In the laboratory or at normal atmospheric condition, the confinement pressure and the pore pressure will be close to equal, i.e. $(\sigma - p)_L = 0$.

For a porous rock sample, where the bulk and rock matrix compressibilities are such that $(c_b(1-\phi) - c_r) > o$, which is the case for practically all porous rock materials, the porosity will increase when the rock sample is brought to the surface, i.e. $\phi_R < \phi_L$.

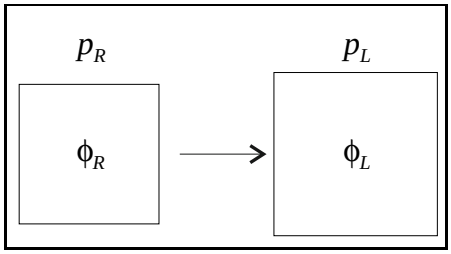


Figure 9.8: Variation of bulk volume during surfacing of core material.

## 9.5 Exercises

1. The reservoir pressure is 1923 psi, connate water saturation is 0.24 and gas saturation is 0.31.

   Find the total compressibility and the effective hydrocarbon compressibility when the following fluid and formation compressibility are known; $c_o = 10 \times 10^{-6}$ psi$^{-1}$, $c_w = 3 \times 10^{-6}$ psi$^{-1}$, $c_g = 1/\text{p}$ psi$^{-1}$ and $c_r = c_b = 5 \times 10^{-6}$ psi$^{-1}$.

2. A reservoir with an initial pressure of 6500 psia has an average porosity of 19 %. Bulk compressibility is $3.8 \times 10^{-6}$ psi$^{-1}$, and estimated abandonment pressure is 500 psia.

   Find the formation porosity when the field is abandoned?

3. A gas reservoir has a gas deviation factor (at $150\,^oF$),

| p [psia] | 0 | 500 | 1000 | 2000 | 3000 | 4000 | 5000 |
|---|---|---|---|---|---|---|---|
| z | 1.00 | 0.92 | 0.86 | 0.80 | 0.82 | 0.89 | 1.00 |

   Plot z versus p and graphically determine the slope at 1000 psia, 2200 psia and 4000 psia. Then, find the gas compressibility at these pressures.

**Answers to questions:**

1. $171.4 \cdot 10^{-6}\, psi^{-1}$, $224.6 \cdot 10^{-6}\, psi^{-1}$, 2. 18.6 %,
3. $1.11 \cdot 10^{-3}\, psi^{-1}$, $0.45 \cdot 10^{-3}\, psi^{-1}$, $0.14 \cdot 10^{-3}\, psi^{-1}$

# Chapter 10

# Properties of Reservoir Fluids

## 10.1 Introduction

Production of oil and gas can be compared to a process where volumes of the reservoir fluids are transformed to the stock tank volumes of oil and gas, see Fig. 10.1. During this process both pressure and temperature are significantly changed. The reservoir production rates of oil and gas will in the event of continuously decreasing pressure and temperature transform, where the phase ratio of oil and gas is changed as well as the *gas-oil ratio* and the composition of both phases.

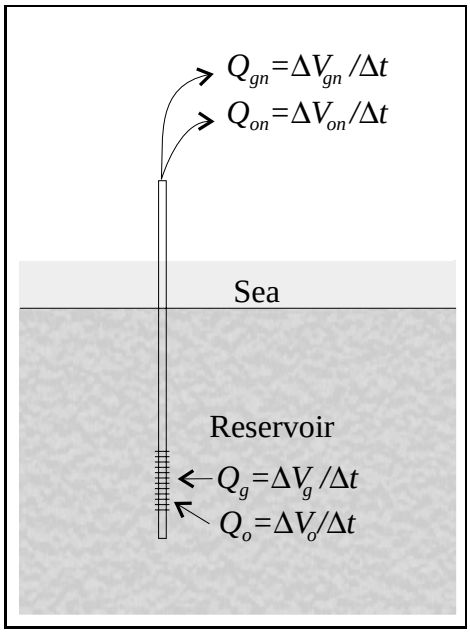


Figure 10.1: Volume transformation of oil and gas.

Primary reservoir production takes place without any temperature change, while the reservoir pressure drops substantially near the well. The composition of oil and/or gas will therefore changed slightly during production. In an oil reservoir we may experience the shrinkage of oil due to the solution gas liberation near the well and in a rich gas reservoir we expect condensa-

tion of liquid hydrocarbons (oil) when the pressure is reduced.

When the reservoir fluid is produced and brought to the surface, pressure is further reduced through different stages of separation. In these processes, temperature is also reduced and consequently the composition of oil and gas undergoes significant change.

In this chapter focus is put on some characteristic aspects of hydrocarbon mixtures and the separation of oil and gas as function of pressure and temperature. We will look at how oil and gas behave in the reservoir and their expansion to stock tank condition.

## 10.2 Definitions

The process by which the different hydrocarbon (HC) components form phases through various chemical reactions is governed by a natural (entropy driven) development towards equilibrium or the lowest energy level. This could be expressed more precisely referring to the Gibbs phase rule.

> The Gibbs phase rule shows a relationship among the number of components $N_C$, number of phases $N_P$, number of chemical reactions $N_R$, and degrees of freedom $N_F$, where;
>
> $$N_F = N_C - N_P + 2 - N_R.$$
>
> The number 2 accounts for *the intensive properties* $p$, $T$, and $N_C - N_R$ defines the number of independent components.

For a pure component (like $H_2O$), then $N_C - N_R = 1$ and

$$N_F = 3 - N_P.$$

For pure components the phase rule says that no more than three phases can form at any temperature and pressure, i.e.

| | | |
|---|---|---|
| When $N_P = 1$ | $N_F = 2$ | Both intensive properties can be changed arbitrarily |
| When $N_P = 2$ | $N_F = 1$ | Only one intensive property can be independent – there are three lines on a (p, T)-plot reflecting this occurrence (sublimation line, melting point line, and vapour pressure line) |
| When $N_P = 3$ | $N_F = 0$ | No degrees of freedom – a single triple point in the phase diagram |

We know that water may appear in different phases like ice, liquid and vapour, all depending on temperature and pressure. The co-existence of different phases, is shown in Fig. 10.2. The different regions are separated by phase boundaries. The phase boundary between water and vapour ends in a critical point where the two phases cease to co-exist. Beyond this point, for temperatures $T > T_C$ and pressures $p > p_C$, there is no distinct difference between water and vapour, hence we call this state the fluid state. (For pure water, i.e. $H_2O$, the critical temperature is 374.1 $^oC$ and the critical pressure is 218.3 atm.)

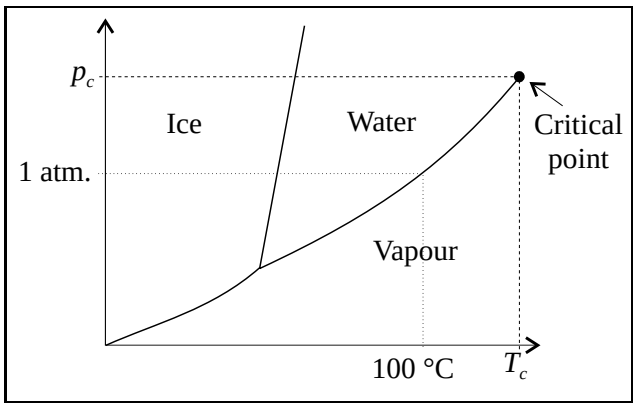


Figure 10.2: PT-diagram for $H_2O$.

## 10.3 Representation of hydrocarbons

Naturally occurring HC are complex in composition and contain a great many members of paraffins (alkanes), naphthenes (cyclo-alkanes) and aromatic series and often some non-hydrocarbon impurities.

Some of the components in the paraffin series are listed below:

| | | | | |
|---|---|---|---|---|
| Methane | $CH_4$ | $C_1$ | Heptane | $C_7H_{16}$ |
| Ethane | $C_2H_6$ | $C_2$ | Octane | $C_8H_{18}$ |
| Propane | $C_3H_8$ | $C_3$ | Nonane | $C_9H_{20}$ |
| Butane | $C_4H_{10}$ | $C_4$ | Decane | $C_{10}H_{22}$ |
| Pentane | $C_5H_{12}$ | $C_5$ | | |
| Hexane | $C_6H_{14}$ | $C_6$ | | |

Some typical non-hydrocarbon impurities are represented by,

| | |
|---|---|
| Nitrogen | $N_2$ |
| Carbon Dioxide | $CO_2$ |
| Hydrogen Sulphide | $H_2S$ |

For mixtures of HC components, $C_7H_{16}$ and higher, it is quite common to write $C_7^+$, meaning all component in the series. The $C_7^+$ characteristic is then the average for all components higher then $C_6$.

In gases, typically light components like $C_1$, $C_2$ and $C_3$ dominate the composition. For light oils, $C_4$, $C_5$ and $C_6$ are the important components and for heavier oils the presence of various decanes and asfaltenes are quit common. However, intermediate components like $C_4 - C_5$ can be in both gaseous and liquid state depending on prevailing pressure and temperature. Components $C_7^+$ are heavy and in most interesting cases of petroleum engineering, can not be evaporized.

For pure components of oil, say, Ethane ($C_2H_6$) and Heptane ($C_7H_{16}$), and their mixture (50% of $C_2H_6$ and 50% of $C_7H_{16}$) the phase PT-diagram is shown in Fig. 10.3. The PT-characteristics of the pure components are somewhat similar to the $H_2O$ case, shown in Fig. 10.2. When two or more HC components are mixed, the phase boundaries form a closed

boundary area in the PT-diagram, where the two phases of oil and gas co-exists. This area is called the two-phase region and has a characteristic shape for that particular composition.

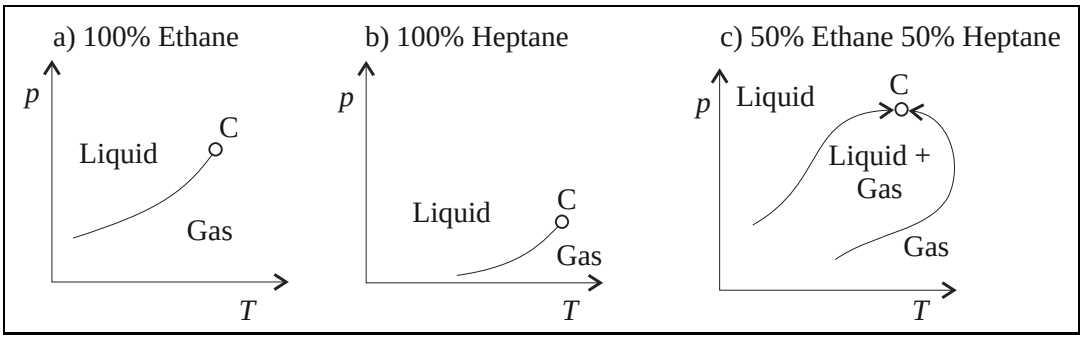


Figure 10.3: PT-diargam for Ethane, Heptane and their mixture.

The equilibrium state is defined as function of $p$ and $T$ and consequently also the volume ratio of oil and gas is PT-dependent. Volume is therefore a dependent function of $p$ and $T$, as shown by the law of real gases. These relations between pressure, volume and temperature are often referred to as PVT-relations. For a mixture of hydrocarbons, a PVT-diagram can be drawn, as shown in Fig. 10.4.

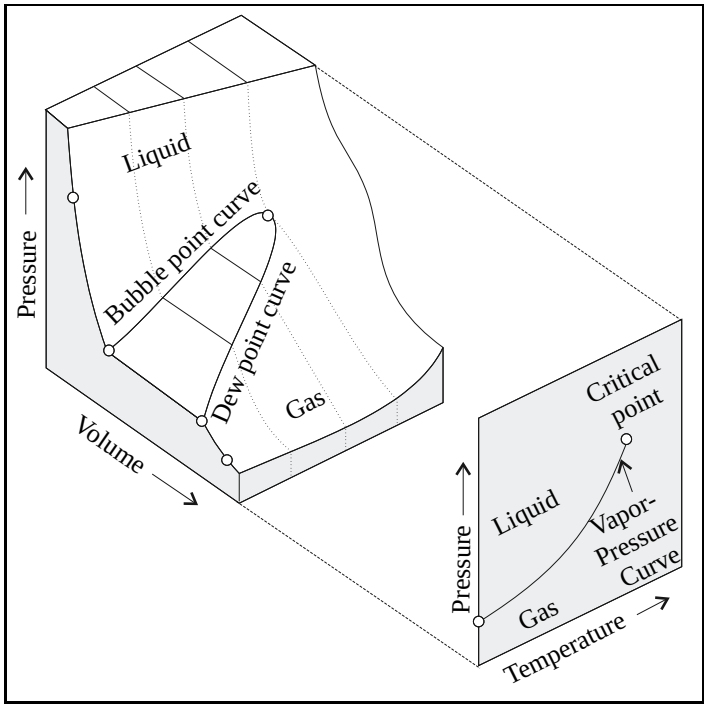


Figure 10.4: PVT diagram for a mixed component system.

The existence of a super critical fluid region to the right of the critical point where phases can not be distinguished, is seen in the PT-diagram in Fig. 10.4 (lower right).

The PV-diagram (upper left) shows how the oil volume is increasing when pressure is

decreasing. For a given temperature, we observe a monotonously volume increase or swelling of the oil phase down to a certain pressure level. At this pressure the volume continues to increase by separation into co-existing oil - and gas phases. Continued volume increase means gradually increased gas-oil ratio at constant pressure. The two-phase region is left when the pressure starts to decrease again and further volume increase is due to gas expansion only.

Another way of representing the PVT discontinuity, represented by the two-phase region, is to present the intensive property of specific - or molar volume, see Fig. 10.5.

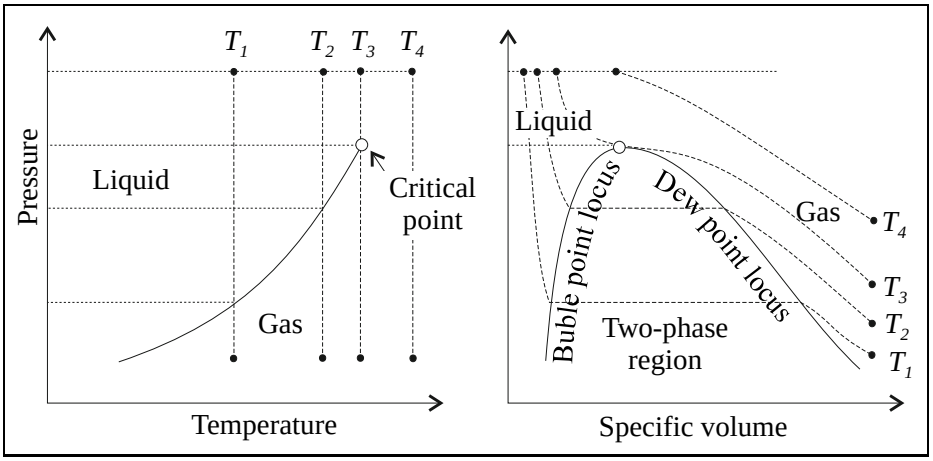


Figure 10.5: Pressure-specific volume diagram for mixed component system.

Specific volume is volume occupied by a unit of mass of a substance, i.e. $[V_s]$ = $m^3$/kg ($ft^3$/lb). Molar volume is equal to volume occupied by one mole of a substance, i.e. $[V_m]$ = $m^3$/kg-mole or $cm^3$/g-mole ($ft^3$/lb-mole).

For temperatures higher than $T_3$, in Fig. 10.5, there is no phase change when pressure is decreased. For lower temperatures, however, a phase transformation will pass through a two-phase region confined by a bubble point locus and a dew point locus where the oil and gas are in equilibrium.

The PT-diagram for a more complex mixtures is presented in Fig. 10.6. It is important to notice that the shape of an envelope A-CP-CT-B depends on the composition of HC mixture, with the following definitions:

CP: **Cricondenbar** – a pressure point, above which a liquid can not be vaporised.

CT: **Cricondentherm** – a temperature point, above which a gas can not be condensed.

C: **Critical Point** – a pressure and temperature point, at which two phases become identical. All the quality lines merge at this point, lines which defines the fractional oil-gas ratio.

A reservoir with initial conditions as indicated by position *1* in Fig. 10.6 is what we would call a gas reservoir. When this reservoir is produced at constant temperature, from *1* to *2*, no phase boundary is crossed, i.e. only gas is produced. If, on the other hand, the production follows the dotted line from *1* to *x*, then oil will gradually drop out of the gas both in the reservoir and on the way to location *x*. The composition of the gas will have changed, where the heavier components are condensed.

A reservoir located at point 3 in Fig. 10.6, should be called a gas condensate reservoir. When this reservoir is produced at constant temperature, from *1* to *5*, condensation of gas in the reservoir starts as soon as the two-phase region is entered, at point *4*. When the pressure continues to decrease, and the dew point line is approached, vaporisation of residual oil can happen and the gas composition may become richer until the dew point line is crossed. Form that point onwards, no change in the composition will occur.

As we have mentioned before, the two-phase region is characterising the reservoir fluid, such that an oil reservoir would have a different shaped two-phase region than seen in Fig. 10.6. Having said this, we can imagine that an oil reservoir is located somewhere in the upper left corner in Fig. 10.6. When this reservoir is produced at constant temperature, no gas will exist in the reservoir until the bubbel point line is crossed. At this time, solution gas will slowly build up to a continuous phase and flow towards the well with a considerably higher mobility than the oil itself.

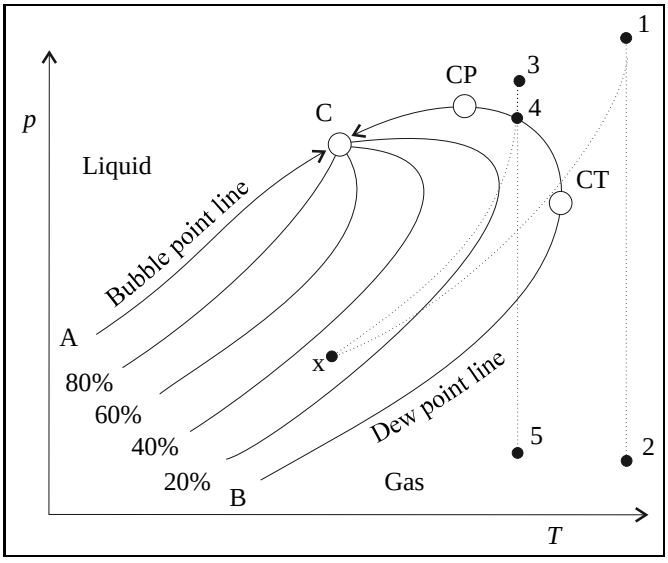


Figure 10.6: PT- diagram for a complex HC mixture.

### 10.3.1 Ternary diagrams

Binary diagrams are often used for representing an overall behaviour of hydrocarbons and for detailed analysis of phase behaviour when the number of components or groups of pure components, do not exceed three . Natural hydrocarbons are complex mixtures of different components and are usually represented by pseudo-components (normally 2 or 3). In order to predict phase behaviour for such compositions ternary diagrams are often used, see Figs. 10.7 and 10.8.

One of the advantages of ternary diagrams is that they enable us to represent both the phase compositions and the overall composition of mixture. Let us assume that the overall composition is represented by point $M$. Then the overall compositions $C_i$ can be expressed through the phase compositions $C_{ij}$,

$$C_i = C_{i1}S_1 + C_{i2}S_2, \quad i = 1,2,3$$

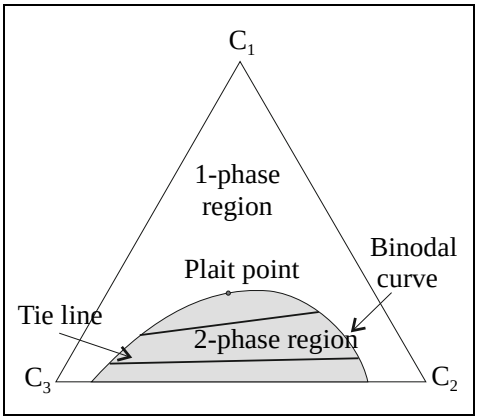


Figure 10.7: Two-phase ternary diagram.

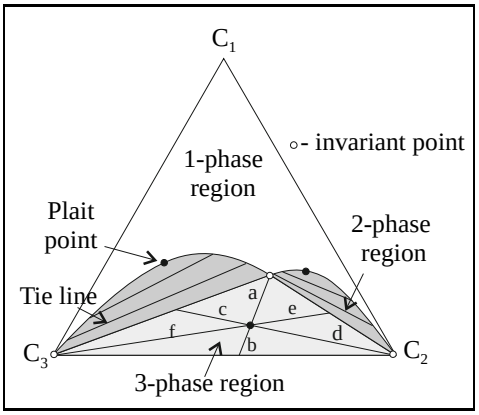


Figure 10.8: Three-phase ternary diagram.

Note that the fraction of each component is 1 at their apex and 0 at the opposite edge. Any unit can be used (mole-, weight- or volume fraction).

Using the fact that $S_1 + S_2 = 1$, we can obtain the following expression for the relative amounts of phases $S_{ij}$ in the overall composition,

$$S_1 = \frac{C_i - C_{i2}}{C_{i1} - C_{i2}}, \qquad S_2 = \frac{C_i - C_{i1}}{C_{i2} - C_{i1}},$$

which is called "the lever rule".

It follows from the Gibbs phase rule that in case of 3 (pseudo) components and 2 phases, where ($p$ and $T$ are expected to be known), the system has only one degree of freedom. This means that if one of the parameters is specified all the other can be easily evaluated.

Fig. 10.8 shows the case when the composition has a 3-phase region which is indicated by the embedded smaller triangle. All sides of this triangle are surrounded by 2- phase regions. There is no degrees of freedom in the three phase region. It means that the compositions of the three phases are given by the apexes of the 3 phase triangle (invariant points). Any total composition $M$ within this triangle gives three phases with the same overall composition. Moving inside the triangle we can only change the fraction of phases and not the overall composition. The lever rule enables us to calculate the relative amounts of these phases,

$$S_1 = \frac{a}{a+b}, \qquad S_2 = \frac{c}{c+d}, \qquad S_3 = \frac{e}{e+f}.$$

In Figs. 10.7 and 10.8 both triangles have a common baseline, which is usually the case for surfactant+oil+brine systems.

## 10.4 Natural gas and gas condensate fields

In a dry gas field, the reservoir temperature is always larger than the critical temperature of the same gas, i.e. the following initial condition is important,

$$T_r > T_{CT}.$$

If initial conditions in the reservoir coincide with point *1* in Fig. 10.6 and gas recovery is performed in such a way that the pressure will decline from *1* to *2*, than the dew point line will never be crossed and only dry gas will exist in the reservoir at any pressure.

When producing the gas to the surface, however, both $p$ and $T$ will decrease and the final state will be at some point $x$ within the two-phase envelope, the position of the point being dependent on surface separation.

Let us imagine initial pressure and temperature at point *3* in Fig. 10.6. During isothermal depletion liquid will start to condense in the reservoir when the pressure has fallen below the dew point at *4*.

The maximum liquid saturation deposited in the reservoir is when the pressure is between points *4* and *5* in the two-phase region. The condensation is generally rather small and frequently below the critical saturation which must be exceeded before the liquid becomes mobile. The process of condensation is called retrograde liquid condensation, where the retrograde liquid condensate is not recovered and, since the heavier components tend to condense first, this represents a loss of a valuable part of the hydrocarbon mixture.

Continued pressure depletion below the point of maximum condensation would lead to re-vaporisation of the liquid condensate. However, this does not occur because once the pressure falls below point *4* the overall composition and hence, the molecular weight of the HC remaining in the reservoir increases and is left behind in the reservoir as retrograde condensate while the light components are mobile and will be produce.

The composite phase envelope for the reservoir fluids tends to move downwards and to the right, thus inhibiting re-vaporisation. Sometimes it is economically advantageous to produce a gas condensate field by the process of gas re-cycling. Starting at point *3* in Fig. 10.9 and separating the liquid condensate from the dry gas at the surface and re-injecting the latter into the reservoir in such a way that the dry gas displaces the wet gas towards the producing wells. However, in practical field developments this is not easily accomplished.

The reservoir pressure is kept almost at the initial level but the composition of the reservoir gas is gradually changed in such a way, that the phase envelope moves to the left and upwards. After breakthrough of the dry gas occurs, the injection is terminated and the remaining dry gas produced. The objective of the gas re-cycling process is to keep reservoir conditions above/or to the right from the dew point curve, as seen in Fig. 10.9.

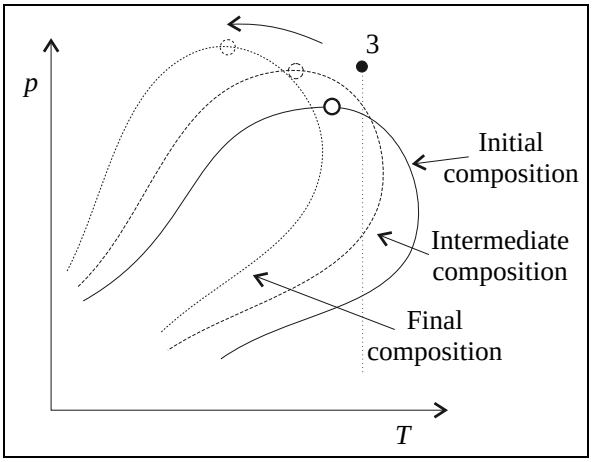


Figure 10.9: Development of the gas field by the gas re-cycling process.

## 10.5 Oil fields

Since the oil contains more of the heavier HC components, a phase diagram for oil will be more elongated in horizontal direction, as compared with gas fields and as shown in Fig. 10.10.

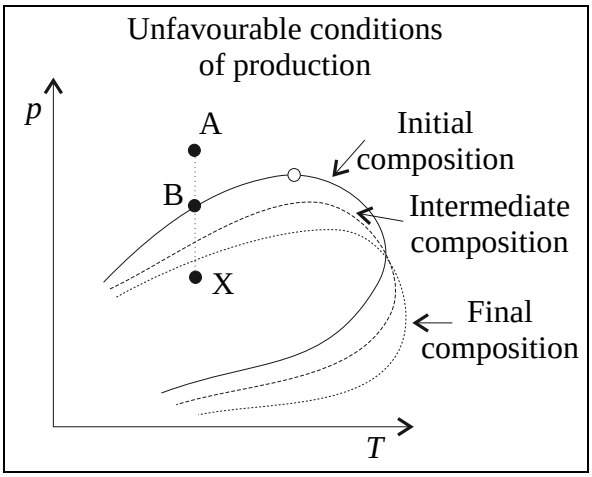


Figure 10.10: Development of the oil field.

If initial conditions in the reservoir coincide with point *A* in Fig. 10.10, there will be only one phase present, namely liquid oil containing dissolved gas. Reducing the pressure isothermally will eventually bring the oil to the bubble point *B*. Further reduction in pressure will lead to solution gas production and the presence of two phases in the reservoir;

- liquid oil, containing an amount of dissolved gas which commensurate with the pressure and
- liberated gas, originally dissolved in the oil.

Keeping production at point *X* below the bubble point, in Fig. 10.10, the overall reservoir HC composition will change due to the fact that the gas, being more mobile, will flow with a much greater velocity than the oil towards the well.

The composition will change to such an extent, that the liquid phase is finally becoming less and less mobile. The relative content of heavier components in oil will increase, and the shape of the phase diagram will change towards more and more unfavourable conditions for oil production. It is therefore preferable to maintain oil production close to, or above the bubble point by using water flooding, gas injection or other enhanced oil recovery methods.

The phase diagram for an oil reservoir with a gas cap must necessarily have a phase envelope which is characterised by both the gas and oil contained in the reservoir. The two-phase area of the reservoir fluid is overlapping the appropriate oil and gas reservoir, as shown in Fig. 10.11.

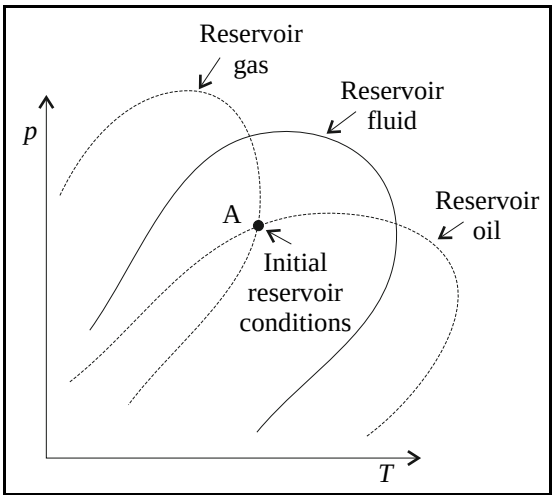


Figure 10.11: Phase diagram for the oil reservoir with a gas cap.

## 10.6 Relation between reservoir and surface volumes

The amount of oil and gas produced form the reservoir, measured in standard volume quantities (at normal pressure and temperature) are converted to reservoir volumes by the use of volume factors; $B_o$, $B_g$, $R_s$ and $R$. These factors are defined in accordance to Fig. 10.12.

Volumes defined at reservoir conditions (or at the surface) are transformed to surface volumes (or reservoir volumes) by use of volume factors. The volume factors are defined by laboratory experiments performed on samples taken from the reservoir oil or gas. The definition of these factors are [21]:

$R_s$ : The solution gas-oil ratio, which is the number of standard cubic meters (feet) of gas which will dissolve in one stock tank cubic meter (barrel) of oil when both are measured at surface conditions.

$$R_s = \frac{V_{ogn}}{V_{on}} \qquad \left[\frac{Sm^3}{Sm^3}\right].$$

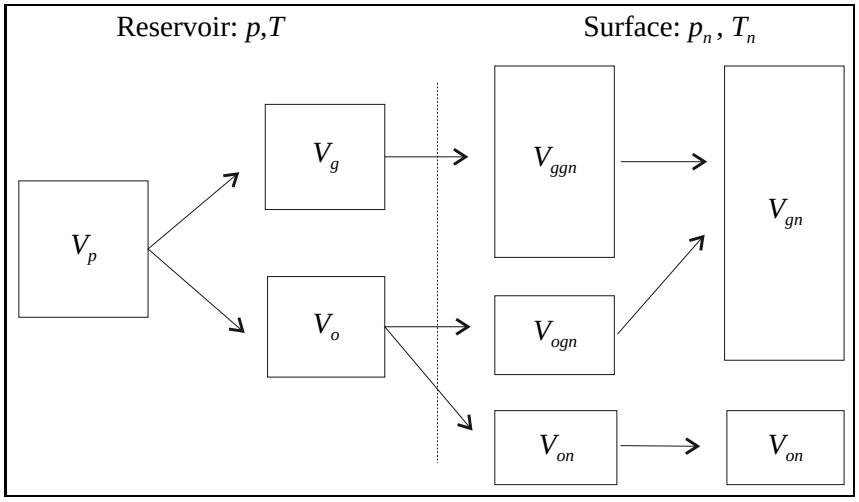


Figure 10.12: Stock tank production through expansion of reservoir oil and -gas from an oil reservoir.

$B_o$: The oil formation volume factor is defined as the volume of oil in cubic meters (or barrels) occupied in the reservoir at the prevailing $p$ and $T$ divided by the volume of oil in stock tank cubic meter (barrel),

$$B_o = \frac{V_o}{V_{on}} \qquad \left[\frac{Rm^3}{Sm^3}\right].$$

$B_g$: The gas formation volume factor is defined as the volume of gas in cubic meters (or barrels) in the reservoir divided by the volume of the same gas at standard cubic meter (foot),

$$B_g = \frac{V_g}{V_{ggn}} \qquad \left[\frac{Rm^3}{Sm^3}\right].$$

$R$: The gas-oil ratio (GOR), is the volume of gas in standard cubic meters (feet) produced divided by volume of stock tank cubic meter (barrel) of oil at surface conditions,

$$R = \frac{V_{gn}}{V_{on}} \qquad \left[\frac{Sm^3}{Sm^3}\right].$$

The following useful relationships between the volume factors can be deduced, simply using Fig. 10.12:

$$V_{gn} = RV_{on} \tag{10.1}$$

$$V_g = B_g(R - R_s)V_{on} \tag{10.2}$$

$$V_o + V_g = [B_o + (R - R_s)B_g]V_{on} \tag{10.3}$$

$$V_g = B_g(1 - \frac{R_s}{R})V_{gn} \tag{10.4}$$

The volume factors $B_o$, $R_s$, $B_g$ and $R$ are all pressure dependent functions, as seen from Fig. 10.13.

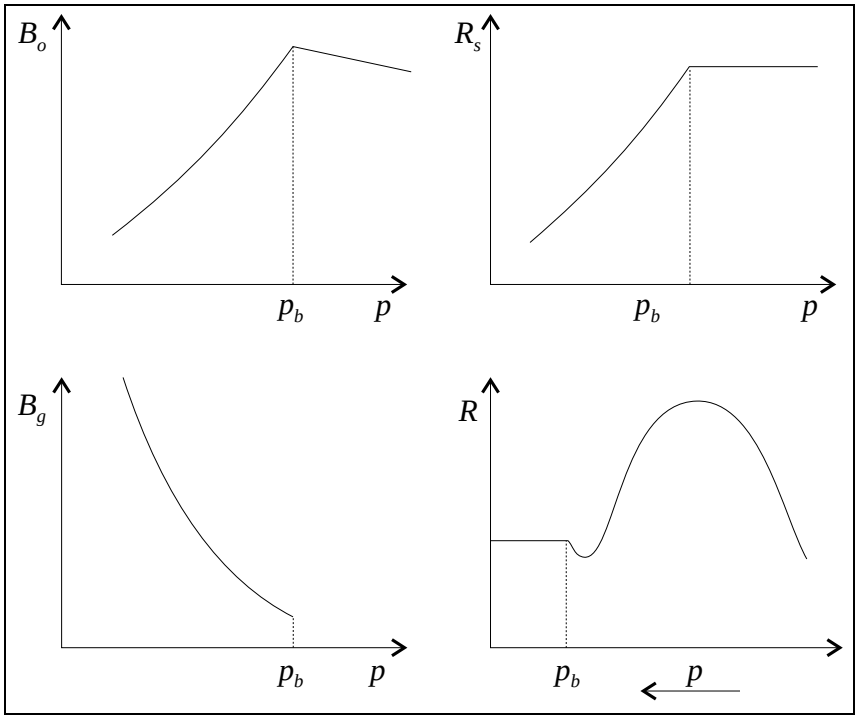


Figure 10.13: Dependency of PVT volum parameters on pressure.

In order to explain the characteristic behaviour of the different volume factors it is natural to follow a decreasing pressure development, i.e. from right to left in Fig. 10.13.

The oil volume factor $B_o$ is seen to increase linearly when pressure is decreasing towards the bubble point pressure $p_b$. This increase in $B_o$ is directly linked to the oil compressibility, i.e. when pressure is released, then volume is increased. For pressure lower then the bubble point, solution gas is gradually leaving the oil phase which leads to a shrinking volume of oil. Finally all gas will evaporate and the oil is said to be *dead* and $B_o \approx 1$. This process continues until standard condition is reached.

The solution gas-oil ratio $R_s$ is constant for pressures higher than the bubble point pressure, since no gas is produced in the reservoir. A unit sample of oil at different pressures ( $p > p_b$) will therefore contain the same amount of gas and oil at standard condition. For pressures lower than the bubble point pressure, we will find a decreasing amount of gas in the reservoir oil sample because some gas has already evaporated and been produced as gas.

In the case of the volum factor for gas, gas in equilibrium with oil can only exist up to its bubble point pressure. For pressure higher than $p_b$, all free gas will be dissolve in the oil. For decreasing pressure lower than the bubble point pressure, the volume of gas will expand as the reciprocal pressure.

The gas-oil ratio $R$, shown in Fig. 10.13, is given as a function of decreasing reservoir

pressure. When the pressure is above the bubble point pressure, no change is observed in the gas-oil ratio at surface condition. Shortly after the reservoir pressure has dropped below the bubble point pressure, the process of solution gas vaporisation will take place, first near the wellbore. For a short while, the gas is not mobile due to gas saturation below critical gas saturation. The presence of discontinuous gas will block some of the path ways for the oil and consequently oil with less gas are being produced. The minimum gas-oil ratio is reached as the gas saturation becomes continuous and starts to flow. When pressure is further decreased, more gas than oil is produced than initially, since gas liberated in the reservoir is more mobile and therefore is produced faster than the oil it originally evaporated from.

**Example: Importance of the GOR**

The GOR is an important parameter, not only because it gives the gas-oil ratio as function of pressure and time, but also because it carries important information about the mobility ratio of gas and oil in the reservoir.

With reference to Figs. 10.1 and 10.12 we may define the gas-oil ratio for a saturated oil reservoir, i.e. with a reservoir pressure lower than bubble point pressure,

$$R = \frac{V_{gn}}{V_{on}} = \frac{Q_{gn}}{Q_{on}},$$

where $Q_{on} = Q_o/B_o$ and where $Q_o$ is the oil rate in the reservoir. Using the relations Eqs.(10.1) - (10.4) we find,

$$\begin{aligned} Q_{gn} &= RQ_{on}, \\ Q_{on} &= Q_g/[B_g(R-R_s)], \end{aligned}$$

where $Q_g$ is the gas rate in the reservoir.

Using the GOR, defined above, and the two relations giving the gas- and oil rate, we may write the following expression for the GOR factor,

$$R = \frac{Q_g}{B_g}\frac{B_o}{Q_o} + R_s.$$

For reservoir flow, we assume Darcy's law to be valid, both for oil- and gas flow, i.e.

$$Q_i = \frac{k_i}{\mu_i} A \frac{dp_i}{dr}, \qquad i = o, g.$$

where $Q_i$ are the reservoir flow rates.

For reservoir flow in the vicinity of the well, we may safely neglect all capillary effects, and the reservoir gas-oil flow ratio is written,

$$\frac{Q_g}{Q_o} = \frac{k_g}{\mu_g}\frac{\mu_o}{k_o}.$$

Substituting this ratio in the GOR equation, we may express the GOR in terms of reservoir parameters,

$$R = \frac{k_g}{\mu_g}\frac{\mu_o}{k_o}\frac{B_o}{B_g} + R_s, \tag{10.5}$$

where the mobility of oil- and gas is defined, $\lambda_i = k_i/\mu_i$, and $i = o, g$.

Eq.(10.5) gives the relation between gas - and oil mobility in the reservoir and the observed gas-oil ration, where the volume factors $B_o$, $B_g$ and $R_s$ are known from laboratory measurements. The GOR as presented in Eq.(10.5) gives a idealized approximation of reservoir dependence and should therefore be interpretated with care.

**Example: Initial reservoir fluids**

The definition of initial in place volumes are somewhat different for oil- and gas reservoirs.

For a general reservoir we may define the following parameters,

| | |
|---|---|
| $V_R$ | Reservoir bulk volume. |
| $\phi$ | Porosity. |
| $B_o$, $B_g$ | Formation factor. |
| $R_s$ | Solution gas-oil ratio. |

The hydrocarbon pore volume, $HCPV = V_R \cdot \phi$, is important in defining the reserves in an oil reservoir,

Oil reserves: $OIIP = HCPV/B_o$,
Gas reserves: $GIIP = OIIP \cdot R_s$.

The reserves coming from a gas reservoir is defined,

Gas reserves: $GIIP = HCPV/B_g$,
Oil reserves: $OIIP = GIIP/R_s$.

## 10.7 Determination of the basic PVT parameters

Conventional analysis of basic PVT parameters follow well established procedures by which the different volume factors are measured:

- Flash expansion of the fluid sample is used to determine the bubble point pressure $p_b$.
- Differential expansion of the fluid sample is used to determine the basic parameters $B_o$, $R_s$ and $B_g$.
- Flash expansion of fluid samples through various separator combinations is used to enable the modification of laboratory derived PVT data to match field separator conditions.

The process differential - and flash expansion, shown in Fig. 10.14, illustrates the difference between flash and differential expansion of the fluid sample.

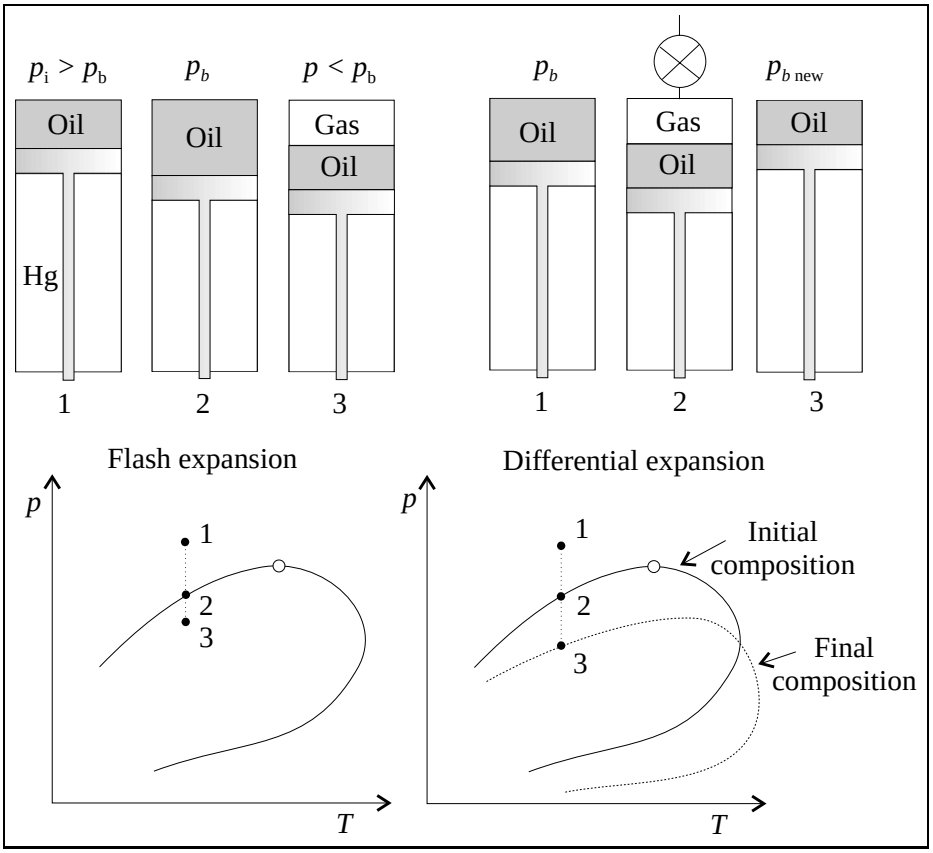


Figure 10.14: Flash and differential expansion of fluid samples.

Note that the flash expansion experiment does not change the overall hydrocarbon composition in the cell while in the differential liberation experiment, at each stage, depletion gas is liberated physically and removed from the cell. Therefore, there is a continous compositional change in the PVT-cell. The remaining hydrocarbones are becoming progressively richer in heavier components and the average molecular weight is increasing. Consequently flash expansion leaves smaller oil volumes then differential expansion.

Reservoir production is most likely reproduced by a non-isothermal differential expansion, where multi-stage separation at the surface is commonly used because differential liberation will normally yield a larger final volume of equilibrium oil than the corresponding flash expansion.

## 10.8 Exercises

1. Calculate the density expressed in SI-units,

   – for a crude oil API gravity of 57.2 and
   – for a natural gas API gravity of 70.7,

   when water density is 1000 $kg/m^3$ at standard condition (1 atm. and $20^0C$).

2. A gas consists of 50% – 50% mixture by weight of two hydrocarbons. The pressure is increased isothermally until two phases appear. The liquid phase consists of 40% by weight of the more volatile component and the vapour phase 65% by weight of this component. What are the weight functions of the liquid and the vapour phase?

3. The following data are obtained in a PVT analysis at $90^0C$.

| Pressure [bar] | 276 | 207 | 172 | 138 | 103 |
|---|---|---|---|---|---|
| Celle (system) volume [$cm^3$] | 404 | 408 | 410 | 430 | 450 |

   a) Estimate the bubble point pressure.

   The system is re-compressed, expanded to 138 bar and the free gas is removed at constant pressure and then measured by further expansion to standard condition. The contained liquid volume is 388 $cm^3$ and the measured gas volume (at 1 atm. and $15.6^0C$) is 5.275 litres.

   The pressure is reduced to normal condition, as above, and residual liquid volume is found to be 295 $cm^3$ and the liberated gas volume is 21 litres.

   Estimate the following PVT parameters,

   b) $c_o$, liquid compressibility at 207 bar,
   c) $B_o$ factor at 207 bar,
   d) $B_o$ and $R_s$ at 172 bar and 138 bar and
   e) $B_g$ and $z$ at 138 bar.

4. Calculate the gas-oil capillary pressure for the following reservoir:

| Gas saturation [%] | Elevation [ft] |
|---|---|
| 75 | -5420 |
| 50 | -5424 |
| 25 | -5426 |
| 0 | -5428 |

   Additional data:

   Oil API gravity; 45.1
   Gas specific gravity; 0.65
   Oil formation volume factor; 1.18 RB/STB
   Gas formation volume factor; 0.0025 RB/SCF
   Solution gas-oil ratio; 480 SCF/STB

**Answers to questions:**

1. 749.5 $kg/m^3$, 699.8 $kg/m^3$ , 2. 2/3, 3. a) 172 bar, b) $14.1 \cdot 10^{-5}\, bar^{-1}$,
c) 1.383 $Rm^3/Sm^3$, d)1.3898 $Rm^3/Sm^3$, 1.315 $Rm^3/Sm^3$,
89.07 $Sm^3/Sm^3$, 71.2 $Sm^3/Sm^3$, e) 0.0079 $Rm^3/Sm^3$, 0.887 4. $\rho_o$ = 735.5 $kg/Rm^3$, $\rho_g$ = 55.7 $kg/Rm^3$.

# Part II

# Reservoir Parameter Estimation Methods

# Chapter 11

# Material Balance Equation

## 11.1 Introduction

The basic principle behind the Material Balance Equation is very fundamental:

> The mass of hydrocarbons (HC) initially in place is equal to sum of the mass produced and the mass still remaining in the reservoir,

$$M_i = \Delta M + M.$$

In material balance calculations we implicitly consider the reservoir as being a tank of constant volume. The pressure in this tank is defined by the volumetric average pressure,

$$\overline{p} = \frac{1}{V_i}\int_{V_i} p dV,$$

where $V_i$ is the initial hydrocarbone volume, i.e. the hydrocarbon pore volume (HCPV).

If we assume the fluid density in the reservoir to be constant during the depletion process, i.e. $\rho \sim$ constant, we may write the mass conservation law in terms of volume conservation,

$$V_i - V = \Delta V \text{ when } p_i \to p. \tag{11.1}$$

Eq.(11.1) is often referred to as *the golden principle*, where

Expansion = Production.

Even though material balance techniques use crude approximations of the reservoir, with limited reference to local information, their application and use have proven to be of great importance in various situations. Being simple in principle, methods based on the material balance equation are commonly used in the following cases:

- Extrapolation of production curves for oil, water and gas (production decline curve analysis).
- Identification of the drive mechanism.
- History matching.

In this chapter we will develop the Material Balance Equation for a general oil and gas reservoir and illustrate the use of the equation by various examples.

## 11.2 Dry gas expansion

Let us consider a dry gas reservoir where the production is modelled using material balance calculations. The HCPV is constant in absence of water influx. The production of gas at surface conditions is $G_p$.

The material balance equation given by Eq.(11.1) is slightly redefined where the volume of gas in the reservoir initially in place is obviously equal to the volume of gas in the reservoir at a given pressure $p$,

$$G \cdot B_{gi} = (G - G_p)B_g, \tag{11.2}$$

where the following definitions are used,

$G$: resources of gas initially in place, $[Sm^3]$,

$G_p$: cumulative volume of gas produced, $[Sm^3]$,

$B_{gi}$: initial gas formation volume factor, $[Sm^3/Rm^3]$ and

$B_g$: gas formation volume factor at current reservoir pressure, $[Sm^3/Rm^3]$.

The relation presented in Eq.(11.2) is illustrated in Fig. 11.1, where the purpose is to visualise the transformation of gas volume under reservoir condition to surface conditions. When a surface volume of $G_p$ has been produced, the volume of gas left in the reservoir is $G - G_p$, in standard units. At a reservoir pressure $p$, the volume occupied by the gas in the reservoir, is equal to $(G - G_p)B_{gp}$, i.e Eq.(11.2).

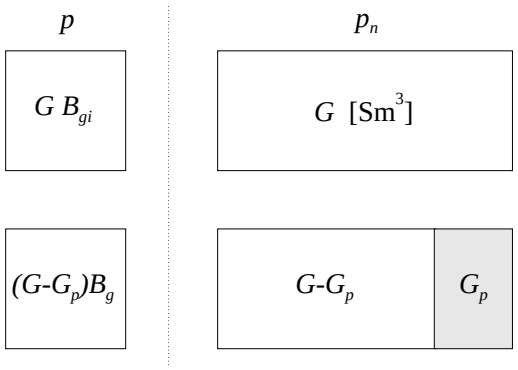


Figure 11.1: Volume transformation using volume formation factors.

It follows from Eq.(11.2) that,

$$\frac{B_{gi}}{B_g} = 1 - \frac{G_p}{G}. \tag{11.3}$$

Using the equation of state for a real gas $pV = znRT$, and assuming isothermal conditions of production one can obtain the relations,

$$B_{gi} \quad = \quad \frac{V_i}{V_n} = \left(\frac{p}{zT}\right)_n \cdot \left(\frac{zT}{p}\right)_i \text{ and}$$

$$B_g = \frac{V_p}{V_n} = \left(\frac{p}{zT}\right)_n \cdot \left(\frac{zT}{p}\right)_p,$$

where the indices *i* and *p* refer to the initial and current pressures respectively .

Eq.(11.3) can now be written,

$$\left(\frac{p}{z}\right) = \left(\frac{p}{z}\right)_i \left(1 - \frac{G_p}{G}\right). \tag{11.4}$$

Using Eq.(11.4), $p/z$ vs. cumulative gas production exhibits a straight line trend, allowing us to estimate the resources of gas, as shown in Fig. 11.2. Two important characteristics are displayed by plotting the data as shown in the figure. When the data follows a linear trend, this serves as a proof for the assumption of no or negligible water influx during gas production and that the main driving force behind the production is gas expansion. Secondly, when a straight line is fitted through the data, the intersection point with the x-axis gives us an estimate for initial gas in place, *G*.

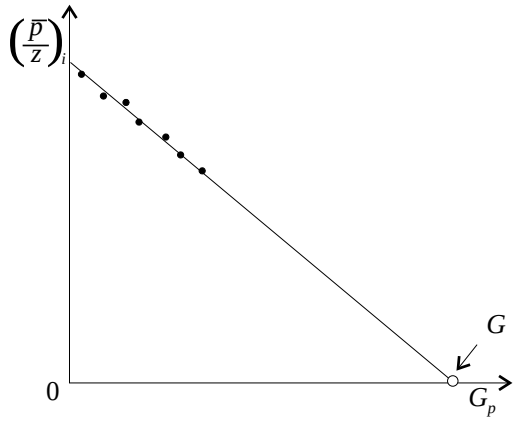


Figure 11.2: Gas reservoir exhibiting a straight line trend in $p/z$ vs. cumulative gas production.

## 11.3 A general oil reservoir

In a general oil reservoir, hydrocarbons will be represented as oil and/or gas. Dependent on the composition of the fluid, reservoir temperature and initial pressure, there may exist a gas cap above the oil zone, as schematically indicated in Fig. 11.3. The gas in the gas cap is in equilibrium with the oil in the oil zone and the volume part of the reservoir occupied by gas relative to oil is constant.

The following nomenclature is used in the derivation of the material balance equation:

*HCPV*: Part of pore volume occupied by hydrocarbons.

*N*: Resources of oil (initial oil in place) in $Sm^3$ .

*m*: Ratio between the resources of gas in the gas cap and resources of oil in the oil zone measured at reservoir conditions.

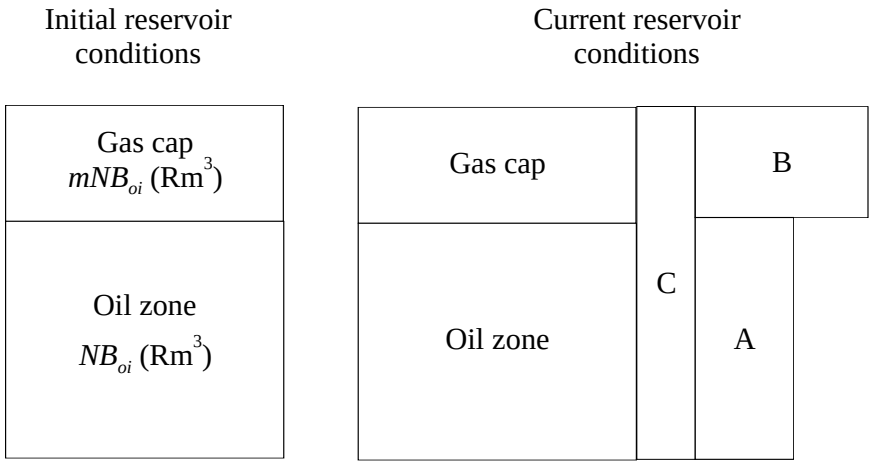


Figure 11.3: Oil reservoir with a gas cap: Illustration of material balance.

$mNB_{oi}$: Resources of gas (initial gas in place) in $Rm^3$.

$N_p$: Volume of oil produced in $Sm^3$.

Production from the oil reservoir (with a gas cap, see Fig. 11.3) is explained as expansion of the oil zone, volume - A, expansion of the gas cap, volume - B and as expansion of initial water present plus reduction of pore volume due to expansion of reservoir formation matrix and possible reduction of bulk volume, volume - C. In dealing with the development of the material balance equation, it is therefore convenient to break up the expansion term into its components. Note that we are here considering underground withdrawal of hydrocarbon fluids, measured in $Rm^3$.

A1: Expansion of oil.

A2: Expansion of originally dissolved gas.

B: Expansion of gas cap gas.

C: Reduction in HCPV due to expansion of connate water and reduction of pore volume.

Reservoir expansion is equal to production, hence: $\Delta V_{prod}$ = A1 + A2 + B + C.

### 11.3.1 A1: Expansion of oil

The oil (liquid phase) expansion at reservoir condition can be defined as,

$$V_o(p) - V_o(p_i) = \Delta V_o(p).$$

Here $V_o(p_i)$ is the oil volume at initial conditions and $V_o(p)$ is the volume of the oil initial in place at pressure $p$, see Fig. 11.4. $\Delta V_o$ is the volume oil produced at reservoir pressure $p$.

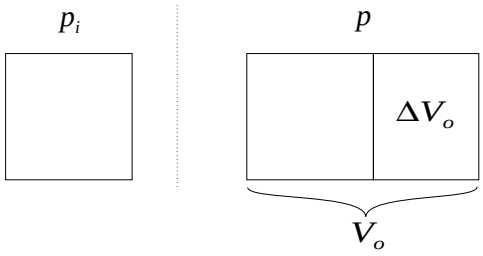


Figure 11.4: Expansion of oil at reservoir pressure.

Oil expansion is written,

$$\Delta V_o = N \cdot B_o - N \cdot B_{oi} = N(B_o - B_{oi}), \tag{11.5}$$

where $\Delta V_o$ is measured in $Rm^3$. $N$ is the initial oil in place [$Sm^3$] and is defined; $N = V_p(1 - S_w)/B_{oi}$, where $S_w$ is the average water saturation and $V_p$ the pore volume.

### 11.3.2 A2: Expansion of originally dissolved gas

At initial conditions oil and gas in the gas cap are in mutual equilibrium . Reducing the pressure below the bubble point pressure, $p_b$ will cause the liberation of solution gas.

The total amount of solution gas in the oil is $NR_{si}$, measured in surface volumes. The amount of gas still dissolved in the oil at current reservoir pressure and temperature is $NR_s$, also in surface volumes. Therefore, the gas volume liberated during the pressure drop, from $p_i$ to $p$, is,

$$NR_{si} - NR_s = N(R_{si} - R_s).$$

This gas volume is measured at surface condition, but since we want to express all expanded volumes at reservoir condition, we have to multiply the surface volume by the volume factor for gas at reservoir pressure, i.e. $B_g$,

$$\Delta V_{og} = N(R_{si} - R_s)B_g. \tag{11.6}$$

### 11.3.3 B: Expansion of gas cap gas

The expansion of gas cap gas follows the same principle as observed for the expansion/production of dry gas given by Eq.(11.2),

$$GB_{gi} = (G - G_p)B_g.$$

The total volume of the gas cap as part of the oil volume in the reservoir, measured at reservoir condition,

$$GB_{gi} = mNB_{oi}.$$

The gas production at current reservoir pressure is then,

$$G_p B_g = \frac{mNB_{oi}}{B_{gi}}(B_g - B_{gi}).$$

The expansion of the gas cap (in reservoir volumes) is therefore written,

$$\Delta V_{gg} = mNB_{oi}\left(\frac{B_g}{B_{gi}} - 1\right). \tag{11.7}$$

### 11.3.4 C: Reduction in HCPV due to expansion of connate water and reduction of pore volume

Reduction in HCPV due to expansion of connate water and reduction of pore volume is in practice equal to the increased production by the same volume. Expansion of connate water and reduction of pore volume are controlled by the compressibility of water and pore volumes, i.e. $c_w$ and $c_p$.

The HCPV compressibility as the compressibility for connate water and formation matrix are defined in accordance with the general law of thermal compressibility,

$$c = \frac{1}{V}\frac{\Delta V}{\Delta p} \quad \Rightarrow \quad \Delta V = cV\Delta p,$$

where the absolute volume change in the HC pore space due to expansion of connate water and reduction of pore volume is,

$$\Delta V_{HCPV} = \Delta V_w + \Delta V_p.$$

$\Delta V_w$ and $\Delta V_p$ are the volume changes due to expansion of connate water and that due to reduction in pore volume, respectively.

Using the definition of compressibility, we get,

$$\Delta V_{HCPV} = c_w V_w \Delta p + c_p V_p \Delta p.$$

From previous considerations, we found that: $V_w = S_w V_p$ and $V_p = V_{HCPV}/(1 - S_w)$ and we get,

$$\Delta V_{HCPV} = V_{HCPV}\left(\frac{c_w S_w + c_p}{1 - S_w}\right)\Delta p,$$

where the pore volume compressibility is; $c_p = (c_b - (1+\phi)c_r)/\phi$ and $V_{HCPV} = V_o + V_g = NB_{oi} + mNB_{oi} = (1+m)NB_{oi}$.

The volume expansion due to initial water and reduction in the pore volume, gives the expansion of the HCPV or volume -C,

$$\Delta V_{HCPV} = (1+m)NB_{oi}\left(\frac{c_w S_w + c_p}{1 - S_w}\right)\Delta p. \tag{11.8}$$

### 11.3.5 Production terms

The production of oil and gas at surface conditions is, $N_p + G_p$. The expansion volumes, A1, A2, B and C, are measured at reservoir conditions. In order to compare the two types of volumes, we have to transform the production volumes to reservoir volumes, i.e. $N_pB_o + G_pB_g$.

Using the relation between gas and oil produced at standard condition, Eqs.(10.1) to (10.4),

$$G_p = (R - R_s)N_p,$$

where $R$ is the gas-oil ratio (GOR) and $R_s$ is the solution gas-oil ratio.

We can now write the overall production term as,

$$\Delta V_{prod} = N_p[B_o + (R - R_s)B_g]. \tag{11.9}$$

## 11.4 The material balance equation

Combining Eqs.(11.5) to (11.9) we can write the material balance equation for a general oil reservoir,

$$N_p[B_o + (R - R_s)B_g] = NB_{oi}\left[\frac{(B_o - B_{oi}) + (R_{si} - R_s)B_g}{B_{oi}} + m(\frac{B_g}{B_{gi}} - 1) + (1 + m)(\frac{c_wS_w + c_p}{1 - S_w})\Delta p\right] + (W_e - W_p)B_w. \tag{11.10}$$

$(W_e - W_p)B_w$ on the right-hand side of Eq.(11.10) accounts for water influx into the reservoir and production of water, respectively.

It is important to notice under which circumstances the material balance equation is developed. The equation gives a static representation of the reservoir and does not include any terms describing the energy loss in the reservoir due to fluid flow behaviour. The following features of the MBE should be noted:

- MBE generally exhibits a lack of time dependence although the water influx has a time dependence.
- Although the pressure only appears explicitly in the water and pore volume compressibility terms, it is implicit in all the other terms of Eq.(11.10) since the PVT parameters $B_o$, $R_s$ and $B_g$ are functions of pressure. The water influx is also pressure dependent.
- Eq.(11.10) is evaluated, in the way it was derived, by comparing the current volumes at pressure $p$ to the original volumes at $p_i$. Note that the material balance equation is not evaluated in a step-wise or differential fashion.

## 11.5 Linearized material balance equation

The linearized material balance equation is particular interesting in connection with reservoir parameter estimation. Results published in 1963-64 by Havlena and Odeh opened a wide range

of applications of the MBE to reservoir engineering [33, 34]. The linear form of equation (11.10) is,

$$F = N(E_o + mE_g + E_c) + W_e B_w, \tag{11.11}$$

where the following definitions are used:

**The underground withdrawal:**

$$F = N_p[B_o + (R - R_s)B_g] + W_p B_w$$

**Expansion of oil and its originally dissolved gas:**

$$E_o = (B_o - B_{oi}) + (R_{si} - R_s)B_g$$

**Expansion of the gas cap gas:**

$$E_g = B_{oi}\left(\frac{B_g}{B_{gi}} - 1\right)$$

**Expansion of the connate water and reduction of pore volume:**

$$E_c = (1+m)\left(\frac{c_w S_w + c_p}{1 - S_w}\right) B_{oi}\Delta p$$

Eq.(11.11) is especially important for revealing the drive mechanism of the reservoir and for estimation of initial oil and gas.

## 11.6 Dissolved gas expansion drive

Fluid samples taken from an oil reservoir, indicate a reservoir pressure larger than the bubble point pressure, i.e. $p > p_b$. From this information alone, important deductions are made:

1. The reservoir fluid exists in only one phase, as undersaturated oil.
2. Production is driven by expansion of undersaturated oil.
3. No gas cap can exist.
4. All produced gas comes from the oil, i.e. $R_{si} = R_s = R$.
5. Production of oil is controlled by compressibility of oil, -water and -formation.

With these restrictions in mind, a simplified material balance equation is written,

$$N_p B_o = N B_{oi}\left[\frac{B_o - B_{oi}}{B_{oi}} + \frac{c_w S_w + c_p}{1 - S_w}\Delta p\right].$$

We have seen earlier that the slow decline of the volume factor $B_o$, for increasing pressures higher than the bubble point pressure, is described by the law of compressibility,

$$c_o = \frac{1}{V_o}\frac{\Delta V_o}{\Delta p},$$

where we may use the definitions; $\Delta p = p_i - p, V_o = V_{on}B_{oi}$ and $\Delta V_o = V_{on}(B_o - B_{oi})$. Note the notation: $N = V_{on}$, in accordance with Fig. 10.12.

Oil compressibility is therefore written,

$$c_o = \frac{1}{V_{on}B_{oi}}\frac{V_{on}(B_o - B_{oi})}{\Delta p} = \frac{B_o - B_{oi}}{B_{oi}}\frac{1}{\Delta p}, \tag{11.12}$$

and the simplified material balance equation above is therefore,

$$N_p B_o = NB_{oi}\left[\frac{c_o S_o + c_w S_w + c_p}{1 - S_w}\Delta p\right].$$

By introducing a total compressibility; $c_t = c_o S_o + c_w S_w + c_p$, we may write the equation above,

$$N_p \cdot B_o = N \cdot B_{oi}\frac{c_t}{1 - S_w}\Delta p, \tag{11.13}$$

and by introducing the reservoir pore volume using the expression, $V_p S_o = N \cdot B_{oi}$, we may find a simple relation between produced oil, $N_p$ and observed pressure drop, $\Delta p$ given by,

$$N_p = \frac{V_p c_t}{B_o}\Delta p.$$

The linear relationship between oil production $N_p$ and pressure drop $\Delta p$ can be used to estimate unknown reservoir parameters such as pore volume $V_p$ or total compressibility $c_t$. Fig. 11.5 shows a linear representation of the data, used to determine $V_p$ and $c_t$.

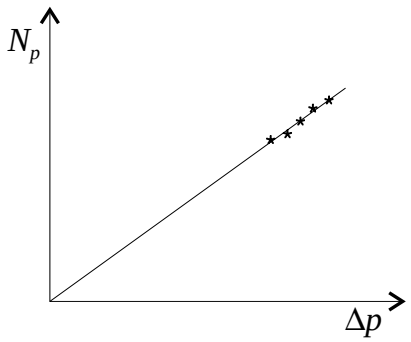


Figure 11.5: Reservoir parameter estimation for dissolved gas expansion data.

$c_w = 3 \cdot 10^{-6} psi^{-1}$ $p_i = 4000\, psi$ $B_{oi} = 1.2417$ RB/STB
$c_p = 8.6 \cdot 10^{-6} psi^{-1}$ $p_b = 3330\, psi$ $B_{ob} = 1.2511$ RB/STB
$S_w = 0.2$

**Example: Oil recovery factor at bubble point pressure**

An undersaturated oil reservoir has been produced down to its bubble point pressure. What is the oil recovery at this time when the following parameters are given?

From Eq.(11.13) we may write,

$$\frac{N_p}{N} = \frac{B_{oi}}{B_{ob}} \frac{c_t \Delta p}{1 - S_w},$$

where $c_t = c_o S_o + c_w S_w + c_p$. Using Eq.(11.12) we have the total compressibility,

$$c_t = \frac{B_{ob} - B_{oi}}{B_{oi} \Delta p}(1 - S_w) + c_w S_w + c_p.$$

Inserting for the numbers from the table above, we find the total compressibility; $c_t = 18.24 \cdot 10^{-6} psi^{-1}$, and the relative production becomes,

$$\left(\frac{N_p}{N}\right)_{3330 psi} = 0.01516,$$

which gives an oil recovery at the bubble point pressure equal to 1.5%.

———— · ————

After some time with continuous production, the reservoir pressure will finally decrease below bubble point pressure. When this happens, gas is produced in the reservoir and the expansion of this gas will become increasingly important for the process of oil production. The material balance equation Eq.(11.10) can now be expressed as,

$$N_p[B_o + (R - R_s)B_g] = N\left[(B_o - B_{oi}) + (R_{si} - R_s)B_g + \frac{c_w S_w + c_p}{1 - S_w}\Delta p\right].$$

When we consider the significance of the different expansion factors, we may assume the gas expansion to be gradually more important than the expansion due to compressibility of initial water and the formation. Consequently, we may neglect the compressibility term and write the simplified material balance equation as,

$$N_p[B_o + (R - R_s)B_g] \approx N[(B_o - B_{oi}) + (R_{si} - R_s)B_g]. \tag{11.14}$$

The use of this approximate equation is justified through a comparison of the different volumes A and C in Fig. 11.3. For reservoir pressures $p < p_b$, we will find that A $\gg$ C in all practical cases.

$$R_{si}(4000psi) = 510 \text{ SCF/STB} \quad B_g(900psi) = 0.00339 \text{ RB/SCF}$$
$$R_s(900psi) = 122 \text{ SCF/STB} \quad B_o(900psi) = 1.0940 \text{ RB/STB}$$

**Example: Oil recovery below the bubble point pressure**

Using the same example as above, we can now calculate the oil recovery down to a pressure $p = 900psi$,where the volume factors are given:

The solution gas produced in the reservoir will change the compressibility in the reservoir drastically. The formula for gas compressibility can be given by $c_g = 1/V(\Delta V/\Delta p)$, indicating a gas compressibility of $c_g \simeq 300 \cdot 10^{-6} psi^{-1}$. This is about 15 times larger than the total compressibility at pressures above the bubble point pressure.

From this simple consideration we may assume all compressibility terms in the material balance equation, Eq.(11.10), to be negligible compared to the solution gas compressibility. We may therefore use the approximation Eq.(11.14),

$$\frac{N_p}{N} = \frac{(B_o - B_{oi}) + (R_{si} - R_s)B_g}{B_o + (R - R_s)B_g},$$

where $R$ is the gas-oil ratio (GOR).

Using the numbers from the tables above, we find the oil recovery equal to,

$$\left(\frac{N_p}{N}\right)_{900psi} = \frac{344.4}{R + 200.7}. \tag{11.15}$$

In order to numerically define the oil recovery, information about the GOR is necessary. On the other hand it is quite obvious that oil recovery is maximised when $R$ is kept as small as possible, i.e. gas should remain in the reservoir if oil production is to be optimized.

From the example above we may state an improtant production strategy for oil reservoirs, namely that:

All production should come from the oil zone.

Since the gas is considered as the driving force in the reservoir production, it should, if possible be produced after the oil is produced. If the gas is produced first, we will not only loose some of the driving force, but the oil will also be smeared out due to the withdrawal of the gas zone. This oil, due to capillary effects, is most probably lost.

## 11.7 Gas cap expansion drive

The presence of a gas cap at initial conditions indicates a saturated oil in equilibrium with the gas. As learned from the example above, production of gas should be minimised since gas acts as the driving force behind oil production. The wells should therefore be drilled and

completed with the purposed of optimising oil production, keeping as much gas in the reservoir as possible.

When a gas cap is discovered in connection with an oil reservoir, we can safely neglect all terms in the material balance equation, Eq.(11.10), containing expansion of connate water or formation matrix. In the case of gas cap expansion drive we therefore get the somewhat simplified material balance equation,

$$N_p[B_o + (R - R_s)B_g] = \\ NB_{oi}\left[\frac{(B_o - B_{oi}) + (R_{si} - R_s)B_g}{B_{oi}} + m(\frac{B_g}{B_{gi}} - 1)\right] + (W_e - W_p)B_w,$$

where the linearized material balance equation is,

$$F = N(E_o + mE_g) + W_eB_w.$$

If we could assume no water influx during oil production, i.e. $W_e = 0$, the linearized material balance equation could then be written,

$$\frac{F}{E_o} = N + mN\frac{E_g}{E_o}, \tag{11.16}$$

which clearly indicates the advantage with linearization, where $mN$ is the slope and $N$ is the constant term ($N$ is the intersection point with the y-axis). The assumption of negligible water influx is rather plausible for reservoirs with a gas cap since the expansion of initial water and formation matrix is small compared to the expansion of gas cap gas, unless the aquifer size is large compared to the oil reservoir.

**Example: Linearization of material balance equation**

The pressure decline in a saturated oil reservoir with a gas cap is driven by expansion of liberated solution gas $E_o$, and gas cap expansion $E_g$, as presented in Eq.(11.16).

In order to estimate initial oil in place $N$, and the size of the gas cap $mN$, we need to know the production data, like produced oil volume at surface condition $N_p$, in addition to the gas-oil ratio $R$. Further information is also acquired with respect to the different volume factors $B_o$, $B_g$ and $R_s$.

The linearized terms used in Eq.(11.16) are defined as below,

$$\begin{aligned} F &= N_p[B_o + (R - R_s)B_g], \\ E_o &= (B_o - B_{oi}) + (R_{si} - R_s)B_g, \\ E_g &= B_{oi}(\frac{B_g}{B_{gi}} - 1), \end{aligned}$$

where we assume no water production or water influx.

For an oil reservoir with a gas cap, we have the following data,

| p [psia] | $F/E_o \cdot 10^6[STB]$ | $E_g/E_o$ |
|---|---|---|
| 3150 | 398.8 | 4.94 |
| 3000 | 371.8 | 4.51 |
| 2850 | 368.5 | 4.29 |
| 2700 | 355.7 | 4.25 |
| 2550 | 340.6 | 3.99 |
| 2400 | 340.7 | 3.93 |

The data in the table above is plotted in Fig. 11.6 which shows a linearization fit taking into account all data points. From the figure we find the initial oil volume to be $N = 109.5 \cdot 10^6$ STB and the slope or gas cap size $mN = 58.7 \cdot 10^6$ STB, indicating a fractional gas cap size of $m = 0.54$.

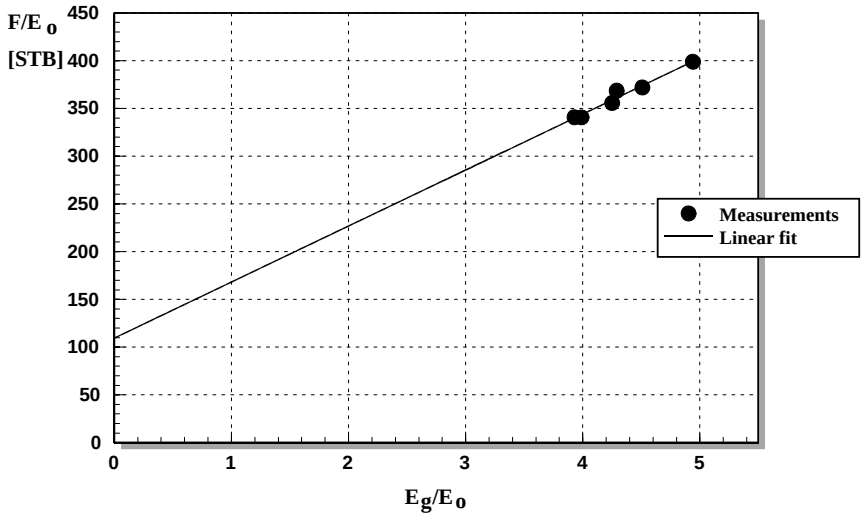


Figure 11.6: Extrapolation of lineraized gas cap expansion data. Note that the units on the y- axis ($F/E_o$) is given in $10^6 STB$.

## 11.8 Water influx

Water influx is more the rule, than the exception for normal oil and gas production, i.e. we expect some influx of water to be present in all situations where reservoir production takes place over some period of time.

Generally we may expect the influx of water to be both time and pressure dependent and we write,

$$W_e = f(p,t),$$

where $f$ is some function which will depend on the reservoir and the extent and volume of the aquifer itself.

This picture could be clarified by considering a reservoir model, as shown in Fig. 11.7, where the periphery pressure (pressure near the boundary) in the aquifer zone is equal to $p_e$. The pressure difference induced, will then cause water to flow into the reservoir volume. This flow will obey Darcy's law,

$$q_w = C(p_e - p),$$

where $C$ is a constant depending on the various reservoir parameters.

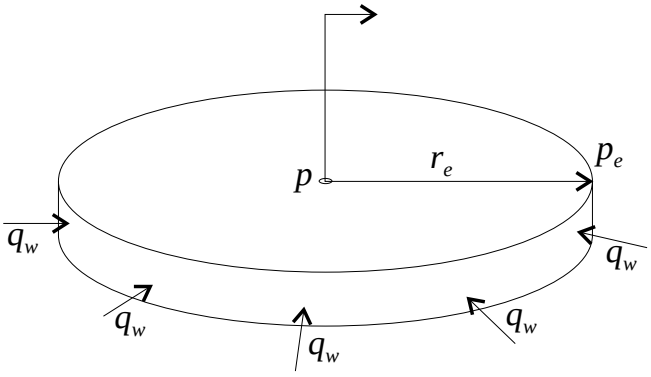


Figure 11.7: Water influx from external aquifer.

The cumulative water influx can be found by integrating over the time this process takes place,

$$W_e = \int_0^t q_w dt \simeq \sum_i q_i \Delta t_i = C \sum_i \Delta p_i \Delta t_i.$$

In the equation above we move from a continuous case to a discrete case by summing over all pressure drops $\Delta p$ for all time periods $\Delta t$.

The use of this equation is important when real data is supposed to be fitted in accordance with a material balance model. The constant $C$ is adjusted in such a way as to secure the match between the model and the real data.

**Example: Pressure maintenance through water injection**

In an attempt to maintain the reservoir pressure we may inject water into the reservoir. Injection water rate will be proportional to the oil production rate and the following simplified material balance equation is applied,

$$N_p[B_o + (R - R_s)B_g] = W_p B_w.$$

Key data for a typical oil reservoir is,

If pressure is maintained, we can conclude from the data above that the relation between produced oil and injected water has to be,

$N_p$ = 10000 STB $B_o$ = 1.2002 RB/STB $R$ = 3000 SCF/STB
$B_g$ = 0.00107 RB/SCF $R_s$ = 401 SCF/STB

$$W_p = 4.0N_p,$$

measured in [STB].

## 11.9 Exercises

1. The following PVT-data is used in material balance calculations.

| p [psia] | $B_o$ | $R_s$ | $B_g$ |
|---|---|---|---|
| 4000 | 1.2417 | 510 | – |
| 3500 | 1.2480 | 510 | – |
| 3330 | 1.2511 | 510 | 0.00087 |
| 3000 | 1.2222 | 450 | 0.00096 |
| 2700 | 1.2022 | 401 | 0.00107 |
| 2400 | 1.1822 | 352 | 0.00119 |
| 2100 | 1.1633 | 304 | 0.00137 |
| 1800 | 1.1450 | 257 | 0.00161 |
| 1500 | 1.1115 | 214 | 0.00196 |
| 1200 | 1.0940 | 167 | 0.00249 |
| 900 | 1.0940 | 122 | 0.00339 |
| 600 | 1.0763 | 78 | 0.00519 |
| 300 | 1.0583 | 35 | 0.01066 |

   a) Find the recovery $N_p/N$, when the pressure decreases from $p_i = 4000\,psia$ to the bubble point, $p = p_b$.

   Compressibility is given; $c_w = 3.0 \cdot 10^{-6} psi^{-1}$, $c_p = 8.6 \cdot 10^{-6} psi^{-1}$ and connate water saturation is $S_{wc} = 0.2$.

   b) Calculate the recovery $N_p/N$ for declining pressure, from $p_i = 4000\,psia$ to $p = 600\,psia$.

   What is the gas saturation at $600\,psia$, when $R = 1000$ SCF/STB ?

   c) The oil rate is 10000 STB/d at pressure $p = 2700\,psia$ and the gas-oil ratio is $R = 3000\,SCF/STB$.

   What is the injection water rate necessary to maintain the production at p=2700 psia ? Use $B_w = 1.0\,RB/STB$.

2. For an oil reservoir with gas cap, the water injection rate is not known. The material balance equation with no water production is,

$$N = \frac{N_p[B_t + B_g(R - R_{si})] - W_i B_w}{(B_t - B_{oi}) + (B_g - B_{gi})mB_{oi}/B_{gi}},$$

   where $B_t = B_o + (R_{si} - R_s)B_g$ and $W_i$ is the water volume injected given in STB.

   a) Calculate the initial oil in place and the size of the gas cap when the following PVT- and production data is given.

   The boiling point pressure is 1850 psia.

| p [psia] | 1850 | 1600 | 1300 | 1000 |
|---|---|---|---|---|
| $R_s$ [SCF/STB] | 690 | 621 | 535 | 494 |
| $B_o$ [RB/STB] | 1.363 | 1.333 | 1.300 | 1.258 |
| $B_g$ [RB/SCF] | 0.00124 | 0.00150 | 0.00190 | 0.00250 |
| $B_t$ [RB/STB] | 1.363 | 1.437 | 1.594 | 1.748 |
| $\rho_o$ [psi/ft] | 0.3014 | 0.3049 | 0.3090 | 0.3132 |
| $N_p$ [STB] | – | $3.1 \cdot 10^8$ | $5.5 \cdot 10^8$ | $5.9 \cdot 10^8$ |
| R [SCF/STB] | – | 1100 | 1350 | 1800 |
| $W_i$ [STB] | – | $1.594 \cdot 10^8$ | $2.614 \cdot 10^8$ | $3.12 \cdot 10^8$ |

Water saturation is 0.24, porosity is 0.17 and the water volume factor is approximately 1.0 RB/STB.

b) Geological information indicates that the reservoir could be approximated to a right circular cone. Calculate the height of the cone when the pressure at the bottom level of the oil zone (cone) is 1919 psia ( –the water-oil contact). [Volume of a right circular cone is $\pi r^2 h/3$].

3. Define an expression giving the gas-oil ratio, GOR [SCF/STB] in a reservoir with supercritical gas saturation.

   Find the GOR using the following data;

   $\mu_o$=0.8 cp  $B_o$=1.363 RB/STB
   $\mu_g$=0.018 cp  $B_g$=0.001162 RB/SCF
   $k_o$=1000 mD  $R_s$= 500 SCF/STB
   $k_g$=96 mD

4. The data in the table below is taken form an oil reservoir.

| p [psia] | $N_p$ [$10^6$ STB] | R [SCF/STB] | $B_o$ [RB/STB] | $R_s$ [SCF/STB] | $B_g$ [RB/SCF] |
|---|---|---|---|---|---|
| 3330 | – | – | 1.2511 | 510 | 0.00087 |
| 3150 | 1.024 | 1050 | 1.2353 | 477 | 0.00092 |
| 3000 | 1.947 | 1060 | 1.2222 | 450 | 0.00096 |
| 2850 | 2.928 | 1160 | 1.2122 | 425 | 0.00101 |
| 2700 | – | – | 1.2022 | 401 | 0.00107 |

a) First, assume there is no gas cap present and the production mechanism is dissolved gas drive. Estimate the initial oil volume in the reservoir.

b) Estimate oil production at $p = 2700$ psia, by a method of comparing $R$, calculated from the material balance equation and secondly calculated from the GOR– equation (as done in Exercise 1),

$$R = R_s + \frac{k_g}{k_o}\frac{B_o \mu_o}{B_g \mu_g}.$$

A relation $k_g/k_o$ exists experimentaly and the gas saturation dependency has been established:

$$\log(k_g/k_o) = 34.5 \cdot S_g - 2.54,$$

where $S_{wc}$=0.30, $\mu_o$=1.0 cp and $\mu_g$=0.1 cp.

c) Data from an other well indicates the existence of a small gas cap. Calculate the initial oil volume, in view of this new information.

**Answer to questions:**

1. a) 1.52%, b) 46%, 0.43, c) 39830 STB/d 2. a) $2.22 \cdot 10^9$ STB, 0.49, b) 738 ft, 3. 5505 SCF/STB,
4. a) $122.8 \cdot 10^6$ STB, b) by iteration c) $108.6 \cdot 10^6$ STB

# Chapter 12

# Well Test Analysis

## 12.1 Introduction

In order to optimise a development strategy for an oil or gas field, we have to consider a reservoir model capable of realistically predicting the dynamic behaviour of the field in terms of production rate and fluid recovery. Such a model is constructed using geological, geophysical and well data. The necessary parameters are obtained from direct measurements (cores, cuttings, formation fluid samples, etc.) and from interpreted data (surface seismic, well logs, well tests, PVT analysis, etc.). While seismic data and well logs provide a static description of the reservoir, only well testing data provide information on dynamic reservoir response. The well test data is therefore a key element in the reservoir model construction, see Fig.12.1.

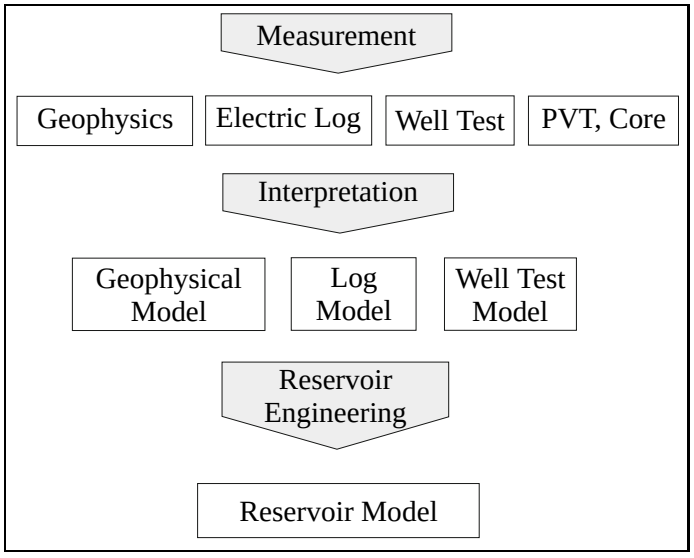


Figure 12.1: Stages of reservoir modelling.

Interpretation of these data leads to individual "models" (what the geophysicist, the petrophysicist and well analyst think the reservoir looks like). A brief understanding of the fundamental aspects of well testing is necessary in order to incorporate dynamic well test data into the reservoir model and it is the function of the reservoir engineer to incorporate these

individual models into a cohesive reservoir model [50].

In the initial phase of well tests, pressure measurements are dominated by wellbore storage effects. During this time, fluid contained in the wellbore and its direct connected volumes are produced. Then, as the production of the reservoir fluid starts, the fluid near the well expands and moves towards the area of lower pressure. This movement will be retarded by friction against the pore walls and the fluid's own inertia and viscosity. However, as the fluid moves it will, in turn, create a pressure imbalance and this will induce neighbouring fluid to move towards the well. This process continues until the drop in pressure, created by the start-up of production, is dissipated throughout the reservoir. The tail portion of the well test data for the test of sufficient duration, is affected by the interference from other wells or by boundary effects such as those that occur when the pressure disturbance reaches the edge of a reservoir. From this time and onwards, the average pressure in the reservoir will decrease in a way similar to emptying a confined volume, like a tank of gas.

In this chapter we will develop simple models that can explain the measured well test data. The models give a rather simplified and idealistic view of the reservoir, characterised by:

- isotropic and homogenous reservoir volume,
- constant porosity, - absolute permeability, - viscosity and - reservoir height (reservoir thickness),
- test production with relative small pressure gradients, i.e. $c\nabla p \cdot \nabla p$ is small (compressibility times pressure gradient squared) ,
- horizontal radial flow paths (no cross flow) and
- constant flow rate.

Even though these items place tight restrictions on the reservoir itself, some important information can be extracted from the models, explaining reservoir behaviour on basis of the well test data.

The wellbore pressure data is subdivided into three different production periods, each describing characteristic well and reservoir pressure response profile:

1. **Wellbore storage period**. Production from the wellbore and nearby cavities.
2. **Semi logarithmic period**. Production from an infinite acting reservoir where no boundary effects are observed.
3. **Semi steady state period**. Production from a confined reservoir (closed volume) where the interference from the boundary dominates pressure decline.

### 12.1.1 Systems of Uunits Used in Well Test Analysis

The following systems of units are traditionally used in well test analysis: SI-Units and Field Units, as presented in Table 12.1.

Some conversion factors mostly used in well test analysis are listed below:

Table 12.1: System of units used in well test analysis

| Parameter | Nomenclature | SI-units | Field units |
|---|---|---|---|
| Flow rate | $q$ | $Sm^3/d$ | STB/d |
| Volume factor | $B$ | $Rm^3/Sm^3$ | RB/STB |
| Thickness | $h$ | m | ft |
| Permeability | $k$ | $\mu m^2$ | mD |
| Viscosity | $\mu$ | mPa·s | cp |
| Pressure | $p$ | kPa | psia |
| Radial distance | $r$ | m | ft |
| Compressibility | $c$ | $(kPa)^{-1}$ | $psi^{-1}$ |
| Time | $t$ | hrs | hrs |

| | | |
|---|---|---|
| 1 STB/d | = | 0.159 $Sm^3/d$ |
| 1 ft | = | 0.3048 m |
| 1 mD | = | $0.987 \cdot 10^{-3}$ $\mu m^2$ |
| 1 cp | = | 1 mPa·s |
| 1 psi | = | 6.895 kPa |

## 12.2 Wellbore Storage Period

Let us consider the initiation of well production at a constant rate at time $t_0 = 0$. First, the fluids contained in the wellbore itself and its continuous cavities will be produced. This production is characterised by the expansion of oil and gas in the well, defined by the fluid compressibility, $c_f$ and the well storage volume, $V_w$.

The definition of the wellbore fluid compressibility is $c_f = \Delta V_w/(V_w \Delta p)$ and the well flowrate is $qB = \Delta V_w/\Delta t$, where the pressure drop in the well is, $\Delta p$. ($B$ is the wellbore fluid volume factor, measured in reservoir volume pr. standard volume.)

$$\Delta p = \frac{qB}{c_f V_w} t, \tag{12.1}$$

where $\Delta p = p_i - p_w(t)$ is the difference between initial and wellbore pressure.

The compressibility is often redefined, where the *wellbore storage*, $c_{ws} = c_f V_w$ is used to characterise particular wells.

**Example: Wellbore storage effect**

A well has a certain volume capacity for fluids. A real well, with an average well radius of $r_w = 0.1m$, at a well depth of $H = 2000\,m$ has a volume $V_w$, accessible to fluids close to 17 $m^3$.

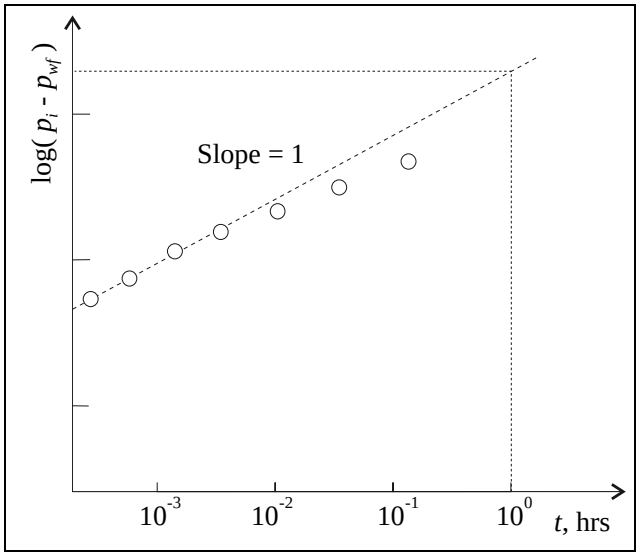


Figure 12.2: Logarithmic analysis of the pressure drawdown data at early times of well testing, i.e. in the wellbore storage period

If well production is measured in standard cubic meter pr. day $[Sm^3/d]$ and time in hours $[hr]$, the well pressure is then given by,

$$p_i - p_w = \frac{qB}{24c_{ws}}t,$$

and the logarithmic pressure difference can be given by,

$$\log(p_i - p_w(t)) = \log(t) + \log\left(\frac{qB}{24c_{ws}}\right),$$

where $p_w$ is the wellbore pressure.

The latter equation, in a logarithmic scale, exhibits the linear relation between time and pressure drop. This straight line behaviour seen in Fig. 12.2, has a slope equal to unity.

The technique of using log-log plots is commonly used in well test analysis for model recognition, but also as here, for estimation of the wellbore storage constant $c_{ws}$:

$$c_{ws} = \frac{qB}{24(p_i - p_w(1hr))}, \tag{12.2}$$

with $p_w$(1 hr) picked from the unit slope line.

———— · ————

When the well is opened (shut-in) to flow, it is opened at the surface. Due to the wellbore storage, where the well itself contains a certain volume of compressible fluid, there is a delay in a flow-rate response at the sand-face (bottom of the well), as seen in Fig. 12.3. This effect must be incorporated into the interpretation model of the pressure test data.

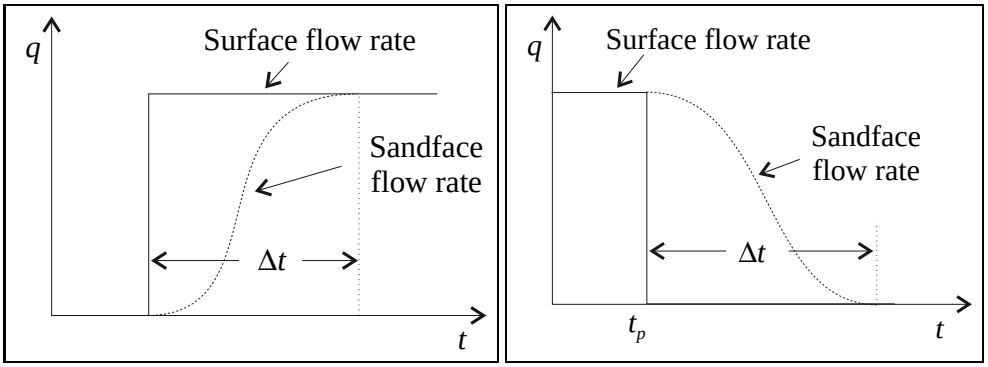


Figure 12.3: The wellbore storage effect on flow-rate during the drawdown (left) and build- up tests (right).

## 12.3 Semi Logarithmic Period

In this section we will focus our attention on what happens in the reservoir when the fluid is drawn towards the well due to the pressure drop in the wellbore. We shall develop a theory for fluid flow in a cylindrical and somewhat idealistic reservoir (see introductory remarks). The production profile in this period is characterised by a semi logarithmic pressure dependence, hence the title of this section.

### 12.3.1 Diffusivity Equation

Transport of oil in porous media is generally described by the law of continuity and Darcy's law. If we consider a volume element, as shown in Fig.12.4, we may define the flow of oil in the x-direction by the equations,

$$\begin{aligned} \frac{d(\rho v_x)}{dx} &= -\frac{\partial(\phi\rho)}{\partial t}, \\ v_x &= -\frac{k}{\mu}\frac{dp}{dx}. \end{aligned}$$

where $\rho$ is density, $\phi$ is porosity, $\mu$ is viscosity, $k$ is permeability and $v_x$ is flow velocity in x-direction.

Using an independent co-ordinate system, we may write the same equations as,

$$\begin{aligned} \nabla\cdot(\rho\vec{v}) &= -\frac{\partial(\phi\rho)}{dt}, \\ \vec{v} &= -\frac{k}{\mu}\nabla p, \end{aligned}$$

Substituting these two equations gives us,

$$\nabla\cdot\left(\rho\frac{k}{\mu}\nabla p\right) = \frac{\partial(\phi\rho)}{\partial t}. \tag{12.3}$$

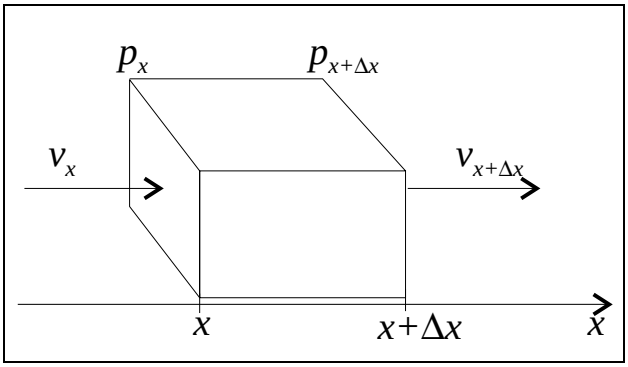


Figure 12.4: Flow of oil in the x-direction through a volume element.

In accordance with an idealistic view of the reservoir, as mentioned above, we will consider both permeability and viscosity to be constant, while oil density and reservoir porosity may vary with pressure, i.e. $\rho = \rho(p)$ and $\phi = \phi(p)$. From these relations we can define the liquid compressibility as well as the matrix compressibility as,

$$c_l = \frac{1}{\rho}\frac{\partial \rho}{\partial p} \text{ and } c_m = \frac{1}{\phi}\frac{\partial \phi}{\partial p}.$$

Eq.(12.3) is further developed using the newly defined compressibilities, $c_l$ and $c_m$, and we write,

$$c_l \nabla p \nabla p + \nabla^2 p = \frac{1}{\eta}\frac{\partial p}{\partial t}, \tag{12.4}$$

where $\eta = k/(\phi c \mu)$ and $c = c_l + c_m$, where $c$ is the total compressibility.

Further simplification of Eq.(12.4) rests on the assumption that $c_l \nabla p \nabla p \ll |\nabla^2 p|$, which is the case in almost all real cases. With this last simplification in mind, we can write the *Diffusitivity equation* (independent of co-ordinate systems),

$$\nabla^2 p = \frac{1}{\eta}\frac{\partial p}{\partial t}. \tag{12.5}$$

The diffusitivity equation in cylindrical co-ordinates gives,

$$\frac{1}{r}\frac{\partial}{\partial r}\left(r\frac{\partial p}{\partial r}\right) + \frac{\partial^2}{\partial z^2} = \frac{1}{\eta}\frac{\partial p}{\partial t}. \tag{12.6}$$

With no crossflow in the reservoir, the linearized diffusitivity equation is written,

$$\frac{1}{r}\frac{\partial}{\partial r}\left(r\frac{\partial p}{\partial r}\right) = \frac{1}{\eta}\frac{\partial p}{\partial t}. \tag{12.7}$$

### 12.3.2 Solution of the Diffusitivity Equation

The solution of the diffusivity equation can be simplified by using *the linear source* approximation implicating a zero wellbore radius. In case of a constant flow rate the following Initial- and Boundary condition are defined. Initial conditions are described by the pressure start-up conditions in the reservoir, while the boundary condition is deduced from Darcy's law.

**Initial condition:**

$$\begin{aligned} i) \quad p(r,0) &= p_i, \ \forall r, \\ ii) \quad \lim_{r\to\infty} &= p_i, \ \forall t. \end{aligned}$$

**Boundary condition:**

$$\begin{aligned} \left(r\frac{\partial p}{\partial r}\right)_{r=r_w} &= \frac{qB\mu}{2\pi hk}, \ \forall t > 0, \\ \text{Line-source solution:} \quad \lim_{r\to\infty}\left(r\frac{\partial p}{\partial r}\right) &= \frac{qB\mu}{2\pi hk}, \ \forall t. > 0 \end{aligned}$$

In solving the linear diffusitivity Eq.(12.7) we may use the well known Boltzmann transformation,

$$y = \frac{r^2}{4t},$$

which gives the following partial derivatives:

$$\partial r = (r/2y)\partial y \ \text{ and } \ \partial t = -(t/y)\partial y.$$

When the Boltzmann transformation is applied to Eq.(12.7), the variable of time is made implicit and the diffusivity equation is reduced to only one variable,

$$\frac{\partial}{\partial y}\left(y\frac{\partial p}{\partial y}\right) = \frac{y}{\eta}\frac{\partial p}{\partial y}. \tag{12.8}$$

We may solve Eq.(12.8), by direct integration and we get,

$$y\frac{\partial p}{\partial y} = K_3 e^{-r^2/(4\eta t)},$$

where $K_3$ is a constant that could be defined, using the boundary condition for the line-source solution, i.e. $K_3 = (qB\mu)/(4\pi hk)$.

Second integration of Eq.(12.8), gives the following expression,

$$p_i - p(r,t) = \frac{qB\mu}{4\pi hk}\int_{r^2/(4\eta t)}^{\infty}\frac{e^{-s}}{s}ds. \tag{12.9}$$

The integral in Eq.(12.9) is known as *the Exponential integral* and is originally defined as,

$$\begin{aligned} Ei(\xi) &\equiv \int_{-\infty}^{\xi}\frac{e^s}{s}ds, \\ -Ei(-\xi) &= \int_{\xi}^{\infty}\frac{e^{-s}}{s}ds. \end{aligned}$$

The general solution of the linear diffusitivity equation, Eq.(12.7), can then be presented as,

$$p_i - p(r,t) = \frac{qB\mu}{4\pi hk}\left[-Ei\left(-\frac{r^2}{4\eta t}\right)\right], \tag{12.10}$$

where $\eta = k/(\phi\mu c)$.

Values of the function $-Ei(-\xi)$ is tabulated in Table 12.2.

Table 12.2: Table of the function $Ei(\xi)$ for $0.01 \leq \xi \leq 10$.

| $\xi$ | $[-Ei(-\xi)]$ | $\xi$ | $[-Ei(-\xi)]$ | $\xi$ | $[-Ei(-\xi)]$ | $\xi$ | $[-Ei(-\xi)]$ |
|---|---|---|---|---|---|---|---|
| 0.01 | 4.0379 | 0.12 | 1.6595 | 0.35 | 0.7942 | 0.90 | 0.2602 |
| 0.02 | 3.3547 | 0.14 | 1.5241 | 0.40 | 0.7024 | 1.00 | 0.2194 |
| 0.03 | 2.9591 | 0.16 | 1.4092 | 0.45 | 0.6253 | 1.50 | 0.1000 |
| 0.04 | 2.6813 | 0.18 | 1.3098 | 0.50 | 0.5598 | 2.00 | 0.0489 |
| 0.05 | 2.4679 | 0.20 | 1.2227 | 0.55 | 0.5034 | 2.50 | 0.0249 |
| 0.06 | 2.2953 | 0.22 | 1.1454 | 0.60 | 0.4544 | 3.00 | 0.0130 |
| 0.07 | 2.1508 | 0.24 | 1.0762 | 0.65 | 0.4115 | 4.00 | 0.0038 |
| 0.08 | 2.0269 | 0.26 | 1.0139 | 0.70 | 0.3738 | 5.00 | 0.0011 |
| 0.09 | 1.9187 | 0.28 | 0.9573 | 0.75 | 0.3403 | 7.00 | 0.0001 |
| 0.10 | 1.8229 | 0.30 | 0.9057 | 0.80 | 0.3106 | 10.00 | 0.0000 |

### 12.3.3 Gas Reservoir

The general form of the basic (material balance) equation, given by Eq. (12.7), is valid for both liquid and gas flow. In the case of more compressible fluids, like gases, some modifications are necessary in order to use the diffusivity equation.

Attempting to obtain a linear type of the diffusivity equation for a highly compressible gas flow, Al-Hussainy, Ramey and Crawford (1966), replaced the dependent variable $p$ by the real gas *pseudo pressure* $m(p)$ in the following manner,

$$m(p) = 2\int_{p_b}^{p} \frac{p}{\mu z} dp, \tag{12.11}$$

where $p_b$ is an arbitrary (datum) pressure.

Using the equation of state for a real gas,

$$\rho = \frac{Mp}{zRT},$$

and a pseudo pressure function $m(p)$ from Eq.(12.11) they derived a simplified linear equation for a real gas flow:

$$\frac{1}{r}\frac{\partial}{\partial r}(r\frac{\partial m(p)}{\partial r}) = \frac{1}{\eta}\frac{\partial m(p)}{\partial t}, \tag{12.12}$$

which is precisely the same as Eq.(12.7) where the term $p$ is replaced by a pseudo pressure function $m(p)$.

It follows from Eq.(12.12) that the behaviour of $m(p)$ vs. time in gas well testing should have identical trends as pressure vs. time in oil well testing. This fact is commonly used in a gas well test analysis.

### 12.3.4 The Solution of the Diffusitivity Equation in Dimensionless Form

In connection with model recognition and practical application of the well test data it is quite often advantageous to plot the measured data in such a way as to initially compare it with a standard and well known function. It is therefore convenient to introduce dimensionless variables, such as,

$$\begin{aligned} r_D &= \frac{r}{r_w}, \\ t_D &= \frac{kt}{\phi\mu c r_w^2}, \\ p_D &= \frac{2\pi hk}{qB\mu}[p_i - p(r,t)]. \end{aligned}$$

Depending on the units preferred; standard- or field units, the above normalisation can be written,

**SI- units:**

$$r_D = \frac{r}{r_w},\ t_D = \frac{0.0036kt}{\phi\mu c r_w^2}\ \textit{and}\ p_D = \frac{\pi hk}{1.842qB\mu}[p_i - p(r,t)],$$

**Field units:**

$$r_D = \frac{r}{r_w},\ t_D = \frac{0.000264kt}{\phi\mu c r_w^2}\ \textit{and}\ p_D = \frac{\pi hk}{141.2qB\mu}[p_i - p(r,t)],$$

Using dimensionless variables for the solution of the linear diffusivity equation, as presented in Eq.(12.10), we get,

$$p_D(r_D,t_D) = -\frac{1}{2}Ei\left(-\frac{r_D^2}{4t_D}\right), \tag{12.13}$$

where the factor $1/2$ in front of the exponential function is of purely historical reasons, related to the presentation of semi logarithmic data.

### 12.3.5 Wellbore Pressure for Semi Logarithmic Data

The wellbore pressure ($r_D = 1$) is given by,

$$p_{wD}(t_D) = -\frac{1}{2}Ei\left(\frac{-1}{4t_D}\right).$$

From mathematical tables we have the following approximation,

$$-Ei(-\xi) = \int_\xi^\infty \frac{e^{-s}}{s}ds \approx (-\ln\xi - \gamma) + \xi - \frac{\xi^2}{2\cdot 2!} + \frac{\xi^3}{3\cdot 3!} - \cdots,$$

where $\gamma \simeq 0.5772157$ is Euler's constant.

The interesting question now is related to the validity of the approximation: $-Ei(-\xi) \approx -\ln\xi - \gamma$, i.e.

$$p_{wD}(t_D) = -\frac{1}{2}Ei\left(-\frac{1}{4t_D}\right) \approx -\frac{1}{2}\left(\ln\frac{1}{4t_D} + \gamma\right). \tag{12.14}$$

We may write the dimensionless wellbore pressure as,

$$\begin{aligned} p_{wD}(t_D) &\approx -\frac{1}{2}(\ln 1 - \ln 4 - \ln t_D + \gamma), \\ &\approx \frac{1}{2}(\ln t_D + 0.80907), \end{aligned}$$

where the next term in the series expansion of Eq. (12.14), is $1/(4t_D)$, is thought to be insignificant.

In order to check the accuracy of this approximation we may look at the relative importance of the next term not included in the approximation Eq.(12.14), i.e.

$$Error = \frac{1/(4t_D)}{\ln t_D + 0.80907}. \tag{12.15}$$

If we assume the dimensionless time; $t_D \geq 25$, then we would expect the *Error* always to be less then 0.25 %.

In order to illustrate the implication of the restriction $t_D \geq 25$, we can consider the constraint on time (in hours), for a "typical" oil reservoir with the following parameters (in field units),

| | | |
|---|---|---|
| k = 100 mD | $\phi$ = 25 % | $\mu$ = 1.0 cP |
| c = $5 \cdot 10^{-6}$ $psi^{-1}$ | $r_w$ = 1 ft | |

Using the definition of the dimensionless time in field units from above, we find that the real time that passes before the approximation, Eq.(12.14) is valid, is not more than 0.0012 hrs, or 4.3 seconds. We therefore conclude that the error done in applying the approximation in Eq.(12.14), is insignificant for all practical purposes.

In cases where the pressure drop observed in one well is induced by an other well a certain lateral distance apart from the observation well, we have to consider the restriction imposed above very carefully. In these cases the approximation may usually not hold.

Generally we may therefore use the following approximation,

$$p_{wD}(r_D, t_D) = \frac{1}{2}\left(\ln \frac{t_D}{r_D^2} + 0.80907\right), \tag{12.16}$$

with the restriction of $t_D/r_D^2 \geq 25$.

**Example: Semi logarithmic analysis of pressure drawdown data**

The wellbore pressure is given by the approximation (in dimensionless form),

$$p_{wD}(t_D) = \frac{1}{2}(\ln t_D + 0.80907)$$

Using the definition of dimensionless variables, given above, we may write,

$$p_i - p_w(t) = \frac{qB\mu}{2\pi hk}\frac{1}{2}\left(\ln \frac{kt}{\phi \mu c r_w^2} + 0.80907\right).$$

Rewriting this equation using *log* term instead of *ln* and standard units,

$$p_i - p_w(t) = \frac{2.1208qB\mu}{hk}\left(\log t + \log\frac{k}{\phi\mu c r_w^2} - 2.0923\right),$$

and in field units,

$$p_i - p_w(t) = \frac{162.6qB\mu}{hk}\left(\log t + \log\frac{k}{\phi\mu c r_w^2} - 3.2275\right).$$

When the well test data is presented in a semi logarithmic plot as shown in Figure 12.5, we may use one of the two equations above in order to extract vital information about the reservoir. In the figure, some early data originates from the wellbore storage period and some late data originates from the period when boundary effects starts to mask the pressure data. These data does not comply with the straight line and should therefore be disregarded when the semi logarithmic data is matched.

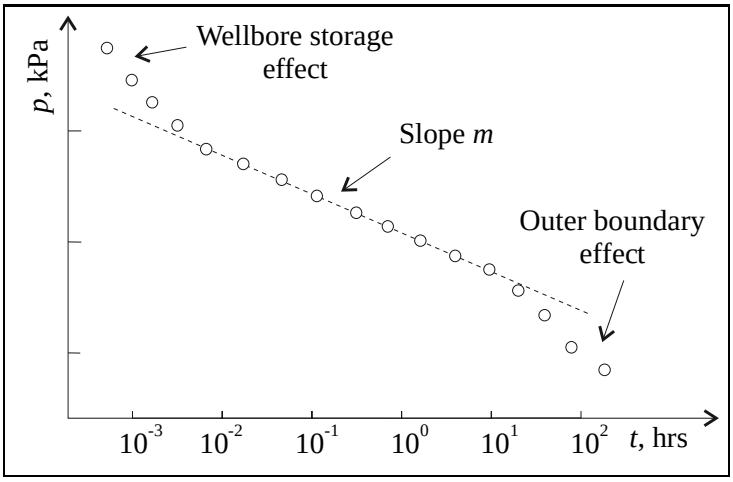


Figure 12.5: Pressure drawdown data.

The straight line through the semi logarithmic data points in Figure 12.5, is defined by the equation,

$$p(t) \sim -m\log t,$$

where $m$ is the slope of the straight line. This line is compared with the model above, and from this comparison we get the following equality (using SI - units),

$$m = 2.1208\frac{qB\mu}{hk}.$$

The reservoir permeability, $k$ could be estimated when information about reservoir height, oil viscosity, oil volume factor and oil rate are known.

## 12.4 Semi Steady State Period

After a period of reservoir production from an infinite reservoir, there comes a period of production where the influence from neighbouring wells or reservoir boundaries, such as lateral extension, faults or sands thinning out, are going to play an increasingly important role. This period is called the *semi steady state* period and a steadily decreasing reservoir pressure is observed (decreased average pressure in a confined reservoir volume). Simultaneously, the pressure profile in the reservoir is maintained unchanged.

It should be emphasised that this is an idealised model of how we think the reservoir responds to boundaries effects, and as such, prudent interpretation of steady state data is highly recommendable.

In Figure 12.6, several pressure profiles are plotted. At constant well production, the drawdown pressure profile is assumed to be constant, i.e. $\partial p(r)/\partial t$ = constant, in the reservoir.

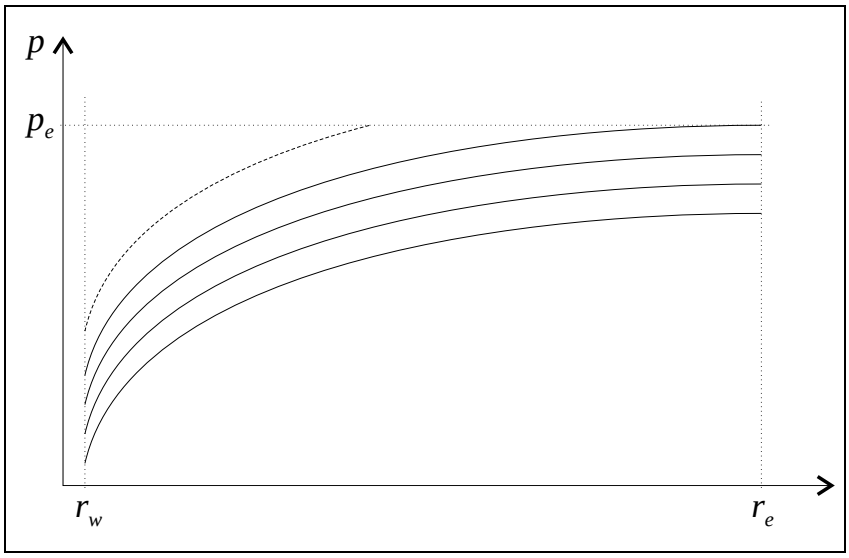


Figure 12.6: Steady state pressure profiles.

Since the pressure profile is assumed to be constant, we expect the diffusitivity equation to be time independent, i.e. a constant $K_1$ balances the diffusitivity equation,

$$\frac{1}{r}\frac{\partial}{\partial r}\left(r\frac{\partial p}{\partial r}\right) = K_1.$$

Integration of the time independent diffusivity equation gives,

$$r\frac{\partial p}{\partial r} = \frac{1}{2}K_1 r^2 + K_2, \tag{12.17}$$

where $K_2$ is also a constant.

The boundary conditions in the semi steady state are partly defined as for the case of the logarithmic period, but in addition we have assumed that the pressure profile does not significantly vary after the reservoir boundary limit is reached. At this limit, the reservoir pressure is steadily decreasing while the pressure profile is conserved.

**Boundary condition in the well:**

$$\left(r\frac{\partial p}{\partial r}\right)_{r=r_w} = \frac{qB\mu}{2\pi hk}.$$

**Boundary condition at infinite reservoir radius:**

$$\left(r\frac{\partial p}{\partial r}\right)_{r=r_e} = 0.$$

Using the boundary conditions to define the constants $K_1$ and $K_2$, and integrating Eq.(12.17) from the well ($r = r_w$), gives,

$$p(r) = p(r_w) + \frac{qB\mu}{2\pi hk}\left(\ln\frac{r}{r_w} - \frac{1}{2}\frac{r^2}{r_e^2}\right), \tag{12.18}$$

where $r_e$ is the radial distance to the boundary of the confined reservoir, i.e. $r_e \gg r_w$ and so $r_w/r_e \to 0$.

### 12.4.1 Average Reservoir Pressure

The average reservoir pressure is not an observable quantity. The average pressure is a weighted function of the pressure in the whole reservoir and could be defined as,

$$\overline{p} = \frac{\int_{r_w}^{r_e} p dV}{\int_{r_w}^{r_e} dV}.$$

Substituting for $p$ given by Eq.(12.18) and integrating, we find the average reservoir pressure,

$$\overline{p} = p(r_w) + \frac{qB\mu}{2\pi hk}\left(\ln\frac{r_e}{r_w} - \frac{3}{4}\right), \tag{12.19}$$

Eq.(12.19) gives the average pressure in a cylindrical reservoir with an outer radius equal to $r_e$ and where the well is located in the centre. In real cases, however, the reservoir shape is seldom cylindrical and more so, the well position is most frequently off centred. In these real cases we may not use Eq.(12.19) directly. Instead a slight modified version given by Eq.(12.20) is used, where $A$ is the top area of the reservoir and $C_A$ is a parameter characterising the shape and relative position of the well.

The average pressure for a general reservoir is then written,

$$\overline{p} = p(r_w) + \frac{qB\mu}{2\pi hk}\left(\frac{1}{2}\ln\frac{4A}{e^{\gamma}C_A r_w^2}\right), \tag{12.20}$$

where $\gamma$ is Euler's constant.

In the case of a cylindrical reservoir, with a centred well location, i.e. $A = \pi(r_e^2 - r_w^2)$, we find the shape-factor $C_A \simeq 4\pi e^{(3/2-\gamma)} = 31.6206$ (Dietz,1965).

### 12.4.2 Well Skin Factor

When a well is drilled it is always necessary to have a positive differential pressure acting from the wellbore to the formation to prevent inflow of the reservoir fluids (blow-out). Consequently, some of the drilling fluid penetrates the formation and particles suspended in the mud can partially penetrate the pore spaces, reducing permeability, and creating a so-called *damaged zone* next to the wellbore.

Assuming modification of the permeability in the damaged zone ($r_w < r < r_s$) is $k_s$, and within the rest of the reservoir ($r_s < r < r_e$) is $k$, as shown in Fig. 12.7.

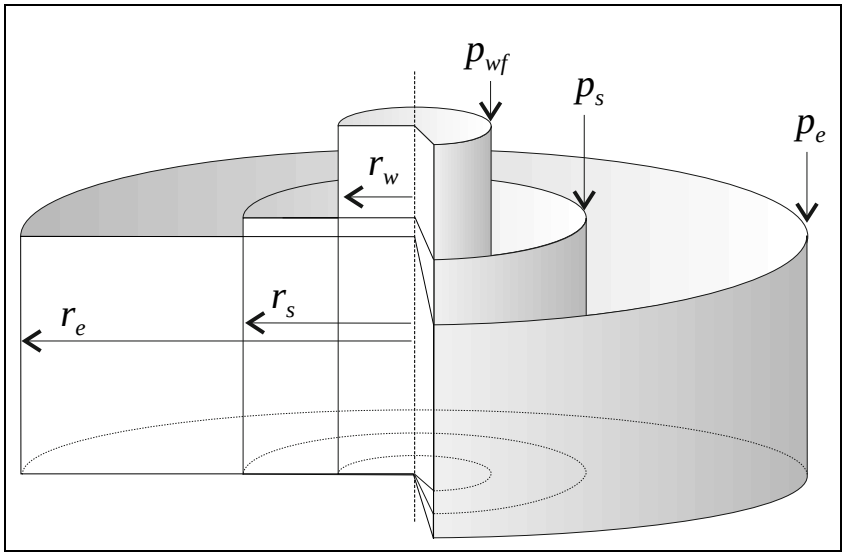


Figure 12.7: Skin effect caused by formation damage.

For the steady state inflow we can write the following equations for a cylindrical reservoir with a centred well, as stated for formation beds in series,

$$p_s - p_w \approx \frac{qB\mu}{2\pi k_s h} \ln \frac{r_s}{r_w},$$
$$p_e - p_s \approx \frac{qB\mu}{2\pi k h} \ln \frac{r_e}{r_s}.$$

Note the approximation made due to the fact that $r_e \gg r_w$ and $r_e \gg r_s$.

The total pressure drop from the wellbore through the reservoir is given by,

$$p_e - p_w = p_e - p_s + p_s - p_w = \frac{qB\mu}{2\pi k h} \left[ \ln \frac{r_e}{r_w} + (\frac{k}{k_s} - 1) \ln \frac{r_s}{r_w} \right], \tag{12.21}$$

where the last term is called the *mechanical skin factor S*,

$$S = (\frac{k}{k_s} - 1) \ln \frac{r_s}{r_w}. \tag{12.22}$$

Hence,

$$p_e - p_w = \frac{qB\mu}{2\pi k h} (\ln \frac{r_e}{r_w} + S), \tag{12.23}$$

where the skin is a number characterising the cylindrical volume next to the wellbore.

As seen from Eq.(12.23), the skin may be associated with a characteristic pressure drop $\Delta p_{skin}$ caused by the reduction in permeability in the skin zone,

$$\Delta p_{skin} = \frac{qB\mu}{2\pi kh} S. \tag{12.24}$$

From this equation it is evident that when the skin $S$ is positive, an increased pressure drop towards the well is observed, while when $S$ is negative the pressure drop is less than expected.

Skin is associated with the condition of reservoir permeability in the closed volume next to the well. If the permeability in the skin zone is reduced, due to drilling or well treatments, then the well will experience an increased pressure drop in this region while the skin is positive. If the well, on the other hand, has a permeability higher than expected, then the skin is negative, i.e.

- Skin factor is *positive*, $S > 0$ when $k_s < k$ and
- Skin factor is *negative*, $S < 0$ when $k_s > k$.

### 12.4.3 Wellbore Pressure at Semi Steady State

The reservoir pressure development in a closed reservoir could be compared to the production from a pressurised closed tank of oil. Production is maintained through volume expansion where the combined compressibility of oil and reservoir rock , $c$, is the important parameter.

The total compressibility of oil and reservoir rock is defined by, $c = -dV/(Vdp)$, which can be rewritten as,

$$\frac{dp}{dt} = -\frac{qB}{cV},$$

where $qB$ is the oil flow in the reservoir and $V = \phi Ah$ is the reservoir pore volume.

At constant reservoir flow rate, we may integrate from initial pressure, $p_i$ to the average pressure $\overline{p}$ and we get the following simple relation between reservoir pressure and time,

$$p_i - \overline{p}(t) = \frac{qB}{cV} t. \tag{12.25}$$

Combining Eq.(12.19) which describes the semi steady state analysis, with Eq.(12.25), we get,

$$p_i - p(r_w) = \frac{qB\mu}{2\pi hk} \left( \frac{1}{2} \ln \frac{4A}{e^{\gamma} C_A r_w^2} + S \right) + \frac{qB}{cV} t \tag{12.26}$$

Note that we in Eq.(12.26) have introduced the skin $S$ as an extra term in the equation, accounting for a partly damaged zone around the well.

Dimensionless variables are introduced, following the same definitions as for the case of semi steady state, with the exception of the dimensionless time $t_{DA}$, which is defined,

$$t_{DA} = \frac{kt}{\phi Ac\mu}. \tag{12.27}$$

In $t_{DA}$ dimensionless time is referenced to the reservoir drainage area $A$.

Hence, Eq.(12.26) can be rewritten using dimensionless variables and we get,

$$p_{wD} = \left(2\pi t_{DA} + \frac{1}{2}\ln\frac{4A}{e^{\gamma}C_A r_w^2} + S\right). \tag{12.28}$$

## 12.5 Wellbore Pressure Solutions

To this time we have developed the pressure function for the three periods of reservoir production, referring to the wellbore storage period, the semi logarithmic period and the semi steady state period, as if they were independent sequences reservoir production. In reality, well test data, originating from the different periods are not easily distinguishable and quite a lot of effort is spent identifying which data belongs to which period of production.

Summing up what we already know, we may write the following three pressure equations,

**Well storage period:**

$$p_i - p_w = \frac{qB}{c_{ws}}t.$$

**Semi logarithmic period:**

$$p_i - p_w = \frac{qB\mu}{2\pi hk}\frac{1}{2}\left(\ln\frac{kt}{\phi\mu c r_w^2} + 0.80907 + 2S\right).$$

**Semi steady state period:**

$$p_i - p_w = \frac{qB\mu}{2\pi hk}\left(\frac{2\pi k}{\phi Ac\mu}t + \frac{1}{2}\ln\frac{4A}{e^{\gamma}C_A r_w^2} + S\right).$$

Using the following set of dimensionless variables,

**SI- units:**

$$r_D = \frac{r}{r_w},\ t_{DA} = \frac{0.0036kt}{\phi Ac\mu},\ p_D = \frac{hk}{1.842qB\mu}(p_i - p(r,t)),$$

**Field units:**

$$r_D = \frac{r}{r_w},\ t_{DA} = \frac{0.000264kt}{\phi Ac\mu},\ p_D = \frac{hk}{141.2qB\mu}(p_i - p(r,t),$$

we get the three wellbore pressure equations in dimensionless form,

**Well storage period:**

$$p_{wD}^{WS} = \frac{A}{c_D}t_{DA},\ \text{where } c_D = \frac{c_{st}}{2\pi h\phi c}.$$

**Semi logarithmic period:**

$$p_{wD}^{SL} = \frac{1}{2}\left(\ln\frac{4A}{r_w^2 e^{\gamma}}t_{DA} + 2S\right).$$

**Semi steady state period:**

$$p_{wD}^{SS} = \left(2\pi t_{DA} + \frac{1}{2}\ln\frac{4A}{e^{\gamma}C_A r_w^2} + S\right).$$

### 12.5.1 Transition Time Between Semi Logarithmic Period and Semi Steady State Period

The difficulties in recognising the semi logarithmic data is primarily related to identification of the time when the wellbore pressure, changes from being semi logarithmic to being semi steady state dominated.

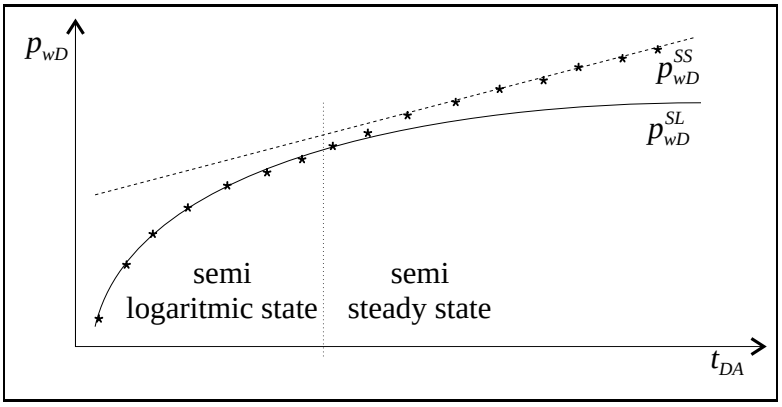


Figure 12.8: Transition between semi logarithmic period and semi steady state period.

Since the wellbore pressure development in the two periods are principally different, as seen in the Fig.12.8, we may define the transient time when one period is followed by the other, by the minimum pressure difference $\min\{p_{wD}^{SS} - p_{wD}^{SL}\}$, such that

$$\frac{d(p_{wD}^{SS}(t_{DA}) - p_{wD}^{SL}(t_{DA}))}{dt_{DA}} = 0.$$

Carrying out the derivation we find the transition time, $t_{DA} = 1/(4\pi)$, which can be transferred to real time by using the definition of dimenisonless time.

### 12.5.2 Recognition of Semi Logarithmic Data

Appropriate plotting of the well test data is an important tool in the process of differentiating the different reservoir production periods.

In a linear-linear plot as shown in Fig. 12.9, we can identify the semi logarithmic data, following a non linear time development. For real data, such identification could be rather difficult to perform and therefore of less practical importance.

The purpose of plotting data is partly to be able to identify the different production periods, but equally important, to facilitate quantitative data analysis. This analysis is mainly performed by plotting the interesting data linearly, i.e. data plotted as a straight line. This technique is shown in Fig. 12.10 where we have plotted the semi logarithmic data as shown in Fig. 12.9, in a linear-log plot. The semi logarithmic data is plotted as a straight line and from the slope of this line, we can get important reservoir information.

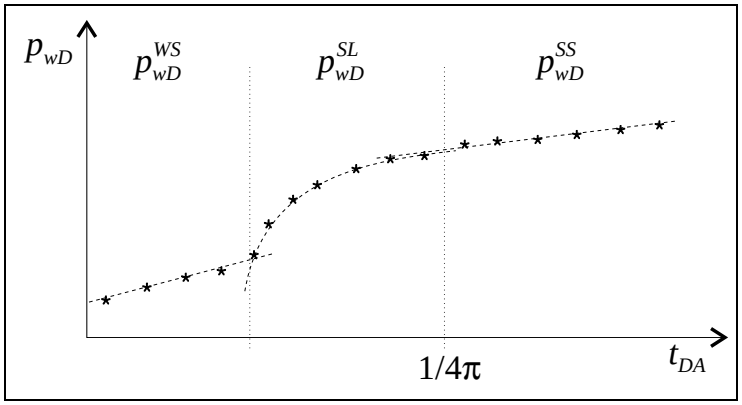


Figure 12.9: Linear-linear plot of well test data..

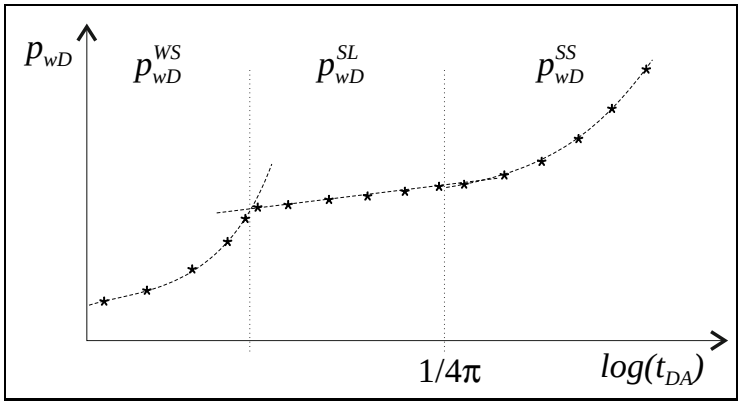


Figure 12.10: Linear-log plot of well test data.

## 12.6 Exercises

1. Claculate the dimensionless time $t_D$ for the following cases,

   a) with data:

   $$\begin{array}{ll} \phi = 0.15 & r = 10cm \\ \mu = 0.3\,cp & t = 10\,s \\ c = 15 \cdot 10^{-5}\,atm^{-1} & k = 0.1\,D \end{array}$$

   b) with data: $\phi$, $\mu$ and $c$ as above and

   $$r = 10\,cm \quad t = 1000\,s \quad k = 0.01\,D$$

2. Find the exponential intergrals and pressure drops for the following cases,

   a) with data:

   $$\begin{array}{ll} \phi = 0.12 & r = 10cm \\ \mu = 0.7\,cp & t = 1\,s \\ c = 10 \cdot 10^{-5}\,atm^{-1} & k = 0.05\,D \\ h = 2400\,cm & q = 10000cm^3/s \end{array}$$

b) with data: $\phi$, $\mu$, $c$ and $h$ as above and

$$r = 30000\,cm \quad t = 24\,h$$

3. In a reservoir at initial pressure, a well with a flow rate of 400 STB/D is shut-in. The reservoir is characterised by the following parameters:

| | | |
|---|---|---|
| k= 50 mD | $\phi$ = 0.3 | c= $10 \cdot 10^{-6}$ $psi^{-1}$ |
| h= 30 ft | $\mu$ = 3.0 cp | $B_o$ = 1.25 RB/STB |
| $r_w$ = 0.5 ft | | |

   a) At what time, after the shut-in, will the approximation $Ei(-x) = -\ln(xe^{\gamma})$ be valid ? (Eulers constant $\gamma$=0.5772.

   b) What is the pressure draw-down in the well after 3 hours of production?

   c) For how long must the well produce, at constant flow rate, until a pressure drop of 1 *psi* is observed in a neighbouring well 2000 $ft$ away?

4. Use the diffusivity equation,

$$\sum_{i=1}^{3} \frac{d}{dx_i}\left(\rho \frac{dp}{dx_i}\right) = \frac{\phi\mu}{k}\frac{d\rho}{dt},$$

   and the expression for the compressibility at constant temperature,

$$c = \frac{1}{\rho}\frac{d\rho}{dp},$$

   to derive the diffusivity equation for one phase liquid flow. (Assume the liquid compressibility to be small and constant for the pressures in mind.) Show that:

$$\sum_{i=1}^{3} \frac{d^2p}{dx_i^2} = \frac{\phi\mu c}{k}\frac{dp}{dt}.$$

5. For a reservoir at initial pressure with 3 wells (W1, W2 and W3) where W1 is an observation well, the following data is given:

| | | |
|---|---|---|
| $P_i$ = 4483 psia | $B_o$ = 1.15 RB/STB | h=30 ft |
| $k_o$ = 7.5 mD | $S_o$ = 0.80 | $c_o$ = $8.0 \cdot 10^{-6}$ $psi^{-1}$ |
| $\mu_o$ = 1.15 cp | $S_w$ = 0.20 | $c_w$ = $3.0 \cdot 10^{-6}$ $psi^{-1}$ |
| $c_f$ = $4.0 \cdot 10^{-6}$ $psi^{-1}$ | $r_w$ = 0.276 ft | |

   Use the total compressibility $c_t = S_o c_o + S_w c_w + c_f$ in the calculations.

   A pressure drop of 4439 *psi* is observed in well W1 after 1600 hours of production at a constant flow rate of 190 STB/D from well W2 and after 1550 hours of production of 80 STB/D from W3. Well W2 is located 2000 $ft$ north of W1 and W3 is 1900 $ft$ west of W1.

   Estimate the average reservoir porosity between the wells.

**Answers to questions:**

1. a) 1481, b) 14815, 2. a) 4.895, b) 0.62, 3. a) 15.4 s, b) 51.3 bar, c) 227 hr, 5. 0.175

# Chapter 13

# Methods of Well Testing

## 13.1 Pressure Tests

Well testing has become a widely used tool for reservoir characterisation and parameter identification. The development of well testing has accelerated from rudimentary productivity tests into a powerful technique which is strengthening the understanding of complex reservoir characteristics. Analysis of pressure trends enables us to evaluate several important reservoir parameters and to appraise the drainage zone.

Pressure tests are classified in accordance with their operation.

- Pressure *drawdown* test (Fig. 13.1,upper left): The well is opened to flow at a constant rate causing pressure drawdown.
- Pressure *build-up* test (Fig. 13.1,upper right): Production of constant flow rate well is shut-in, causing pressure build-up.
- *Falloff* test (Fig. 13.1,lower left): Injecting at constant rate and injection well shut-in, causing pressure falloff.
- *Multiple rate* (Fig. 13.1,lower right): Well tested at different flow rates, each lasting until the flowing pressure stabilises. This is followed by a shut-in period, which again lasts until the pressure stabilises.

Drawdown and build-up tests are the two most common types of well tests and the selection of which one to use depends on the practical field requirements.

A drawdown test simply involves flow rate measurements and pressure decline in a flowing well. In a conventional drawdown test, the well is first shut-in until wellbore pressures stabilise, and then opened and produced at a steady rate while the pressure decrease within the well bore is monitored.

Unfortunately, flow rates are still measured at the surface in most well tests. Such flow rates do not reflect the true downhole conditions as they are considerably affected by wellbore storage, fluid segregation and gas liberation. This poses a problem as well testing theory requires downhole flow rates.

Build-up tests are basically the opposite of drawdown tests. Instead of measuring pressures in a flowing well, as in drawdown testing, the well is shut-in and the increase or build-up in

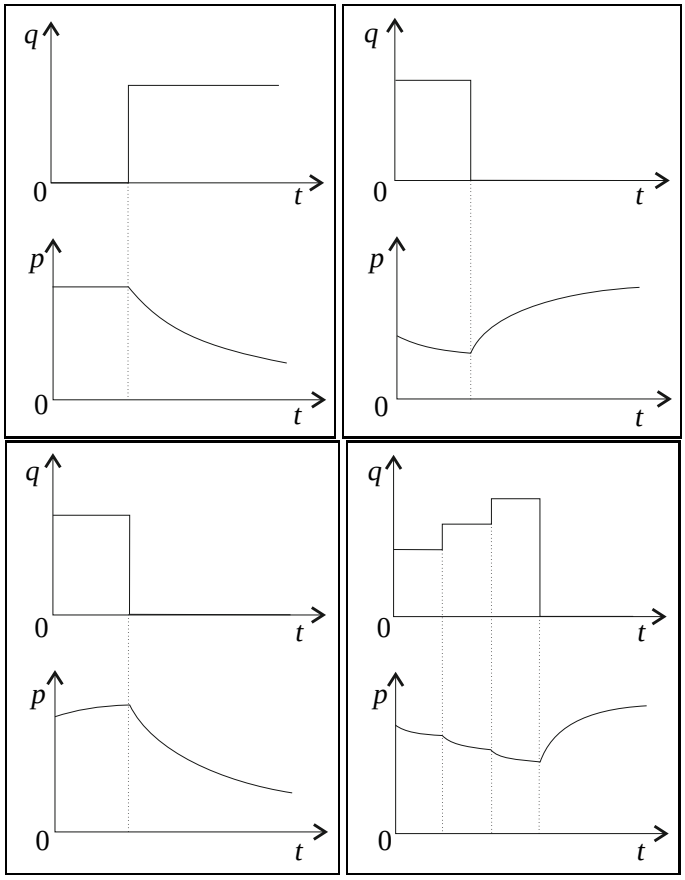


Figure 13.1: Methods of well testing.

pressure is monitored. Nevertheless, as with drawdown tests, build-up tests are still affected by wellbore storage effects during the initial stages or "early time"-part of the test. Therefore pressure readings taken from the beginning of the test has to be ignored and all analysis is done on the later part of the pressure response, even though it has been realised that this discarded early time data contains a considerable amount of information.

In practice, it is not so easy to carry out a "pure" drawdown or build-up test as the production schedule prior to the test, is usually complex. For example, a Drill-Stem Test (DST) is performed by carrying out a series of build-up and drawdown tests in relatively quick succession. The observed pressure build-up/drawdown response, within a given time, incorporates all the pressure transient effects caused by every previous step-change in production rate. However, multiple rate tests are not as simple as it might appear, while it relies on additional reservoir information as well as complex interpretation of pressure data using analysis based on theoretical models.

## 13.2 Pressure Drawdown Test

Drawdown test analysis are done by direct application of the wellbore pressure solutions, presented in the previous chapter.

A plot of pressure versus the log of time $(p, \log(t))$, will show the radial flow solution as a straight line, see Fig. 13.2. This fact provides us with an easy and seemingly precise graphical procedure for interpretation of the pressure data. The slope and intercept of the portion of the curve forming a straight line is used for permeability and skin factor calculations.

The early portion of the data is unfortunately, distorted by wellbore storage and skin effects as indicated in Fig. 13.2. Well tests have therefore to be made long enough to overcome both effects and to produce a straight line in a semi logaritmic plot.

But even this approach presents drawbacks. Sometimes more than one "apparent" straight line appears and analysis finds it difficult to decide which one to use. An alternative straight line could be the signature of a fault located near the well.

The latter portion of the pressure transient is affected by the interference from other wells or by boundary effects such as those that occur when the pressure response reaches the edge of the reservoir.

### 13.2.1 Pressure Drawdown Test Under Semi Logarithmic Conditions

From the previous chapter in section "Wellbore pressure solutions", we may formulate the semi logarithmic pressure solutions in *SI-units* and *Field-units* as:

**SI-units:**

$$p_w = p_i - 2.1208\frac{qB\mu}{kh}(\log t + \log\frac{k}{\phi\mu c r_w^2} - 2.0923 + \frac{S}{1.151}). \tag{13.1}$$

**Field-units:**

$$p_w = p_i - 162.6\frac{qB\mu}{kh}(\log t + \log\frac{k}{\phi\mu c r_w^2} - 3.2275 + \frac{S}{1.151}). \tag{13.2}$$

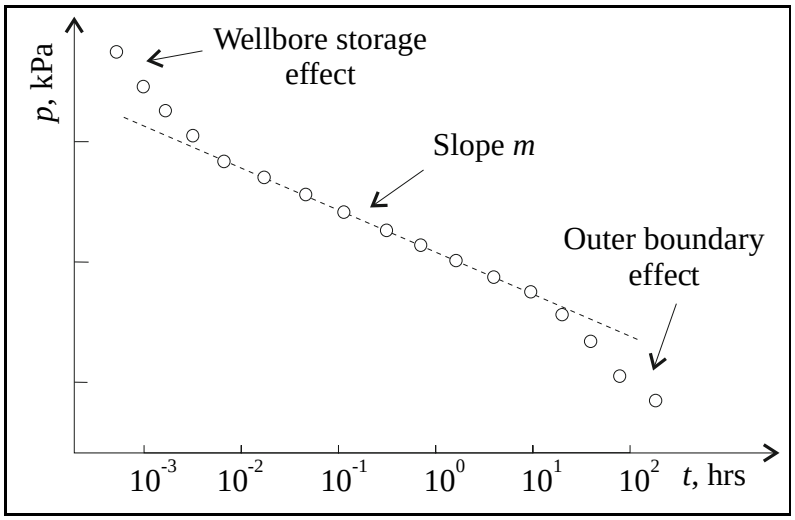


Figure 13.2: Semi-logarithmic plot of pressure drawdown test data.

In Fig. 13.2 we recognise the semi logarithmic data, as the data points being plotted on a straight line, where $m$ is the slope of the straight line. If we define the slope as a positive number,

$$m = \frac{(p_i - p_w(t_1)) - (p_i - p_w(t_2))}{\log(t_1) - \log(t_2)} > 0,$$

we may use Eqs. (13.1) or (13.2), to define the reservoir permeability, $k$. The known $m$-value yields a permeability value.

$$\begin{array}{cc} \text{SI-units:} & \text{Field-units:} \\ k = \frac{2.1208 qB\mu}{mh} \ [\mu m^2], & k = \frac{162.6 qB\mu}{mh} \ [mD]. \end{array}$$

The skin factor $S$ is conventionally identified from the same plot, see Fig. 13.2. The linear pressure at time $t = 1$ hr is used in Eqs. (13.1) or (13.2) and the skin is directly calculated. (Note that $p_w(1hr)$ in the equations below, is a data point on the straight line which needs not necessarily correspond to an observed pressure.)

**SI-units:**

$$S = 1.151 \left[ \frac{p_i - p_w(1hr)}{m} - \log \frac{k}{\phi \mu c r_w^2} + 2.0923 \right].$$

**Field-units:**

$$S = 1.151 \left[ \frac{p_i - p_w(1hr)}{m} - \log \frac{k}{\phi \mu c r_w^2} + 3.2275 \right].$$

### 13.2.2 Pressure Drawdown Test Under Semi Steady State Conditions

When the pressure transient is affected by the interference from boundary effects or other wells, the pressure curve deviates downwards from the straight line behaviour. Sometimes such disturbances overlap with other kinds of "early time" effects like large scale reservoir inhomogeneity, neighbouring sealing faults or other pressure disturbing zones. These effects can completely mask the all-important pressure response such that proper pressure analysis becomes impossible.

Under semi steady state test conditions we are investigating a sealed-off reservoir, where the well is producing from its own drained area. At these late times in the development of the well test procedure we may likely observe complicated pressure data which is masked by several effects. Semi steady state tests are therefore normally not preferred when typical reservoir parameters like permeability, productivity and skin are estimated. The analysis of semi steady state data is more rigorous than might possible be interpreted by the wellbore pressure equation.

The semi steady state equation is written,

$$p_w(t) = p_i - \frac{qB\mu}{2\pi kh} \left( \frac{2\pi kt}{\phi c \mu A} + \frac{1}{2} \ln \frac{4A}{e^{\gamma} C_A r_w^2} + S \right), \tag{13.3}$$

where the pressure is a linear function of time.

Semi steady state data is plotted as a straight line in a line-line plot, as seen in Fig. 13.3. The asymptotic pressure value $p_0 = p_w(t = 0)$, in the figure, enables us to define the Dietz shape factor $C_A$. In *Field Units*, Eq. (13.3) can re-written,

$$p_0 = p_i - \frac{162.6qB\mu}{kh}\left(\log\frac{4A}{e^{\gamma}r_w^2} - \log C_A + \frac{S}{1.151}\right). \tag{13.4}$$

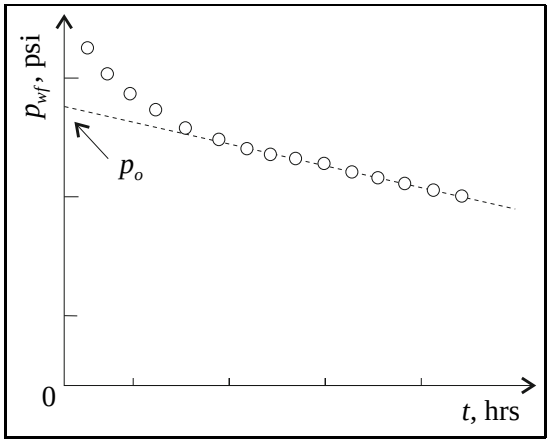


Figure 13.3: Semi steady state analysis of pressure drawdown data.

## 13.3 Pressure Build-Up Test

In analysing drawdown data, we could directly apply the "Wellbore pressure solutions" from the previous chapter, since pressure is decreasing with time, at constant wellbore rate. In the case of pressure build-up, when the well is closed, the "Wellbore pressure solutions" may not be used directly. Fortunately, the same equations can be applied since the process, the bottomhole pressure drawdown is, in principle, similar too the process of pressure build-up.

Normally, the build-up pressure data is considered to be more reliable than the pressure drawdown data, since the influence from dynamical effects near the well is of lesser importance.

If a well is shut-in at a certain time $t$, the no-flow conditions, as shown in Fig. 13.4, can be described by a superposition technique.

> As a theoretical assumption we may consider the wellbore rate to be both positive, $+q$ and *negative*, $-q$, as indicated in Fig. 13.4. The no-flow condition is obtained when the positive and negative well rate are summed, i.e. $(+q)+(-q) = 0$. Consequently, the no-flow condition can be described by adding the pressure solutions for the positive flow rate and the pressure solution for the negative flow rate, using the "Wellbore pressure solutions" (drawdown pressure analysis).

The technique of superposition is depicted in Fig. 13.5. At time $t$ when the well is shut-in, the wellbore pressure is influenced by the continuos production at positive rate $+q$ causing the pressure to decrease. The influence by the negative rate $-q$ is to increase the wellbore pressure. For times greater than $t$, we will observe a combined pressure development caused

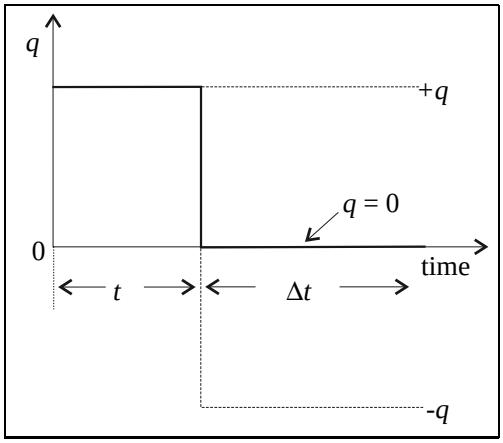


Figure 13.4: Pressure build-up test. Representation of a non-flowing well performance by a superposition technique.

by a decreasing pressure due to the positive well rate ($-q$) and a increasing pressure due to the negative well rate ($-q$).

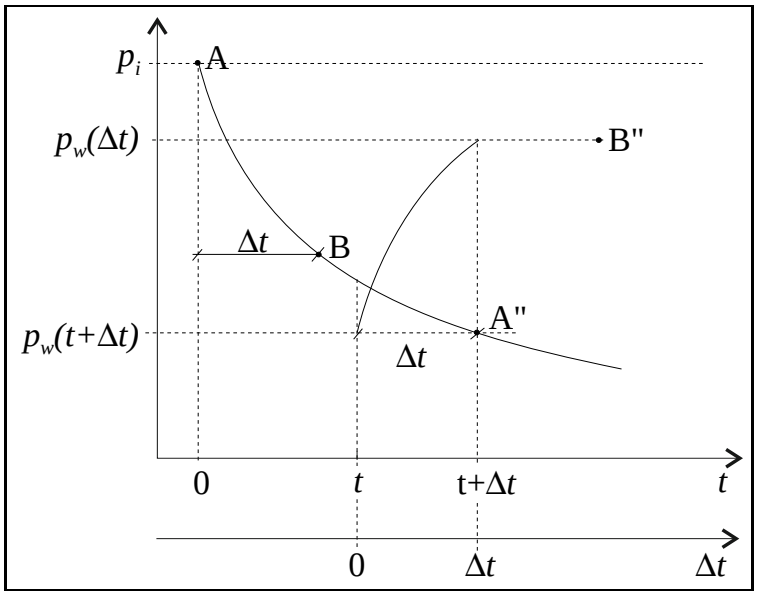


Figure 13.5: Pressure formation by superposition in build-up tests.

Using wellbore pressure, we define,

| | |
|---|---|
| $p_w(\Delta t)$: | Pressure in the well after shut-in. |
| $p_w(t+\Delta t)$: | Pressure in the well given by continuos production at positive well rate. |
| $p_i - p_w(\Delta t)$: | Pressure in the well given by start-up of continuos production at negative well rate (increasing pressure contribution). |

The superposition principle gives,

$$p_w(\Delta t) = p_w(t+\Delta t) + p_i - p_w(\Delta t),$$

where $p_w$ on the left side of the equallity is the well shut-in pressure, while $p_w$ on the right side is the well flow pressure. Using dimensionless pressures, the well shut-in pressure is given,

$$p_i - p_w(\Delta t) = \frac{qB\mu}{2\pi hk}[p_{wD}(t_D+\Delta t_D) - p_{wD}(\Delta t_D)].$$

If skin is included and the wellbore pressure at shut-in is $p_w(\Delta t_D = 0) = p_{ws}$, we have

$$p_i - p_{ws} = \frac{qB\mu}{2\pi hk}[p_{wD}(t_D) + S].$$

From the above equations, we may derive the following expressions for the wellbore pressure.

$$p_w(\Delta t) = p_i - \frac{qB\mu}{2\pi hk}[p_{wD}(t_D+\Delta t_D) - p_{wD}(\Delta t_D)], \tag{13.5}$$

$$p_w(\Delta t) = p_{ws} + \frac{qB\mu}{2\pi hk}[p_{wD}(t_D) - p_{wD}(t_D+\Delta t_D) + p_{wD}(\Delta t_D) + S], \tag{13.6}$$

$$p_w(\Delta t) = \overline{p} - \frac{qB\mu}{2\pi hk}[p_{wD}(t_D+\Delta t_D) - p_{wD}(\Delta t_D) - 2\pi t_{DA}]. \tag{13.7}$$

Pressure build-up data is analysed using the three equations above, where Eq. (13.6) is applied to estimate the reservoir permeability and skin, while Eq. (13.7) is used to determine the average pressure $\overline{p}$. Eq. (13.7) is derived on the basis of average pressure development, where

$$p_i - \overline{p} = \frac{qB}{c_t V}t = \frac{qB\mu}{2\pi hk}2\pi t_{DA},\ \ t_{DA} = \frac{k}{\phi Ac\mu}t.$$

It is important to notice that the dimensionless pressures $p_D$ in Eqs. (13.5) to (13.7) could represent the equations describing both semi logarithmic period as well as semi steady state period, i.e. depending on the analysis to be performed, we may chose which set of equations we think will fit the data best.

## 13.4 Pressure Test Analysis

Based on Eqs. (13.5) to (13.7), we may perform different analysis, where certain assumptions are made about the nature of pressure test data. In the following, two examples are give on how pressure build-up data might be analysed.

### 13.4.1 Miller - Dyes - Hutchinson (MDH) Analysis

In this analysis [43] we will assume that the semi logarithmic period is long enough to recognise a straight line behaviour in a semi logarithmic plot, i.e. we need to be able to differentiate between the three different periods, described in the previous chapter.

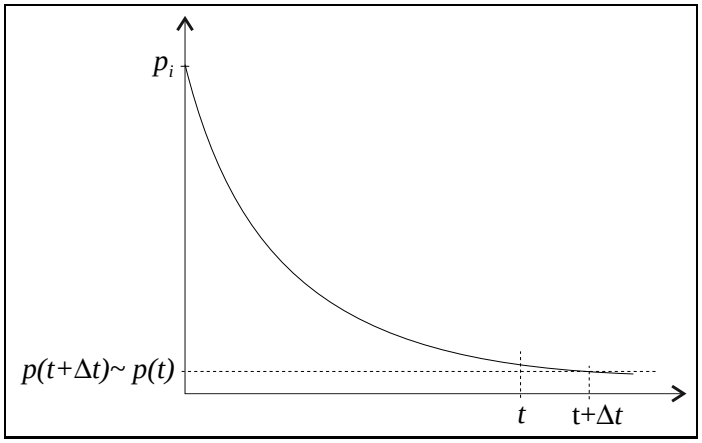


Figure 13.6: Pressure approximation in MDH-analysis.

Shortly after the well is shut-in, at time $t$, we start to monitor the wellbore pressure $p_w(\Delta t)$. For some period of time we may assume $t \gg \Delta t$ and during this period the dimensional pressure approximation $p_{wD}(t_D + \Delta t_D) \simeq p_{wD}(t_D)$ is valid, as depicted in Fig. 13.6.

Combining Eq. (13.6) and the above assumption, gives the wellbore pressure

$$p_w(\Delta t) = p_{ws} + \frac{qB\mu}{2\pi hk}[p_{wD}(\Delta t_D) + S]. \tag{13.8}$$

If the pressure development is assumed to have reached the semi logarithmic state, after shut-in of the well, we may write: $p_{wD}(\Delta t) = p^{SL}_{wD}(\Delta t_D)$, with reference to the definitions of semi logarithmic solutions in the previous chapter.

Using the definitions of dimensionless time and pressure for semi logarithmic data, we get the following pressure expression,

$$p_w(\Delta t) = p_{ws} + m\left[\log \Delta t + \log \frac{k}{\phi \mu c r_w^2} - 2.0923 + \frac{S}{1.151}\right],$$

where $m$ is the slope of the linearized semi logarithmic data (see Fig. 13.7) and the number 2.0923 is a conversion factor to SI-units.

SI-units or Field units depends on preference and the following definitions.

| | | | |
|---|---|---|---|
| SI-units: | $m = \frac{2.1208qB\mu}{hk}$ | and | $-2.0923$ |
| Field units: | $m = \frac{162.6qB\mu}{hk}$ | and | $-3.2275$ |

From Eq. (13.8), we find the skin factor by direct substitution, see also Fig. 13.7,

$$S = 1.151\left[\frac{p_w(\Delta t = 1hr) - p_{ws}}{m} - \log \frac{k}{\phi \mu c r_w^2} + 2.0923\right].$$

The average reservoir pressure $\overline{p}$, could be evaluated on the basis of Eq. (13.7), using the same approximation as above, namely; $p_{wD}(t_D + \Delta t_D) \simeq p_{wD}(t_D)$.

$$p_w(\Delta t) = \overline{p} - \frac{m}{1.151}[p_{wD}(t_D) - p_{wD}(\Delta t_D) - 2\pi t_{DA}].$$

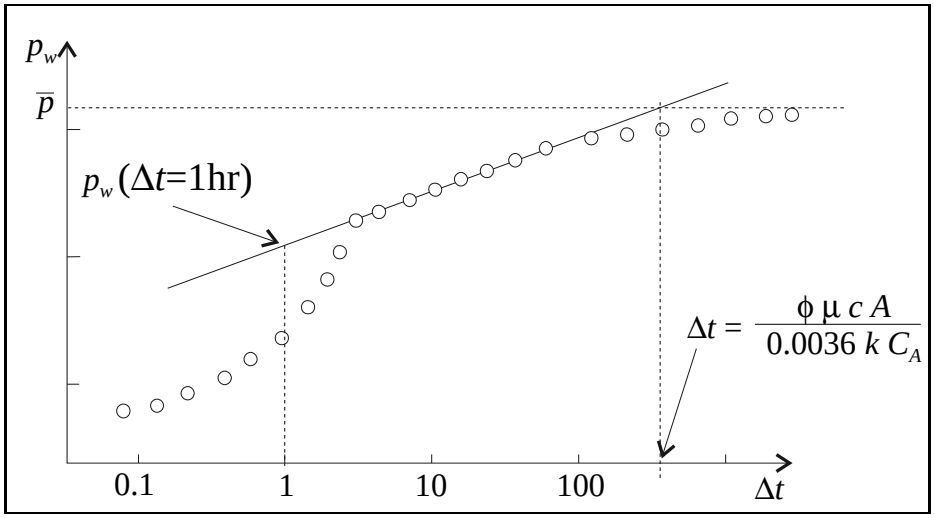


Figure 13.7: MDH analysis of semi logarithmic pressure data.

We shall now assume that the reservoir had reached its semi steady state period before or shortly after the well was shut-in. The interpretation of the different dimensionless pressures are accordingly,

$$p_{wD}(t_D) = p_{wD}^{SS}(t_D) \quad \text{and} \quad p_{wD}(\Delta t_D) = p_{wD}^{SL}(\Delta t_D),$$

and the wellbore pressure is the written,

$$\begin{aligned} p_w(\Delta t) &= \overline{p} - \frac{m}{1.151}[p_{wD}^{SS}(t_D) - p_{wD}^{SL}(\Delta t_D) - 2\pi t_{DA}], \\ &= \overline{p} - \frac{m}{1.151}\left[2\pi t_{DA} + \frac{1}{2}\ln\frac{4A}{e^{\gamma}C_A r_w^2} - \frac{1}{2}\ln\frac{4\Delta t_D}{e^{\gamma}} - 2\pi t_{DA}\right], \\ &= \overline{p} - \frac{m}{1.151}\left[\frac{1}{2}\ln\frac{A}{C_A r_w^2 \Delta t_D}\right]. \end{aligned}$$

Using SI-units we get,

$$p_w(\Delta t) = \overline{p} - \frac{m}{1.151}\left[\frac{1}{2}\ln\frac{\phi\mu cA}{0.0036kC_A\Delta t}\right].$$

If the reservoir has reached its semi steady state period before (or shortly after) the well was shut-in, the average reservoir pressure $\overline{p}$ is found by following the semi logarithmic line to the time $\Delta t = \phi\mu cA/(0.0036kC_A)$, as shown in Fig. 13.7, where the average pressure is,

$$\overline{p} = p_w\left(\Delta t = \frac{\phi\mu cA}{0.0036kC_A}\right).$$

### 13.4.2 Matthews - Brons - Hazebroek (MBH) Analysis (Horner plot)

Following the same approach as in the above section, we have assumed the pressure difference $p_{wD}(t_D + \Delta t_D) - p_{wD}(t_D)$ to be small but finite, i.e.,

$$p_{wD}(t_D + \Delta t_D) - p_{wD}(t_D) = \frac{1}{2} \ln \frac{t + \Delta t}{t}. \tag{13.9}$$

In practical terms, compared to MDH - analysis, this means that the well could be closed somewhat earlier in the MBH - analysis [36]. The pressure difference is depicted in Fig. 13.8, which points out that the time of shut-in $t_D$, may come earlier and further up on the pressure decline curve. In Fig. 13.8 we have $p_w(t) \geq p_w(t + \Delta t)$, while for dimension less pressures $p_{wD}(t_D + \Delta t_D) \geq p_{wD}(t_D)$, since $p_{wD} \propto (p_i - p_w)$.

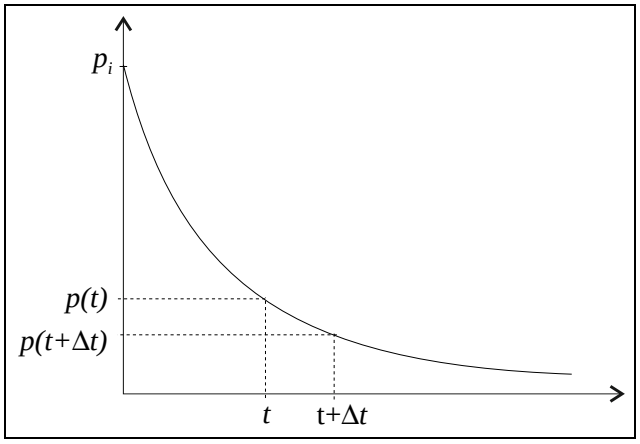


Figure 13.8: Wellbore pressure difference at the shut-in time, in MBH - analysis.

Combining the approximation given by Eq. (13.9) and the wellbore pressure solution Eq. (13.6), we get

$$p_w(\Delta t) = p_{ws} + \frac{m}{1.151} \left[ -\frac{1}{2} \ln \frac{t + \Delta t}{t} + p_{wD}(\Delta t_D) + S \right], \tag{13.10}$$

where $p_{wD}(\Delta t_D) = p_{wD}^{SL}(\Delta t_D)$, is considered to be in the semi logarithmic period.

Using SI-units this gives,

$$\begin{aligned} p_w(\Delta t) &= p_{ws} + m \left[ -\log \frac{t + \Delta t}{t} + \log \Delta t + \log \frac{k}{\phi \mu c r_w^2} - 2.0923 + \frac{S}{1.151} \right], \\ &= p_{ws} + m \left[ \log \frac{\Delta t}{t + \Delta t} + \log t + \log \frac{k}{\phi \mu c r_w^2} - 2.0923 + \frac{S}{1.151} \right]. \end{aligned} \tag{13.11}$$

Permeability and skin are estimated by plotting the build-up pressures $p_w(\Delta t)$ against the time function $\Delta t/(t + \Delta t)$ on a semi logarithmic plot, as indicated by Eq. (13.11). The slope of the linear data is $m$ and hence $k$ or $kh$ are found by substitution. The skin is calculated at the time $\Delta t = 1$, where $t + 1 \simeq t$ is assumed, i.e.,

$$S = 1.151 \left[ \frac{p_w(\Delta t = 1hr) - p_{ws}}{m} - \log \frac{k}{\phi \mu c r_w^2} + 2.0923 \right].$$

The pressure $p_w(\Delta t = 1)$ is read directly from the plot, as shown in Fig. 13.9.

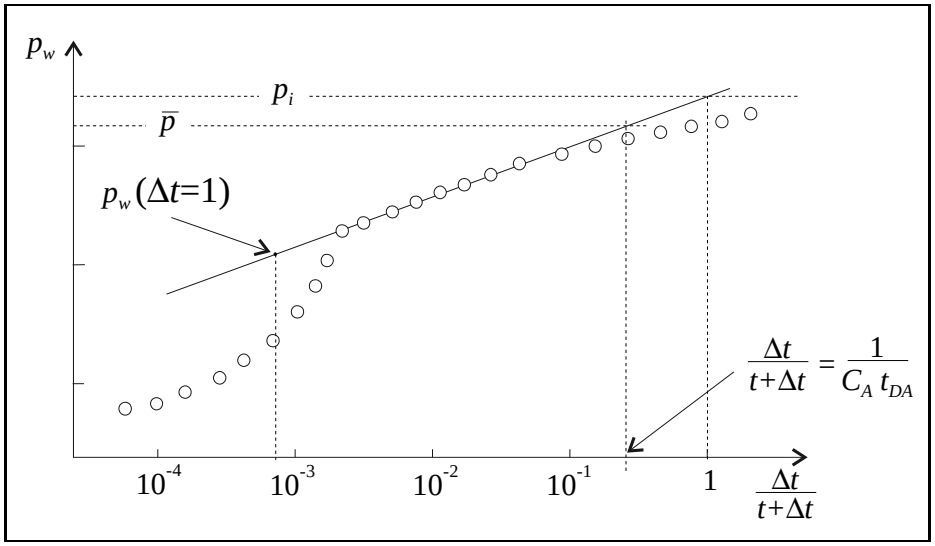


Figure 13.9: Horner plot. Wellbore pressure data plotted for MBH - analysis.

The pressure approximation Eq. (13.9) may be applied in a similar way as done above, for defining the average reservoir pressure $\overline{p}$. Substituting Eq. (13.9) in Eq. (13.7), we get

$$\begin{aligned}
p_w(\Delta t) &= \overline{p} - \frac{m}{1.151}\left[\frac{1}{2}\ln\frac{t+\Delta t}{t} + - p_{wD}(\Delta t_D) - 2\pi t_{DA}\right], \\
&= \overline{p} - \frac{m}{1.151}\left[\frac{1}{2}\ln\frac{t+\Delta t}{t} + p_{wD}(t_D) - \frac{1}{2}(\ln\Delta t_D + 0.80907) - 2\pi t_{DA}\right], \\
&= \overline{p} - \frac{m}{1.151}\left[\frac{1}{2}\ln\frac{t+\Delta t}{\Delta t} + p_{wD}(t_D) - \frac{1}{2}(\ln t_D + 0.80907) - 2\pi t_{DA}\right], \\
&= \overline{p} - \frac{m}{1.151}\left[\frac{1}{2}\ln\frac{t+\Delta t}{\Delta t} + p_{wD}(t_D) - p^{SL}_{wD}(t_D) - 2\pi t_{DA}\right]. \qquad (13.12)
\end{aligned}$$

If we then assume that the well is in its semi steady state at the time of shut-in, i.e. $p_{wD}(t_D) = p^{SS}_{wD}(t_D)$, the we get

$$\begin{aligned}
p_w(\Delta t) &= \overline{p} - \frac{m}{1.151}\left[\frac{1}{2}\ln\frac{t+\Delta t}{\Delta t} - \frac{1}{2}\ln\frac{4t_D}{e^{\gamma}} + 2\pi t_{DA} + \frac{1}{2}\ln\frac{4A}{e^{\gamma}C_A r_w^2} - 2\pi t_{DA}\right], \\
&= \overline{p} - m\left[\log\left(\frac{t+\Delta t}{\Delta t}\frac{A}{C_A r_w^2}\frac{1}{t_D}\right)\right]. \qquad (13.13)
\end{aligned}$$

Since $t_D$ in Eq. (13.13) is a well defined time (time of shut-in), we may estimate the average reservoir pressure as the pressure on the straight line (see Fig. 13.9) at the time,

$$\frac{\Delta t}{t+\Delta t} = \frac{A}{C_A r_w^2 t_D} = \frac{1}{C_A t_{DA}}.$$

If we now assume that the well is in its semi logarithmic state at the time of shut-in, i.e. $p_{wD}(t_D) = p^{SL}_{wD}(t_D)$, we then get by substitution into Eq. (13.12),

$$p_w(\Delta t) = \overline{p}\frac{m}{1.151}\left[\frac{1}{2}\ln\frac{t+\Delta t}{\Delta t} - 2\pi t_{DA}\right]$$

At the time $\Delta t/(t+\Delta t) = 1$, we get

$$\begin{aligned} p_w\left(\frac{\Delta t}{t+\Delta t}=1\right) &= \overline{p} + \frac{m}{1.151}[2\pi t_{DA}], \\ &= \overline{p}\frac{qB\mu}{2\pi hk}\left[2\pi\frac{kt}{\phi Ac\mu}\right], \\ &= \overline{p} + \frac{qBt}{Vc}, \text{ where } V = \phi Ah \end{aligned} \tag{13.14}$$

Under semi steady state conditions we have seen that,

$$p_i - \overline{p} = \frac{qBt}{Vc},$$

and consequently we may write,

$$p_w\left(\frac{\Delta t}{t+\Delta t}=1\right) = \overline{p} + (p_i - \overline{p}) = p_i.$$

The initial reservoir pressure is defined in Fig. 13.9 on the straight line at time $\Delta t/(t+\Delta t) = 1$.

## 13.5 Exercises

1. A well is tested by exploiting it at a constant rate of 1500 STB/d for a period of 100 hours. It is suspected, from seismic and geological evidence, that the well is draining an isolated reservoir block which has approximately a 2:1 rectangular geometrical shape and the extended drawdown test is intended to confirm this. The reservoir data and the flowing bottom hole pressures recorded during the test are detailed below.

$$\begin{array}{ll} h = 20\,ft & c = 15 \cdot 10^{-6}\,psi^{-1} \\ r_w = 0.33\,ft & \mu_o = 1\,cp \\ \phi = 0.18 & B_o = 1.20\,RB/STB \end{array}$$

| Time (hours) | $p_w$ (psi) | Time (hours) | $p_w$ (psi) | Time (hours) | $p_w$ (psi) |
|---|---|---|---|---|---|
| 0 | 3500 ($p_i$) | 7.5 | 2848 | 50 | 2597 |
| 1 | 2917 | 10 | 2830 | 60 | 2545 |
| 2 | 2900 | 15 | 2794 | 70 | 2495 |
| 3 | 2888 | 20 | 2762 | 80 | 2443 |
| 4 | 2879 | 30 | 2703 | 90 | 2392 |
| 5 | 2869 | 40 | 2650 | 100 | 2341 |

   a) Calculate the effective permeability and skin factor of the well.

   b) Make an estimate of the area being drained by the well and the Dietz shape factor.

   (after L.P.Dake)

2. A discovery well is produced for a period of approximately 100 hours proir to closure for an initial pressure buildup survey. The production data and estimated reservoir and fluid properties are listed below.

$$\begin{array}{ll} q = 123\,STB/d & \phi = 0.2 \\ N_p = 500\,STB & \mu = 1\,cp \\ h = 20\,ft & B_{oi} = 1.22\,RB/STB \\ r_w = 0.3\,ft & c = 20 \cdot 10^{-6} psi^{-1}(c_o S_o + c_w S_w + c_f) \\ A = 300\,\text{acers} & \end{array}$$

| Time (hours) | $p_w$ (psi) | Time (hours) | $p_w$ (psi) | Time (hours) | $p_w$ (psi) |
|---|---|---|---|---|---|
| 0.0 | 4506 | 1.5 | 4750 | 4.0 | 4766 |
| 0.5 | 4675 | 2.0 | 4757 | 6.0 | 4770 |
| 0.66 | 4705 | 2.5 | 4761 | 8.0 | 4773 |
| 1.0 | 4733 | 3.0 | 4763 | 10.0 | 4775 |

   a) What is the initial reservoir pressure?

   b) If the well is completed across the entire formation thickness, calculated the effective permeability.

c) Calculate the value of the mechanical skin factor.

d) What is the additional pressure drop in the wellbore due to the skin?

e) If it is initially assumed that the well is draining from the centre of a circle, is it valid to equate $p_i$ to the asymptotic value $\log(t+\Delta t)/(\Delta t) = 0$?

(after L.P.Dake)

3. A reservoir has 3 wells; W1, W2 and W3. Well W1 has been producing at a constant flow rate of 120 STB/D for 70 hours and is then converted to an observation well. Well W2, located 2500 $ft$ straight north of well W1, is producing at a flow rate of 190 STB/D. Well W3, located 1900 $ft$ west of W1, is producing at a rate of 80 STB/D. At the time when well W1 was shut-down, well W2 had produced for 100 hours and well W3 for 50 hours.

   Pressure data from well W1 is given in the table:

| $\Delta t$ [hours] | 0 | 5 | 10 | 20 | 30 | 40 | 50 | 100 | 150 |
|---|---|---|---|---|---|---|---|---|---|
| $P_{ws}$ [psia] | 4213 | 4380 | 4413 | 4433 | 4443 | 4450 | 4455 | 4466 | 4472 |
| $\Delta t$ | 200 | 250 | 300 | 400 | 500 | 800 | 1200 | 1500 | – |
| $P_{ws}$ | 4473 | 4474 | 4478 | 4480 | 4470 | 4461 | 4448 | 4439 | – |

   Additional reservoir data:

| | | |
|---|---|---|
| $\mu_o$ = 0.8 cp | $B_o$ = 1.15 RB/STB | $c_f = 4.0 \cdot 10^{-6}\ psi^{-1}$ |
| $S_o$ = 0.80 | $S_w$ = 0.20 | $c_o = 8.0 \cdot 10^{-6}\ psi^{-1}$ |
| h = 30 ft | $r_w$ = 0.276 ft | $c_w = 3.0 \cdot 10^{-6}\ psi^{-1}$ |

   Assume that the pressure development in well W1 can be expressed by the formula below:

$$P_{ws} = P_i - 162.6\frac{Q_1\mu B}{kh}\log\left(\frac{t_1+\Delta t}{\Delta t}\right) - 70.6\frac{Q_1\mu B}{kh}\left[\frac{Q_2}{Q_1}Ei(x_1) + \frac{Q_3}{Q_1}Ei(x_2)\right]$$

   where

$$x_1 = \frac{\phi\mu c_t d_{12}^2}{0.00105kt_2} \qquad x_2 = \frac{\phi\mu c_t d_{13}^2}{0.00105kt_3}$$

   and where $d_{12}$ and $d_{13}$ is the distance between W1 and W2 and W1 and W3, respectively. $t_1$ is the time of production for well W1.

   a) Calculate the average reservoir compressibility $c_t$.

   b) Estimate the initial pressure $P_i$, assuming the interference between well W2 and W3 is negligible for early pressure data.

   c) Calculate the average reservoir oil permeability ,$k$.

   d) Calculate the mechanical skin, S.

   e) Use the pressure observation form $\Delta t$ = 1500 hours to find the average reservoir porosity between the wells.

4. An oil well has been producing 1484 STB at a flow rate of 124 STB/D, when it was shut down. The pressure build-up data is given in the table below:

| $\Delta t$ [hours] | 4 | 8 | 12 | 16 | 20 | 24 |
|---|---|---|---|---|---|---|
| $P_{ws}$ [psia] | 2857 | 3027 | 3144 | 3252 | 3283 | 3298 |
| $\Delta t$ | 28 | 32 | 36 | 40 | 44 | 48 |
| $P_{ws}$ | 3308 | 3315 | 3323 | 3331 | 3338 | 3342 |

Additional reservoir data:

$\mu$ = 3.2 cp $\quad B_o$ = 1.21 RB/STB
h = 8.4 ft $\quad c_t = 12 \cdot 10^{-6}\ psia^{-1}$
$\phi$ = 0.02

a) Find the reservoir pressure at the outer boundary, $P_e$.

b) Calculate the average reservoir oil permeability, $k_o$.

**Answers to questions:**

1. a) 240 mD, b) 4.5, 2. a) 4800 psi, b) 50 mD, c) 6.0, d) 128 psi, 3. a) $11 \cdot 10^{-6}\ psi^{-1}$, b) 4485 psi, c) 7.6 mD, d) -3.5, e) 0.135, 4. a) 3475 psi, b)58 mD.

# Chapter 14

# Modern Well Test Analysis

## 14.1 Advantages of a Transient Well Testing Techniques

Advances in downhole control and modern computer processing of well test data have transformed well testing into a powerfool tool that helps to better understand the reservoir complexity and obtain much more information than just single values of permeability, skin and reservoir pressure.

Methods of well test analysis described in previous chapters, enable to obtain reliable results in simple cases of a "well behaving reservoirs". As we have already learned, the early portion of the well test data is controlled by the wellbore storage and skin effect. Often a long time testing is required to overcome these effects and obtain a desired straight line in the standard linear-log plot. However, a straight line behavior can be often distorted or even masked by other wells interfering with the tested one, and complex reservoirs features (dual porosity, sealing barriers, stratified reservoirs, etc.). In such cases, interpretation of well test data can be very uncertain and thus, unreliable.

Number of publications made in late 70s-early 80s ([6, 17, 24, 32, 55]) have shown that the downhole pressure derivative coupled with conventional pressure plotted versus time functions, can be substantially more informative than thaditional plot. It follows from the fact that pressure derivative is much more sensitive than pressure to reservoir characteristics and, therefore, responds more distinctly to their changes (see Fig. 14.1).

Another advantage of introducing the pressure derivative to the well test analysis is that it allows, in principle, to terminate the test before the development of full radial flow corresponding to a straight line in the plot and thus, reduce duration of the test without affecting the accuracy of the analysis [5].

Most of the drawbacks inherent in *surface shut-in testing* have been eliminated by introducing *downhole shut-in valves* and *downhole measurements*. This technique enables to accurately measure dowhole flowrates and corresponding pressure and directly evaluate the wellbore storage coefficient $C$ by using the following simple material balance equation written for the downhole chamber conditions [3]:

$$q_s = C \cdot dp/dt, \tag{14.1}$$

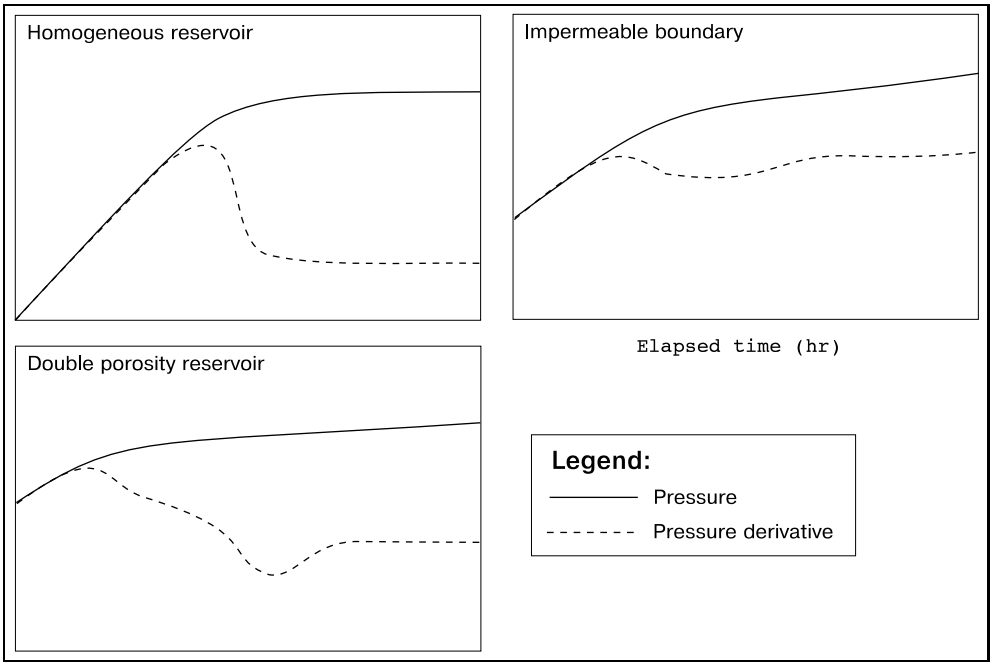


Figure 14.1: Transient pressure and pressure derivative plots showing different types of responses that might occur due to various reservoir characteristics (Schlumberger Educational Series: "Modern Reservoir Testing", 1994)

where: $q_s$ – sand face production flow rate;
$C = c_f \cdot V_{ch}$ – wellbore storage coefficient;
$c_f$ – compressibility of fluids trapped in the chamber;
$V_{ch}$ – chamber volume

As follows from Eq. (14.1) a sand face flow rate can only be related to the downhole pressure if the wellbore storage and, resprectively, compressibility of fluids remain constant during the test. This assumption holds for a downhole shut-in valves and does not satisfy conditions of the earlier used surface shut-in testing. Due to the fact that the whole well test analysis is based on a constant compressibility concept, this recently introduced technique provides with more accurate analysis of the well data. Moreover, it allows to use type curves and type-curve matching technique that is a key element of modern well test analysis.

## 14.2 Use of Type Curves

As it has been mentioned before, a large number of type curves exists to cover different reservoir models. Each reservoir model is represented by the downhole pressure and its derivative versus time in a log-log plot. Using dimensionless pressure, time and wellbore storage coefficient as shown below:

$$\begin{array}{ll} \underline{\text{Field Units}} & \underline{\text{SI Units}} \\ p_D = 0.00708\frac{kh}{qB\mu}[p_i - p_{wf}(t)] & p_D = 0.543\frac{kh}{qB\mu}[p_i - p_{wf}(t)] \\ t_D = 0.0002637\frac{kt}{\mu\phi C_t r_w^2} & t_D = 0.0036\frac{kt}{\mu\phi C_t r_w^2} \\ C_D = 0.8937\frac{C}{\phi h C_t r_w^2} & C_D = 2.308\frac{C}{\phi h C_t r_w^2} \end{array} \tag{14.2}$$

this set of type curves can be expressed in a more universal way (i.e. independent of actual well/reservoir parameters) revealing dependence on only the reservoir model. For example, two production wells acting in the same type of reservoir with different characteristics (flow rate, wellbore radius, porosity, oil viscosity, etc.) would result in the same dimensionless type curves.

Using dimensionless parameteres specified by Eq. (14.2) the pressure drawdown in the infinite-acting reservoir expressed in Field Units is,

$$p_i - p_{wf} = 162.6\frac{qB\mu}{kh}(\log t + \log\frac{k}{\phi\mu C_t r_w^2} - 3.2275 + \frac{S}{1.151}) \tag{14.3}$$

and its derivative can be written as follows (Gringarten *et al.*, 1979):

$$p_D = 0.5[\ln(\frac{t_D}{C_D} + 0.80907 + \ln(C_D e^{2S}) \tag{14.4}$$

$$p'_D(t_D/C_D) = 0.5 \tag{14.5}$$

Eqs. (14.4) and (14.5) show that the infinite-acting response with constant wellbore storage and skin, when subjected to a single-step change in flow rate, can be described by three dimensionless groups, i.e.

$$p_D, \qquad t_D/C_D, \qquad p'_D \cdot t_D/C_D$$

The graphical representation of $p_D$ and $p'_D \cdot t_D/C_D$ versus $t_D/C_D$ in a log-log plot provides one of the most widely used type curves and is fundamental to a modern well test analysis.

Typical set of type curves for different values of $C_D e^{2S}$ is shown in Fig. 14.2 [1].

## 14.3 Type Curve Matching Technique

Modern well test interpretation consists of two distinct stages [3]:

- Model recognition stage.
- Parameter estimation stage.

First the analyst must, using his/her experience, available software, carefully study specific features of the reservoir response during pressure drawdown/build-up and isentify a theoretical reservoir model.

Pressure transient and especially its derivative are the tools to identify these features (dual porosity or layered reservoir, reservoir with sealing faults, impermeable boundaries, etc.) and

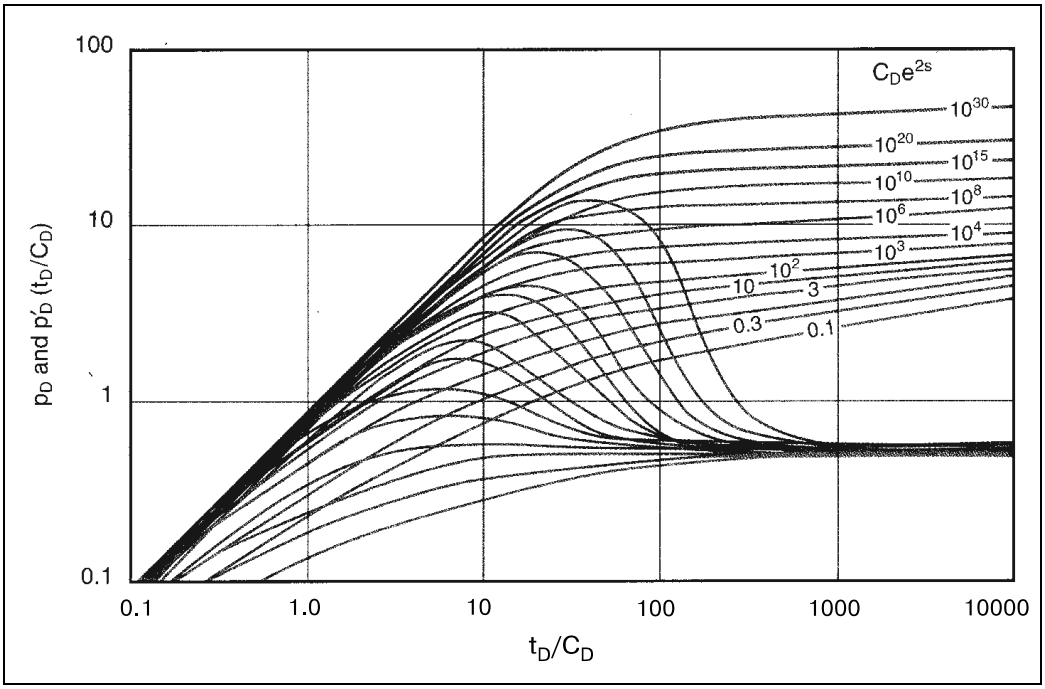


Figure 14.2: True type curves for a well with constant wellbore storage and skin in an infinite- acting reservoir (from Bourdet *et al.*, 1983

thus, recognize the model. Fig. 14.3 gives an example of how different reservoir features affect the bottomhole pressure and its derivative [5].

Since the reservoir model has been identified the definition of reservoir parameters can be done using the type-curve matching technique. Data obtained during the well testing are plotted in terms of $\Delta p = p_i - p_{wf}(t)$ and $(\Delta p' \cdot \Delta t)$ versus elapsed time $\Delta t$ in a log-log plot and superimposed over the type curves. This procedure is illustrated in Fig. 14.4.

Once both pressure and its derivative are matched with the corresponding type curves the following data can be read directly from the plot (Fig. 14.4):

- $C_D e^{2S}$
- pressure match, $(p_D/\Delta p)_M$
- time match, $(t_D/C_D/\Delta t)_M$

Using dimensionless groups of parameters ( 14.2), the permeability-thickness product (flow capacity) *kh*, wellbore storage coefficient *C* and skin factor *S* can be readily estimated as follows [5]:

$$k \cdot h = 141.2 q B \mu \left(\frac{p_D}{\Delta p}\right)_M \tag{14.6}$$

$$C = \left(\frac{0.000295 kh}{\mu}\right)\left(\frac{\Delta t}{t_D/C_D}\right)_M \tag{14.7}$$

[1]Note that these type curves are derived under assumption that wellbore storage remains constant during well test. This assumption is valid only if tests have been prformed using downhole shut-in devices.

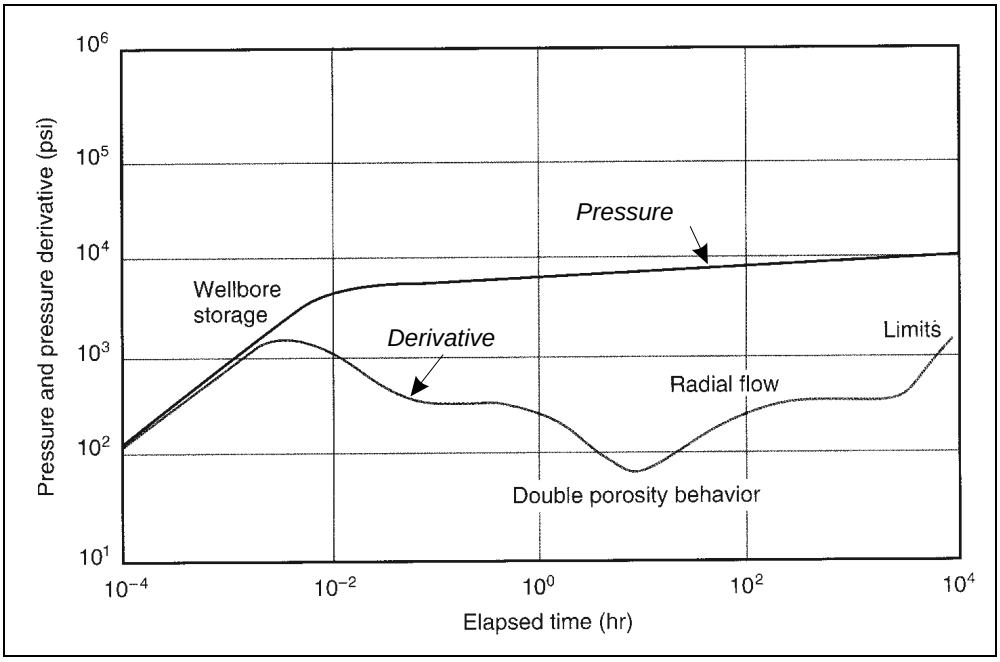


Figure 14.3: Example showing how different reservoir features affect the transient downhole pressure and its derivative (from Schlumberger Educational Services: "Modern Reservoir Testing", 1994)

$$S = 0.5 \ln[\frac{(C_D e^{2S})_M}{C_D}] \tag{14.8}$$

Material presented above serves as an introduction to a modern well test analysis. For a more comprehensive acquaintance with this technique we recommend the following literature [6, 17, 26, 50, 20, 55, 3, 5].

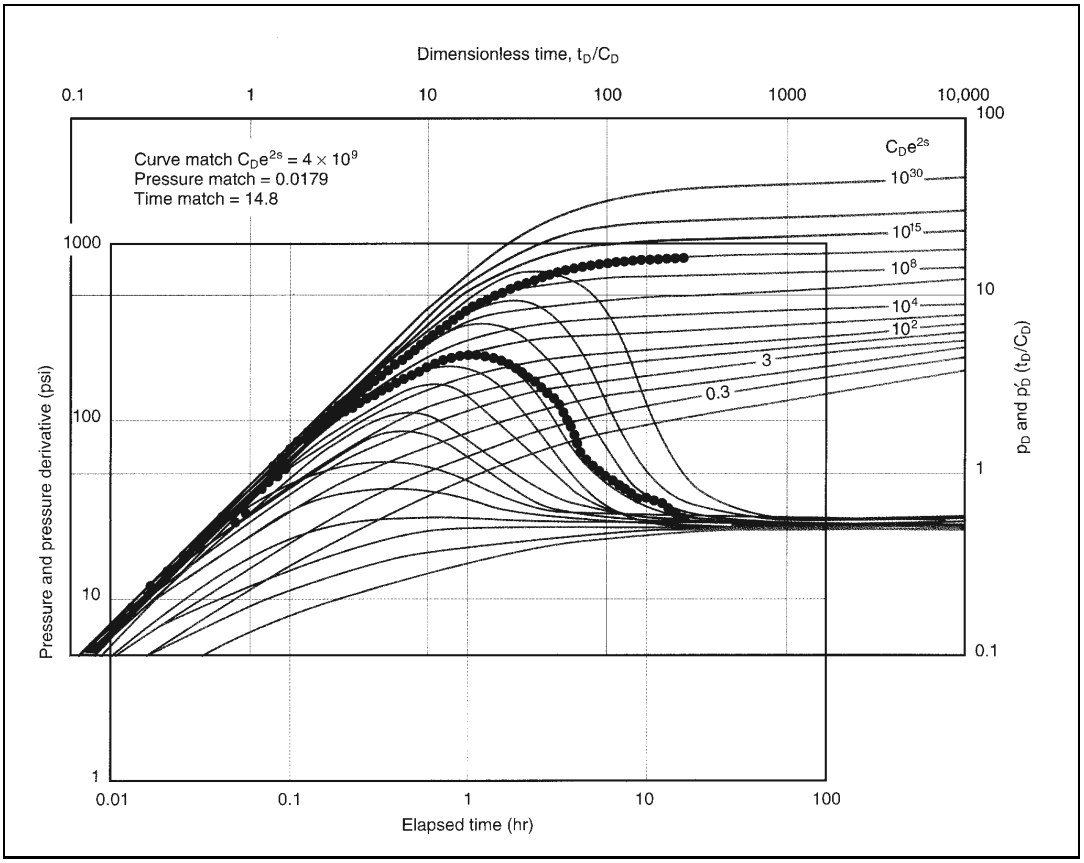


Figure 14.4: Type-curve matching technique for the estimation of reservoir parameters (from Bourdet *et al.*, 1983)

## 14.4 Exercises

1. Using results of tupe-curve matching shown in Fig. 14.4) and the following reservoir parameters:

| | | |
|---|---|---|
| $S_o = 0.8$ | $\mu_o = 1.0$ cp | $B = 1.2$ Rb/STb |
| $c_o = 10^{-5}$ psi$^{-1}$ | $c_w = 3{\cdot}10^{-6}$ psi$^{-1}$ | $c_r = 3{\cdot}10^{-6}$ psi$^{-1}$ |
| $\phi = 0.18$ | $r_w = 0.3$ ft | $h = 100$ ft |
| $q = 1200$ b/d | | |

estimate the reservoir permeability $k$, wellbore storage coefficient $C$ and skin factor $S$.

# Bibliography


[1] *Reservoir and Production Fundamentals*. Textbook published by Schlumberger, 1982.

[2] *Monograph 1: Guidelines for Application of the Definitions for Oil and Gas Reserves*. The Society of Petroleum Evaluation Engineers, Houston, TX, 1988.

[3] *Middle East Well Evaluation Review: Reservoir Testing*. Schlumberger Technical Services, Dubai, revised edition, 1991.

[4] *Petroleum Resources: Norwegian Continental Shelf*. Norwegian Petroleum Directorate, 1993.

[5] *Schlumberger Educational Service: Modern Reservoir Testing*. Schlumberger, SMP-7055, Houston, 1994.

[6] R.G. Agarval. A new method to account for producing time effects when drawdown type curves are used to analyse pressure build-up and other test data. *Paper SPE 9289*, 1980.

[7] J.W. Amyx, Jr. Bass, D.M., and R.L. Whiting. *Petroleum Reservoir Engineering*. McGraw-Hill, New York, 1960.

[8] J.S. Archer and P.G. Wall. *Petroleum Engineering: Principles and Practice*. Graham & Trotman, London, 1991.

[9] T. Austad, I. Fjelde, K. Veggeland, and K. Taugbøl. Physicochemical principles of low tension polymer flood. *Proceedings of the 7th Symposium on Improved Oil Recovery*, 1:208–219, 1993.

[10] K. Aziz and A. Settari. *Petroleum Reservoir Simulation*. Applied Science Publishers, London, 1979.

[11] G.I. Barenblatt. *Dimensional Analysis*. Moscow Physico-Technical University, Moscow, 1987. (in Russian).

[12] G.I. Barenblatt, V.M. Entov, and V.M. Ryzhik. *Theory of Non-Stationary Filtration of Liquids and Gases*. Nedra, Moscow, 1972. (in Russian).

[13] K.S. Basniev, I.N. Kochina, and V.M. Maximov. *Undeground Hydrodynamics*. Nedra, Moscow, 1993. (in Russian).

[14] M. Baviere, editor. *Basic Concepts in Enhanced Oil Recovery Processes*. Elsevier Applied Science, 1991.

[15] J. Bear. *Dynamics of Fluids in Porous Media*. American Elsevier Publ. Co., New York, 1972.

[16] P.G. Bedrikovetsky. *Mathematical Theory of Oil and Gas Recovery*. Kluwer Acad. Publ., Dordrecht, 1993.

[17] D.P. Bourdet, T.M. Whittle, A.A. Douglas, and Y.M. Pilard. A new set of type curves simplifies well test analysis. *World Oil*, (6):95–106, May 1983.

[18] T. Bu, I. Sørende, and T. Kydland. Ior screening: What went wrong? *Proceedings of the 7th European Symposium on IOR*, 1:30–35, 1993.

[19] Jr. Creig, F.F. *Reservoir Engineering Aspects of Waterflooding*, volume 3 of *Monorgaph Series*. SPE, Richardson, 1971.

[20] G. Da Prat. *Well Test Analysis for Fractured Reservoir Evaluation*. Elsevier, Amsterdam, 1990.

[21] L.P. Dake. *Fundamentals of Reservoir Engineering*. Elsevier, Amsterdam, twelfth edition, 1991.

[22] D. Dubois and H. Prade. *Fuzzy Sets and Systems: Theory and Applications*. Academic Press, New York, 1980.

[23] F.A.L. Dullien. *Porous Media: Fluid Transport and Pore Structure*. Academic Press, Inc., San Diego, 1979.

[24] R.C. Jr. Earlougher. *Advances in Well Test Analysis*. Society of Petroleum Engineers of AIME, Dalls, monograph series edition, 1977.

[25] D.A. Efros. Determination of relative permeability and distribution functions in the displacement of petroleum by water. *Proceedings of the USSR Academy of Sciences*, 110(5):746, 1956.

[26] C.A. Ehlig-Economides, P. Hegeman, and S. Vik. *Guidelines Simplify Well Test Interpretation*. Schlumberger: Wireline and Testing, SMP-3101, Houston, 1994.

[27] V.M. Entov. *Physico-chemical Hydrodynamics of Processes In Porous Media*. Istitute of Applied Mechanics of the USSR Academy of Sciences, Moscow, 1980. (in Russian).

[28] J.H. Fang and H.C. Chen. Uncertainties are better handled by fuzzy arothmetic. *AAPG Bull.*, 74(8):1228–1233, 1990.

[29] Jr. Forrest F. Craig. *The Reservoir Engineering Aspects Of Waterflooding*. Society of Petroleum Engineers of AIME, Dallas, 1971.

[30] S.M. Skjæveland G.A. Virnovsky, Y. Guo. Relative permeability and capillary pressure concurrently determined from steady-state flow experiments. *Proceedings of the IOR Symposium, Vienna, May 1995*, 1995.

[31] J. Geertsma. The effect of fluid pressure decline on volumetric changes of porous rock. *Trans.AIME*, 210:331–340, 1957.

[32] A.C. Gringarten, D.P. Bourdet, P.A. Landel, and V.J. Kniazeff. A comparison between different skin and wellbore storage type curves for early-time transient analysis. *Paper SPE 8205*, 1979.

[33] D. Havlena and A.S. Odeh. The material balance as an equation of a straight line. *JPT*, pages 896–900, August 1963.

[34] D. Havlena and A.S. Odeh. The material balance as an equation of a straight line. part ii - field cases. *JPT*, pages 815–822, July 1964.

[35] Z.E. Heinemann. *Flow in Porous Media*, volume 1 of *Textbook Series*. Mining University Leoben, Leoben, 1988.

[36] D.R. Horner. Pressure build-up in wells. *World Petr. Congress*, (3):503–521, 1951.

[37] N.J. Hyne. *Geology for Petroleum Exploration, Drilling and Production*. McGraw-Hill, New York, 1984.

[38] E.F. Johnson, D.P. Bossler, and V.O. Naumann. Calculation of relative permeability from displacement experiments. *Transactions of AIME*, 216:370 – 372, 1959.

[39] J. Kolnes. *Improved Oil Recovery*. Stavanger, 1993.

[40] Larry W. Lake. *Enhanced Oil Recovery*. Prentice Hall, Englewood Cliffs, New Jersey, 1989.

[41] M. Latil. *Enhanced Oil Recovery*. Editions Technip, Paris, 1980.

[42] W. Littmann. *Polymer Flooding*. Elsevier, Amsterdam, 1988.

[43] C.C. Miller, A.B. Dyes, and C.A. Hutchinson. Estimation of permeability and reservoir pressure from bottom-hole pressure build-up characteristics. *Trans. AIME*, (189):91–104, 1950.

[44] Nærings og energidepartementet. *Faktaheftet; Norsk petroleumsvirksomhet*. Nærings og energidepartementet, Oslo, Norge, 1994.

[45] D.W. Peaceman. *Fundamentals of Numerical Reservoir Simulation*. Elsevier, Amsterdam, 3rd edition, 1977.

[46] G.A. Pope. The application of fractional flow theory to enhanced oil recovery. *Society of Petroleum Engineers Journal*, 20(3):191–205, 1980.

[47] E.J. Finnemore R.B. Daugherty, J.B. Franzini. *Fluid Mechanics with Engineering Applications*. McGraw-Hill, New York, 1990.

[48] F.W. Sears, M.W. Zemansky, and H.D. Young. *University Physics, Seventh Edition*. Addison-Wesley, 1986.

[49] R.C. Selley and David C. Morill. *GL 101: Basic Concepts of Petroleum Geology*. IHRDC Video Library for Exploration and Production Specialists, Boston, 1991.

[50] R.C. Selley and David C. Morill. *PE 401: Introduction to Well Testing and Measurement Technique*. IHRDC Video Library for Exploration and Production Specialists, Boston, 1991.

[51] Briann J. Skinner and Stephen C. Porter. *The Dynamic Earth (An introduction to physical geology)*. Second Edition, 1991.

[52] S.M. Skjæveland and J. Kleppe, editors. *SPOR Monograph*. Norwegian Petroleum Directorate, Stavanger, 1992.

[53] H.C. Slider. *Practical Petroleum Reservoir Engineering Methods*. Petroleum Publishing Company, Tulsa, 1976.

[54] M.R. Spiegel. *Theory and Problems of Probability and Statistics*. McGraw-Hill Book Company, New York, 1975.

[55] T.D. Streltsova and R.M. McKinley. Effect of flow time duration on build-up pattern for reservoirs with heterogeneous properties. *Paper SPE 11140*, 1982.

[56] T. Terano, K. Asai, and M Sugeno. *Fussy Systems Theory and Its Applications*. Academic Press, New York, 1992.

[57] D. Tiab and E.C. Donaldson. *Petrophysics, Theory and Practice of Measuring Reservoir Rock and Fluid Transport Properties*. Gulf Publishing Company, Houston, Texas, 1996.

[58] Ya.M Vainberg, G.A. Virnovsky, and M.I. Shwidler. On some inverse problems of two-phase filtration theory. *Numerical Methods for Solving the Incompressible Fluids Filtration Problems*, pages 73–78, 1975. (in Russian).

[59] R.C. Weast and M.J. Astle. *Handbook og Chemistry and Physics, 62,nd Edition*. CRC Press, Inc., Boca Raton, Florida, 1981 - 1982.

[60] Henry J. Welge. A simplified method for computing oil recovery by gas or water drive. *Petroleum Transactions, AIME*, 195:91–98, 1952.

[61] L.A. Zade. Fuzzy sets. *Inform. and Controll*, 8(3):338–353, 1965.

[62] R.W. Zimmerman. *Compressibility of sandstones*. Elsvier, 1991.